Development of a model error estimation strategy and application to multi-scale model adaptation

Mouad Fergoug

PSL
UNIVERSITÉ PARIS

THÈSE DE DOCTORAT

DE L'UNIVERSITÉ PSL

Préparée à MINES Paris

Développement d'une stratégie d'estimation d'erreur de modèle et application à l'adaptation de modèle multi-échelle

Development of a model error estimation strategy and application to multi-scale model adaptation

Soutenance par

Mouad FERGOUG

prévue le 03 février 2023

École doctorale n°621

Ingénierie des Systèmes, Matériaux, Mécanique, Energétique

Spécialité

Mécanique

Composition du jury :

Claude BOUTIN Directeur de recherche, ENTPE	*Rapporteur*
Varvara KOUZNETSOVA Associate Professeur, Eindhoven University of Technology	*Rapporteur*
Ludovic CHAMOIN Professeur, ENS Paris-Saclay	*Examinateur*
Julien YVONNET Professeur, Université Gustave Eiffel	*Président*
Basile MARCHAND Ingénieur de recherche, Mines Paris	*Examinateur*
Augustin PARRET-FRÉAUD Ingénieur de recherche, Safran Tech	*Examinateur*
Nicolas FELD Ingénieur de recherche, Safran Tech	*Co-directeur de thèse*
Samuel FOREST Directeur de recherche, Mines Paris CNRS	*Directeur de thèse*

MINES PARIS | PSL

Abstract

Homogenized models are often used in multiscale analysis of composite materials because of their computational efficiency. However they frequently fail to provide sufficient accuracy in regions with considerable gradients in solution fields. One approach to overcome this issue is to adaptively couple the homogeneous model with a full field, heterogeneous model in selected zones of interest which need to be determined somehow. For this purpose, I have proposed a new modeling error estimate based on a higher-order asymptotic homogenization method associated with an original general boundary layer correction, shown to provide accurate estimation of heterogeneous fields even for cases with a weak scale separation between the characteristic lengths of the heterogeneities and the structural problem. This modeling error estimation quantifies the terms neglected by classical first-order homogenization, which become significant for weak separation of scales. An original multiscale coupling strategy is also developed to more effectively couple the homogeneous and heterogeneous domains as a step toward hierarchical modeling of elastic heterogeneous structures.

Keywords

Modeling error, multiscale analyses, asymptotic homogenization, boundary layer effect, global-local analysis.

Résumé

Les modèles homogénéisés sont souvent utilisés dans l'analyse multi-échelle des matériaux composites en raison de leur efficacité de calcul, cependant ils ne fournissent souvent pas une précision suffisante dans les régions présentant des forts gradients dans les champs de solution. Une approche pour surmonter cette difficulté est de coupler de manière adaptative le modèle homogène avec un modèle hétérogène dans des zones d'intérêt identifiées. J'ai développé un nouvel estimateur d'erreur de modélisation afin de détecter ces régions où le raffinement du modèle de matériau est nécessaire. Cet estimateur est formulé en se basant sur la méthode d'homogénéisation asymptotique d'ordre supérieur associée à une correction originale des effets de bords que j'ai proposée. En effet, il est démontré que l'homogénéisation d'ordre supérieur fournit une estimation précise des champs hétérogènes même dans les cas où la séparation d'échelle entre les longueurs caractéristiques des hétérogénéités et le problème structurel est faible. Cette estimation de l'erreur de modélisation quantifie la différence entre une estimation d'ordre supérieur introduisant l'effet des gradients macroscopiques et une estimation classique de premier ordre. Une stratégie de couplage adéquate est également développée pour coupler efficacement les domaines homogènes et hétérogènes, constituant une étape vers la modélisation hiérarchique des structures élastiques hétérogènes.

Mots clés

Erreur de modélisation, analyse multi-échelle, homogénéisation asymptotique, effets de bords, couche limite, analyse globale/locale.

Contents

Chapter 1

Introduction

"Pour ce qui est de l'avenir, il ne s'agit pas de le prévoir, mais de le rendre possible. "

Antoine de Saint Exupéry,
Citadelle, 1948

Global warming is one of the biggest threats humankind faces nowadays. It leads and continues to cause several environmental problems like an increasing number of climate cataclysms, sea level rise, precipitation problems, forest fires, and so on. Scientists have high confidence that global temperatures will continue to rise for many decades, mainly due to greenhouse gases (GHG) produced by human activities.

To address this emergency, the European Union (EU) aims to be climate-neutral by 2050 and has reinforced its emissions targets for 2030, committing to reduce greenhouse gas (GHG) by at least 55% compared to 1990. This requires unprecedented and deep changes for the industry, especially the transportation sector which is very energy-intensive and difficult to decarbonize.

Consequently, the aerospace industry has already planned several evolutionary technologies, particularly for engines which are the main source of aircraft emissions. Safran Group and GE Aviation, international leaders in aircraft engines, launched the CFM RISE (Revolutionary Innovation for Sustainable Engines) program with the objective, among others, of improving engine efficiency.

For the RISE demonstrator engine (see figure 1.1), an open fan architecture has been chosen. It is expected to reduce fuel consumption and carbon dioxide (CO2) emissions by more than 20% compared with the current generation of LEAP engines [CFM International, 2022] while maintaining comparable thrust and noise performance. The LEAP engine has already achieved fuel burn and CO2 emissions reductions of about 15% compared with the previous generation of engines (CFM56) [CFM International, 2022]. One key to reach this efficiency is to increase the engine bypass ratio, the main contributor to the total thrust. This is achievable by increasing the size of the fan blades size (see figure 1.2). Major scientific challenges arise such as reducing the excess mass due to the

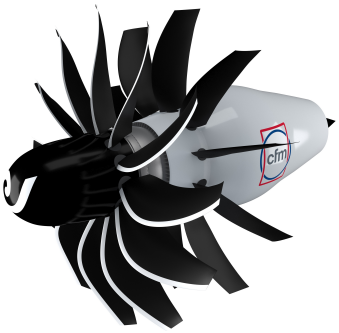

Figure 1.1: *RISE demonstrator engine. [CFM International, 2022]*

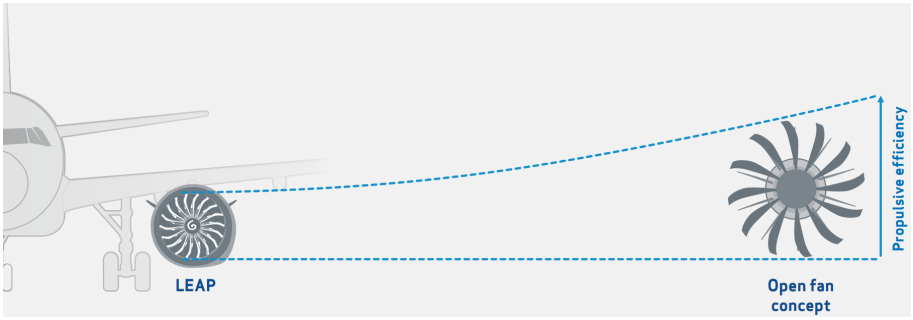

Figure 1.2: *New open fan size compared with the current generation of LEAP engine [CFM International, 2022].*

increasing size of the engine and improving the mechanical design of fan blades, especially regarding fatigue and bird ingestion. Numerical methods and simulations play a crucial role in answering these questions to avoid performing expensive laboratory experiments.

The new fan blades are manufactured using 3D woven carbon composites with an RTM (Resin Transfer Molding) process. Three scales may be used to describe such a material (see figure 1.3). The smallest scale occurs at the packing level of the individual fibril on the order of fiber diameters ($\sim \mu m$), and the biggest scale is the specimen macroscale ($\sim m$). The intermediate length scale, between the micro and macroscale, is the mesoscale ($\sim mm$) characteristic of the yarn architecture. It is possible to adapt the mesostructure of 3D woven composite components throughout the manufacturing process according to targeted local aerodynamics and mechanical requirements. To this end, there is a need to investigate what could occur in the mesoscale (or microscale) but if all mesoscopic (or microscopic) heterogeneities are taken into account, we will be facing intractable computational problems due to the extremely fine spatial discretization mesh (around 500 million degree of freedom for a full 3D woven fan blade simulation).

The homogenization methods have been developed to tackle this by modeling the heterogeneous material as a simpler homogeneous material based on the mechanics of the underlying heterogeneities.

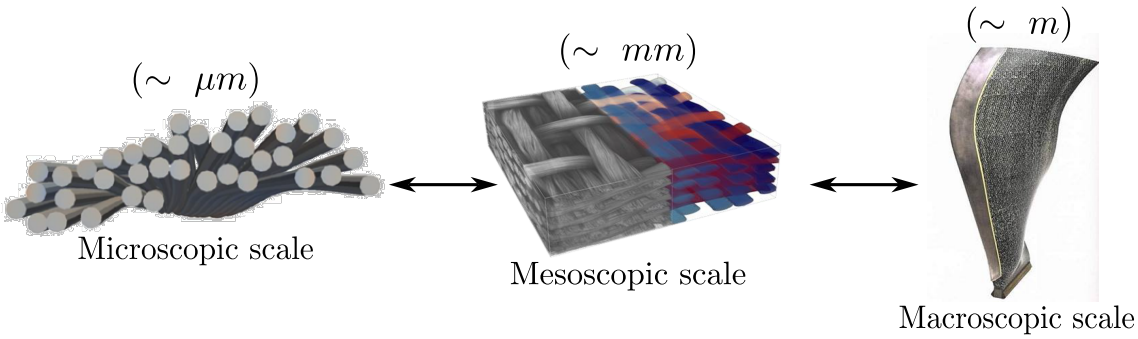

Figure 1.3: *Scale zoom on engine fan blade [CFM International, 2022].*

1.1 Homogenization methods

Numerous homogenization methods exist in the literature. They can be divided into two main categories: Closed-form (often analytical) homogenization methods and computational homogenization methods.

The simplest analytical methods are based on the assumption that either strains or stresses are uniform within the unit-cell, leading to the well known Voigt [1889] and Reuß [1929] bounds. Hill [1952] has proved rigorously that the Voigt and the Reuss approximations are the upper and lower bounds of the true homogeneous stiffness. Nevertheless, the width of these bounds grows with the heterogeneities' volume fraction and the contrast in their properties. A more sophisticated method is the mean field homogenization method that uses formulations based on Eshelby's solution [Eshelby, 1957] for a composite made of particles dispersed in a matrix. It is assumed that there is no particle interaction so that the problem can be considered as a single inclusion immersed in an infinite matrix domain with uniform outer loading. Eshelby [1957] has proven that the strain state inside the ellipsoidal inclusion is uniform and depends only upon each individual phase property and the inclusions aspect ratio. The strong assumption of non-interacting particles may provide inaccurate results, leading to the development of other methods incorporating particle interaction such as the Mori–Tanaka method [Mori and Tanaka, 1973; Benveniste, 1987], the Self Consistent method [Hill, 1965], and the Generalized Self Consistent method [Christensen, 1990]. Mean field methods exhibit difficulties to take into account the clustering effect and lose their accuracy for material with high contrast [Hashin, 1983]. It is possible to determine better (narrower) bounds compared to the Voigt and the Reuss bounds by using the principle of minimum potential energy and the concept of polarization [Hashin and Shtrikman, 1963] leading to several variational bounding methods [Willis, 1981; Hashin, 1983; Castaneda and Suquet, 1997].

Asymptotic homogenization [Sanchez-Palencia, 1983; Bensoussan et al., 2011], also known as periodic or mathematical homogenization, is one of the most rigorous closed-form homogenization methodologies available in the literature. It is based on the assumption of the microstructure's spatial periodicity, where the unit-cell specifies the Repre-

sentative Volume Element (RVE) without any ambiguity. This method consists in using asymptotic expansions of the mechanical fields of the full-scale problem in order to split it into a decoupled set of microscale unit-cell problems and a macroscale problem. Solving the former allows one to compute the effective properties of the equivalent homogeneous medium but also to estimate, by a relocalization process, local heterogeneous fields within the material. Nevertheless, this estimation remains inaccurate in the vicinity of the boundaries due to the loss of periodicity assumption in these regions.

Computational homogenization methods [Moulinec and Suquet, 1998; Feyel and Chaboche, 2000; Kouznetsova et al., 2001, 2002; Miehe and Koch, 2002; Kanit et al., 2003] do not lead to closed-form overall constitutive equations but consider the solution of a microscale boundary value problem at every macroscopic point to deduce the macroscopic homogenized constitutive response. Although these methods are computationally expensive, they are well adapted for nonlinear analyses. In this thesis, I will mainly treat linear elastic materials.

We use asymptotic homogenization in a finite element framework for multiscale linear elastic analyses. Also, only periodic heterogeneous structures are taken into account. The periodicity assumption of the underlying mesostructure is hardly verified in realistic engineering composite structures as the fan blades which display irregular domains and locally nonperiodic zones. Nevertheless, the periodicity assumption can fairly be considered for a specimen or coupon of the global structure. For instance in [Gras et al., 2013] an identification of the macroscopic elastic parameters of a 3D woven composite used in the fan blades is performed by confronting periodic homogenization numerical results with experimental full-field measurements. When the periodicity assumption is considered, asymptotic homogenization remains the most accurate method to determine the macroscopic overall characteristics (homogenization) and also to estimate heterogeneity effects on the macroscopic behavior (relocalization), without computing the response of the *full* mesostructure in the global analysis.

1.2 Limitation: scale separation

Asymptotic homogenization introduces a scale factor $\varepsilon = l/L$, where l and L are the characteristic lengths of the mesostructure and macrostructure, respectively. First-order asymptotic homogenization, which considers only the first term in the asymptotic expansion, assumes a complete separation of scales in materials, *i.e.* $\varepsilon \ll 1$, and remains effective in capturing uniform macroscopic strain fields without large gradients.
Nevertheless, the fan blade contains critical regions of high gradients as discussed by Gras et al. [2015] and illustrated in figure 1.4. As also argued by Boisse et al. [2018], the scale-independent Cauchy-type continuum obtained by first-order homogenization is unable to correctly describe the mechanical behavior of woven composites because of its inability to describe the slipping between the fibers and their resulting bending stiffness. Consequently, a first-order homogenization is not adapted for some real engineering cases. Indeed, for weak scale separation scenarios, *i.e.* $\varepsilon < 1$, first-order asymptotic homoge-

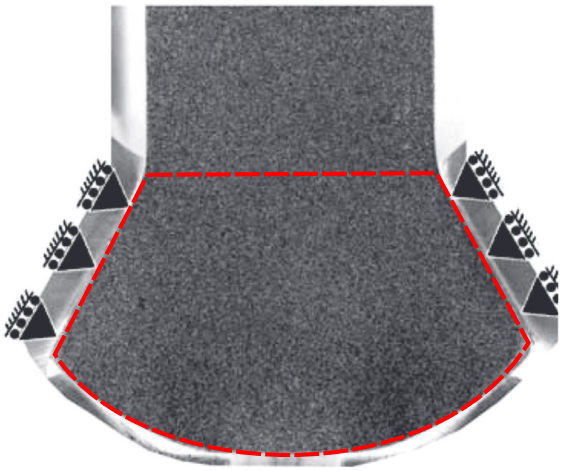

Figure 1.4: *Schematic view of a fan blade root made of 3D woven composite [Gras et al., 2015]. The region highlighted in red is expected to exhibit high gradients of the solution fields, where first-order homogenization becomes inaccurate.*

nization becomes inaccurate [Ameen et al., 2018]. Solution fields, however, can be approximated by keeping higher-order terms in the series expansion. Indeed, successive gradients of macroscale strain and tensors characteristic of the mesostructure are introduced, which results in inducing a non-local effect in the material behavior [Boutin et al., 2010].

While asymptotic homogenization may estimate local heterogeneous fields, even in cases of a weak separation of scales, by a higher-order relocalization process, the construction of a solution in the vicinity of the boundaries remains beyond the capabilities of this method. This is mainly explained by the loss of periodicity assumption in these regions. One approach to tackle the non-periodicity in the boundary layers is to introduce, for each relocalization process, evanescent corrective terms that would decay toward the interior of the material [Dumontet, 1986].

There is still a lack in literature regarding numerical frameworks to perform higher-order asymptotic homogenization/relocalization in order to deal with low scale separation cases as encountered for 3D woven composites, especially around stress concentrations. Also, there is still a need for a general higher-order correction strategy to account for non-periodicity in the boundary layers.

1.3 Modeling error

As stated by Fish et al. [1994b]; Zohdi et al. [1996], while conducting a finite element simulation, two sources of error generally occur: *discretization* and *modeling* error. The first one is due to the inherent inaccuracies incurred in the discretization of mathematical models of the events, and the second one is due to the natural imperfections in models of

the actual physical phenomena, as expressed by Oden and Prudhomme [2002].

The discretization error estimation techniques can be distinguished with respect to three main categories:

- Averaging-based error estimators [Zienkiewicz and Zhu, 1987, 1992a,c] make use of the fact that the gradient of the discretized solution is discontinuous across the inter-element boundaries. Hence, a comparison between the computed field and a smoothed one is conducted to estimate the error.

- Residual-based error estimators [Babuška and Rheinboldt, 1978; Bank and Weiser, 1985; Ainsworth et al., 2007] make use of the fact that the approximate FE solution does not satisfy equilibrium. Therefore, a residual is estimated either directly from the equilibrium equation (*explicit* estimation) or by solving local problems where the load function is given by the local residuals (*implicit* estimation).

- Constitutive relation-based estimators [Ladevèze and Leguillon, 1983; Ladevèze et al., 1999] are built upon the computation of admissible fields which satisfy both compatibility and equilibrium equations. Thereafter, the residual on the constitutive equation between the two fields is evaluated.

The modeling error, has raised the interest of researchers since the mid-1990s, *i.e.*, several years after the discretization error, with a less extensive bibliography. It quantifies the error emanating from replacing an actual exact model with a simplified one in order to improve computational efficiency.
In the context of our study, the exact model is the heterogeneous one and the simplified model is the one obtained by homogenization methods, as in Fish et al. [1994b]; Zohdi et al. [1996]. In these works, error estimation techniques have been used to steer adaptive processes, as shown in figure 1.5.

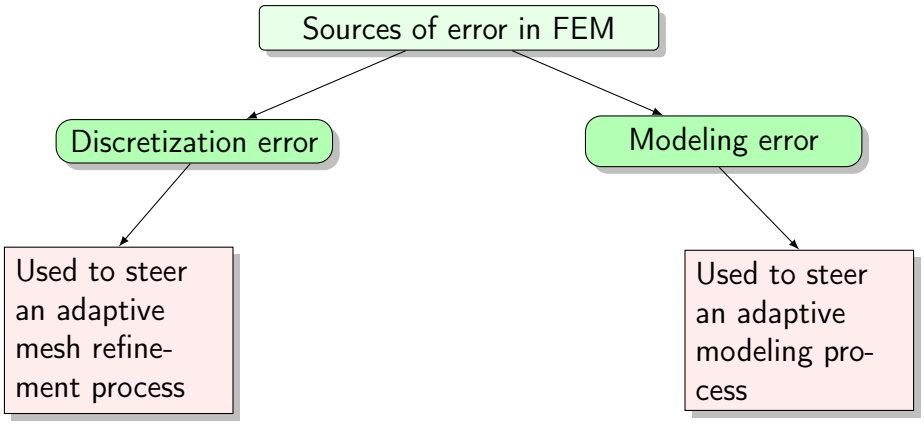

Figure 1.5: *Errors in FEM used to steer adaptive processes.*

1.4 Hierarchical modeling

The main focus is not to estimate the exact modeling error value but to use the relative magnitude of this error to detect areas where refining the material model is necessary, this process is referred as *hierarchical modeling*. It couples, adaptively, a fine material description in some regions of the domain and a coarse, less accurate macroscopic model in regions of homogeneous deformation. This is analogous to the *mesh refinement* in the FEM controlled by the discretization error, except that, here, the refinement is in terms of the material model, as shown in figure 1.6.

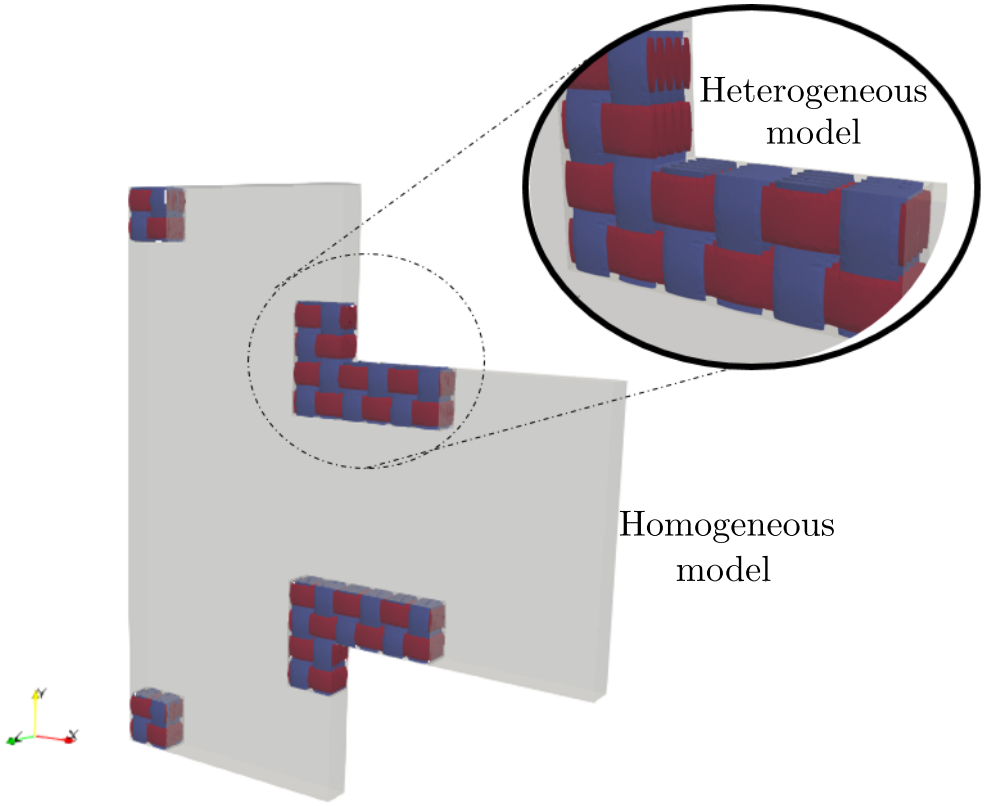

Figure 1.6: *Illustration of adaptive modeling strategy for a T-shape structure. Two regions are differentiated: regions requiring macroscopic analysis using homogenized material properties e.g., regions of relatively benign deformation, and regions that require an explicit representation of the local mesostructure.*

Hierarchical modeling raises the challenge of adequately coupling the homogeneous and heterogeneous models which are different with dissimilar discretization. Several coupling techniques have been proposed in the literature such as the volume coupling of the Arlequin method [Ben Dhia, 1998], and surface coupling techniques such as the mortar coupling [Bernardi et al., 1993; Belgacem, 1999] or the Nitsche coupling [Hansbo and Hansbo, 2002]. Another coupling strategy is the submodeling technique [Schwartz, 1981;

Kelley, 1982], which consists in performing a global homogeneous analysis whose solution is used as input for a local analysis on a chosen heterogeneous model. This technique is a *descending* process in the sense that there is no feedback from the heterogeneous computation toward the homogeneous one. A such feedback has been proposed in Gendre et al. [2009]. We are particularly interested in the submodeling technique since it is largely used in the industry and is supported by most commercial finite element software programs.
These techniques have not been originally developed to deal with incompatible homogeneous and heterogeneous models, which may result in high interface coupling errors. For example, it can be necessary, in the submodeling technique, to enlarge the chosen local heterogeneous model to avoid spurious coupling errors in a region of interest, which can be computationally expensive. Recently, a second-order homogenization-based coupling has been proposed by Wangermez et al. [2020] and demonstrated to provide better results than a mortar coupling.

1.5 Objectives & Methodology

The ultimate goal of this research is the development of modeling error estimation, in a finite element framework, to steer hierarchical modeling of periodic heterogeneous structures. By doing so, we aim to couple a heterogeneous material description in regions with a low scale separation, *i.e*, critical areas of high gradients, and a homogeneous, less accurate macroscopic model in regions of benign deformation. Therefore, in a comparison with a full heterogeneous computation, this process could reduce the computational cost considerably. Also, this thesis attempts to propose a robust/efficient technique in order to adequately couple the homogeneous and heterogeneous domains.

To this end, we use asymptotic homogenization to derive a modeling error estimator quantifying the terms neglected by classical first-order homogenization, which become significant for weak separation of scales. The proposed estimation quantifies the modeling error that occurs at the boundaries as well. Also, a multiscale enhancement of the classical submodeling is suggested based on estimates derived from a higher-order relocalization process.

Regarding the aforementioned aspects, this thesis serves to investigate the following research topics:

- Scale separation limits of classical and higher-order asymptotic homogenization/relocalization.
- Boundary layer correction to account for the non-periodicity in regions near the boundaries.
- Modeling error estimation and its competition with discretization error.
- Hierarchical modeling and coupling of incompatible models.

1.6 Thesis outline

The thesis contains 3 additional self-contained chapters than can be read separately. They are organized as follows:

In chapter 2, a post-processing scheme is proposed to conduct the relocalization step. A new general boundary layer correction method, effective for various boundary conditions (Dirichlet, Neumann, or mixed), is presented. The scale separation limit of the classical first-order relocalization is highlighted as well.

The effectiveness of higher-order relocalization for cases with low scale separation is demonstrated in chapter 3, in order to estimate correctly the heterogeneous fields within the material. An extension of the previously suggested boundary layer correction is proposed for these higher-order estimates. In chapter 2 and 3, the relocalization process is conducted while considering that the heterogeneous and homogeneous meshes are identical.

An extension of the post-processing relocalization scheme to deal with arbitrary homogeneous meshes is proposed in chapter 4. A modeling error estimation is derived, and its competition with the discretization error is also investigated. A multiscale enhancement of the classical displacement-based submodeling technique is proposed as well.

Chapter 2

First-order asymptotic homogenization with boundary layer correction

Abstract

The asymptotic homogenization method is often used in multiscale analysis of periodic structures instead of conducting a full field heterogeneous analysis, to achieve computational feasibility and efficiency. When completed with a relocalization process, this method may provide relevant estimates of microscale fields within the material. Nevertheless, the construction of a solution near the boundaries remains beyond the capabilities of classical relocalization schemes due to the loss of periodicity in the vicinity of the boundaries, unless a boundary layer correction is applied. This chapter proposes a post-processing scheme to conduct the relocalization step within a finite element framework for periodic linear elastic composite materials. It also assesses the boundary layer effect and a new general method, effective for various boundary conditions (Dirichlet, Neumann, or mixed), is proposed based on the idea of computing corrective terms as a solution to auxiliary problems on the unit-cell. These terms are finally added to the usual fields obtained from the relocalization process to obtain the corrected solution near the boundaries. The efficiency, accuracy, and limitation of the proposed approach are studied on various numerical examples.

Résumé

La méthode d'homogénéisation asymptotique est largement utilisée dans l'analyse multi-échelle des structures périodiques comme une alternative à une analyse hétérogène qui représente un coût conséquent en temps de calcul. Lorsqu'elle est complétée par un processus de relocalisation, cette méthode peut fournir des estimations pertinentes des champs hétérogènes au sein du matériau. Néanmoins, la construction d'une solution près des frontières reste au-delà des capacités des schémas de relocalisation classiques en raison de la perte de périodicité au voisinage des frontières, à moins qu'une méthode de correction des bords est appliquée. Dans ce chapitre, je propose une méthode de correction des effets de bords en homogénéisation asymptotique valable pour différents types de conditions aux limites (Dirichlet, Neumann et mixte). Des correcteurs de couche limite sont rajoutés dans les développements asymptotiques au premier ordre et au niveau du voisinage des bords. L'ajout de ces termes permet de satisfaire de façon exacte les con-

ditions aux limites sur les bords. Des exemples numériques sur structures en composite sont présentés pour démontrer l'efficacité de la méthode ainsi que ses limites.

Contents

Reproduced from:
Mouad Fergoug, Augustin Parret-Fréaud, Nicolas Feld, Basile Marchand and Samuel Forest.
A general boundary layer corrector for the asymptotic homogenization of elastic linear composite structures.
Composite Structures, 2022, 285:115091.
doi: 10.1016/j.compstruct.2021.115091

2.1 Introduction

Composite materials' microstructure can be varied, ranging from randomly distributed phases to a perfectly periodic microstructure. Direct Numerical Simulations (DNS, *i.e.* when the geometry of the microstructure is explicitly described in simulations) of composite materials are often difficult to perform because of the resulting complexity and size of the computational problems. Therefore, to fully realize the benefits offered by these materials, it is essential to develop reliable computational methods, bypassing DNS, to predict their behavior.
Homogenization of periodic structures has been successfully used to determine their effective properties at the macroscale from the knowledge of local mechanical properties of one unit-cell, representative of the material microstructure. The obtained effective properties can then be used for numerical simulations of the homogeneous problem without conducting DNS. The unit-cell problem can be solved either analytically or numerically.
The simplest analytical methods are based on the assumption that either strains or stresses are uniform within the unit-cell, leading to the well known Voigt [Voigt, 1889] and Reuss [Reuß, 1929] bounds. More accurate analytical methods were developed, among which the composite sphere model and the self-consistent scheme [Hashin and Shtrikman, 1963; Hill, 1965; Mori and Tanaka, 1973]. Numerical homogenization using computational methods like the Finite Element Method (FEM) has also been used for solving the unit-cell problem [Ghosh et al., 1995; Feyel and Chaboche, 2000; Terada and Kikuchi, 2001], among many others.
Most of these methods are known to be effective for materials with large scale separation between the scale of heterogeneity and the macroscale dimension. For low scale separation, however, they generally become inaccurate. In such a case, the wavelength of variation of the macroscale fields is not sufficiently large compared to the size of the heterogeneities. Thus, the predicted effective properties may fail to describe the local or global response of the composite [Ameen et al., 2018]. To tackle this, higher-order gradients of macroscale strain may be taken into account in the homogenization of the unit-cell. At least two approaches exist regarding this subject:

- The first approach uses Quadratic Boundary Conditions (QBCs) applied to the unit-cell [Kouznetsova et al., 2004; Yuan et al., 2008; Forest and Trinh, 2011], deduced from the macroscale higher-order strain-stress fields. This method has a major flaw as shown in Forest and Trinh [2011]. Indeed, the effective strain-gradient properties remain non zero when the material is homogeneous, which seems to be a physically unreasonable result. To tackle this, a correction has been proposed in Yvonnet et al. [2020] by adding adequate body forces to QBCs.

- The second approach considers higher-order problems in the asymptotic expansion at the basis of the homogenization method, introduced in Sanchez-Palencia [1983]; Bensoussan et al. [2011]. This method consists in using asymptotic expansions of mechanical fields of the microscale problem in order to split them into separate microscale and macroscale problems. It is shown in Boutin [1996] that the higher-order terms in asymptotic homogenization introduce successive gradients of macroscale strain and tensors, characteristic of the microstructure, which results in introducing a non-local effect in the material behavior.

These methods allow the prediction of both the local, by a relocalization process, and the overall averaged properties of the structure. A recent comparison between the asymptotic homogenization and QBCs-based method [Monchiet et al., 2020] shows that a modification of the QBCs-based method, by adding body forces, is necessary to be consistent with the asymptotic homogenization.
Asymptotic homogenization has been applied in a wide range of engineering problems, *e.g.* to optimize structures [Sigmund, 1995; Suzuki and Kikuchi, 1991; Hassani and Hinton, 1998], compute the effective elastic behavior of woven fabric composites [Chung and Tamma, 1999] and evaluate localized stiffness degradation [Visrolia and Meo, 2013]. Different numerical methods have been applied in conjunction with the asymptotic homogenization theory. The Fast Fourier Transform [Moulinec and Suquet, 1994; Michel et al., 2000] (FFT) method was used to apply the homogenization theory on microstructures defined on regular grids [Tran et al., 2012]. FEM has also been successfully applied for the analysis of linear and non-linear microstructures with arbitrary discretization, albeit at a higher computing cost. Different implementation strategies [Chung et al., 2001; Cheng et al., 2013; Oliveira et al., 2009; Dutra et al., 2020] were proposed for the homogenization of composites using the FEM. However, the validity of the relocalization process is usually not verified, except asymptotically in an idealized setting. The analysis of local gradients and boundary effects requires additional effort.
The response of a composite structure near its geometric boundaries has been studied both experimentally and analytically [Pipes et al., 1973; Tang and Levy, 1975; Hsu and Herakovich, 1977; Pagano, 1978]. It has been shown that complex stress states with a rapid change of gradients occur within a very local region near the boundaries, frequently referred to as a *boundary layer effect*. Ultimately, the high stresses developed in these regions may be responsible for the failure initiation of the structure [Pipes et al., 1973].
While asymptotic homogenization allows estimating local fields within the structure by a relocalization method, the construction of a solution near the vicinity of the boundaries remains beyond the capabilities of the classical homogenization [Sanchez-Palencia, 1986] for two reasons:

- First, in asymptotic homogenization, the solution is considered to be periodic. However the loads are no longer periodic in the vicinity of boundaries, and consequently, the solution is not periodic either.
- Second, the boundary condition on the composite domain cannot be satisfied by a periodic unit-cell solution.

One approach to tackle the non-periodicity in the boundary layers is to introduce evanescent corrective terms that would exponentially decay toward the interior of the body [Dumontet, 1986; Lefik and Schrefler, 1996]. These corrective terms are obtained by solving auxiliary problems on the unit-cell. An application of this approach is found in Abdelmoula and Leger [2005], in which heterogeneous stress fields are estimated by considering a Neumann boundary condition correction as in Dumontet [1986]. More recently, a numerical study was conducted to investigate the decay of the boundary layer in a three dimensional periodic homogenization for different fiber orientations using a domain with fixed edges (Dirichlet boundary) [Koley et al., 2019]. It is worth remarking that these papers have not proposed a boundary layer correction strategy for various types of boundary conditions.

Regarding the aforementioned aspects, the present work proposes a general boundary layer correction methodology for asymptotic homogenization to approximate real microscale fields near the boundaries. The main idea is to compute corrective terms obtained from the resolution of different problems over the unit-cell. The nature of the problems to be solved depends on the actual boundary conditions applied locally to the structure. Then, the corrective terms are added to the estimated local fields. The obtained results demonstrate the significance of boundary layer corrections even in the general case. Indeed, the proposed method is valid for different Boundary Conditions (BCs): Dirichlet, Neumann, or mixed. The authors are unaware of a similar general boundary layer correction strategy for asymptotic homogenization in the literature.
The outline of this chapter is as follows. In Sec. 2.2, we first recall briefly the asymptotic expansion homogenization method and describe the proposed relocalization process. In Sec. 2.3, we detail the proposed general boundary layer correction procedure. Numerical examples are presented and discussed in Sec. 2.4, to demonstrate the efficiency and limitations of the suggested approach.

2.2 Estimation of microscale fields based on asymptotic homogenization

This section briefly recalls the asymptotic homogenization approach in linear elasticity. The reader is referred to seminal works in Sanchez-Palencia [1983]; Bensoussan et al. [2011] and other recent references [Boutin, 1996; Chung et al., 2001; Hassani and Hinton, 1999] for further details. We also describe the proposed estimation of microscale fields based on the relocalization process, derived from asymptotic homogenization. This relocalization stage is associated with a given macroscale equilibrium state detailed in this section.

2.2.1 Statement of the boundary value problem and homogenization procedure

An inhomogeneous body is considered as a linearly elastic solid in static equilibrium, whose heterogeneity arises from the distribution of separate phases at the microscale. We define the bounded domain Ω^ε occupied by this heterogeneous body and corresponding to the microscale (see Fig. 2.1) and subjected to a body force $\boldsymbol{f}$ per unit volume. The boundary $\partial\Omega^\varepsilon$ consists of a portion Γ_u, on which the displacements are prescribed to the value $\boldsymbol{u}^d$, and a portion Γ_t on which surface tractions $\boldsymbol{F}^d$ per unit area are prescribed such that $\partial\Omega^\varepsilon = \Gamma_u \cup \Gamma_t$, and $\Gamma_u \cap \Gamma_t = \emptyset$.
Due to its heterogeneity, the mechanical behavior of the body is assumed to depend on two scales:

- Macroscale, free of heterogeneities, having L as a characteristic length and global coordinates $\boldsymbol{x} \in \Omega$ with the assumption that $\partial\Omega^\varepsilon = \partial\Omega$ (see Fig. 2.1).
- Microscale, having l as a characteristic length and with local coordinates $\boldsymbol{y} \in Y$, where Y is the unit-cell domain, typically chosen to be an open rectangular parallelepiped $Y =]0, Y_1[\times]0, Y_2[\times]0, Y_3[$ (see Fig. 2.1).

The coarse and fine scales are related by the parameter ε such that:

$$\varepsilon = \frac{l}{L}, \qquad \boldsymbol{y} = \frac{\boldsymbol{x}}{\varepsilon}. \tag{2.1}$$

The domain Ω^ε can be considered as the product space $\Omega \times Y$:

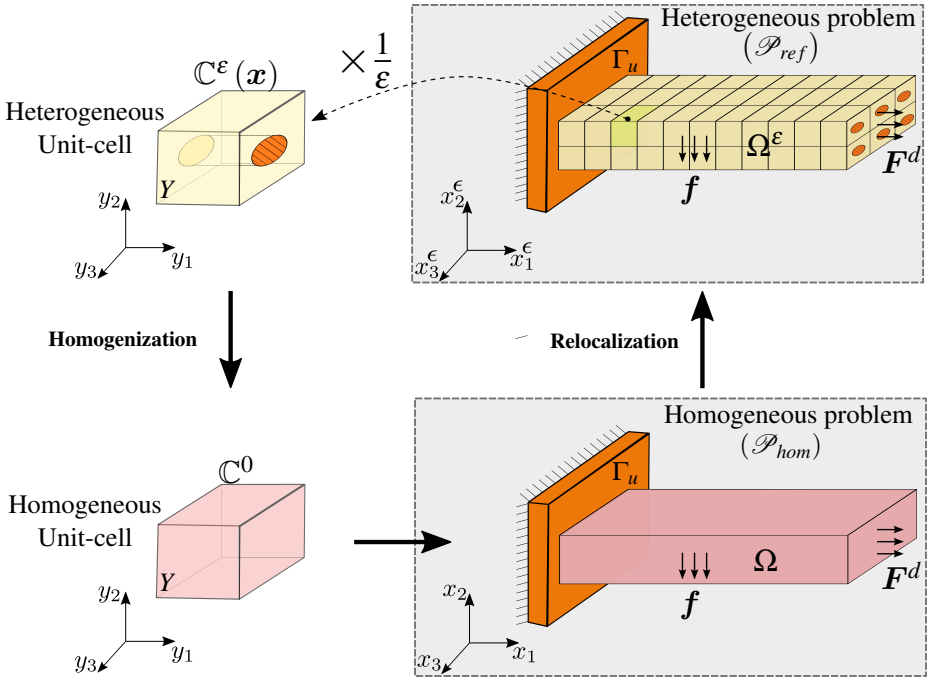

Figure 2.1: *Illustration of the heterogeneous problem* $(\mathscr{P}_{ref})$ *with domain* Ω^ε*, constructed by translating the unit-cell* Y *characterized by an oscillatory behavior* $\mathbb{C}^\varepsilon(\boldsymbol{x})$ *over the three-space directions. The homogenized problem* $(\mathscr{P}_{hom})$ *with homogeneous domain* Ω *is characterized by the homogenized elasticity tensor* $\mathbb{C}^0$ *obtained from the homogenization step. Microscale fields are estimated from a relocalization process.*

$$\Omega^\varepsilon = \left\{ \boldsymbol{x} \in \Omega \middle| \left(\boldsymbol{y} = \frac{\boldsymbol{x}}{\varepsilon} \right) \in Y \right\}. \tag{2.2}$$

We further consider that, at each material point of Ω^ε, there exists a periodically repeating microstructure. Owing to this periodicity, one can define the elasticity tensor $\mathbb{C}$ as $Y-$periodic:

$$\mathbb{C} = \mathbb{C}(\boldsymbol{y}). \tag{2.3}$$

Expressed in global coordinates, the heterogeneous stiffness tensor would read $\mathbb{C}^\varepsilon(\boldsymbol{x}) = \mathbb{C}(\boldsymbol{x}/\varepsilon) = \mathbb{C}(\boldsymbol{y})$, the superscript indicating fine-scale dependence. Similarly, the microscale displacement, strain and stress fields in global coordinates read $\boldsymbol{u}^\varepsilon$, $\boldsymbol{\varepsilon}^\varepsilon$, and $\boldsymbol{\sigma}^\varepsilon$, respectively.
In the ensuing sections, we will define the following boundary value problems:

- The heterogeneous problem $(\mathscr{P}_{ref})$ corresponding to microscale and generated by translating the unit-cell Y characterized by an oscillatory behavior $\mathbb{C}^\varepsilon(\boldsymbol{x})$ over the three-space directions.

- The first-order periodic problem $\left(\mathscr{P}^{1^{st}}_{order}\right)$ used to deduce the homogenized elasticity tensor $\mathbb{C}^0$ and localization tensors.
- The homogenized problem $(\mathscr{P}_{hom})$ corresponding to the macroscale characterized by the homogenized elasticity tensor $\mathbb{C}^0$.

The proposed first-order estimate of microscale fields will also be defined.

Definition of the heterogeneous problem $\left(\mathscr{P}_{ref}\right)$

The boundary value problem of the heterogeneous linear elastic body Ω^ε reads:

Find $(\boldsymbol{u}^\varepsilon, \boldsymbol{\sigma}^\varepsilon)$ such that:

$$\begin{cases} \operatorname{div}\left(\boldsymbol{\sigma}^\varepsilon(\boldsymbol{x})\right) + \boldsymbol{f}(\boldsymbol{x}) = 0, & \forall \boldsymbol{x} \in \Omega^\varepsilon, \quad (2.4a) \\ \boldsymbol{\sigma}^\varepsilon(\boldsymbol{x}) = \mathbb{C}^\varepsilon(\boldsymbol{x}) : \boldsymbol{\varepsilon}^\varepsilon(\boldsymbol{x}), & \forall \boldsymbol{x} \in \Omega^\varepsilon, \quad (2.4b) \\ \boldsymbol{u}^\varepsilon(\boldsymbol{x}) = \boldsymbol{u}^d, & \forall \boldsymbol{x} \in \Gamma_u, \quad (2.4c) \\ \boldsymbol{\sigma}^\varepsilon(\boldsymbol{x}) \cdot \boldsymbol{n} = \boldsymbol{F}^d, & \forall \boldsymbol{x} \in \Gamma_t, \quad (2.4d) \end{cases}$$

where Eq. (2.4a) is the balance equation, Eq. (2.4b) is the constitutive equation and Eq. (2.4c), Eq. (2.4d) are the applied boundary conditions, with $\boldsymbol{n}$ the outward unit normal vector to Γ_t. The traction and displacement fields are assumed to be continuous across the interfaces. The strain field $\boldsymbol{\varepsilon}^\varepsilon$ is given by:

$$\boldsymbol{\varepsilon}^\varepsilon = \operatorname{sym}\left(\nabla \boldsymbol{u}^\varepsilon\right) = \frac{1}{2}\left(\nabla \boldsymbol{u}^\varepsilon + \left(\nabla \boldsymbol{u}^\varepsilon\right)^\top\right), \quad (2.5)$$

where $\operatorname{sym}(\bullet)$ indicates the symmetric part of second-order tensors.
Thus, by considering Einstein's convention for tensor notation, the resolution of $\left(\mathscr{P}_{ref}\right)$ consists in determining the displacement field corresponding to the solution $\boldsymbol{u}^\varepsilon$ of the following variational problem:

$$\int_{\Omega^\varepsilon} C_{ijkl} \frac{\partial u_k^\varepsilon}{\partial x_l^\varepsilon} \frac{\partial v_i}{\partial x_j^\varepsilon} \, d\Omega^\varepsilon = \int_{\Omega^\varepsilon} f_i \, v_i \, d\Omega^\varepsilon + \int_{\Gamma_t} F_i^d \, v_i \, d\Gamma, \qquad \forall v_i \in \mathscr{V}^0_{\Omega^\varepsilon}, \quad (2.6)$$

where $\mathscr{V}^0_{\Omega^\varepsilon}$ are the sets of sufficiently regular functions, zero-valued in Γ_u.
Mechanical fields, solution of $\left(\mathscr{P}_{ref}\right)$, are approximated with an asymptotic expansion in powers of the small parameter ε as:

$$\boldsymbol{u}^\varepsilon(\boldsymbol{x}) = \boldsymbol{u}^0(\boldsymbol{x},\boldsymbol{y}) + \varepsilon \boldsymbol{u}^1(\boldsymbol{x},\boldsymbol{y}) + \mathscr{O}\left(\varepsilon^2\right), \quad (2.7)$$

$$\boldsymbol{\varepsilon}^\varepsilon(\boldsymbol{x}) = \boldsymbol{\varepsilon}^0(\boldsymbol{x},\boldsymbol{y}) + \varepsilon \boldsymbol{\varepsilon}^1(\boldsymbol{x},\boldsymbol{y}) + \mathscr{O}\left(\varepsilon^2\right), \quad (2.8)$$

$$\boldsymbol{\sigma}^\varepsilon(\boldsymbol{x}) = \boldsymbol{\sigma}^0(\boldsymbol{x},\boldsymbol{y}) + \varepsilon \boldsymbol{\sigma}^1(\boldsymbol{x},\boldsymbol{y}) + \mathscr{O}\left(\varepsilon^2\right). \quad (2.9)$$

The quantities $\boldsymbol{u}^n$, $\boldsymbol{\varepsilon}^n$ and $\boldsymbol{\sigma}^n$ are $Y-$periodic functions called correctors of order n of the displacement, strain and stress fields, respectively.

The existence of two scales means that a function $f^{\varepsilon}(\boldsymbol{x})$ is associated with the function $f(\boldsymbol{x},\boldsymbol{y})$, where the chain rule is applied:

$$f^{\varepsilon}(\boldsymbol{x}) = f(\boldsymbol{x},\boldsymbol{y}), \quad \frac{\mathrm{d}}{\mathrm{d}x} f^{\varepsilon} = \frac{\partial}{\partial x} f + \frac{1}{\varepsilon}\frac{\partial}{\partial y} f, \tag{2.10}$$

The expansion of strains is obtained by substituting the expansion of displacements (2.7) into the strain definition (2.5), and making use of the chain rule (2.10). The expansion of stresses is obtained by substituting the resulting strains into the constitutive equation (2.4b). The stress expansion is substituted into the balance equation (2.4a) and, by collecting the terms of like powers of ε, we obtain a sequence of equilibrium equations of different orders with respect to powers of ε, defined on the unit-cell [Boutin, 1996]. We choose to ignore higher-order homogenization problems and restrict our study to the resolution of the first-order problem. It is shown that $\boldsymbol{u}^0(\boldsymbol{x},\boldsymbol{y}) = \boldsymbol{u}^0(\boldsymbol{x})$, meaning that the displacement $\boldsymbol{u}^0$ is independent of the microscale coordinates $\boldsymbol{y}$ and can be identified with the macroscale displacement field.

First-order periodic problem $\left(\mathscr{P}^{1^{st}}_{order}\right)$

This problem is defined on the unit-cell Y. Its solution is the first-order displacement corrector $\boldsymbol{u}^1$ and stress $\boldsymbol{\sigma}^0$. It reads:

Find $(\boldsymbol{u}^1, \boldsymbol{\sigma}^0)$ such that:

$$\begin{cases} \operatorname{div}_y\left(\boldsymbol{\sigma}^0(\boldsymbol{x},\boldsymbol{y})\right) = 0, & \forall \boldsymbol{y} \in Y, \quad (2.11a) \\ \boldsymbol{\sigma}^0(\boldsymbol{x},\boldsymbol{y}) = \mathbb{C}(\boldsymbol{y}) : \left(\boldsymbol{E}^0(\boldsymbol{x}) + \boldsymbol{\varepsilon}_y(\boldsymbol{u}^1)\right), & \forall \boldsymbol{y} \in Y, \quad (2.11b) \\ \boldsymbol{u}^1(\boldsymbol{x},\boldsymbol{y}), & \text{is } Y-\text{periodic}, \quad (2.11c) \\ \boldsymbol{\sigma}^0(\boldsymbol{x},\boldsymbol{y}) \cdot \boldsymbol{n}, & \text{is } Y-\text{antiperiodic}, \quad (2.11d) \end{cases}$$

where $\boldsymbol{E}^0(\boldsymbol{x}) = \boldsymbol{\varepsilon}_x(\boldsymbol{u}^0(\boldsymbol{x}))$ is a prescribed macroscale strain, $\operatorname{div}_y(\bullet)$ is the divergence operator with respect to local variable $\boldsymbol{y}$, and $\boldsymbol{\varepsilon}_x$, $\boldsymbol{\varepsilon}_y$ are the strain tensors calculated according to the global variable $\boldsymbol{x}$ and local variable $\boldsymbol{y}$, respectively:

$$\boldsymbol{\varepsilon}_{\bullet} = \operatorname{sym}\left(\nabla_{\bullet} \boldsymbol{u}^{\varepsilon}\right) = \frac{1}{2}\left(\nabla_{\bullet} \boldsymbol{u}^{\varepsilon} + \left(\nabla_{\bullet} \boldsymbol{u}^{\varepsilon}\right)^{\top}\right). \tag{2.12}$$

The periodic fluctuation solution of the first-order problem takes the following form:

$$\boldsymbol{u}^1(\boldsymbol{x},\boldsymbol{y}) = \mathbb{D}^0(\boldsymbol{y}) : \boldsymbol{E}^0(\boldsymbol{x}), \tag{2.13}$$

where $\mathbb{D}^0(\boldsymbol{y})$ is a third-order tensor, called the displacement localization tensor. It is periodic over unit-cell Y and verifies $\left\langle \mathbb{D}^0 \right\rangle_Y = 0$, where $\langle \bullet \rangle_Y = \frac{1}{|Y|}\int_Y \bullet \, dY$ indicates the volume average over unit-cell Y. Note that $\mathbb{D}^0$ is symmetric with respect to its two last indices.

The displacement localization tensor components are the solutions $D_{ijk} \in \mathscr{V}_Y^{\#}$ of the

variational problem:

$$\int_Y C_{ijkl}\,\frac{\partial D^0_{kmn}}{\partial y_l}\,\frac{\partial v_i}{\partial y_j}dY = \int_Y C_{ijmn}\,\frac{\partial v_i}{\partial y_j}\,dY, \qquad \forall v_i \in \mathscr{V}_Y^{\#}, \tag{2.14}$$

where $\mathscr{V}_Y^{\#}$ is the set of Y-periodic sufficiently regular functions with zero average value in Y.
The total first-order microscale strain field reads:

$$\boldsymbol{\varepsilon}^0(\boldsymbol{x},\boldsymbol{y}) = \boldsymbol{\varepsilon}_y(\boldsymbol{u}^1(\boldsymbol{x},\boldsymbol{y})) + \boldsymbol{E}^0(\boldsymbol{x}) = \mathbb{A}^0(\boldsymbol{y}) : \boldsymbol{E}^0(\boldsymbol{x}), \tag{2.15}$$

where $\mathbb{A}^0(\boldsymbol{y})$ is a fourth-order tensor, called the strain localization tensor:

$$\mathbb{A}^0(\boldsymbol{y}) = \mathbb{I} + \boldsymbol{\varepsilon}_y(\mathbb{D}^0(\boldsymbol{y})), \tag{2.16}$$

where $\mathbb{I}$ is the fourth-order identity tensor operating on symmetric second order tensors.
We therefore can define the first-order microscale stress field as:

$$\boldsymbol{\sigma}^0(\boldsymbol{x},\boldsymbol{y}) = \mathbb{C}(\boldsymbol{y}) : \boldsymbol{\varepsilon}^0(\boldsymbol{x},\boldsymbol{y}) = \mathbb{B}^0(\boldsymbol{y}) : \boldsymbol{E}^0(\boldsymbol{x}), \tag{2.17}$$

where

$$\mathbb{B}^0(\boldsymbol{y}) = \mathbb{C}(\boldsymbol{y}) : \mathbb{A}^0(\boldsymbol{y}), \tag{2.18}$$

is the stress localization tensor. Note that $\mathbb{A}^0$ and $\mathbb{B}^0$ possess minor symmetries.
The homogenized elasticity tensor $\mathbb{C}^0$ is deduced from the volume average of the stress localization tensor over the unit-cell:

$$\mathbb{C}^0 = \left\langle \mathbb{B}^0(\boldsymbol{y}) \right\rangle_Y. \tag{2.19}$$

It can be proved that $\mathbb{C}^0$ possesses the minor and major symmetries as required for an elasticity tensor.

Definition of the homogeneous problem $(\mathscr{P}_{hom})$

The boundary value problem on the macroscale for the homogeneous linear elastic body Ω reads:

Find $(\boldsymbol{U}, \boldsymbol{\Sigma})$ such that:

$$\begin{cases} \operatorname{div}_x(\boldsymbol{\Sigma}(\boldsymbol{x})) + \boldsymbol{f}(\boldsymbol{x}) = 0, & \forall \boldsymbol{x} \in \Omega, \quad (2.20a)\\ \boldsymbol{\Sigma}(\boldsymbol{x}) = \mathbb{C}^0 : \boldsymbol{E}(\boldsymbol{x}), & \forall \boldsymbol{x} \in \Omega, \quad (2.20b)\\ \boldsymbol{U}(\boldsymbol{x}) = \boldsymbol{u}^d, & \forall \boldsymbol{x} \in \boldsymbol{\Gamma}_u, \quad (2.20c)\\ \boldsymbol{\Sigma}(\boldsymbol{x}) \cdot \boldsymbol{n} = \boldsymbol{F}^d, & \forall \boldsymbol{x} \in \boldsymbol{\Gamma}_t, \quad (2.20d) \end{cases}$$

where $\operatorname{div}_x(\bullet)$ is the divergence operator with respect to global variable $\boldsymbol{x}$, the macroscale displacement is $\boldsymbol{U} = \boldsymbol{u}^0$ and the macroscale strain $\boldsymbol{E}$ and stress $\boldsymbol{\Sigma}$ are equal to the volume

average over the unit-cell of their microscopic counterparts $\boldsymbol{\varepsilon}^0$ and $\boldsymbol{\sigma}^0$, respectively.

$$\boldsymbol{E} = \left\langle \boldsymbol{\varepsilon}^0 \right\rangle_Y, \quad \boldsymbol{\Sigma} = \left\langle \boldsymbol{\sigma}^0 \right\rangle_Y. \tag{2.21}$$

The resolution of $(\mathscr{P}_{hom})$ consists in finding the displacement field corresponding to the solution $\boldsymbol{u}^0$ of the following variational problem:

$$\int_\Omega C^0_{ijkl} \frac{\partial u^0_k}{\partial x_l} \frac{\partial v_i}{\partial x_j} d\Omega = \int_\Omega f_i \, v_i \, d\Omega + \int_{\Gamma_t} F^d_i \, v_i \, d\Gamma \qquad \forall v_i \in \mathscr{V}^0_\Omega, \tag{2.22}$$

where $\mathscr{V}^0_\Omega$ is the set of sufficiently regular functions, zero-valued in Γ_u.
It is apparent from Eq. (2.20c) and (2.20d) that macroscale fields $(\boldsymbol{U}, \boldsymbol{\Sigma})$ verify given boundary conditions. However, as we will demonstrate later, the microscale fields estimated after the relocalization process, do not necessarily verify these boundary conditions. For instance, the estimated local stresses $\boldsymbol{\sigma}^0$ do not verify in general the Neumann boundary conditions:

$$\boldsymbol{\sigma}^0 \cdot \boldsymbol{n} \neq \boldsymbol{F}^d. \tag{2.23}$$

2.2.2 Proposed first-order estimate

The design and reliability analysis of composite structures taking into account the state of microscale fields can be more accurate than an entirely macroscale analysis. To tackle this, it is possible to bind the macroscale with the microscale based on a relocalization process derived from asymptotic homogenization.
As mentioned before, periodic homogenization is based on the assumption of scale separation between that of heterogeneities (with local coordinates $\boldsymbol{y}$) and the characteristic macroscale dimension (with global coordinates $\boldsymbol{x}$). This assumption induces a local invariance by translation and the periodicity of microscale fields. The scale separation assumption leads to:

$$\varepsilon \ll 1, \tag{2.24}$$

with ε defined in Eq. (2.1). In what follows, we propose to investigate situations where the scale separation assumption is *not* verified, meaning that the size of the heterogeneities can be comparable to the characteristic macroscale length scale, *e.g.* near the boundaries. Thus, the macroscale gradients could be such that it is no longer possible to assume a uniform mechanical field acting on the unit-cell. Therefore, we will consider:

$$\varepsilon = 1 \implies \boldsymbol{x} = \boldsymbol{y}. \tag{2.25}$$

This directly implies that the separation of scales assumption is *not* verified. Therefore, the mechanical fields of the reference problem depend only on $\boldsymbol{x}$, representing *both* microscale and macroscale coordinates.
For the purpose of this study, the reference problem is tractable by Direct Numerical Simulation (DNS) and its mechanical fields are used as reference results. However, in the more general case where a DNS would be out of reach, common practice would call for a best estimate. This estimate is built here using the solution of the homogeneous problem $(\mathscr{P}_{hom})$ and localization tensors $(\mathbb{D}^0, \mathbb{A}^0, \mathbb{B}^0)$ obtained after the resolution

of $\left(\mathscr{P}^{1^{st}}_{order}\right)$. The proposed estimate fields read:

$$\begin{cases} \boldsymbol{u}^{est}(\boldsymbol{x}) = \boldsymbol{U}(\boldsymbol{x}) + \mathbb{D}^0(\boldsymbol{x}) : \boldsymbol{E}(\boldsymbol{x}), & \forall \boldsymbol{x} \in \Omega, \quad (2.26a) \\ \boldsymbol{\varepsilon}^{est}(\boldsymbol{x}) = \mathbb{A}^0(\boldsymbol{x}) : \boldsymbol{E}(\boldsymbol{x}), & \forall \boldsymbol{x} \in \Omega, \quad (2.26b) \\ \boldsymbol{\sigma}^{est}(\boldsymbol{x}) = \mathbb{B}^0(\boldsymbol{x}) : \boldsymbol{E}(\boldsymbol{x}), & \forall \boldsymbol{x} \in \Omega. \quad (2.26c) \end{cases}$$

The displacement $\boldsymbol{U}(\boldsymbol{x})$ and the strain $\boldsymbol{E}(\boldsymbol{x})$ are obtained from the resolution of the homogeneous problem $(\mathscr{P}_{hom})$.

2.2.3 Proposed relocalization procedure

Once $\left(\mathscr{P}^{1^{st}}_{order}\right)$ is solved, the resulting homogenized elasticity tensor $\mathbb{C}^0$ is used to compute the homogeneous structure problem conducted at the macroscale, whose solution fields are $(\boldsymbol{U}, \boldsymbol{E}, \boldsymbol{\Sigma})$. To carry out the relocalization process, an intermediate step is performed to locate each unit-cell on the macroscale structure. To eliminate mesh-sensitivity and facilitate the computation of error estimates, we considered that the macroscale mesh was constructed by translating the unit-cell mesh over the three space directions, *i.e.* macroscale and microscale meshes are identical. If not, a mapping of the homogeneous fields on the microscale mesh could be considered as shown in Kruch [2007]. We considered the relocalization process improvement proposed in Kruch and Forest [1998], which is a simple way of taking into account macroscale gradients in relocalization formulation. For instance, the microscopic estimated strain (or stress), in a given point of the unit-cell, is determined using localization tensors combined with the value of the current macroscale strain *at this point*, and not its average over the unit-cell.

2.3 Boundary layer correction

Asymptotic homogenization may provide an estimate of the microscale fields within the material if the macroscale computation is complemented by a relocalization process. Nevertheless, the construction of a solution near the boundaries remains beyond the capabilities of classic homogenization/relocalization. This is mainly due to the loss of periodicity in the vicinity of boundaries.

We propose a new approach to account for non-periodicity in the boundary layers based on the idea of introducing corrective terms that would decay as one moves toward the interior of the body, which can be seen as an extension of Dumontet [1986]; Koley et al. [2019].

The main objective of this section is to describe the proposed *general* boundary layer correction procedure, effective for various types of *boundary conditions* (Dirichlet, Neumann, or mixed), see Fig. 2.3.

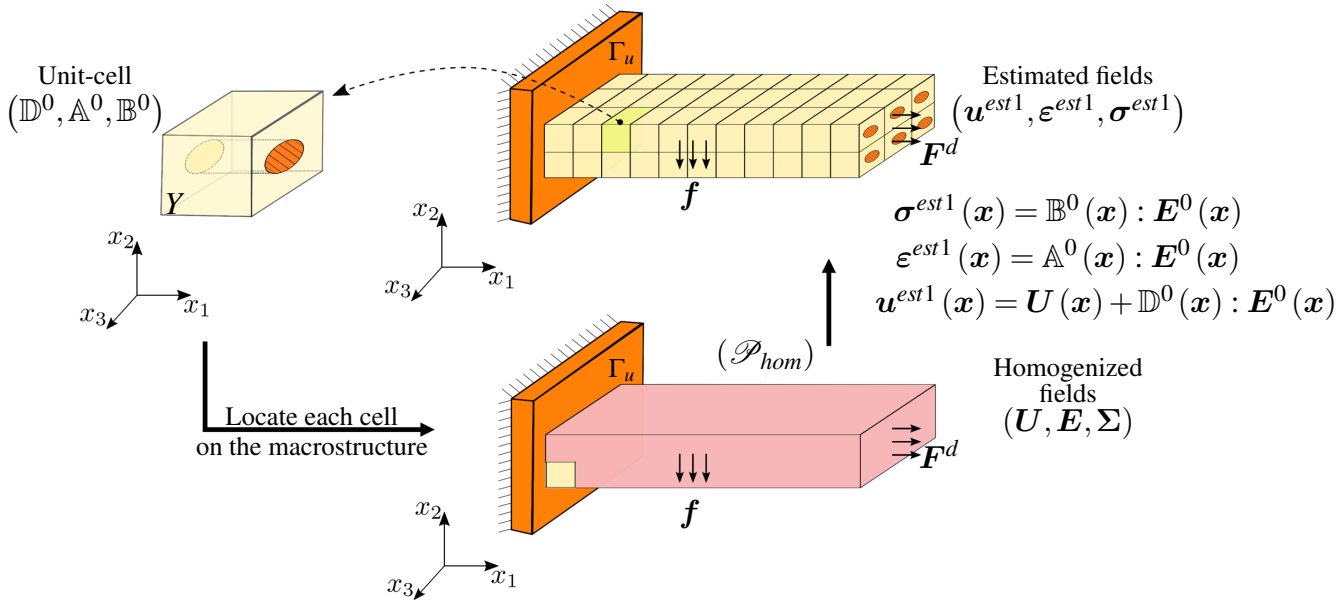

Figure 2.2: *Illustration of the proposed relocalization procedure scheme without scale separation. Mechanical fields depend only on $\boldsymbol{x}$, representing* both *microscale and macroscale coordinates.*

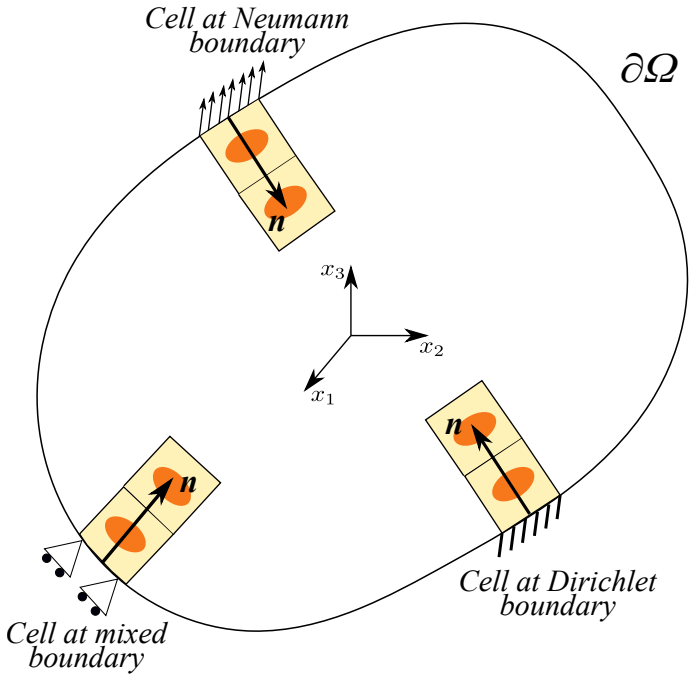

Figure 2.3: *Illustration of the boundary layers for Dirichlet, Neumann, and mixed boundary conditions. With $\boldsymbol{n}$ is the normal direction of the boundary.*

2.3.1 Correctors for Neumann BCs

The homogenized problem ($\mathscr{P}_{hom}$) could be written as:

$$\begin{cases} \operatorname{div}\left\langle \boldsymbol{\sigma}^{est}(\boldsymbol{x})\right\rangle_Y + \boldsymbol{f}(\boldsymbol{x}) = 0, & \forall \boldsymbol{x} \in \boldsymbol{\Omega}, \quad (2.27a) \\ \left\langle \boldsymbol{\sigma}^{est}(\boldsymbol{x})\right\rangle_Y = \mathbb{C}^0 : \boldsymbol{E}(\boldsymbol{x}), & \forall \boldsymbol{x} \in \boldsymbol{\Omega}, \quad (2.27b) \\ \left\langle \boldsymbol{u}^{est}(\boldsymbol{x})\right\rangle_Y = \boldsymbol{u}^d, & \forall \boldsymbol{x} \in \boldsymbol{\Gamma}_{\boldsymbol{u}}, \quad (2.27c) \\ \left\langle \boldsymbol{\sigma}^{est}(\boldsymbol{x})\right\rangle_Y \cdot \boldsymbol{n} = \boldsymbol{F}^d, & \forall \boldsymbol{x} \in \boldsymbol{\Gamma}_{\boldsymbol{t}}, \quad (2.27d) \end{cases}$$

with the macroscale stress: $\langle \boldsymbol{\sigma}^{est}\rangle_Y = \boldsymbol{\Sigma}$ and strain: $\langle \boldsymbol{\varepsilon}^{est}\rangle_Y = \boldsymbol{E}$.
It is apparent from problem (2.27d) that the boundary condition on $\boldsymbol{\Gamma}_{\boldsymbol{t}}$ is only satisfied by the mean value of $\boldsymbol{\sigma}^{est}$, therefore:

$$\boldsymbol{\sigma}^{est} \cdot \boldsymbol{n} \neq \boldsymbol{F}^d. \quad (2.28)$$

For this reason, added to the fact that the local stress field is generally not periodic in the vicinity of the Neumann boundaries, $\boldsymbol{\sigma}^{est}$ is inaccurate near the boundaries. To overcome this, it was proposed in Dumontet [1986] to correct the expansion of the displacement and the associated expansion of the stresses in the neighborhood of the boundary of a 2D problem. Boundary layers term $\boldsymbol{\sigma}^{bl}$ are introduced whose sum with local stresses satisfies exactly boundary conditions at each microscopic point.
We propose to compute $\boldsymbol{\sigma}^{bl}$ by considering six auxiliary problems on the unit-cell subjected to six characteristic loads F_{kl} with $kl = \{11,22,33,23,31,12\}$ on the surface where the Neumann boundary condition is applied. The opposite surface is fixed, and other surfaces of the unit-cell are subjected to periodicity conditions. The characteristic load is defined as follows:

$$F_{ikl} = -B^0_{ijkl} \cdot n_j + \frac{1}{|Y|}\int_Y B^0_{ijkl} \cdot n_j \, dY \quad \text{with fixed index } j, \quad (2.29)$$

where n_j is the normal direction of $\boldsymbol{\Gamma}_{\boldsymbol{t}}$ and the fixed index $j \in \{1,2,3\}$ is the index of this normal direction. B_{inkl} are the components of the stress localization tensor $\mathbb{B}^0$.
The resulting displacements, strains, and stresses solving each auxiliary problem are the components of the boundary-layer localization tensors $\mathbb{D}^{0,bl}$, $\mathbb{A}^{0,bl}$, and $\mathbb{B}^{0,bl}$, respectively. Thus, the boundary layer corrective terms are computed as follows:

$$\begin{cases} \boldsymbol{\sigma}^{bl} = \mathbb{B}^{0,bl} : \boldsymbol{E}, & (2.30) \\ \boldsymbol{\varepsilon}^{bl} = \mathbb{A}^{0,bl} : \boldsymbol{E}, & (2.31) \\ \boldsymbol{u}^{bl} = \mathbb{D}^{0,bl} : \boldsymbol{E}. & (2.32) \end{cases}$$

As a result, the stress field $\boldsymbol{\sigma}^{cor}$

$$\boldsymbol{\sigma}^{cor} = \boldsymbol{\sigma}^{est} + \boldsymbol{\sigma}^{bl}, \quad (2.33)$$

satisfies the Neumann BC.

2.3.2 Correctors for Dirichlet BCs

We recall that the proposed estimated displacement field is given by equation (2.26a):

$$\boldsymbol{u}^{est}(\boldsymbol{x}) = \boldsymbol{U}(\boldsymbol{x}) + \boldsymbol{u}^{1}(\boldsymbol{x}), \tag{2.34}$$

with $\boldsymbol{u}^{1} = \mathbb{D}^{0} : \boldsymbol{E}$ is the first-order corrector of the displacement field obtained from the resolution of $\left(\mathscr{P}^{1^{st}}_{order}\right)$. The displacement $\boldsymbol{u}^{est}$ estimates correctly the real displacement in the interior of the material where the structure is periodic. Nevertheless, we need to ensure that $\boldsymbol{u}^{est}$ verifies the Dirichlet boundary condition $\boldsymbol{u}^{est} = \boldsymbol{u}^{d}$ on $\boldsymbol{\Gamma}_{u}$. But since $\boldsymbol{U} = \boldsymbol{u}^{d}$ on $\boldsymbol{\Gamma}_{u}$ is enforced then $\boldsymbol{u}^{est}$ do not necessarily verify the Dirichlet boundary conditions. Therefore, a correction is needed that is the negative of $\boldsymbol{u}^{1}$ at the boundary and decays inward, and such that the corrected field would read:

$$\boldsymbol{u}^{cor}(\boldsymbol{x}) = \boldsymbol{U}(\boldsymbol{x}) + \left(\boldsymbol{u}^{1}(\boldsymbol{x}) + \boldsymbol{u}^{bl}(\boldsymbol{x})\right). \tag{2.35}$$

The correction $\boldsymbol{u}^{bl}$ must verify:

$$\boldsymbol{u}^{bl}(\boldsymbol{x}) = -\boldsymbol{u}^{1}(\boldsymbol{x}) \qquad \forall \boldsymbol{x} \in \boldsymbol{\Gamma}_{\boldsymbol{u}}. \tag{2.36}$$

As in the Neumann case, an auxiliary problem is considered on which the boundary layer fields will be computed. In this case, corrective displacements $\boldsymbol{\varrho}_{kl}$ with $kl = \{11,22,33,23,31,12\}$ are applied to the unit-cell and defined as:

$$\boldsymbol{\varrho}_{ikl} = -D^{0}_{ikl}, \tag{2.37}$$

where D_{ijk} are the components of the displacement localization tensor $\mathbb{D}^{0}$. The corrective boundary layer fields are obtained by conducting the same analyses defined in Eq. (2.30),(2.31), and (2.32).

2.3.3 Mixed BCs

The correction for boundary layers with mixed BCs is conducted by considering six auxiliary problems on the unit-cell subjected to both six characteristic loads F_{ikl} defined in Eq. (2.29) and displacements $\boldsymbol{\varrho}_{ikl}$ defined in Eq. (2.37), with $kl = \{11,22,33,23,31,12\}$. The correction to be ultimately applied for each i index depends on the actual (Neumann or Dirichlet) BC applied in this specific direction. For the purpose of illustration, we shall consider the following simple of a composite in tension (see Fig. 2.4):

2.3.4 Proposed general boundary correction scheme

The proposed boundary correction strategy is summarized in Fig. 2.6. For the sake of simplicity and clarity, an invariance along the thickness direction is considered. The structure in Fig. 2.6 is fixed on Γ_{u}, a surface traction is applied on Γ_{t} and other boundaries of Γ_{t} are kept free of forces. The estimated fields are correct in the bulk region where the structure is periodic and the boundary layers to be corrected are divided into five regions. For what follows, $kl = \{11,22,33,23,31,12\}$ and $i \in \{1,2,3\}$. The five regions are:

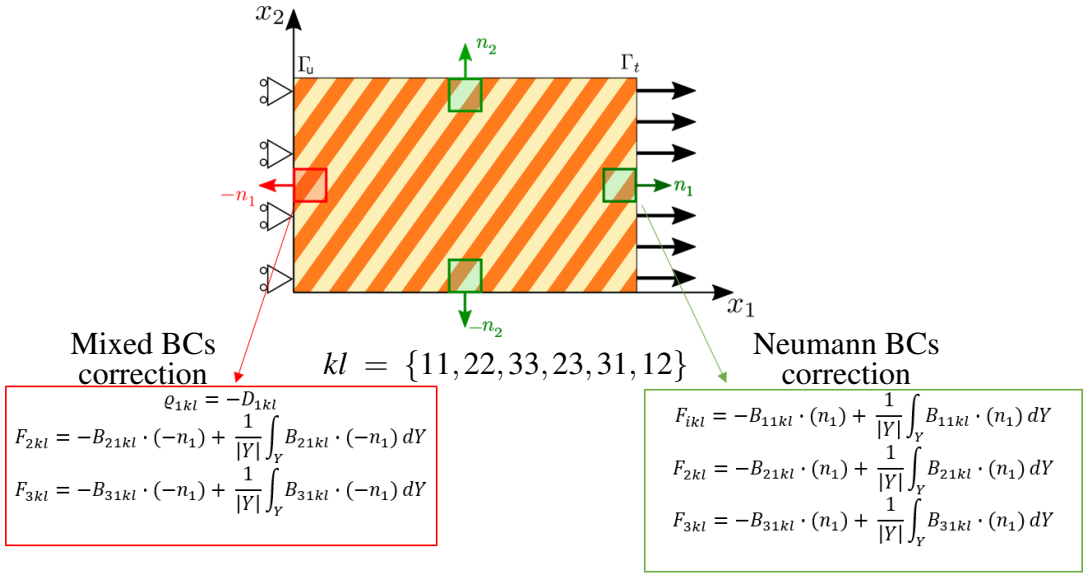

Figure 2.4: *Illustration of the Neumann and mixed BCs corrections to be applied to the unit-cell.*

1. Boundary layers subjected to Dirichlet BCs:
   The unit-cell is subjected to six displacement vectors $\boldsymbol{\varrho}_{ikl}$ (2.37) on the face where Dirichlet BCs are applied, the opposite face is kept free of forces. The remaining faces of the unit-cell are subjected to periodicity conditions (see Fig. 2.5a).

2. Corner cells subjected to both Neumann and Dirichlet BCs:
   The unit-cell, which is a corner cell in this case as shown Fig. 2.6, is subjected to six displacement vectors $\boldsymbol{\varrho}_{ikl}$ (2.37) on the face where Dirichlet BCs are applied and six loads $\boldsymbol{F}_{ikl}$ (2.29) on the face where Neumann BCs are applied. The remaining faces of the unit-cell are kept free of forces (see Fig. 2.5b).

3. Free forces boundary layers:
   The unit-cell is subjected to six loads $\boldsymbol{F}_{ikl}$ (2.29) where the unit-cell is free of forces. The opposite face where the loads are applied is fixed. The remaining faces of the unit-cell are subjected to periodicity conditions (see Fig. 2.5c).

4. Boundary layers subjected to Neumann BCs:
   The unit-cell is subjected to six loads $\boldsymbol{F}_{ikl}$ (2.29) on the face where Neumann BCs are applied. The opposite face where the loads are applied is fixed. The remaining faces of the unit-cell are subjected to periodicity conditions (see Fig. 2.5d).

5. Corner cells subjected to Neumann BCs:
   The unit-cell is subjected to six loads $\boldsymbol{F}_{ikl}$ (2.29) where Neumann BCs are applied and where the unit-cell is free of forces. The remaining faces of the unit-cell are fixed (see Fig. 2.5e).

The boundary layer correction and localization tensors $\mathbb{D}^{0,bl}$, $\mathbb{A}^{0,bl}$, and $\mathbb{B}^{0,bl}$ are constructed from the resolution of auxiliary problems. Thereafter corrective boundary layer fields are computed and added to estimated fields as summarized in Fig. 2.6.

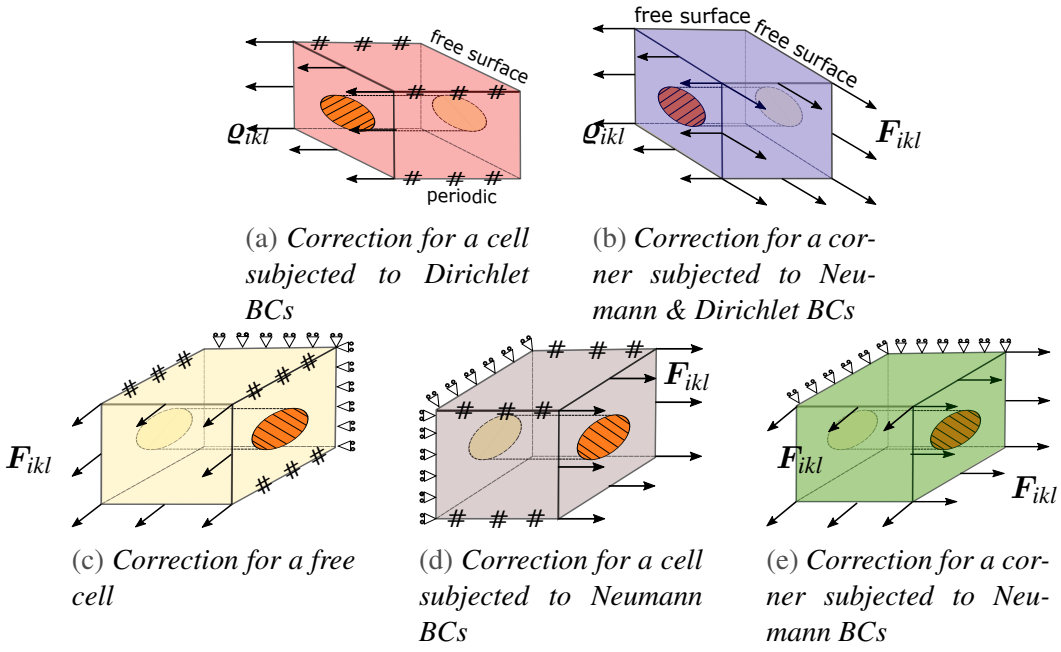

(a) *Correction for a cell subjected to Dirichlet BCs*

(b) *Correction for a corner subjected to Neumann & Dirichlet BCs*

(c) *Correction for a free cell*

(d) *Correction for a cell subjected to Neumann BCs*

(e) *Correction for a corner subjected to Neumann BCs*

Figure 2.5: *Illustration of auxiliary problems for boundary layers correction.*

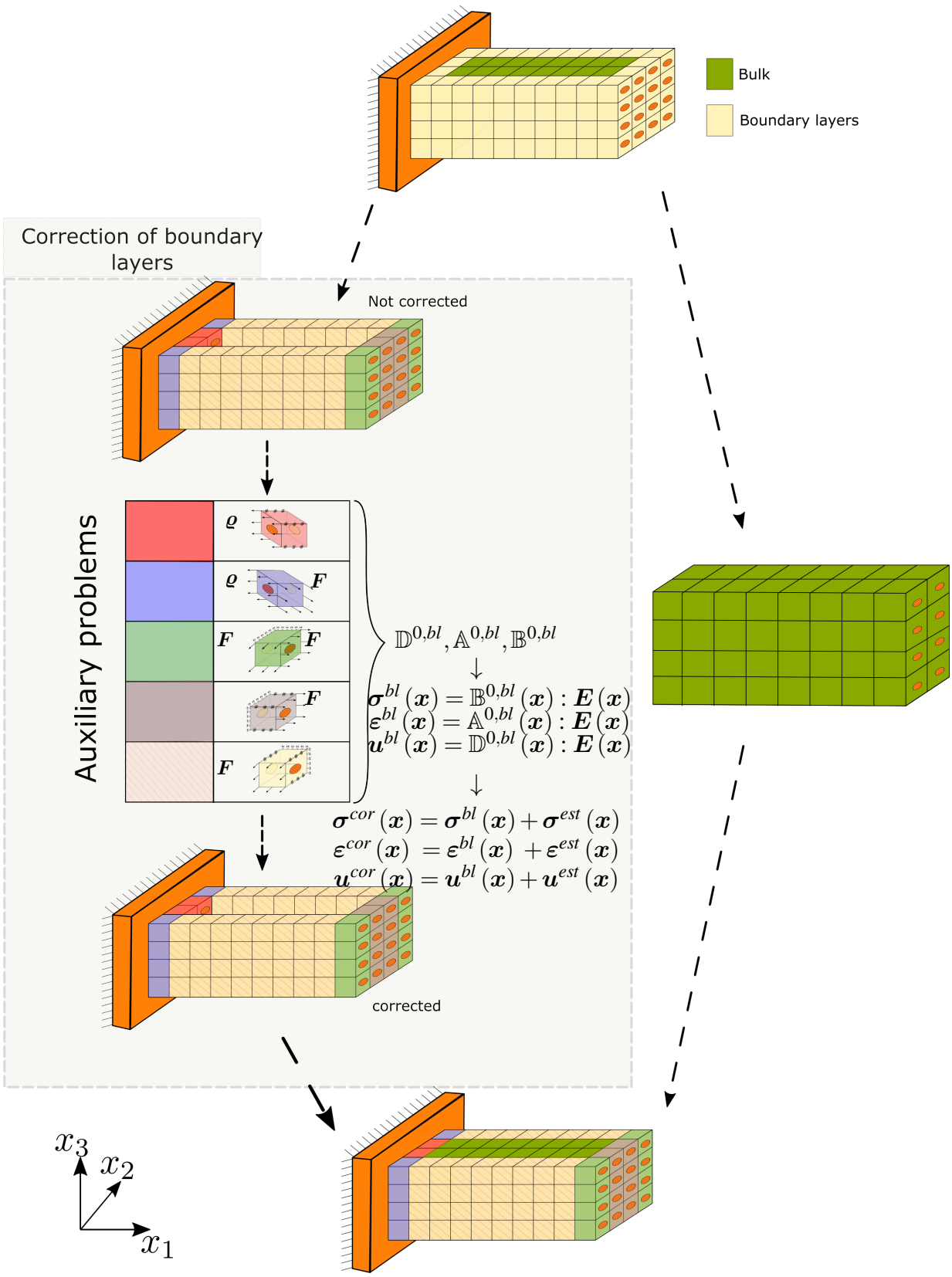

Figure 2.6: *Illustration of the boundary layer correction process. An invariance along the vertical (thickness) direction is considered for simplicity.*

2.4 Numerical examples

In this section, numerical examples are presented and discussed to demonstrate the efficiency and limitations of the suggested approach. For illustrative purposes, a simple study conducted on a uni-directional laminate in tension is presented in appendix A.2.

2.4.1 Matrix-inclusion composite

We consider the plane strain linear elasticity problem of a matrix-inclusion composite in tension as depicted in Fig. 2.7. The size of the structure is $L = 8$ mm, $H = 5$ mm and $W = 1$ mm, and the diameter of the fibers is $D = 0.2$ mm. The matrix and the spherical inclusions are assumed to be isotropic linear elastic with coefficients ($E_m = 1000$ MPa, $\nu_m = 0.3$) and (E_f, $\nu_f = 0.3$) where E_f is varied in the examples, respectively. We propose to estimate the microscale fields by using the relocalization procedure

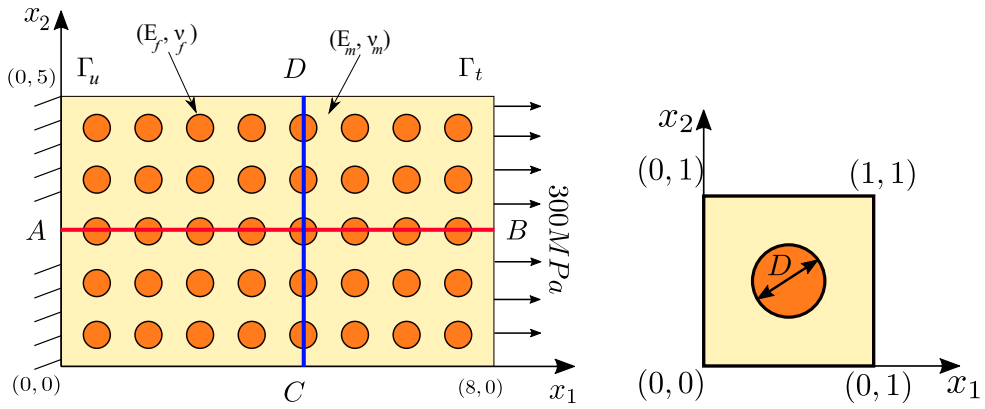

(a) *Structure geometry* (b) *unit-cell domain*

Figure 2.7: *Illustration of matrix-inclusion composite. The structure is fixed on Γ_u and a non-zero surface traction is applied on Γ_t, other boundaries are kept free. The results will be plotted along AB and CD lines.*

described in subsection. 2.2.3, and correct these estimates on the boundaries based on the proposed boundary correction scheme described in Sec. 2.3.
In this study we will compare the ensuing stress fields:

- The microscale stress field obtained by solving the problem $(\mathscr{P}_{ref})$ using DNS, which will be considered as our reference, indexed *ref*.
- The homogeneous stress field obtained from solving the problem $(\mathscr{P}_{hom})$, indexed *hom*.
- The proposed estimate of the microscale stress field obtained by the relocalization process, indexed *est*.
- The correction of the microscale stress field corrected with the proposed boundary layer correction scheme, indexed *cor*.

We will also quantify the difference between the reference and estimated fields by computing the modeling error. For this purpose, we define the following local (element wise) error in energy norm:

$$\begin{aligned}\|\boldsymbol{e}\|_{E(\Omega_e)} &= \|\boldsymbol{u}^{ref}(\boldsymbol{x}) - \boldsymbol{u}^{k}(\boldsymbol{x})\|_{E(\Omega_e)} \\ &= \left(\int_{\Omega_e} \nabla^s\left(\boldsymbol{u}^{ref}(\boldsymbol{x}) - \boldsymbol{u}^{k}(\boldsymbol{x})\right) : \mathbb{C} : \nabla^s\left(\boldsymbol{u}^{ref}(\boldsymbol{x}) - \boldsymbol{u}^{k}(\boldsymbol{x})\right) d\Omega_e\right)^{\frac{1}{2}},\end{aligned} \tag{2.38}$$

where Ω_e denotes the domain of an element and $\boldsymbol{u}^k(\boldsymbol{x})$ denotes the estimated displacement field whose error is measured ($k = est$ or $k = cor$). The global error $\|\boldsymbol{e}\|_{E(\Omega)}$ is then defined as:

$$\|\boldsymbol{e}\|^2_{E(\Omega)} = \sum_e \|\boldsymbol{e}\|^2_{E(\Omega_e)}. \tag{2.39}$$

Comparison of stress fields

We consider a contrast $\frac{E_f}{E_m} = 10$, where E_f and E_m are Young's moduli of the fiber and matrix phases, respectively. Comparison of resulting stress fields along AB and CD lines

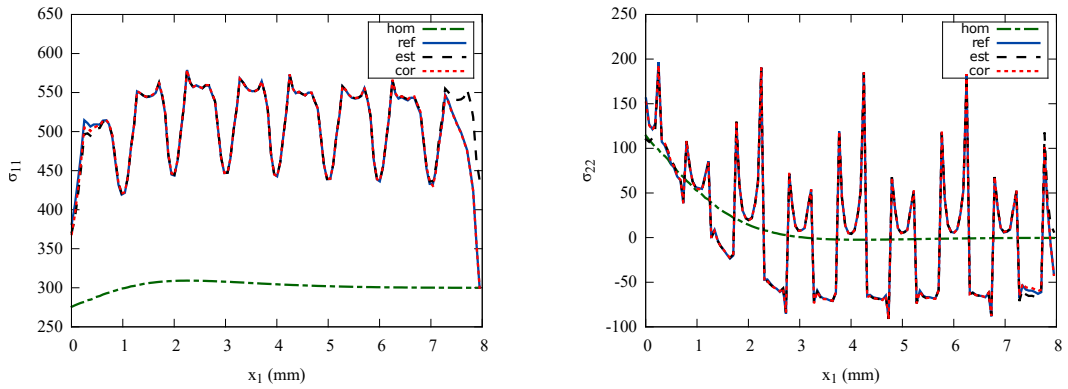

(a) σ_{11} *(MPa)* (b) σ_{22} *(MPa)*

Figure 2.8: *Results of the homogenized (hom), reference (ref), estimated (est) and corrected (cor) stress fields plotted along the AB line with* $\frac{E_f}{E_m} = 10$ *for the matrix-inclusion composite in tension.*

are presented in Fig. 2.8 and Fig. 2.9, respectively. The corresponding AB and CD lines are defined in Fig. 2.7. Both σ_{11}^{est} and σ_{22}^{est} perfectly coincide with reference ones in the inner domain of the composite, where they are periodic. Nevertheless, accuracy is lost near the boundaries. After the boundary layer correction, the corrected fields provide a good approximation of the reference near the boundaries. In particular, σ_{11}^{cor} verifies the applied Neumann condition (300 MPa) at $x_1 = 8$ mm as for the reference and the homogeneous counterparts, but it is not the case for σ_{11}^{est}. A more precise quantification of the error is provided in the next subsection.

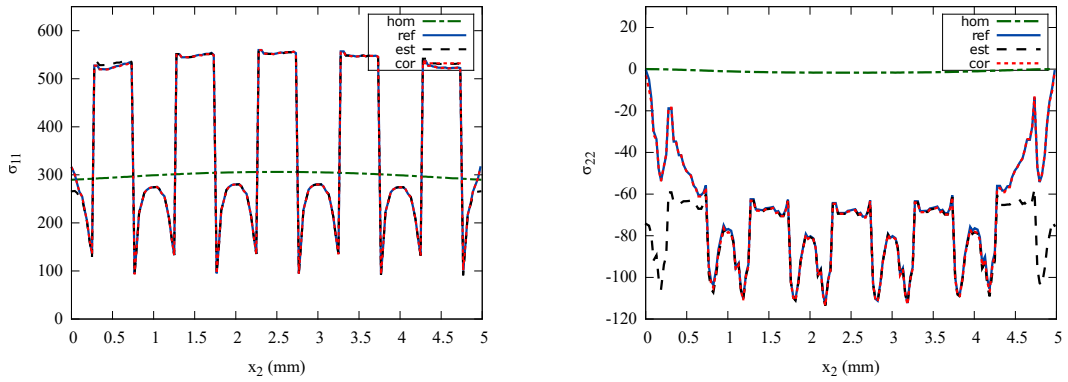

(a) σ_{11} *(MPa)* (b) σ_{22} *(MPa)*

Figure 2.9: *Results of the homogenized (hom), reference (ref), estimated (est) and corrected (cor) stress fields plotted along the CD line with* $\frac{E_f}{E_m} = 10$ *for the matrix-inclusion composite in tension.*

Modeling error

The local relative modeling error without the boundary layer correction, presented in Fig. 2.10a, is concentrated near the boundaries and maximal in the vicinity of the applied Neumann boundary. This is mainly explained by the loss of periodicity in the vicinity of the boundaries. After the correction, the error is significantly reduced near the boundaries. We notice that the remaining error is mainly concentrated at the corners, especially near the Neumann boundary. We recall that a particular treatment was considered for the corners correction, as explained in Fig. 2.6. This correction improves the overall result but seems to be still imperfect since errors remain at the interfaces. Table 2.1 summarizes the

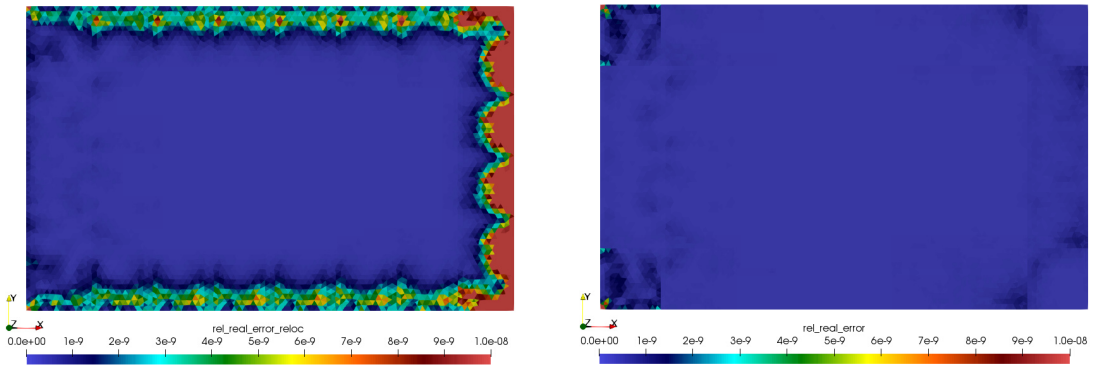

(a) $\frac{\|\boldsymbol{u}^{ref}-\boldsymbol{u}^{est}\|^2_{E(\Omega_e)}}{\|\boldsymbol{u}^{ref}\|^2_{E(\Omega)}}$ (b) $\frac{\|\boldsymbol{u}^{ref}-\boldsymbol{u}^{cor}\|^2_{E(\Omega_e)}}{\|\boldsymbol{u}^{ref}\|^2_{E(\Omega)}}$

Figure 2.10: *Comparison of the local relative modeling error results with* $\frac{E_f}{E_m} = 10$ *for the matrix-inclusion composite in tension.*

global relative modeling error for different contrast ratios. The boundary layer correction allows to drastically reduce the modeling error by a factor of 4 to 5 for the four ratios. This demonstrates that the correction process is effective even for higher contrast between fiber and matrix phases.

Table 2.1: *Comparison of the global relative modeling error for different contrast ratios for the matrix-inclusion composite in tension.*

Global modeling error	Contrast 10	Contrast 25	Contrast 50	Contrast 100
$\frac{\|\boldsymbol{u}^{ref}-\boldsymbol{u}^{est}\|_{E(\Omega)}}{\|\boldsymbol{u}^{ref}\|_{E(\Omega)}}$	0.038	0.044	0.046	0.048
$\frac{\|\boldsymbol{u}^{ref}-\boldsymbol{u}^{cor}\|_{E(\Omega)}}{\|\boldsymbol{u}^{ref}\|_{E(\Omega)}}$	0.009	0.010	0.011	0.012

2.4.2 Laminated composite in tension

We consider a plane strain elasticity problem of a laminated composite made of two layers as presented in Fig. 2.11. The size of the structure is $L = 8$ mm, $H = 5$ mm and $W = 1$ mm. The two layers are assumed to be isotropic linear elastic with coefficients ($E_m = 1000$ MPa, $\nu_m = 0.3$) and ($E_f, \nu_f = 0.3$) where E_f is varied in the examples. We conduct the same study as in the previous example. In order to correct the Γ_u boundary layer, it is necessary to apply both the Neumann and Dirichlet boundary corrections.

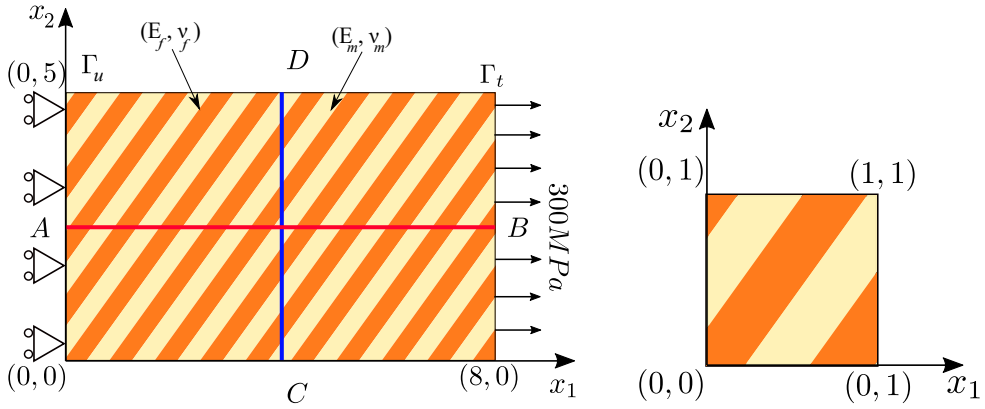

(a) *Structure geometry* (b) *unit-cell domain*

Figure 2.11: *Illustration of the laminated composite in tension. The structure is sliding on Γ_u and surface tension is applied on Γ_t. Other boundaries are kept free. Results will be plotted along AB and CD lines.*

Comparison of stress fields

Figs. 2.12 and 2.13 show that σ^{cor} is in agreement with σ^{ref} in the inner domain of the composite *and* on the boundaries. We also notice that high stresses are developed in the vicinity of the sliding boundary Γ_u, especially for higher contrast ratios. For a ratio of 50, the estimated stress is 3 times smaller than the real stress for σ_{11} and 7 times smaller for σ_{12}, which may result in underestimating failure criteria if the design is conducted without any boundary layer correction.

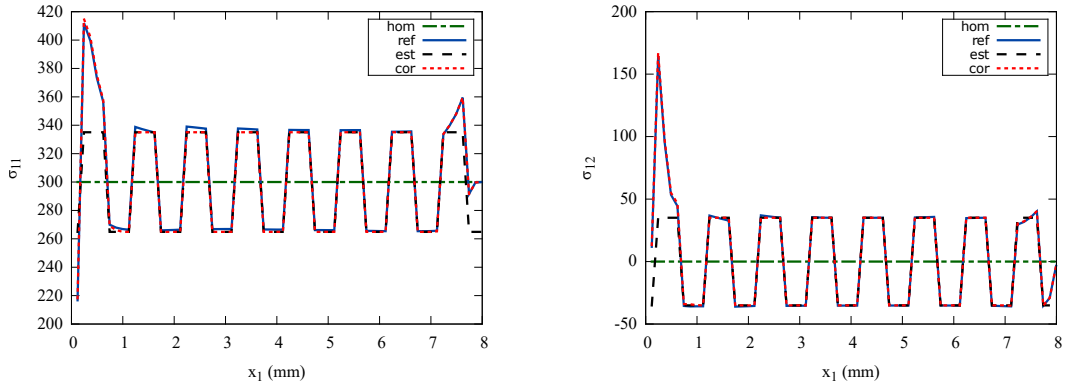

(a) σ_{11} *(MPa)* (b) σ_{12} *(MPa)*

Figure 2.12: *Results of the homogenized (hom), reference (ref), estimated (est) and corrected (cor) stress fields plotted along the AB line with* $\frac{E_f}{E_m} = 10$ *for the laminated composite in tension.*

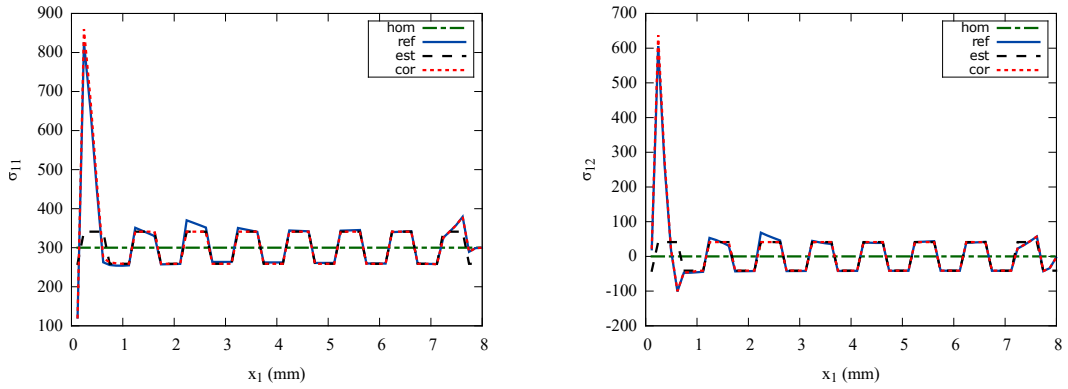

(a) σ_{11} *(MPa)* (b) σ_{12} *(MPa)*

Figure 2.13: *Results of the homogenized (hom), reference (ref), estimated (est) and corrected (cor) stress fields plotted along the AB line with* $\frac{E_f}{E_m} = 50$ *for the laminated composite in tension.*

Modeling error

The local relative modeling error between the reference and estimated fields (Fig. 2.14a) is negligible in the inner domain of the composite but significant on the boundaries, especially in the vicinity of the sliding boundary Γ_u. After the correction (Fig. 2.14b), the modeling error is significantly reduced, and remains concentrated at the corners of Γ_u.
Table 2.2 summarizes the relative modeling error for different contrast ratios. Similarly, by correcting the boundary layers, the remaining error is divided by 3 for the four ratios.

2.4.3 Laminated composite in bending

The same composite as in the previous example is now subjected to bending as shown in Fig. 2.15. This specific load will create high macroscale strain gradients. In this case, the

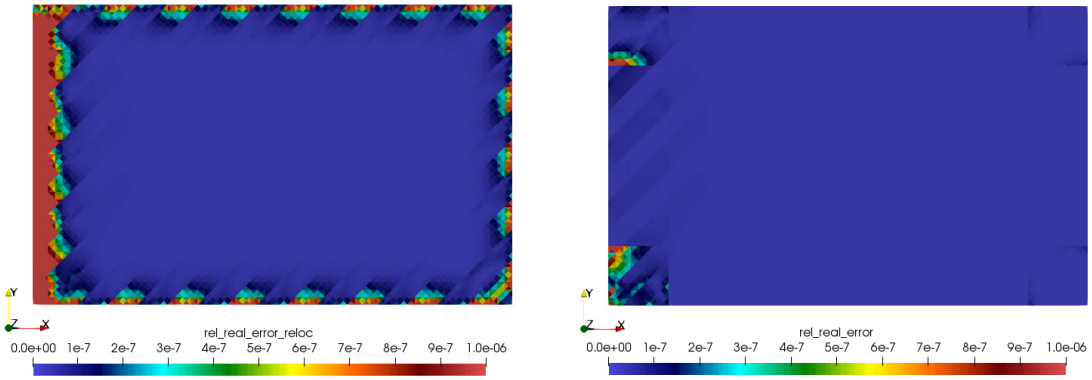

(a) $\frac{\|\boldsymbol{u}^{ref}-\boldsymbol{u}^{est}\|^2_{E(\Omega_e)}}{\|\boldsymbol{u}^{ref}\|^2_{E(\Omega)}}$ (b) $\frac{\|\boldsymbol{u}^{ref}-\boldsymbol{u}^{cor}\|^2_{E(\Omega_e)}}{\|\boldsymbol{u}^{ref}\|^2_{E(\Omega)}}$

Figure 2.14: *Comparison of the local relative modeling error results for* $\frac{E_f}{E_m} = 10$ *for the laminated composite in tension.*

Table 2.2: *Comparison of the global relative modeling error for different contrast ratios for the laminated composite in tension.*

Global modeling error	Contrast 10	Contrast 25	Contrast 50	Contrast 100
$\frac{\|\boldsymbol{u}^{ref}-\boldsymbol{u}^{est}\|_{E(\Omega)}}{\|\boldsymbol{u}^{ref}\|_{E(\Omega)}}$	0.10	0.14	0.17	0.20
$\frac{\|\boldsymbol{u}^{ref}-\boldsymbol{u}^{cor}\|_{E(\Omega)}}{\|\boldsymbol{u}^{ref}\|_{E(\Omega)}}$	0.027	0.036	0.047	0.066

first-order approximation is expected to lose its accuracy *even* in the inner domain of the structure. To illustrate this, the same study is conducted by comparing stress fields and computing the modeling error.

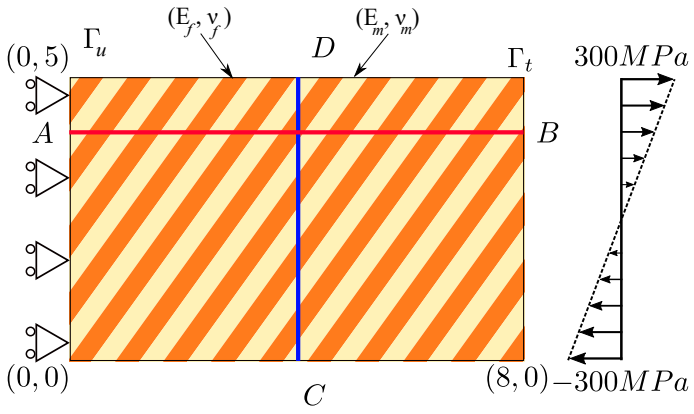

Figure 2.15: *Structure composed of a laminated composite subjected to bending. Results will be plotted along AB and CD lines.*

Comparison of stress fields

We only consider a contrast of 10 in this example, as it will be sufficient to illustrate our point. Comparisons of the stress fields along the AB line are presented in Fig. 2.16 and along the CD line in Fig. 2.17.

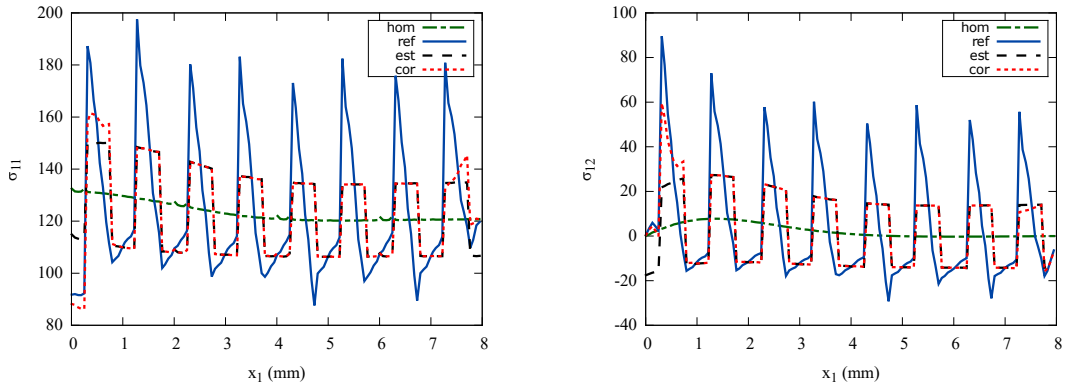

(a) σ_{11} *(MPa)* (b) σ_{12} *(MPa)*

Figure 2.16: *Results of the homogenized (hom), reference (ref), estimated (est) and corrected (cor) stress fields plotted along the AB line with* $\frac{E_f}{E_m} = 10$ *for the laminated composite in bending.*

The results show that the estimated fields, contrary to the previous examples, are inaccurate *even* in the inner domain of the structure. This is mainly explained by high macroscale strain gradients induced by the bending. To overcome this shortcoming, higher-order terms must be introduced in the asymptotic expansion which features higher-order gradients of macroscale strain and characteristic tensors of the microstructure [Boutin, 1996]. Despite this clear limitation, the corrected estimated stresses are still a better approximation of the real stresses near the boundaries.

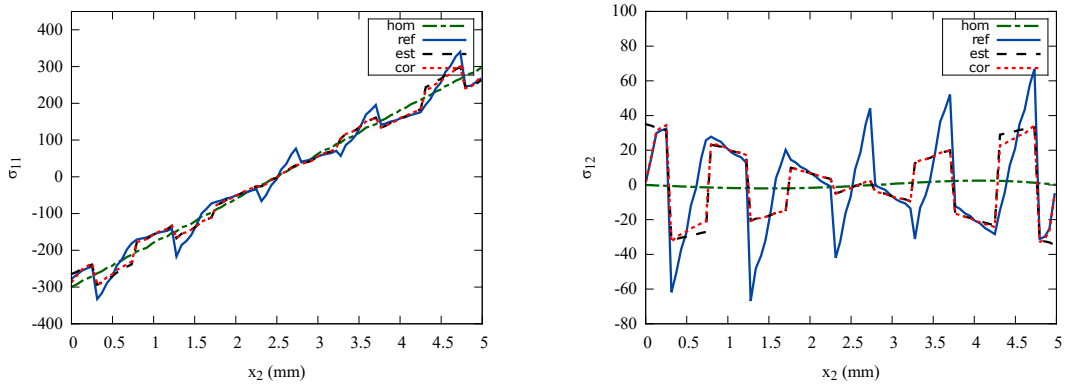

(a) σ_{11} *(MPa)* (b) σ_{12} *(MPa)*

Figure 2.17: *Results of the homogenized (hom), reference (ref), estimated (est) and corrected (cor) stress fields plotted along the CD line with* $\frac{E_f}{E_m} = 10$ *for the laminated composite in bending.*

Modeling error

The local relative modeling error before the correction is maximal in the vicinity of the sliding boundary Γ_u but also spread across the structure as shown in Fig. 2.18a. After the boundary layer correction, the error is considerably reduced on the boundaries but still present inside the structure as shown in Fig. 2.18b.

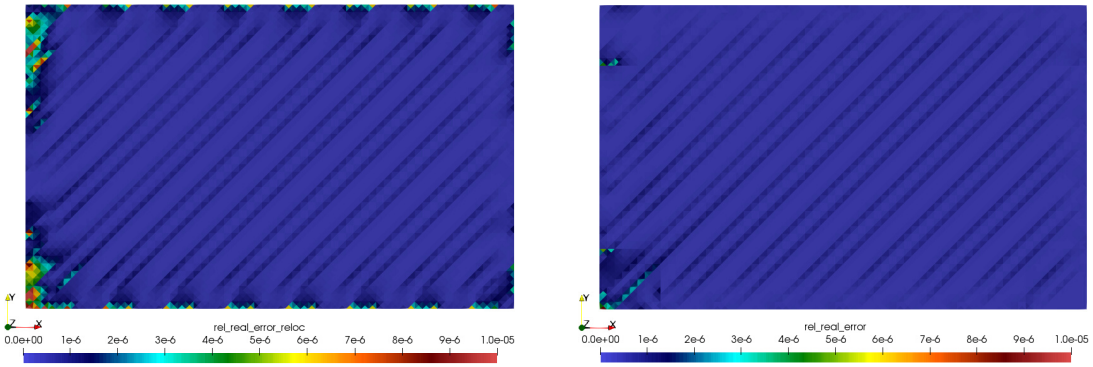

(a) $\frac{\|\boldsymbol{u}^{ref}-\boldsymbol{u}^{est}\|^2_{E(\Omega_e)}}{\|\boldsymbol{u}^{ref}\|^2_{E(\Omega)}}$ (b) $\frac{\|\boldsymbol{u}^{ref}-\boldsymbol{u}^{cor}\|^2_{E(\Omega_e)}}{\|\boldsymbol{u}^{ref}\|^2_{E(\Omega)}}$

Figure 2.18: *Comparison of the local relative modeling error results for* $\frac{E_f}{E_m} = 10$ *for the laminated composite in bending.*

2.5 Conclusions

In this study, we propose a general boundary layer correction based on asymptotic homogenization to estimate consistent microscale fields in the vicinity of the boundaries. The main idea of the method is to compute corrective terms from solving different auxiliary problems on the unit-cell. The nature of the problem to solve depends on the local boundary conditions. These corrective terms are added to the usual fields obtained from the relocalization process, drastically improving the solution near the boundaries.
It was shown, by means of three numerical examples, that the corrected fields successfully predict stress or strain concentrations near the boundaries, which can be responsible for the failure of the individual phases. The proposed method was developed for different boundary conditions (Dirichlet, Neumann, and mixed). The associated computational cost is relatively inexpensive since the corrective terms are computed over the unit-cell. All localization tensors can be computed off-line and used for any composite structure involving the same unit-cell.
The major conclusions that can be drawn from this study are as follows:

- The first-order estimated fields, obtained from the relocalization process, are a good approximation of the heterogeneous (reference) fields in the inner domain of the structure. This result is not true for cases when high gradients of macroscale strains exist.
- The boundary layer correction allows to reduce the global modeling error by a factor of 3 to 4 for different ratios $\frac{E_f}{E_m}$.

- The corrected stress field captures high stresses developed near the boundaries. Particularly, for the laminated composite in tension (ratio of $\frac{E_f}{E_m} = 50$) shown in Sec. 2.4.2, the estimated stress component is 3 times smaller than the real stress for σ_{11} and 7 times smaller for σ_{12}. This may result in underestimating failure criteria if the design is conducted without any boundary layer correction.

The method can now be applied with confidence to more realistic engineering composite structures, especially in the 3D case for which DNS are more expensive to achieve. This also implies the use of coarse macroscale finite element meshes and proper projection/interpolation to the unit-cell mesh.
The limitation of the proposed approach has also been evidenced in some cases where boundary conditions are not the only source of modeling error. Second-gradient effects, which first-order asymptotic homogenization neglects, may also play a prominent role. Combining higher-order and boundary correctors could be a path toward efficient error estimation or adaptive model refinement as we will see in the following chapters.

Chapter 3

Higher-order asymptotic homogenization with boundary layer correction

Abstract

I have demonstrated in the previous chapter that first-order homogenization generally becomes inaccurate for materials with a weak scale separation between characteristic lengths of the heterogeneities and the structural problem. I have also shown that it is unable to provide a correct solution in the vicinity of the boundaries due to the loss of periodicity in these regions. In this chapter, I demonstrate the effectiveness of higher-order homogenization, up to the third-order, in estimating correctly the heterogeneous solution, for cases with a low scale separation in elastic composite materials. I also propose an extension of the previously proposed general boundary layer method to correct higher-order estimates obtained near the boundaries. The efficiency and accuracy of the proposed methods are studied on various numerical examples dealing with elastic laminates and fiber-matrix composites.

Résumé

J'ai démontré dans le chapitre précédent que l'homogénéisation asymptotique au premier ordre est généralement imprécise pour les matériaux avec une faible séparation d'échelle entre les longueurs caractéristiques des hétérogénéités et le problème structurel. J'ai également montré qu'elle est incapable de fournir une solution correcte au voisinage des bords en raison de la perte de périodicité près de ces régions. Dans ce chapitre, je démontre l'efficacité de l'homogénéisation d'ordre supérieur, et ce, jusqu'au troisième ordre, afin d'estimer correctement la solution hétérogène, sur des cas avec une faible séparation d'échelle. Je propose également une extension de la méthode de correction de couche limite afin de corriger les estimations aux ordres supérieurs obtenues près des bords. L'efficacité des méthodes proposées sont étudiées sur divers exemples numériques portant sur des laminés élastiques et des composites à matrice de fibres.

Contents

Reproduced from:
Mouad Fergoug, Augustin Parret-Fréaud, Nicolas Feld, Basile Marchand and Samuel Forest. Multiscale analysis of composite structures based on higher-order asymptotic homogenization with boundary layer correction.
European Journal of Mechanics - A/Solids, 2022, 96:104754.
doi: 10.1016/j.euromechsol.2022.104754

3.1 Introduction

Classical or first-order homogenization methods assume a complete separation of scales in composite materials. This assumption is only valid when the scale of the microstructure or microstructural fluctuation is much smaller than the characteristic dimension of the macrostructure. Most of these homogenization methods are known to be effective in capturing uniform macroscopic strain fields without large gradients. For weak separation of scales, however, they generally become inaccurate [Ameen et al., 2018]. Such cases can occur mainly when: (a) The size of the microstructure is of the same order of magnitude as that of the macrostructure, and (b) the wave length of variation of macroscale fields is not sufficiently large compared to the size of the microstructure. In such cases, the predicted properties obtained by first-order homogenization may fail to describe the local or global responses of the composite [Ameen et al., 2018; Kouznetsova et al., 2002; He and Pindera, 2020a]. This is mainly explained by two reasons:

- The scale separation assumption implicitly implies macroscopic quasi-uniformity of the strain field over the microstructure. Therefore, only first-order deformation modes (tension, compression, and shear) are considered. In contrast, in the case of weak separation of scales, capturing a bending mode, for example, remains beyond the capabilities of classical homogenization [Kouznetsova et al., 2002; Fergoug et al., 2022a], as will be shown later in this chapter.

- Higher-order homogenization may require consideration of non-local media. Indeed, classical homogenization methods take into account the influence of the volume fraction, distribution, and morphology of the microstructure [Sanchez-Palencia and Zaoui, 1987; Suquet, 2014], but cannot account for geometrical size effects in the mechanical behavior of heterogeneous materials.

To overcome these limitations, generalized continuum theories (higher-order continua or higher-grade theories) are used to describe the behavior of either the microscopic scale or the macroscopic one or both levels simultaneously. Indeed, enriched continuum theories extend the range of applicability of homogenization methods beyond the strict assumption of scale separation. They also enable relaxation of the local action principle by introducing some additional length scale parameters to take into account the influence of the surrounding physical state on the behavior of a continuum point.
Two main categories of generalized continua are distinguished:

- Higher-order continua that introduce additional degrees of freedom, like the Cosserat medium proposed by the Cosserat brothers [Cosserat and Cosserat, 1909] where local micro-rotations are introduced at each continuum point in addition to the displacement field. This enhancement can be extended further to obtain the micromorphic elasticity [Mindlin, 1964; Germain, 1973].

- Higher-grade continua according to Mindlin [1964]; Mindlin and Eshel [1968] that include higher-order gradients of kinematic or internal variables in the expression of the (elastic) energy density.

The strain-gradient continuum offers some advantages compared to higher-order continua as stated in Yvonnet et al. [2020]. Indeed, this model is rich enough to incorporate a characteristic length of the microstructure without introducing a large number of parameters as

in micromorphic elasticity [Auffray et al., 2015]. Furthermore, such a model can be constructed by asymptotic analyses [Boutin, 1996; Smyshlyaev and Cherednichenko, 2000; Peerlings and Fleck, 2004; Tran et al., 2012].

In most cases, it is agreed that including higher gradients of the macroscopic field in the homogenization of a Representative Volume Element (RVE) is a natural way to introduce the internal length scale characterizing the microstructure. At least two approaches exist regarding this subject.

The first approach uses Quadratic Boundary Conditions (QBCs) applied to the unit-cell [Gologanu et al., 1997; Forest, 1998; Forest et al., 2001; Kouznetsova et al., 2002; Yvonnet et al., 2020]. This method is an extension of the classical Kinematic Uniform Boundary Conditions (KUBC) [Huet, 1990; Kanit et al., 2003] which consist in applying, on the boundary of the RVE, the displacement field that would occur if the strain field was uniform. Indeed, a displacement that has a quadratic dependence with the position vector is applied, with the macroscopic gradient of strain being the considered enforcing term. This method has a major flaw: QBCs lead to non-zero fluctuations when the material is homogeneous, which seems to be physically unreasonable as stated by Yuan et al. [2008], Forest and Trinh [2011], Tran et al. [2012], Monchiet et al. [2020], and Yvonnet et al. [2020], since these fluctuations are due to the heterogeneity of the microstructure. To tackle this, a correction has been proposed in Monchiet et al. [2020] by adding adequate body forces to QBCs and has been successfully used in Yvonnet et al. [2020].

The second approach considers higher-order problems in the asymptotic homogenization method. This approach of series expansion initially presented by Sanchez-Palencia [1983]; Bensoussan et al. [2011] for periodic heterogeneous materials, introduces a scale factor $\varepsilon = l/L$, where l and L are the characteristic lengths of the microstructure and macrostructure, respectively. In the case of strict scale separation, *i.e.* $\varepsilon \ll 1$, classical homogenization gives adequate estimate properties. In cases of weak scale separation, *i.e.* $\varepsilon < 1$, the solution can be approximated by keeping higher-order terms in the series expansion. These terms are obtained by resolving a hierarchical set of elasticity problems with prescribed body forces and eigenstrains, obtained from the solution at the lower-order. It is shown in Boutin [1996] that higher-order terms in asymptotic homogenization introduce successive gradients of the macroscale strain and tensors characteristic of the microstructure, which result in introducing a non-local effect on material behavior. The analytical solutions of these characteristic tensors were provided by Boutin [1996] for a laminate. The agreement with the phenomenological strain-gradient theories was established by Smyshlyaev and Cherednichenko [2000]; Peerlings and Fleck [2004]; Tran et al. [2012] by combining the asymptotic method with a variational technique.

In the present chapter, the retained method for our multiscale analyses is the asymptotic homogenization method. Consequently, only periodic heterogeneous materials are considered where the period, *i.e.* the unit-cell, defines the RVE without any ambiguity.

We establish a general numerical framework to evaluate the effect of macroscopic strain gradients on the local response of the composite. This framework is implemented, in this chapter, using the Finite Element Method (FEM) but could be implemented using another discretization method. We perform a relocalization process to estimate heterogeneous local fields by considering higher-order homogenization problems, up to the third-order in the asymptotic expansion. This relocalization process is associated with a macroscale problem, which remains, in this work, a scale-independent Cauchy type. Indeed, commer-

cial FE software is usually limited to the computation of Cauchy media and our approach is an attempt to conduct relocalization in such a situation. My numerical implementation of the localization tensors will be verified based on analytical solutions provided by Boutin [1996] (see appendix B.1).
While asymptotic homogenization may estimate local fields within the composite by a relocalization process, the construction of a solution at the vicinity of the boundaries remains beyond the capabilities of classical homogenization [Sanchez-Palencia, 1986; Dumontet, 1986; Koley et al., 2019; Fergoug et al., 2022a]. Indeed, asymptotic homogenization assumes a periodic solution, which is not the case on the boundaries. It has been shown by Pipes et al. [1973]; Tang and Levy [1975]; Hsu and Herakovich [1977]; Pagano [1978] that complex stress states with a rapid change of gradients occur within a local region near the boundaries, frequently referred to as a *boundary layer effect*. This effect is often responsible for the initiation of structural failure, *e.g.* in laminates [Pipes et al., 1973].
In a previous work [Fergoug et al., 2022a], a general boundary layer correction was proposed. It is valid for different Boundary Conditions (BCs): Dirichlet, Neumann, or mixed. The main idea of this method is to enrich, on boundaries, the first-order relocalized solution fields by adding decaying corrective terms obtained by the resolution of independent auxiliary problems over the unit-cell. The nature of the problems to be solved depends on the actual boundary conditions applied locally to the structure. These corrective terms are then added to the first-order relocalized fields.
In the present chapter, we propose an extension of this general boundary layer correction to rectify higher-order relocalization fields up to the third-order. Indeed, matching boundary conditions requires the introduction of boundary layers in each order.
Regarding the aforementioned aspects, the present work proposes two main aspects:

- A higher-order relocalization process up to the third-order. This means that we the introduce effects of the macroscopic strain, its gradient, and its second gradient on the local response of the composite. By doing so, we extend the range of applicability of relocalization to cases subjected where a first-order homogenization/relocalization is generally not valid anymore.

- A general boundary layer correction to accurately estimate higher-order relocalized fields, up to the third-order, on the boundaries.

To the best knowledge of the authors, such an extension of first-order boundary layer correction has not been yet proposed in the literature.
A computing workflow is proposed to perform both the relocalization step and the boundary layer correction within a finite element framework.
The outline of this chapter is as follows. In Sec. 3.2, we first briefly recall the asymptotic expansion homogenization method and describe the proposed higher-order relocalization process. In Sec. 3.3, we detail the proposed general boundary layer correction procedure. A numerical implementation procedure is proposed in Sec. 3.4. Numerical examples are presented and discussed in Sec. 3.5, with the objective of demonstrating the efficiency of the suggested approach.

3.2 Higher-order estimation of micromechanical fields

Conventionally in mechanical homogenization, asymptotic series are truncated at the first-order. It follows that the obtained effective macroscopic continuum is a scale-independent Cauchy type continuum. The consequence of taking into account additional terms of the expansion, up to the third-order, as derived by Boutin [1996], is to introduce scale-dependent corrective terms on material behavior.
The objective of this section is to describe the proposed estimation of local heterogeneous fields based on a higher-order relocalization process. This relocalization stage is associated with a given macroscale equilibrium state also elaborated in this section.

3.2.1 Statement of the boundary value problem and homogenization procedure

Consider a problem domain Ω^ε, formed by the spatial repetition of a heterogeneous unit-cell, as shown in Fig. 3.1. This body, considered as a linear elastic solid in static equilibrium, is subjected to a body force $\boldsymbol{f}$ per unit volume. The boundary $\partial\Omega^\varepsilon$ consists of a portion Γ_u, on which the displacements are prescribed to the value $\boldsymbol{u}^d$, and a portion Γ_t on which surface traction $\boldsymbol{F}^d$ per unit area are prescribed, such that $\partial\Omega^\varepsilon = \Gamma_u \cup \Gamma_t$, and $\Gamma_u \cap \Gamma_t = \emptyset$.
Because of the heterogeneous nature of the material, the corresponding mechanical behavior depends on two scales:

- Macroscale with domain Ω, free of heterogeneities, having L as a characteristic length and global coordinates $\boldsymbol{x} \in \Omega$ with the assumption that $\partial\Omega^\varepsilon = \partial\Omega$ (see Fig. 3.1).
- Microscale, having l as a characteristic length and with local coordinates $\boldsymbol{y} \in Y$, where Y is the unit-cell domain, typically chosen here to be an open rectangular parallelepiped $Y =]0, Y_1[\times]0, Y_2[\times]0, Y_3[$ (see Fig. 3.1).

The coarse and fine scales are related by the parameter ε such that:

$$\varepsilon = \frac{l}{L}, \qquad \boldsymbol{y} = \frac{\boldsymbol{x}}{\varepsilon}. \tag{3.1}$$

The domain Ω^ε can be considered as the product space $\Omega \times Y$:

$$\Omega^\varepsilon = \left\{ \boldsymbol{x} \in \Omega \middle| \left(\boldsymbol{y} = \frac{\boldsymbol{x}}{\varepsilon} \right) \in Y \right\}. \tag{3.2}$$

Since the heterogeneity of the material arises from the periodically repeating unit-cell, and owing to this periodicity, one can define the elasticity tensor $\mathbb{C}$ as $Y-$periodic:

$$\mathbb{C} = \mathbb{C}(\boldsymbol{y}). \tag{3.3}$$

The heterogeneous stiffness tensor reads $\mathbb{C}^\varepsilon(\boldsymbol{x}) = \mathbb{C}(\boldsymbol{x}/\varepsilon) = \mathbb{C}(\boldsymbol{y})$, the superscript indicating fine-scale dependence. Similarly, the microscale displacement, strain, and stress fields read $\boldsymbol{u}^\varepsilon$, $\boldsymbol{\varepsilon}^\varepsilon$, and $\boldsymbol{\sigma}^\varepsilon$, respectively.

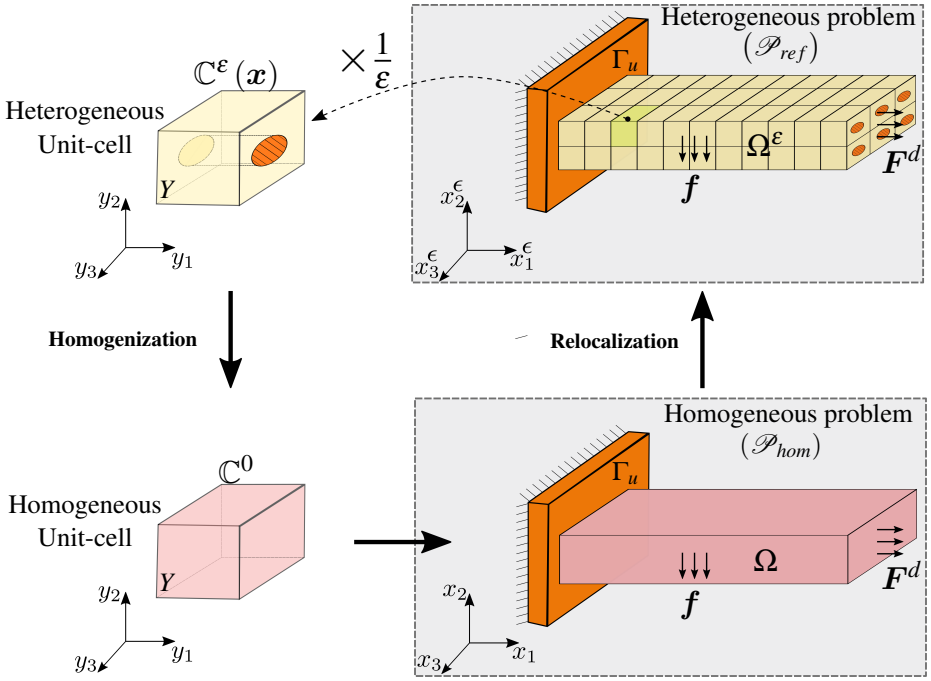

Figure 3.1: *Illustration [Fergoug et al., 2022a] of the heterogeneous problem* $(\mathscr{P}_{ref})$ *with domain* Ω^{ε}*, constructed by translating the unit-cell* Y *characterized by an oscillatory behavior* $\mathbb{C}^{\varepsilon}(\boldsymbol{x})$ *over the three space directions. The homogenized problem* $(\mathscr{P}_{hom})$ *with homogeneous domain* Ω *is characterized by the homogenized elasticity tensor* $\mathbb{C}^0$ *obtained from the homogenization step. Microscale fields are estimated by a relocalization process.*

In our previous work [Fergoug et al., 2022a], we have defined the following boundary value problems:

- Heterogeneous problem $(\mathscr{P}_{ref})$ with solution $(\boldsymbol{u}^{\varepsilon}, \varepsilon^{\varepsilon}, \boldsymbol{\sigma}^{\varepsilon})$. This problem is usually intractable by Direct Numerical Simulation (DNS, *i.e.* when the geometry of the microstructure is explicitly described in simulations). Common practice would call for a tractable estimate.

- First-order periodic problem $\left(\mathscr{P}^{1^{st}}_{order}\right)$ used to deduce the homogenized elasticity tensor $\mathbb{C}^0$ and first-order displacement, strain, and stress localization tensors: $\mathbb{D}^0$, $\mathbb{A}^0$, and $\mathbb{B}^0$, respectively.

- Homogenized problem $(\mathscr{P}_{hom})$ corresponding to the macroscale with solution (displacement $\boldsymbol{U}$, strain $\boldsymbol{E}$, stress $\boldsymbol{\Sigma}$), characterized by the homogenized elasticity tensor $\mathbb{C}^0$.

Formal definitions of these problems are omitted here for conciseness; we refer the reader to Fergoug et al. [2022a] for more details.
We aim to truncate the asymptotic expansion up to the third-order. Therefore, mechanical fields, solution to $(\mathscr{P}_{ref})$, are approximated with an asymptotic expansion in powers of

the small parameter ε as:

$$\boldsymbol{u}^{\varepsilon}(\boldsymbol{x}) = \boldsymbol{u}^{0}(\boldsymbol{x},\boldsymbol{y})+\varepsilon\boldsymbol{u}^{1}(\boldsymbol{x},\boldsymbol{y})+\varepsilon^{2}\boldsymbol{u}^{2}(\boldsymbol{x},\boldsymbol{y})+\varepsilon^{3}\boldsymbol{u}^{3}(\boldsymbol{x},\boldsymbol{y})+\mathscr{O}\left(\varepsilon^{4}\right), \tag{3.4}$$

$$\boldsymbol{\varepsilon}^{\varepsilon}(\boldsymbol{x}) = \boldsymbol{\varepsilon}^{0}(\boldsymbol{x},\boldsymbol{y})+\varepsilon\boldsymbol{\varepsilon}^{1}(\boldsymbol{x},\boldsymbol{y})+\varepsilon^{2}\boldsymbol{\varepsilon}^{2}(\boldsymbol{x},\boldsymbol{y})+\mathscr{O}\left(\varepsilon^{3}\right), \tag{3.5}$$

$$\boldsymbol{\sigma}^{\varepsilon}(\boldsymbol{x}) = \boldsymbol{\sigma}^{0}(\boldsymbol{x},\boldsymbol{y})+\varepsilon\boldsymbol{\sigma}^{1}(\boldsymbol{x},\boldsymbol{y})+\varepsilon^{2}\boldsymbol{\sigma}^{2}(\boldsymbol{x},\boldsymbol{y})+\mathscr{O}\left(\varepsilon^{3}\right). \tag{3.6}$$

The quantities $\boldsymbol{u}^{n}$, $\boldsymbol{\varepsilon}^{n}$ and $\boldsymbol{\sigma}^{n}$ are $Y-$periodic functions called *correctors* of the displacement, strain, and stress fields, respectively.
The following formulation for higher-order homogenization is classical without new developments. Nevertheless, efforts have been made to detail the formulation of hierarchical periodic problems, up to the third-order. Details of the prescribed body forces and eigenstrains, used to solve these periodic problems, are provided. Furthermore, since our objective is to conduct a higher-order relocalization process, the localization tensors at different orders are also provided.

Second-order periodic problem $\left(\mathscr{P}^{2^{nd}}_{order}\right)$

This problem is defined on the unit-cell Y. Its solution are the displacement corrector $\boldsymbol{u}^{2}$ and stress $\boldsymbol{\sigma}^{1}$. It reads:

Find $(\boldsymbol{u}^{2},\boldsymbol{\sigma}^{1})$ such that:

$$\left(\mathscr{P}^{2^{nd}}_{order}\right):\begin{cases}\operatorname{div}_{y}\left(\boldsymbol{\sigma}^{1}(\boldsymbol{x},\boldsymbol{y})\right)+\boldsymbol{L}^{1}(\boldsymbol{x},\boldsymbol{y})=0, & \forall\boldsymbol{y}\in Y, \quad (3.7a)\\ \boldsymbol{\sigma}^{1}(\boldsymbol{x},\boldsymbol{y})=\mathbb{C}(\boldsymbol{y}):\left(\varepsilon_{y}(\boldsymbol{u}^{2})+\boldsymbol{\eta}^{1}(\boldsymbol{x},\boldsymbol{y})\right), & \forall\boldsymbol{y}\in Y, \quad (3.7b)\\ \boldsymbol{u}^{2}(\boldsymbol{x},\boldsymbol{y}) & \text{is } Y-\text{periodic}, \quad (3.7c)\\ \boldsymbol{\sigma}^{1}(\boldsymbol{x},\boldsymbol{y})\cdot\boldsymbol{n} & \text{is } Y-\text{antiperiodic}, \quad (3.7d)\end{cases}$$

with:

$$\varepsilon_{y}(\boldsymbol{u}^{2})=\operatorname{sym}\left(\nabla_{y}\boldsymbol{u}^{2}\right)=\frac{1}{2}\left(\nabla_{y}\boldsymbol{u}^{2}+\left(\nabla_{y}\boldsymbol{u}^{2}\right)^{\top}\right). \tag{3.8}$$

The body force $\boldsymbol{L}^{1}(\boldsymbol{x},\boldsymbol{y})$ and the strain field $\boldsymbol{\eta}^{1}(\boldsymbol{x},\boldsymbol{y})$ read:

$$\begin{cases}\boldsymbol{L}^{1}(\boldsymbol{x},\boldsymbol{y})=\left(\mathbb{B}^{0}(\boldsymbol{y})-\left\langle\mathbb{B}^{0}(\boldsymbol{y})\right\rangle_{Y}\right)\vdots\boldsymbol{\nabla}_{x}\boldsymbol{E}(\boldsymbol{x}),\\ \boldsymbol{\eta}^{1}(\boldsymbol{x},\boldsymbol{y})=\operatorname{sym}\left(\mathbb{D}^{0}(\boldsymbol{y}):\boldsymbol{\nabla}_{x}\boldsymbol{E}(\boldsymbol{x})\right).\end{cases} \tag{3.9}$$

The periodic fluctuation $\boldsymbol{u}^{2}$ takes the following form:

$$\boldsymbol{u}^{2}(\boldsymbol{x},\boldsymbol{y})=\mathbb{D}^{1}(\boldsymbol{y})\vdots\boldsymbol{\nabla}_{x}\boldsymbol{E}(\boldsymbol{x}), \tag{3.10}$$

where $\mathbb{D}^{1}(\boldsymbol{y})$ is a fourth-rank tensor, called second-order displacement localization tensor. It is periodic over unit-cell Y and verifies $\left\langle\mathbb{D}^{1}\right\rangle_{Y}=0$, where $\langle\bullet\rangle_{Y}=\frac{1}{|Y|}\int_{Y}\bullet\,dY$ indicates the volume average over unit-cell Y.

The second-order strain corrector reads:

$$\boldsymbol{\varepsilon}^1(\boldsymbol{x},\boldsymbol{y}) = \mathbb{A}^1(\boldsymbol{y}) \vdots \boldsymbol{\nabla}_x \boldsymbol{E}(\boldsymbol{x}), \tag{3.11}$$

where $\mathbb{A}^1(\boldsymbol{y})$ is a fifth-rank tensor, called second-order strain localization tensor. We therefore can define the second-order stress corrector as:

$$\boldsymbol{\sigma}^1(\boldsymbol{x},\boldsymbol{y}) = \mathbb{C}(\boldsymbol{y}) : \boldsymbol{\varepsilon}^1(\boldsymbol{x},\boldsymbol{y}) = \mathbb{B}^1(\boldsymbol{y}) \vdots \boldsymbol{\nabla}_x \boldsymbol{E}(\boldsymbol{x}), \tag{3.12}$$

where

$$\mathbb{B}^1(\boldsymbol{y}) = \mathbb{C}(\boldsymbol{y}) : \mathbb{A}^1(\boldsymbol{y}), \tag{3.13}$$

is the fifth-rank stress localization tensor.
The effective, fifth-rank, elasticity tensor $\mathbb{C}^1$, which depends on the microstructure, is deduced from the volume average of the stress localization tensor over the unit-cell:

$$\mathbb{C}^1 = \left\langle \mathbb{B}^1(\boldsymbol{y}) \right\rangle_Y. \tag{3.14}$$

The tensor $\mathbb{C}^1$ is of odd rank and therefore equals to *zero* in the case of centro-symmetric unit-cell.

Third-order periodic problem $\left(\mathscr{P}^{3^{rd}}_{order}\right)$

This problem is defined on the unit-cell Y. Its solution are the displacement corrector $\boldsymbol{u}^3$ and stress $\boldsymbol{\sigma}^2$. It reads:

Find $(\boldsymbol{u}^3, \boldsymbol{\sigma}^2)$ such that:

$$\left(\mathscr{P}^{3^{rd}}_{order}\right): \begin{cases} \operatorname{div}_y\left(\boldsymbol{\sigma}^2(\boldsymbol{x},\boldsymbol{y})\right) + \boldsymbol{L}^2(\boldsymbol{x},\boldsymbol{y}) = 0, & \forall \boldsymbol{y} \in Y, \quad (3.15a) \\ \boldsymbol{\sigma}^2(\boldsymbol{x},\boldsymbol{y}) = \mathbb{C}(\boldsymbol{y}) : \left(\boldsymbol{\varepsilon}_y(\boldsymbol{u}^3) + \boldsymbol{\eta}^2(\boldsymbol{x},\boldsymbol{y})\right), & \forall \boldsymbol{y} \in Y, \quad (3.15b) \\ \boldsymbol{u}^3(\boldsymbol{x},\boldsymbol{y}) & \text{is } Y-\text{periodic}, \quad (3.15c) \\ \boldsymbol{\sigma}^2(\boldsymbol{x},\boldsymbol{y}) \cdot \boldsymbol{n} & \text{is } Y-\text{antiperiodic}. \quad (3.15d) \end{cases}$$

The body force $\boldsymbol{L}^2(\boldsymbol{x},\boldsymbol{y})$ and the strain field $\boldsymbol{\eta}^2(\boldsymbol{x},\boldsymbol{y})$ read:

$$\begin{cases} \boldsymbol{L}^2(\boldsymbol{x},\boldsymbol{y}) = \left(\mathbb{B}^1(\boldsymbol{y}) - \left\langle \mathbb{B}^1(\boldsymbol{y}) \right\rangle_Y\right) :: \boldsymbol{\nabla}_x \boldsymbol{\nabla}_x \boldsymbol{E}(\boldsymbol{x}), \\ \boldsymbol{\eta}^2(\boldsymbol{x},\boldsymbol{y}) = \operatorname{sym}\left(\mathbb{D}^1(\boldsymbol{y}) \vdots \boldsymbol{\nabla}_x \boldsymbol{\nabla}_x \boldsymbol{E}(\boldsymbol{x})\right). \end{cases} \tag{3.16}$$

Similarly to the second-order, a body force and eigenstrain based on the solution to the previous order are prescribed over the unit-cell.
The periodic fluctuation $\boldsymbol{u}^3$, solution to the third-order problem, reads:

$$\boldsymbol{u}^3(\boldsymbol{x},\boldsymbol{y}) = \mathbb{D}^2(\boldsymbol{y}) :: \boldsymbol{\nabla}_x \boldsymbol{\nabla}_x \boldsymbol{E}(\boldsymbol{x}), \tag{3.17}$$

where $\mathbb{D}^2(\boldsymbol{y})$ is a fifth-rank tensor, called third-order displacement localization tensor. It is periodic over unit-cell Y and verifies $\langle \mathbb{D}^2 \rangle_Y = 0$.
The third-order strain corrector reads:

$$\boldsymbol{\varepsilon}^2(\boldsymbol{x},\boldsymbol{y}) = \mathbb{A}^2(\boldsymbol{y}) :: \boldsymbol{\nabla}_x \boldsymbol{\nabla}_x \boldsymbol{E}(\boldsymbol{x}), \tag{3.18}$$

where $\mathbb{A}^2(\boldsymbol{y})$ is a sixth-rank tensor, called third-order strain localization tensor. We can therefore define the third-order stress corrector as:

$$\boldsymbol{\sigma}^2(\boldsymbol{x},\boldsymbol{y}) = \mathbb{C}(\boldsymbol{y}) : \boldsymbol{\varepsilon}^2(\boldsymbol{x},\boldsymbol{y}) = \mathbb{B}^2(\boldsymbol{y}) :: \boldsymbol{\nabla}_x \boldsymbol{\nabla}_x \boldsymbol{E}(\boldsymbol{x}), \tag{3.19}$$

where

$$\mathbb{B}^2(\boldsymbol{y}) = \mathbb{C}(\boldsymbol{y}) : \mathbb{A}^2(\boldsymbol{y}), \tag{3.20}$$

is the third-rank stress localization tensor.
The effective, sixth-rank, elasticity tensor $\mathbb{C}^2$ reads:

$$\mathbb{C}^2 = \langle \mathbb{B}^2(\boldsymbol{y}) \rangle_Y. \tag{3.21}$$

For both second and third-order problems, the applied body forces and eigenstrains are related to successive gradients of the macroscopic strain tensor. Hence, the resolution of these problems introduces a non-local effect on material behavior. When strain gradients are significant, contributions of higher-order correctors become significant as well. In contrast, a weaker contribution is expected for quasi-homogeneous deformation cases. For these reasons, the possible drawback of QBCs approaches highlighted in the introduction, that strain gradient effects persist even when the material is homogeneous, does not concern periodic homogenization based on asymptotic series expansion.

3.2.2 Proposed micromechanical fields estimates

Fergoug et al. [2022a] have shown that a first-order relocalization may provide an accurate estimate of DNS fields, provided that macroscale strain gradients remain sufficiently small. Indeed, for a bending case, it was shown that the first-order estimate may not be accurate anymore [Fergoug et al., 2022a].
We propose a better estimate of DNS fields by conducting a higher-order relocalization process which takes into account additional terms of the asymptotic expansion, up to the third-order. This is expected to capture the effect of macroscopic successive gradients, and thus introduce a length scale in the modeling.
This estimate is built here using:

- The macroscale strain and its successive gradients obtained from the resolution of the homogeneous problem $(\mathscr{P}_{hom})$. We recall that the homogenized macroscopic continuum is a scale-independent Cauchy type.
- localization tensors $(\mathbb{D}^0, \mathbb{A}^0, \mathbb{B}^0)$, $(\mathbb{D}^1, \mathbb{A}^1, \mathbb{B}^1)$, and $(\mathbb{D}^2, \mathbb{A}^2, \mathbb{B}^2)$ obtained from the resolution of $\left(\mathscr{P}^{1^{st}}_{order}\right)$, $\left(\mathscr{P}^{2^{nd}}_{order}\right)$, and $\left(\mathscr{P}^{3^{rd}}_{order}\right)$, respectively.

The proposed estimates in the composite read:

$$\left.\begin{aligned} \boldsymbol{u}^{est}(\boldsymbol{x},\boldsymbol{y}) &= \boldsymbol{U}(\boldsymbol{x}) \\ &+ \boldsymbol{\varepsilon}\, \mathbb{D}^0(\boldsymbol{y}) : \boldsymbol{E}(\boldsymbol{x}) \\ &+ \boldsymbol{\varepsilon}^2\, \mathbb{D}^1(\boldsymbol{y}) \vdots \boldsymbol{\nabla}_x \boldsymbol{E}(\boldsymbol{x}) \\ &+ \boldsymbol{\varepsilon}^3\, \mathbb{D}^2(\boldsymbol{y}) :: \boldsymbol{\nabla}_x \boldsymbol{\nabla}_x \boldsymbol{E}(\boldsymbol{x}) \end{aligned}\right\} \quad \forall \boldsymbol{x} \in \Omega,\ \forall \boldsymbol{y} \in Y, \tag{3.22}$$

$$\left.\begin{aligned} \boldsymbol{\varepsilon}^{est}(\boldsymbol{x},\boldsymbol{y}) &= \mathbb{A}^0(\boldsymbol{y}) : \boldsymbol{E}(\boldsymbol{x}) \\ &+ \boldsymbol{\varepsilon}\, \mathbb{A}^1(\boldsymbol{y}) \vdots \boldsymbol{\nabla}_x \boldsymbol{E}(\boldsymbol{x}) \\ &+ \boldsymbol{\varepsilon}^2\, \mathbb{A}^2(\boldsymbol{y}) :: \boldsymbol{\nabla}_x \boldsymbol{\nabla}_x \boldsymbol{E}(\boldsymbol{x}) \end{aligned}\right\} \quad \forall \boldsymbol{x} \in \Omega,\ \forall \boldsymbol{y} \in Y, \tag{3.23}$$

$$\left.\begin{aligned} \boldsymbol{\sigma}^{est}(\boldsymbol{x},\boldsymbol{y}) &= \mathbb{B}^0(\boldsymbol{y}) : \boldsymbol{E}(\boldsymbol{x}) \\ &+ \boldsymbol{\varepsilon}\, \mathbb{B}^1(\boldsymbol{y}) \vdots \boldsymbol{\nabla}_x \boldsymbol{E}(\boldsymbol{x}) \\ &+ \boldsymbol{\varepsilon}^2\, \mathbb{B}^2(\boldsymbol{y}) :: \boldsymbol{\nabla}_x \boldsymbol{\nabla}_x \boldsymbol{E}(\boldsymbol{x}) \end{aligned}\right\} \quad \forall \boldsymbol{x} \in \Omega,\ \forall \boldsymbol{y} \in Y. \tag{3.24}$$

3.3 Boundary layer correction

While asymptotic homogenization may provide an accurate estimate of local fields within the structure based on a relocalization process, the construction of a solution near the boundaries remains beyond its capability. This is mainly explained by the loss of the periodicity assumption in the vicinity of boundaries.
Fergoug et al. [2022a] have proposed a new approach to correct first-order estimates, constructed by a first-order relocalization process. This approach is based on the idea of introducing corrective terms that would decay inward the material, far from boundaries. These terms are obtained from the resolution of various problems over the unit-cell. The nature of the problems to be solved depends on the actual boundary conditions applied to the structure. The proposed approach is general, *i.e.* valid for different BCs: Dirichlet, Neumann, or mixed.
In this section, an extension of this method is proposed to correct higher-order estimated fields, $(\boldsymbol{u}^{est}, \boldsymbol{\varepsilon}^{est}, \boldsymbol{\sigma}^{est})$ defined in Eq. (3.22), (3.23), (3.24), respectively. To do so, supplementary problems over the unit-cell, besides those of a first-order correction, must be considered: 18 additional problems for second-order correction and 54 for third-order correction.

3.3.1 Correctors for Neumann BCs

The homogenized problem $(\mathscr{P}_{hom})$ can be written as:

$$\begin{cases} \operatorname{div}(\boldsymbol{\Sigma}(\boldsymbol{x})) + \boldsymbol{f}(\boldsymbol{x}) = 0, & \forall \boldsymbol{x} \in \boldsymbol{\Omega}, \quad (3.25a) \\ \boldsymbol{\Sigma}(\boldsymbol{x}) = \mathbb{C}^0 : \boldsymbol{E}(\boldsymbol{x}), & \forall \boldsymbol{x} \in \boldsymbol{\Omega}, \quad (3.25b) \\ \boldsymbol{U}(\boldsymbol{x}) = \boldsymbol{u}^d, & \forall \boldsymbol{x} \in \boldsymbol{\Gamma}_{\boldsymbol{u}}, \quad (3.25c) \\ \boldsymbol{\Sigma}(\boldsymbol{x}) \cdot \boldsymbol{n} = \boldsymbol{F}^d, & \forall \boldsymbol{x} \in \boldsymbol{\Gamma}_{\boldsymbol{t}}, \quad (3.25d) \end{cases}$$

with the macroscale stress: $\langle \boldsymbol{\sigma}^{est} \rangle_Y = \boldsymbol{\Sigma}$ and strain: $\langle \boldsymbol{\varepsilon}^{est} \rangle_Y = \boldsymbol{E}$.
It is apparent from problem (3.25d) that the boundary condition on $\boldsymbol{\Gamma}_{\boldsymbol{t}}$ is only satisfied by the mean value of $\boldsymbol{\sigma}^{est}$, therefore, in general:

$$\boldsymbol{\sigma}^{est} \cdot \boldsymbol{n} \neq \boldsymbol{F}^d. \quad (3.26)$$

Corrective term $\boldsymbol{\sigma}^{bl}$ is introduced, whose sum with the estimated stress field $\boldsymbol{\sigma}^{est}$ satisfies exactly the Neumann boundary condition at each microscopic point, then:

$$\left(\boldsymbol{\sigma}^{est} + \boldsymbol{\sigma}^{bl}\right) \cdot \boldsymbol{n} = \boldsymbol{F}^d. \quad (3.27)$$

We propose to compute $\boldsymbol{\sigma}^{bl}$ by considering auxiliary problems on the unit-cell, subjected to characteristic loads F_i with $i \in \{1,2,3\}$ where the Neumann boundary condition is applied. The opposite surface is fixed, and other remaining surfaces are subjected to periodicity conditions (see [Fergoug et al., 2022a] for more details). The expression of characteristic loads depends on the order of the boundary correction:

- First-order corrective load:

$$F^0_{ikl} = -B^0_{ijkl}\, n_j + \frac{1}{|Y|} \int_Y B^0_{ijkl}\, n_j \, dY. \quad (3.28)$$

B^0_{ijkl} are components of the first-order stress localization tensor $\mathbb{B}^0$ and $kl = \{11,22,33,23,31,12\}_6$. Therefore, 6 loads are applied successively over the unit-cell.

- Second-order corrective load:

$$F^1_{iklm} = -B^1_{ijklm}\, n_j + \frac{1}{|Y|} \int_Y B^1_{ijklm}\, n_j \, dY. \quad (3.29)$$

B^1_{ijklm} are components of the second-order stress localization tensor $\mathbb{B}^1$ and $klm = \{111,211,311,...,112,212,312\}_{18}$. Therefore, 18 loads are applied successively over the unit-cell.

- Third-order corrective load:

$$F^2_{iklmn} = -B^2_{ijklmn}\, n_j + \frac{1}{|Y|}\int_Y B^2_{ijklmn}\, n_j\, dY. \tag{3.30}$$

B^2_{ijklmn} are components of the third-order stress localization tensor $\mathbb{B}^2$ and $klmn = \{1111, 2111, 3111, ..., 1312, 2312, 3312\}_{54}$. Therefore, 54 loads are applied successively over the unit-cell.

Note that $\boldsymbol{n}$ is the normal direction of $\boldsymbol{\Gamma_t}$. For instance, the normal vector $\boldsymbol{n}$ will be equal to $\frac{1}{\sqrt{2}}\begin{pmatrix}1 & 1 & 0\end{pmatrix}^\top$ in the case of a macroscopic boundary that has a 45° direction. The resulting displacement, strain, and stress fields obtained for each loading case provide a component of first, second, or third order boundary layer displacement, strain, and stress localization tensors ($\mathbb{D}^{0,bl}, \mathbb{A}^{0,bl}, \mathbb{B}^{0,bl}$), ($\mathbb{D}^{1,bl}, \mathbb{A}^{1,bl}, \mathbb{B}^{1,bl}$), and ($\mathbb{D}^{2,bl}, \mathbb{A}^{2,bl}, \mathbb{B}^{2,bl}$), respectively.
Therefore, the boundary layer correctors read:

$$\left.\begin{aligned}\boldsymbol{u}^{bl}(\boldsymbol{x},\boldsymbol{y}) = {}& \varepsilon \mathbb{D}^{0,bl}(\boldsymbol{y}) : \boldsymbol{E}(\boldsymbol{x}) \\ &+ \varepsilon^2\, \mathbb{D}^{1,bl}(\boldsymbol{y}) \vdots \boldsymbol{\nabla}_x \boldsymbol{E}(\boldsymbol{x}) \\ &+ \varepsilon^3\, \mathbb{D}^{2,bl}(\boldsymbol{y}) :: \boldsymbol{\nabla}_x \boldsymbol{\nabla}_x \boldsymbol{E}(\boldsymbol{x})\end{aligned}\right\} \quad \forall \boldsymbol{x} \in \boldsymbol{\Gamma_t},\ \forall \boldsymbol{y} \in Y, \tag{3.31}$$

$$\left.\begin{aligned}\boldsymbol{\varepsilon}^{bl}(\boldsymbol{x},\boldsymbol{y}) = {}& \mathbb{A}^{0,bl}(\boldsymbol{y}) : \boldsymbol{E}(\boldsymbol{x}) \\ &+ \boldsymbol{\varepsilon}\, \mathbb{A}^{1,bl}(\boldsymbol{y}) \vdots \boldsymbol{\nabla}_x \boldsymbol{E}(\boldsymbol{x}) \\ &+ \varepsilon^2\, \mathbb{A}^{2,bl}(\boldsymbol{y}) :: \boldsymbol{\nabla}_x \boldsymbol{\nabla}_x \boldsymbol{E}(\boldsymbol{x})\end{aligned}\right\} \quad \forall \boldsymbol{x} \in \boldsymbol{\Gamma_t},\ \forall \boldsymbol{y} \in Y, \tag{3.32}$$

$$\left.\begin{aligned}\boldsymbol{\sigma}^{bl}(\boldsymbol{x},\boldsymbol{y}) = {}& \mathbb{B}^{0,bl}(\boldsymbol{y}) : \boldsymbol{E}(\boldsymbol{x}) \\ &+ \boldsymbol{\varepsilon}\, \mathbb{B}^{1,bl}(\boldsymbol{y}) \vdots \boldsymbol{\nabla}_x \boldsymbol{E}(\boldsymbol{x}) \\ &+ \varepsilon^2\, \mathbb{B}^{2,bl}(\boldsymbol{y}) :: \boldsymbol{\nabla}_x \boldsymbol{\nabla}_x \boldsymbol{E}(\boldsymbol{x})\end{aligned}\right\} \quad \forall \boldsymbol{x} \in \boldsymbol{\Gamma_t},\ \forall \boldsymbol{y} \in Y. \tag{3.33}$$

As a result, the stress field $\boldsymbol{\sigma}^{cor}$

$$\boldsymbol{\sigma}^{cor} = \boldsymbol{\sigma}^{est} + \boldsymbol{\sigma}^{bl}, \tag{3.34}$$

satisfies the Neumann BC.

3.3.2 Correctors for Dirichlet BCs

It is clear from (3.25c) that the homogenized displacement field $\boldsymbol{U}$ verifies the Dirichlet BC, *i.e.* $\boldsymbol{U} = \boldsymbol{u}^d$ on $\boldsymbol{\Gamma}_u$. Therefore, $\boldsymbol{u}^{est}$ defined in Eq. (3.22) does not necessarily satisfy this BC. Therefore, a correction is needed that verifies:

$$\boldsymbol{u}^{cor}(\boldsymbol{x},\boldsymbol{y}) = \boldsymbol{U}(\boldsymbol{x}) + \Big(\boldsymbol{v}(\boldsymbol{x},\boldsymbol{y}) + \boldsymbol{u}^{bl}(\boldsymbol{x},\boldsymbol{y})\Big), \tag{3.35}$$

where the periodic fluctuation $\boldsymbol{v}$ reads:

$$\boldsymbol{v} = \boldsymbol{\varepsilon}\boldsymbol{u}^1(\boldsymbol{x},\boldsymbol{y}) + \boldsymbol{\varepsilon}^2\boldsymbol{u}^2(\boldsymbol{x},\boldsymbol{y}) + \boldsymbol{\varepsilon}^3\boldsymbol{u}^3(\boldsymbol{x},\boldsymbol{y}), \tag{3.36}$$

then

$$\begin{aligned}\boldsymbol{v} =& \boldsymbol{\varepsilon}\, \mathbb{D}^0(\boldsymbol{y}) : \boldsymbol{E}(\boldsymbol{x}) \\ &+ \boldsymbol{\varepsilon}^2\, \mathbb{D}^1(\boldsymbol{y}) \vdots \boldsymbol{\nabla}_x \boldsymbol{E}(\boldsymbol{x}) \\ &+ \boldsymbol{\varepsilon}^3\, \mathbb{D}^2(\boldsymbol{y}) :: \boldsymbol{\nabla}_x \boldsymbol{\nabla}_x \boldsymbol{E}(\boldsymbol{x}).\end{aligned} \tag{3.37}$$

The correction $\boldsymbol{u}^{bl}$ must verify:

$$\boldsymbol{u}^{bl}(\boldsymbol{x},\boldsymbol{y}) = -\boldsymbol{v}(\boldsymbol{x},\boldsymbol{y}), \qquad \forall \boldsymbol{x} \in \boldsymbol{\Gamma}_{\boldsymbol{u}},\ \forall \boldsymbol{y} \in Y. \tag{3.38}$$

Similarly to the Neumann boundary case, several auxiliary problems are considered providing boundary layer correctors. In this case, corrective displacements ρ_i with $i \in \{1,2,3\}$ are applied to the unit-cell and defined as:

- First-order corrective displacement:

$$\rho^0_{ikl} = -D^0_{ikl}, \tag{3.39}$$

with $kl = \{11,22,33,23,31,12\}_6$ and D^0_{ikl} are components of the first-order displacement localization tensor $\mathbb{D}^0$.

- Second-order corrective displacement:

$$\rho^1_{iklm} = -D^1_{iklm}, \tag{3.40}$$

with $klm = \{111,211,311,...,112,212,312\}_{18}$ and D^1_{iklm} are components of the second-order displacement localization tensor $\mathbb{D}^1$.

- Third-order corrective displacement:

$$\rho^2_{iklmn} = -D^2_{iklmn}, \tag{3.41}$$

with $klmn = \{1111,2111,3111,...,1312,2312,3312\}_{54}$ and D^2_{iklmn} are components of the third-order displacement localization tensor $\mathbb{D}^2$.

The corrective boundary layer fields are obtained by conducting the same analyses defined in Eq. (3.31), (3.32), and (3.33).

Remark 1 *We recall that in order to compute boundary layer localization tensors, for Neumann boundary conditions, at different orders: ($\mathbb{D}^{0,bl}, \mathbb{A}^{0,bl}, \mathbb{B}^{0,bl}$), ($\mathbb{D}^{1,bl}, \mathbb{A}^{1,bl}, \mathbb{B}^{1,bl}$), and ($\mathbb{D}^{2,bl}, \mathbb{A}^{2,bl}, \mathbb{B}^{2,bl}$), auxiliary problems are solved over the unit-cell. In this case, the loads F^0_{ikl}, F^1_{iklm} and F^2_{iklmn} defined in Eq. (3.28), (3.29), and (3.30), are applied on the unit-cell. Similarly for Dirichlet boundary conditions, displacement fields ρ^0_{ikl}, ρ^1_{iklm}, and ρ^2_{iklmn}, defined in Eq. (3.39), (3.40), and (3.41), are applied on the unit-cell. Details concerning the formulation of auxiliary problems, at the first-order, are provided in Fergoug et al. [2022a], and are omitted here for higher-orders for the sake of conciseness.*

Remark 2 *For mixed BCs, the correction is derived by applying both characteristic load F_i and displacement ρ_i. The correction to be ultimately applied depends on the actual (Neumann or Dirichlet) BC applied in this specific direction. For more details, the reader is referred to Fergoug et al. [2022a].*

3.4 Numerical implementation

The objective of the relocalization process is to compute estimated fields $(\boldsymbol{u}^{est}, \boldsymbol{\varepsilon}^{est}, \boldsymbol{\sigma}^{est})$ defined in Eq. (3.22), (3.23), (3.24), respectively. To do so, three hierarchical sets of elasticity problems are solved over the unit-cell, with applied Periodic Boundary Conditions (PBC):

• **First-order problem** $\left(\mathscr{P}^{1^{st}}_{order}\right)$: After discretizing the unit-cell domain, six linearly independent unit strain loads are applied (for 3D cases). By using the modified Voigt notations, the macroscale strain field reads:

$$\boldsymbol{E} = \left(E_{11}, E_{22}, E_{33}, \sqrt{2}E_{23}, \sqrt{2}E_{31}, \sqrt{2}E_{12}\right)_6. \tag{3.42}$$

The solutions to these problems are first-order displacement, strain, and stress localization tensors: $\mathbb{D}^0$, $\mathbb{A}^0$, and $\mathbb{B}^0$, respectively. The homogenized elasticity tensor reads: $\mathbb{C}^0 = \left\langle \mathbb{B}^0(\boldsymbol{y}) \right\rangle_Y$.

• **Second-order problem** $\left(\mathscr{P}^{2^{nd}}_{order}\right)$: A body force $\boldsymbol{L}^1$ and eigenstrain $\boldsymbol{\eta}^1$ defined in Eq. (3.9), which depend on the resolution of $\left(\mathscr{P}^{1^{st}}_{order}\right)$, are prescribed over the unit-cell. Since these enforcing terms are connected with the gradient of strain $\boldsymbol{E}$, then one should apply 18 loads on the unit-cell. Indeed, $\boldsymbol{\nabla}_x \boldsymbol{E}$ is symmetric according to its first two indices $\left(E_{ij,k} = E_{ji,k}\right)$, then it is possible to represent it by a vector of dimension 18 as:

$$\boldsymbol{\nabla}_x \boldsymbol{E} = \left(E_{11,k}, E_{22,k}, E_{33,k}, \sqrt{2}E_{23,k}, \sqrt{2}E_{31,k}, \sqrt{2}E_{12,k}\right)_{18}, \text{ with } k = 1,2,3. \tag{3.43}$$

The solutions to these problems are second-order displacement, strain, and stress localization tensors: $\mathbb{D}^1$, $\mathbb{A}^1$, and $\mathbb{B}^1$, respectively.

• **Third-order problem** $\left(\mathscr{P}^{3^{rd}}_{order}\right)$: A body force $\boldsymbol{L}^2$ and eigenstrain $\boldsymbol{\eta}^2$ defined in Eq. (3.16), which depend on the resolution of $\left(\mathscr{P}^{2^{nd}}_{order}\right)$, are prescribed over the unit-cell. Since these enforcing terms are connected with the second gradient of strain $\boldsymbol{E}$, one should apply 54 loads on the unit-cell. Indeed, $\boldsymbol{\nabla}_x \boldsymbol{\nabla}_x \boldsymbol{E}$ can be represented by a vector of dimension 54:

$$\boldsymbol{\nabla}_x \boldsymbol{\nabla}_x \boldsymbol{E} = \left(E_{11,kj}, E_{22,kj}, E_{33,kj}, \sqrt{2}E_{23,kj}, \sqrt{2}E_{31,kj}, \sqrt{2}E_{12,kj}\right)_{54}, \text{ with } k,j = 1,2,3. \tag{3.44}$$

The solutions to these problems are third-order displacement, strain, and stress localization tensors: $\mathbb{D}^2$, $\mathbb{A}^2$, and $\mathbb{B}^2$, respectively.

Remark 3 *From a practical standpoint, solving* $\left(\mathscr{P}^{1^{st}}_{order}\right)$, $\left(\mathscr{P}^{2^{nd}}_{order}\right)$ *and* $\left(\mathscr{P}^{3^{rd}}_{order}\right)$ *corresponds to subjecting the unit-cell to 6, 18 or 54 gradients of various order of the strain field.*

Remark 4 *Localization tensors, of various orders, are functions of microstructural characteristics only, and are independent of the homogenized problem. Thus, these quantities are computed only once for each type of unit-cell.*

After discretizing the macroscale mesh, one can solve the homogenized problem $(\mathscr{P}_{hom})$ whose solution fields are $(\boldsymbol{U}, \boldsymbol{E}, \boldsymbol{\Sigma})$. Successive macroscale strain gradients are used to compute estimated fields defined in Eq. (3.22), (3.23), (3.24).

Remark 5 *Successive gradients of the macroscale strain, involved in higher-order relocalization processes, are resolved numerically. For instance, the gradient of the macroscale strain field,* $\nabla_x \boldsymbol{E}$*, has been evaluated by extrapolating corresponding strain values between integration points to the nodes and then appropriately differentiating them using the usual finite element shape functions. The same procedure is used to evaluate the second gradient of the macroscale strain field* $\nabla_x \nabla_x \boldsymbol{E}$*. Sufficient order of finite element shape functions is required.*

To eliminate mesh sensitivity and facilitate the computation of error estimates, we consider that the macroscale mesh is identical to the microscale one, but endowed with homogenized properties. If not, a mapping of the homogeneous fields on the microscale mesh could be considered as shown by Kruch [2007]. An intermediate step is then considered to locate each unit-cell on the macroscale mesh as in Fergoug et al. [2022a].
The relocalization process improvement proposed by Kruch and Forest [1998] is considered. Estimated fields, in a given point of the unit-cell, are determined using localization tensors combined with the value of the current macroscale strain or its gradients *at this point*, and not its average over the unit-cell.
Once homogenization problems are solved, localization tensors are used to construct corrective loads and displacements for the boundary layer correction. Afterwards, boundary layer localization tensors $(\mathbb{D}^{0,bl}, \mathbb{A}^{0,bl}, \mathbb{B}^{0,bl})$, $(\mathbb{D}^{1,bl}, \mathbb{A}^{1,bl}, \mathbb{B}^{1,bl})$ and $(\mathbb{D}^{2,bl}, \mathbb{A}^{2,bl}, \mathbb{B}^{2,bl})$ are computed and used to compute boundary layer correctors defined in Eq. (3.31), (3.32), and (3.33).
Higher-order relocalization and boundary layer correction processes are summarized in Fig. 3.2.

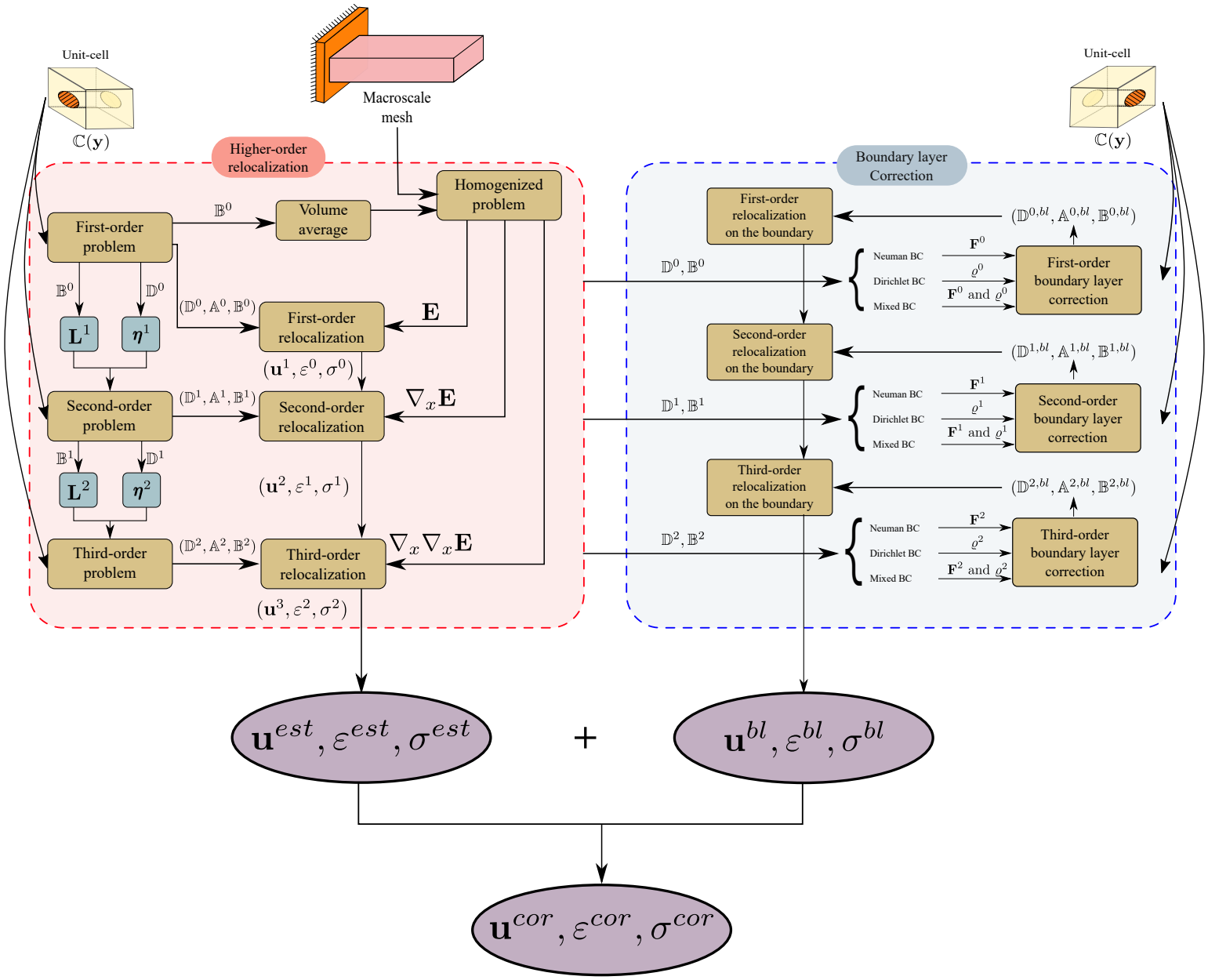

Figure 3.2: *Workflow describing higher-order relocalization and boundary layer correction processes.*

3.5 Numerical examples

To demonstrate the effectiveness of the proposed relocalization and boundary layer correction processes, two numerical examples of composite structures in linear elasticity are presented.
In these examples, we will compare the following fields:

- Microscale fields obtained by solving problem $\left(\mathscr{P}_{ref}\right)$ using DNS, which will be considered as our reference, indexed *ref*.
- Homogeneous fields obtained by solving problem $(\mathscr{P}_{hom})$, indexed *hom*.
- Proposed first, second, and third-order estimates of microscale fields obtained by the first, second, and third-order relocalization processes, indexed *est1*, *est2*, and *est3*, respectively.
- Proposed first, second, and third-order boundary layer corrections of estimated fields indexed *cor1*, *cor2*, and *cor3*, respectively.

We will also quantify the difference between the reference and estimated fields by computing the modeling error. For this purpose, the following local (element-wise) error in energy norm is defined:

$$\begin{aligned}\|\boldsymbol{e}\|_{E(\Omega_e)} &= \|\boldsymbol{u}^{ref}(\boldsymbol{x}) - \boldsymbol{u}^{k}(\boldsymbol{x})\|_{E(\Omega_e)} \\ &= \left(\int_{\Omega_e} \nabla^s\left(\boldsymbol{u}^{ref}(\boldsymbol{x}) - \boldsymbol{u}^{k}(\boldsymbol{x})\right) : \mathbb{C} : \nabla^s\left(\boldsymbol{u}^{ref}(\boldsymbol{x}) - \boldsymbol{u}^{k}(\boldsymbol{x})\right) d\Omega_e\right)^{\frac{1}{2}},\end{aligned} \tag{3.45}$$

where Ω_e denotes the domain of an element and $\boldsymbol{u}^k(\boldsymbol{x})$ denotes the estimated displacement field whose error is measured. The global error $\|\boldsymbol{e}\|_{E(\Omega)}$ is then defined as:

$$\|\boldsymbol{e}\|^2_{E(\Omega)} = \sum_e \|\boldsymbol{e}\|^2_{E(\Omega_e)}. \tag{3.46}$$

3.5.1 Laminated composite in bending

We consider a plane strain elasticity problem of a laminated composite made of two layers as presented in Fig. 3.3. The size of the structure is $L = 8$ mm, $H = 5$ mm and $W = 1$ mm. The two layers are assumed to be isotropic linear elastic with coefficients ($E_m = 500$ MPa, $\nu_m = 0.3$) and ($E_f = 5000, \nu_f = 0.3$).

In this example, we consider that $\varepsilon = 1$. Therefore, mechanical fields depend only on $\boldsymbol{x}$, representing *both* microscale and macroscale coordinates. The finite element mesh describing the unit-cell is composed of 1600 fifteen-node wedge elements as shown in Fig. 3.3. The mesh describing the entire structure including all heterogeneities is composed of 64 000 elements, corresponding to 867 909 degrees of freedom.

Remark 6 *In order to correct the mixed boundary Γ_s, it is necessary to apply both the Neumann and Dirichlet boundary corrections.*

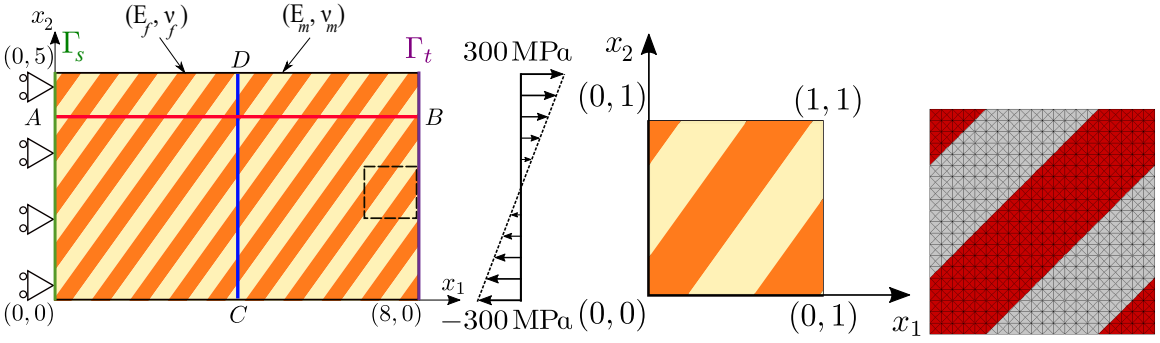

(a) *Structure geometry* (b) *Unit-cell domain* (c) *Unit-cell mesh*

Figure 3.3: *Illustration of the laminated composite subjected to bending. The structure is sliding on Γ_s and a surface bending is applied on Γ_t. Other boundaries are kept free of forces. Results will be plotted along AB and CD lines. Boundary layer correctors will be plotted for the boundary cell with a dashed line.*

Comparison of stress fields

Comparison of resulting stress fields along AB and CD lines are presented in Fig. 3.4. First-order estimates, *i.e.* σ_{11}^{est1} and σ_{12}^{est1}, obtained by the first-order relocalization process, are inaccurate in the inner domain of the structure. This is mainly explained by high macroscale strain gradients induced by the bending and neglected by classical first-order relocalization.
We propose to conduct a higher-order relocalization process, up to the third-order, to introduce the effects of the macroscale strain gradients. As noticed in Fig. 3.6, second-order estimates, *i.e.* σ_{11}^{est2} and σ_{12}^{est2}, and third-order estimates, *i.e.* σ_{11}^{est3} and σ_{12}^{est3}, perfectly coincide with the reference inside the structure.

Remark 7 *In this example, the contribution of third-order relocalization is negligible compared to second-order relocalization. This is explained by the low second gradient of the macroscale strain field, $\nabla_x\nabla_x \boldsymbol{E}$, induced by the bending. For the sake of conciseness, upcoming analyses will be restricted up to the second-order.*

The estimated fields lose their accuracy near the boundaries. This is due to the loss of periodicity in the vicinity of these regions.
We propose a boundary layer correction method based on the computation of corrective terms, that decay toward the interior of the body. Figures 3.5a and 3.5b show first and second-order boundary layer correctors σ_{11}^{bl1}, and σ_{11}^{bl2}, respectively. The decay of both boundary corrections takes place over one unit-cell. These corrective terms are added to the estimated fields obtained from the relocalization processes.
First-order ($cor1$) and second-order ($cor2$) corrected fields plotted along AB and CD lines are presented in Fig. 3.6.

Remark 8 *Boundary layer correctors are introduced at each order. Thus, for instance: $\sigma_{11}^{cor1} = \sigma_{11}^{est1} + \sigma_{11}^{bl1}$, and $\sigma_{11}^{cor2} = \sigma_{11}^{cor1} + \sigma_{11}^{bl2}$.*

First-order corrected fields are still inaccurate on the boundaries, contrarily to second-order corrected fields which are in good agreement with the reference fields. In particular, σ_{11}^{cor2} verifies the applied Neumann condition at $x_1 = 8$ mm similarly to the reference

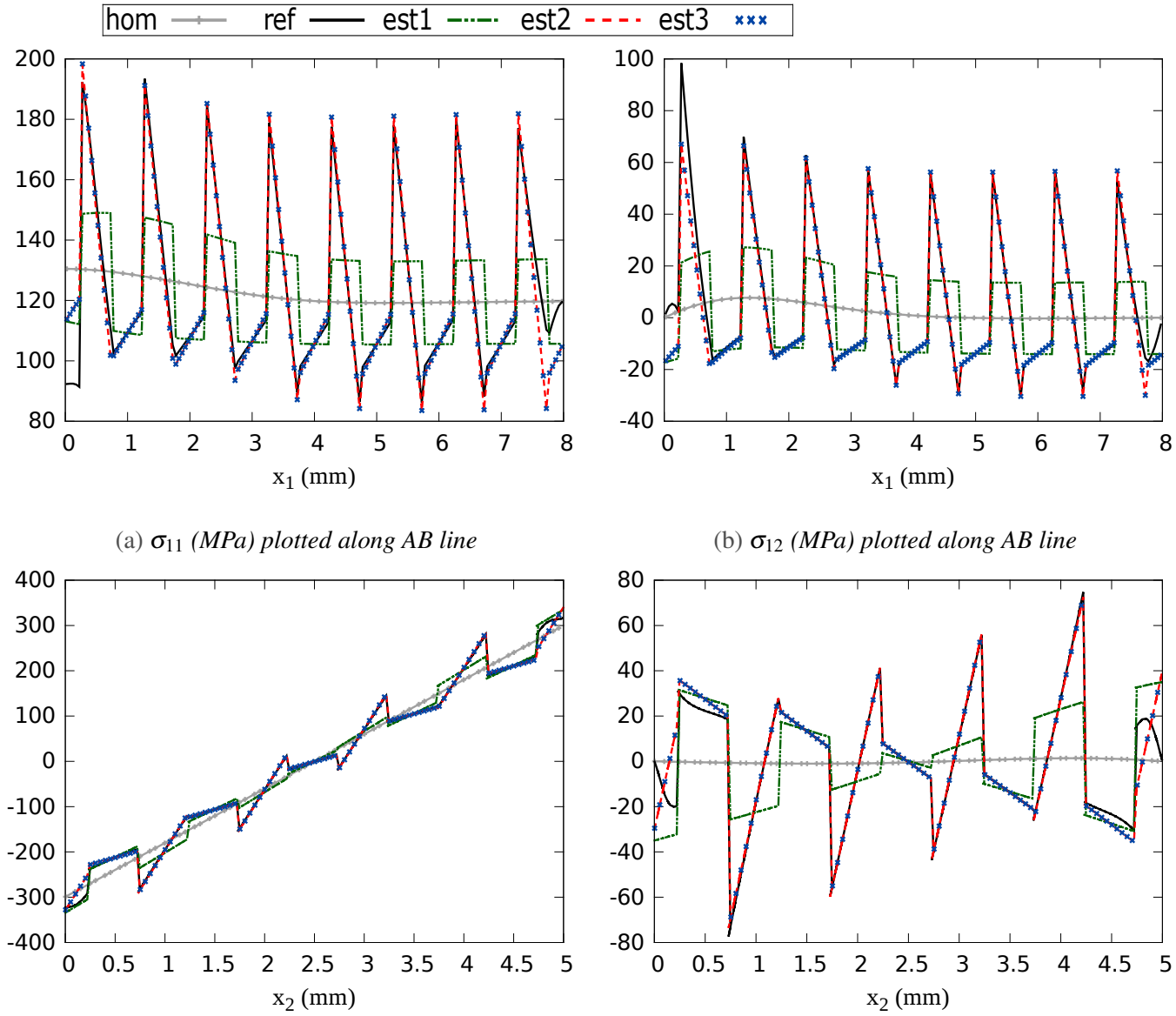

(a) σ_{11} *(MPa) plotted along AB line*

(b) σ_{12} *(MPa) plotted along AB line*

(c) σ_{11} *(MPa) plotted along CD line*

(d) σ_{12} *(MPa) plotted along CD line*

Figure 3.4: *Results of the homogenized (hom) and reference (ref) fields compared with the first-order (est1), second-order (est2), and third-order (est3) estimates for the laminated composite in bending.*

and the homogeneous counterparts, but it is not the case for σ_{11}^{est1}.
We also notice that high stresses are developed inside the structure *and* in the vicinity of the sliding boundary Γ_s as shown in figure 3.6, which may result in underestimating failure criteria if the design is conducted without the higher-order relocalization and boundary layer correction.
A more precise quantification of the error is provided in the next subsection.

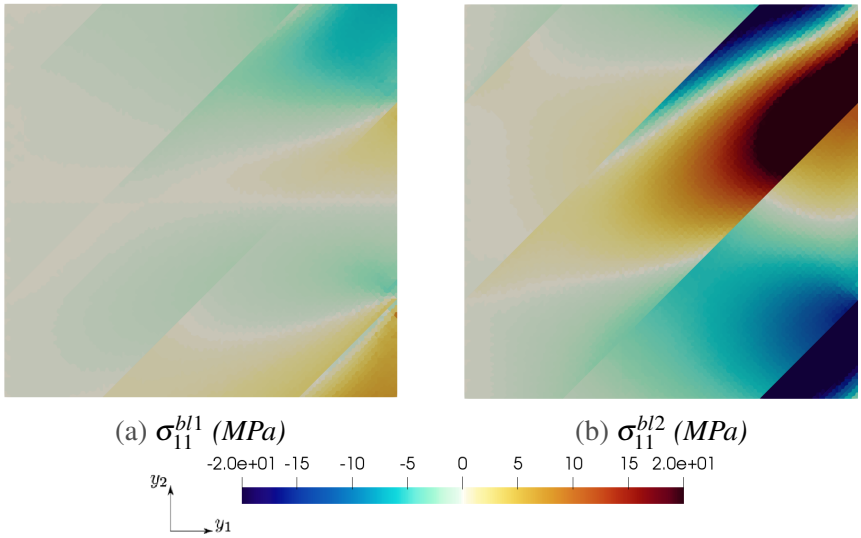

Figure 3.5: *First-order (σ_{11}^{bl1}) and second-order (σ_{11}^{bl2}) boundary layer correctors for the boundary cell with a dashed line in Fig. 3.3. The decay inward (left side of the unit-cell) of both boundary corrections takes place over one unit-cell.*

Modeling error

Local relative modeling errors between the reference and first-order relocalized fields, before and after the boundary layer correction, are shown in Fig. 3.7a and 3.7b, respectively. After the boundary layer correction, the error is reduced on the boundaries, yet still spread inside the structure. For second-order fields, the error before the correction (Fig. 3.7c), is negligible in the inner domain of the structure but significant on the boundaries, especially in the vicinity of the sliding boundary Γ_s. After the correction, the modeling error is drastically reduced but remains concentrated at the corners, as shown in Fig. 3.7d.

Remark 9 *A particular treatment was considered for corner cells correction, as explained by Fergoug et al. [2022a]. This correction improves the overall result, yet leaves some residual errors because of the loss of periodicity conditions. Indeed, as shown in Fergoug et al. [2022a], Periodic Boundary Conditions (PBC) are not applied for corner cells, contrary to other boundaries where PBC are considered. The corner cells correction can be improved by considering a boundary layer correction applied to four unit-cells instead of one, as shown in appendix D.2.*

Table 3.1 summarizes the global relative modeling error for different fields. Second-order relocalization combined with the boundary layer correction allows to drastically reduce the global modeling error by a factor of 3 to 4.

Remark 10 *The use of a Cauchy continuum on the macroscale can lead to errors in the relocalization process for some microstructures and loading conditions as shown in appendix B.3. In these cases, a higher continuum should be considered at the macroscale.*

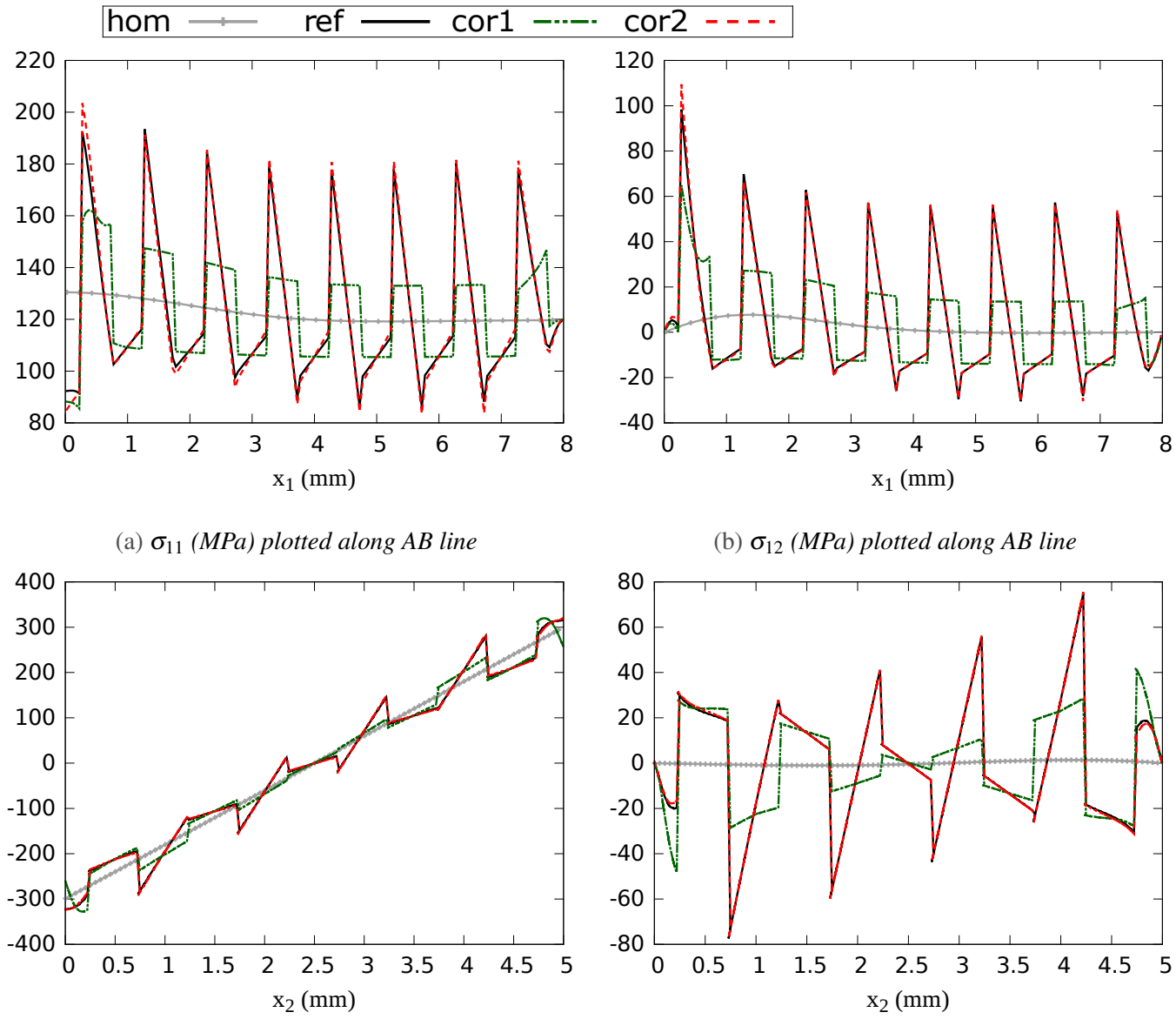

(a) σ_{11} *(MPa) plotted along AB line*

(b) σ_{12} *(MPa) plotted along AB line*

(c) σ_{11} *(MPa) plotted along CD line*

(d) σ_{12} *(MPa) plotted along CD line*

Figure 3.6: *Results of the homogenized (hom) and reference (ref) fields compared with the corrected first-order (cor1), and second-order (cor2) estimates for the laminated composite in bending.*

Table 3.1: *Comparison of the global relative modeling error for different fields.*

Global modeling error	$k =$ *est*1	$k =$ *cor*1	$k =$ *est*2	$k =$ *cor*2
$\frac{\|\boldsymbol{u}^{ref}-\boldsymbol{u}^{k}\|_{E(\Omega)}}{\|\boldsymbol{u}^{ref}\|_{E(\Omega)}}$	16.6%	10.9%	14.4%	4.7%

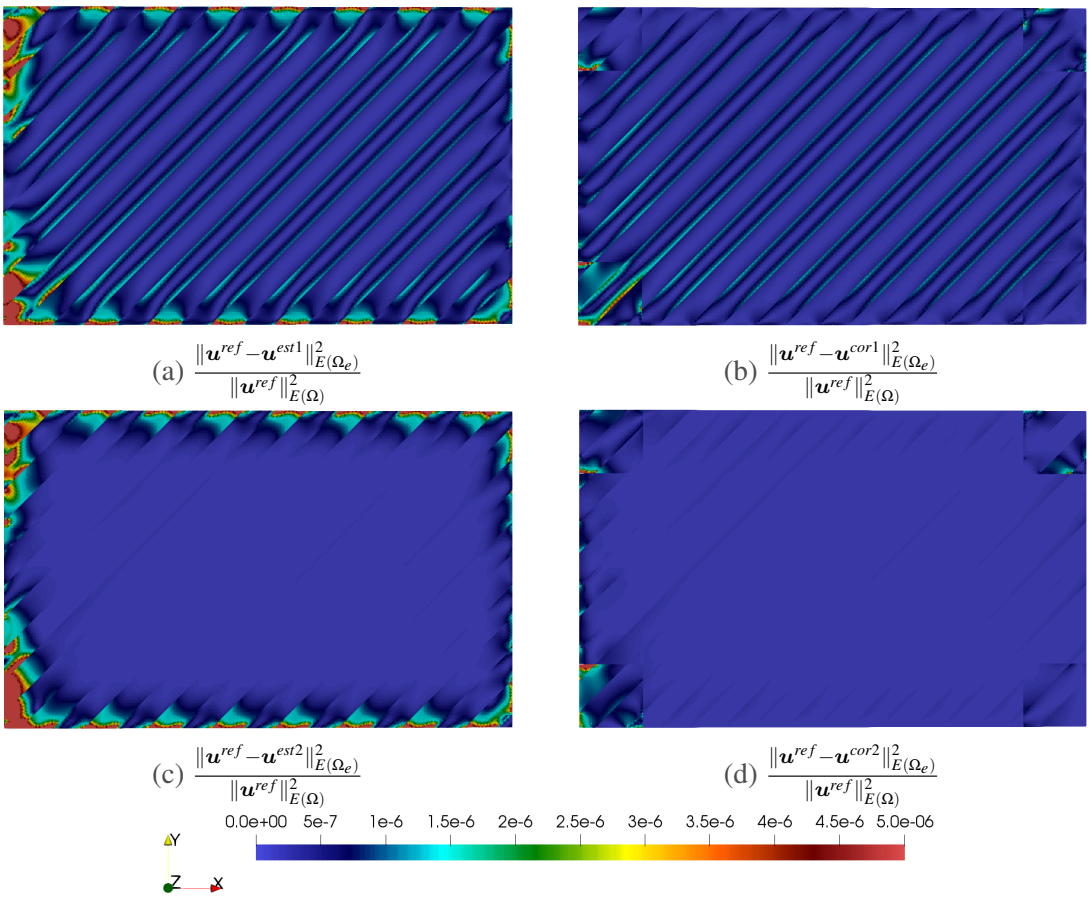

Figure 3.7: *Comparison of the local relative modeling error results for the laminated composite in bending. The modeling error is drastically reduced by increasing the order of the relocalization and boundary layer correction.*

3.5.2 Matrix-inclusion composite subjected to prescribed body forces

We consider the in-plane linear elasticity problem of a matrix-inclusion composite, as depicted in Fig. 3.8, subjected to body forces (f_1 and f_2) in the two space directions, with Γ_u fixed. The size of the structure is $L = 1$ mm and $H = 1$ mm with fiber volume fraction of 0.25; matrix and inclusions are assumed to be isotropic linear elastic with coefficients ($E_m = 1$ MPa, $\nu_m = 1/3$) and ($E_f = 100$, $\nu_f = 1/3$), respectively. In this example, the scale ratio $\varepsilon = 1/3$. The finite element mesh describing the unit-cell is composed of 6300 twenty-node brick elements as shown in Fig. 3.8. The mesh describing the entire structure including all heterogeneities is composed of 56 700 elements, corresponding to 1 193 409 degrees of freedom.

Body forces are prescribed in the form:

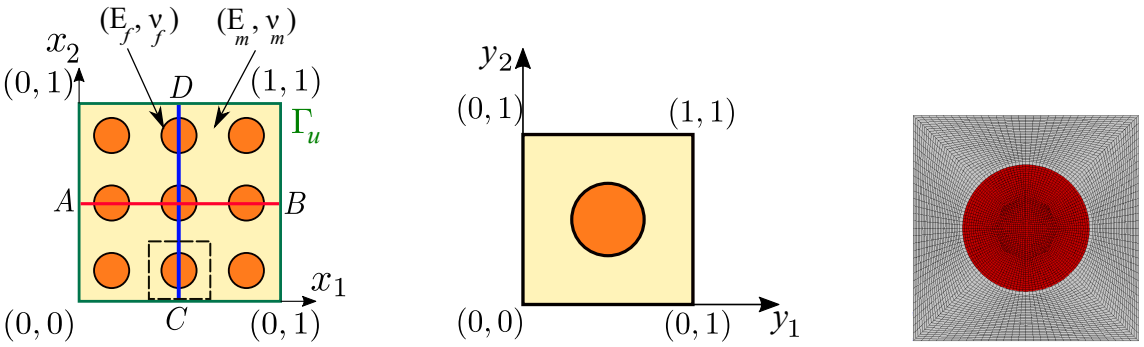

(a) *Structure geometry* (b) *Unit-cell domain* (c) *Unit-cell mesh*

Figure 3.8: *Illustration of matrix-inclusion composite. The structure is fixed on Γ_u, body forces f_1 and f_2 are applied in the two directions of space. Results will be plotted along AB and CD lines. Boundary layer correctors will be plotted for the boundary cell with a dashed line.*

$$\begin{cases} f_1 = \sin(\pi x_1)\sin(\pi x_2) - \dfrac{C^0_{1122} + C^0_{1212}}{C^0_{2222} + C^0_{1212}} \cos(\pi x_1)\cos(\pi x_2), & \text{(3.47a)} \\ f_2 = \sin(\pi x_1)\sin(\pi x_2) - \dfrac{C^0_{2211} + C^0_{1212}}{C^0_{1111} + C^0_{1212}} \cos(\pi x_1)\cos(\pi x_2). & \text{(3.47b)} \end{cases}$$

The choice of the applied body forces f_1 and f_2 is justified by the resulting simple analytical solutions obtained for the homogenized problem ($\mathscr{P}_{hom}$). Indeed, the homogenized displacement field is:

$$\begin{cases} U_i = X_i \sin(\pi x_1)\sin(\pi x_2), & \text{(3.48a)} \\ X_1 = \dfrac{1}{\pi^2 \left(C^0_{1111} + C^0_{1212}\right)}, \; X_2 = \dfrac{1}{\pi^2 \left(C^0_{2222} + C^0_{1212}\right)}, & \text{(3.48b)} \end{cases}$$

where C^0_{ijkl} are the components of the effective tensor $\mathbb{C}^0$, and the homogenized material is orthotropic.

Remark 11 *Successive gradients of the macroscale strain are computed analytically.*

Therefore, numerical errors resulting from higher-order spatial derivatives of $\boldsymbol{E}$ *are avoided. In the general case,* $\boldsymbol{E}$ *and its successive gradients must be obtained numerically, as in the previous example 3.5.1.*

This problem 3.5.2 has also been treated by He and Pindera [2020b], where third-order relocalization is performed using a finite volume method. The boundary layer correction is conducted by applying the third-order relocalized displacement field, defined in Eq. 3.22, in the inner domain of the *fully* detailed, *i.e.* using DNS, boundary. This may be computationally cumbersome when the boundary domain is large. We propose an *alternative* boundary layer method, where corrective terms are obtained by the resolution of independent auxiliary problems over a *single unit-cell*, and then added to the relocalized fields as explained in section 3.3. The nature of the problems to be solved depends on the actual boundary conditions applied locally to the structure [Fergoug et al., 2022a]. A comparative study is performed in appendix B.2.

Comparison of stress fields

Comparisons of stress fields, before the boundary layer correction, along the AB and CD lines are presented in Fig. 3.9. Second and third-order estimates perfectly coincide with reference fields in the inner domain of the composite but are inaccurate near the boundaries. The first-order estimate, however, provides a poor approximation of the whole plotted domain. It is noticed, in Fig. 3.9, that third-order estimates provide slightly more accurate solutions than second-order estimates, especially near the boundaries, albeit at a higher computation cost.

First (σ_{11}^{bl1}), second (σ_{11}^{bl2}) and third-order (σ_{11}^{bl3}) boundary layer correctors are shown in figures 3.10a, 3.10b, and 3.10b, respectively. It is observed that the decay of the correction takes place over one unit-cell and becomes less pronounced by increasing the order of the correction.

Comparisons of stress fields, after the boundary layer correction, along the AB and CD lines are presented in Fig. 3.11. It is shown that corrected fields, near the boundaries, get closer to the reference by increasing the order of the correction.

Modeling error

The local relative modeling error, without the boundary layer correction, is presented in figures 3.12a, 3.12b, and 3.12c. By increasing the order of the relocalization, the error is drastically reduced in the inner domain of the composite, but remains concentrated near the fixed boundary Γ_u.

The local relative modeling error, after the boundary layer correction, is presented in figures 3.12d, 3.12e, and 3.12f. The modeling error significantly decreases near the boundaries but remains mainly concentrated at the corners.

Table 3.2 summarizes the global relative modeling error for different fields. The global modeling error is reduced by a factor of 3 to 4 for third-order relocalization combined with boundary layer correction.

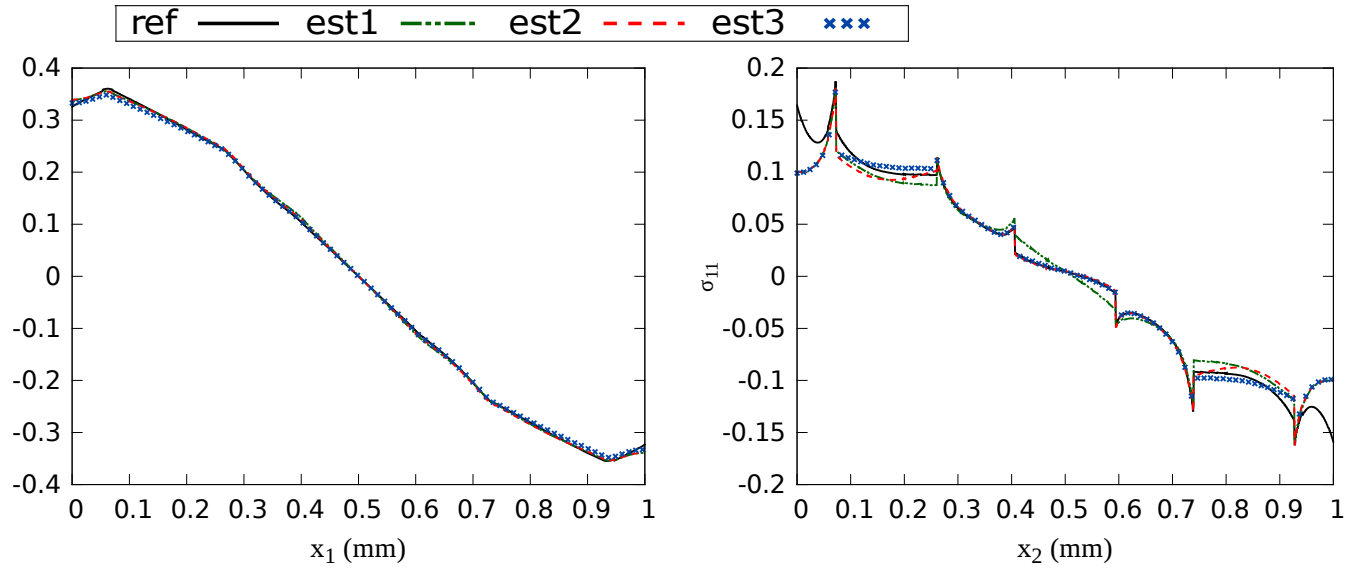

(a) σ_{11} *(MPa) plotted along AB line*

(b) σ_{12} *(MPa) plotted along CD line*

(c) σ_{11} *(MPa) plotted along AB line*

(d) σ_{12} *(MPa) plotted along CD line*

Figure 3.9: *Results of the reference (ref) field compared with the first-order (est1), second-order (est2), and third-order (est3) estimates.*

Table 3.2: *Comparison of the global relative modeling error for different fields.*

Global modeling error	$k =$ *est*1	$k =$ *cor*1	$k =$ *est*2	$k =$ *cor*2	$k =$ *est*3	$k =$ *cor*3
$\frac{\|\boldsymbol{u}^{ref}-\boldsymbol{u}^{k}\|_{E(\Omega)}}{\|\boldsymbol{u}^{ref}\|_{E(\Omega)}}$	16.4%	12.7%	12.6%	6.1%	12.3%	5.1%

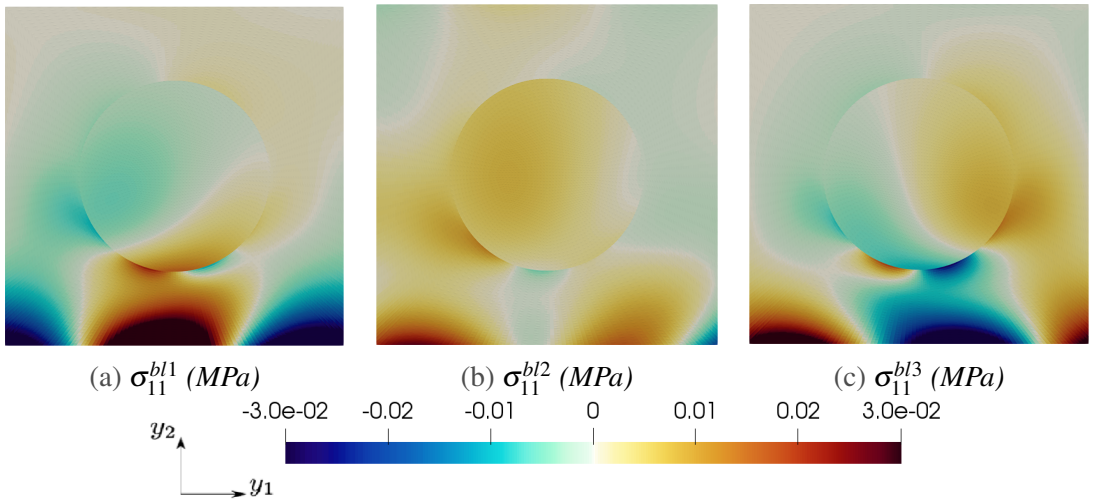

Figure 3.10: *First (σ_{11}^{bl1}), second (σ_{11}^{bl2}), and third-order (σ_{11}^{bl3}) boundary layer correctors for the boundary cell with a dashed line in Fig. 3.8. The decay inward (upper side of the unit-cell) of the corrections takes place over one unit-cell, but is less pronounced for the second and third-order corrections.*

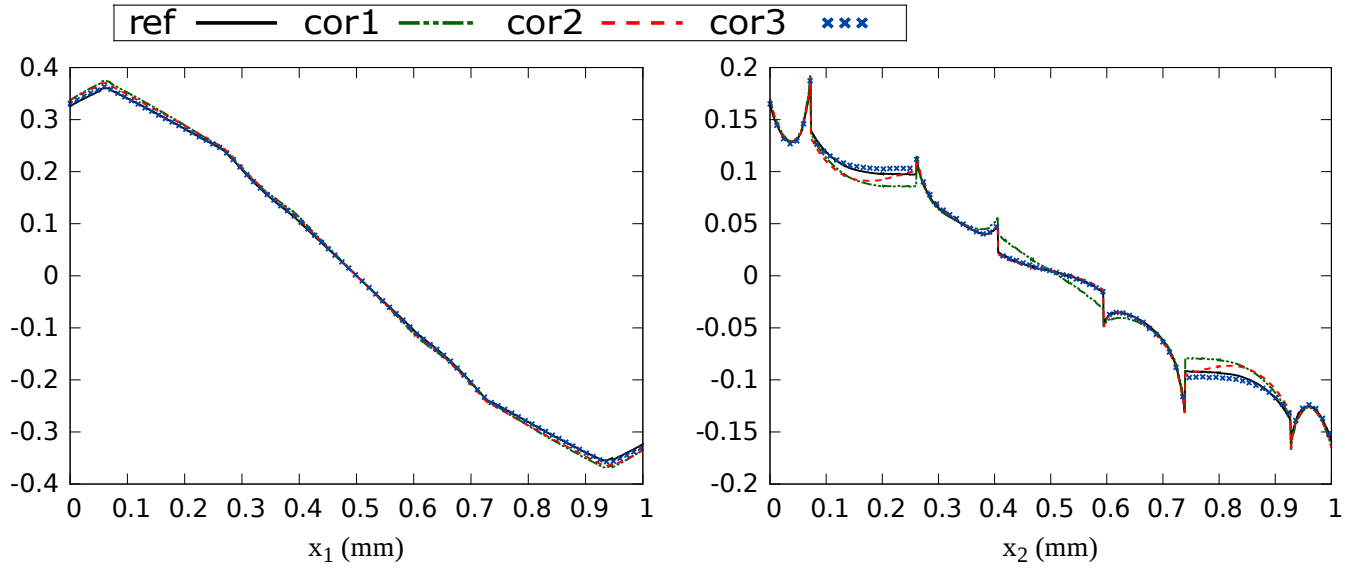

(a) σ_{11} *(MPa) plotted along AB line*

(b) σ_{12} *(MPa) plotted along CD line*

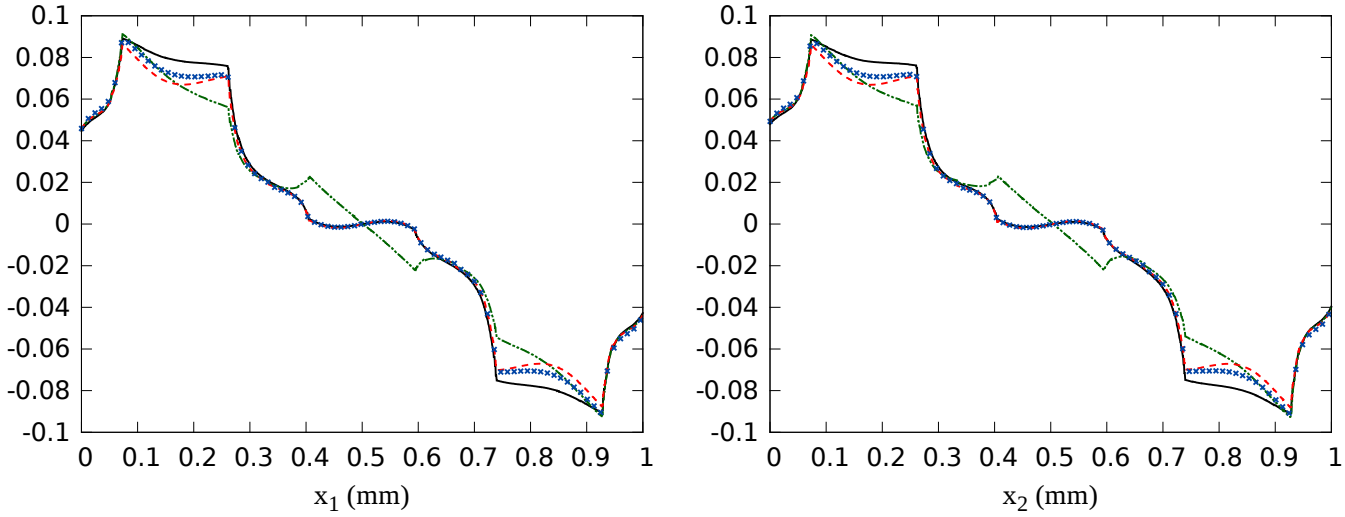

(c) σ_{11} *(MPa) plotted along AB line*

(d) σ_{12} *(MPa) plotted along CD line*

Figure 3.11: *Results of the reference (ref) field compared with the first-order (est*1*), second-order (est*2*), and third-order (est*3*) estimates.*

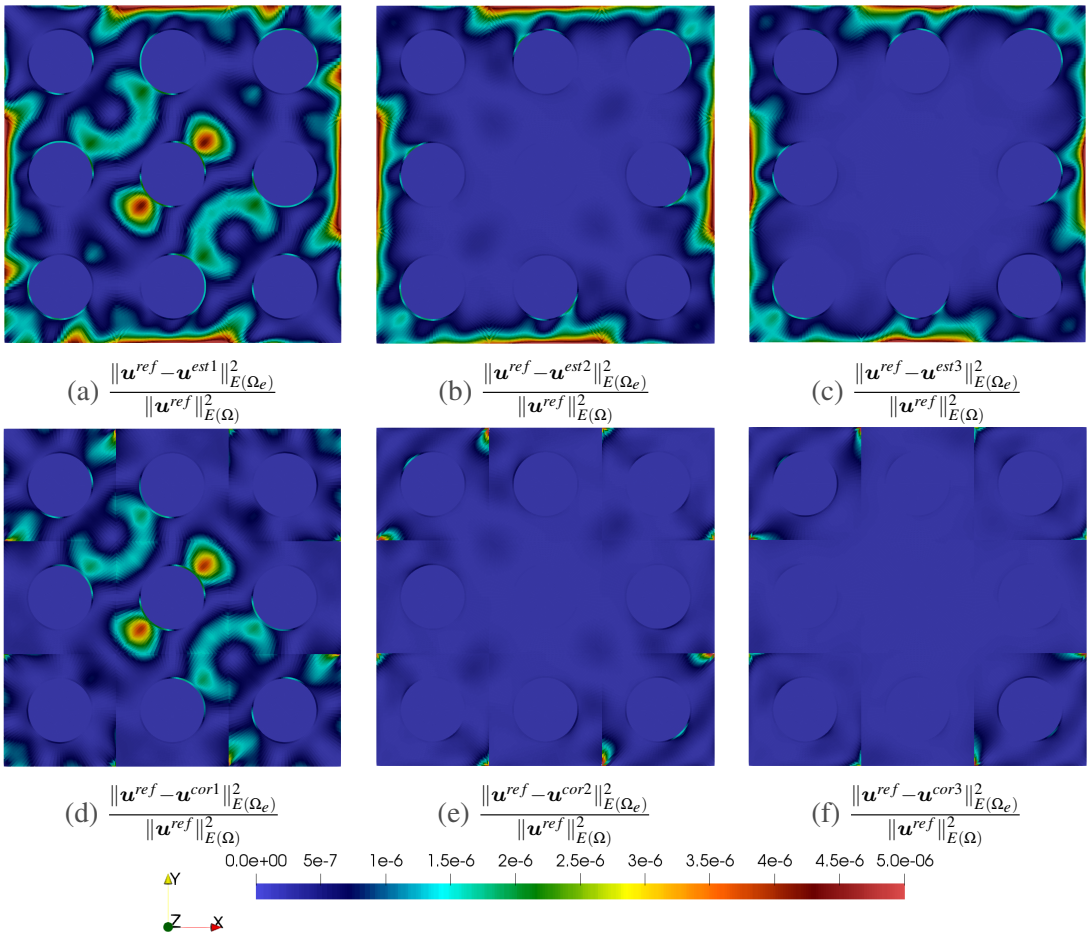

Figure 3.12: *Comparison of the local relative modeling error results. The error is drastically reduced by increasing the order of the relocalization and boundary layer correction.*

3.6 Conclusions

In this work, we have proposed a higher-order relocalization process, up to the third-order, to estimate heterogeneous fields without conducting DNS. The proposed relocalization captures the effects of the macroscale strain gradients, generally neglected by classical first-order homogenization. As a result, the range of applicability of asymptotic homogenization/relocalization is extended to cases subjected to strong macroscale strain gradients. My implementation of localization tensors has been verified, up to the third-order, based on analytical solutions provided by Boutin [1996]. These tensors can be computed off-line and used for any composite structure involving the same unit-cell.
We have also proposed a general boundary layer correction based on asymptotic homogenization, up to the third-order, in order to estimate consistent microscale fields in the vicinity of the boundaries. Classical asymptotic relocalization is modified at the boundaries by adding corrective terms, that decay toward the interior of the structure. These terms are obtained from the resolution of different problems over the unit-cell. The nature of the problems to be solved depends on the actual boundary conditions applied locally to the composite structure. The proposed boundary layer method is valid for different boundary conditions: Dirichlet, Neumann, or mixed.
The major conclusions that can be drawn from this study are as follows:

- The boundary layer correction decays within one unit-cell. The theoretical work of Allaire and Amar [1999] provides a mathematical proof of the exponential decay of the boundary layer correction in a rectangular plate and this for any considered order. The characteristic decay length may extend over one or more cells. This may be numerically tested and improved by considering two or three layers of the cell as done by Dumontet [1986]. This was not necessary for the presented examples.

- First-order estimates may be inaccurate on the boundaries *and* in the inner domain of the structure. In contrast, second and third-order estimates are in good agreement with the reference fields inside the structure, but remain inaccurate at the boundaries.

- By increasing the order of the boundary layer correction, corrected fields progressively converge towards the reference.

- Higher-order relocalization combined with boundary layer correction allows to drastically reduce the global modeling error by a factor of 3 to 4.

- Second and third-order corrected stress fields capture high stresses developed inside the structure *and* near boundary regions. In particular, for the laminated composite in bending shown in Sec. 3.5.1, $\sigma_{12}^{est\,1}$ is 3 times smaller, inside the structure, than σ_{12}^{ref} and 5 times smaller near the sliding boundary. This may result in underestimating failure criteria if the design is conducted without higher-order relocalization and boundary layer correction.

The proposed higher-order relocalization and boundary layer correction are applicable to 3D cases, but only 2D examples were provided for the sake of conciseness. The suggested methods could be a path toward estimating microscale fields of 3D realistic

engineering composite structures. This implies the use of irregular structure domains, coarse macroscale finite element meshes, and locally nonperiodic zones. Early work on the extension of the asymptotic homogenization method to non-periodic zones has been investigated in the work of Americo De Almeida [2022] (see appendix D.3), an intern I supervised for one year.

Chapter 4

Modeling error estimation & hierarchical modeling

Abstract

Homogenized models are widely used in multiscale analysis for their computational efficiency, but they often fail to provide sufficient accuracy in regions exhibiting high variations in the solution fields. One way to address this limitation is to adaptively couple the homogeneous model with a full field, heterogeneous one in designated zones of interest. Within the framework of finite-element based higher-order asymptotic homogenization, this work introduces a modeling error estimator in order to detect regions where refining the material model is necessary. I also analyze the competition between discretization and modeling errors. I finally propose a multiscale enhancement of the classical displacement-based submodeling technique in order to adequately couple the homogeneous and heterogeneous domains. The promise of the proposed methods and the overall associated strategy is illustrated on various numerical examples of elastic fiber-matrix composites.

Résumé

Les modèles homogénéisés sont largement utilisés dans l'analyse multi-échelle pour leur efficacité de calcul, mais ils ne parviennent souvent pas à fournir une précision suffisante dans les régions présentant de fortes variations dans les champs solution. Une façon de remédier à cette limitation est de coupler de manière adaptative le modèle homogène avec un modèle hétérogène dans des zones d'intérêt désignées. Dans le cadre éléments finis de l'homogénéisation asymptotique d'ordre supérieur, ce travail introduit un estimateur d'erreur de modélisation afin de détecter les régions où le raffinement du modèle matériel est nécessaire. J'analyse également la compétition entre les erreurs de discrétisation et de modélisation. Je propose enfin une amélioration multi-échelle de la technique classique de zoom structural afin de coupler de manière adéquate les domaines homogènes et hétérogènes. L'efficacité des méthodes proposées sont illustrées par divers exemples numériques de composites élastiques à fibres et matrices.

Contents

Reproduced from:
Mouad Fergoug, Augustin Parret-Fréaud, Nicolas Feld, Basile Marchand and Samuel Forest. Toward hierarchical modeling of heterogeneous structures driven by a modeling error estimator based on asymptotic homogenization.
Submitted to: Computer Methods in Applied Mechanics and Engineering

4.1 Introduction

Analyses of heterogeneous structures are conventionally performed using effective or homogenized material properties, instead of explicitly taking into account each material phase and the geometrical arrangements of the microstructure. These effective properties are usually obtained by homogenization methods, which can be broadly divided into two main categories: closed-form (or analytical) methods and computational methods.

Asymptotic homogenization, firstly introduced in the theoretical work of Sanchez-Palencia [1983] and Bensoussan et al. [2011], is one of the most rigorous closed-form homogenization approaches available in the literature. It is based on the assumption of spatial periodicity of the microstructure where the unit-cell defines the Representative Volume Element (RVE) without any ambiguity. This method consists in using asymptotic expansions of the mechanical fields of the full-scale problem in order to split it into a decoupled set of microscale unit-cell problems and a macroscale problem. Solving the former allows one to compute the effective properties of the equivalent homogeneous medium but also to estimate, by a relocalization process, local fields within the material. Asymptotic homogenization, as an engineering tool, has been explored in the seminal works of Kikuchi and coworkers [Guedes and Kikuchi, 1990; Hollister and Kikuchi, 1992; Terada and Kikuchi, 1995] where the finite element method has been used to solve the unit-cell problems to compute equivalent material properties, as well as local fields estimation. Such multiscale computational analyses have been conducted by Ghosh et al. [1995, 2001] where the asymptotic homogenization theory has been combined with the Voronoi cell finite element method (VCFEM) to study elastic and elasto-plastic material behavior. Fish and coworkers [Fish et al., 1994b; Fish and Belsky, 1995; Fish and Yu, 2001] have used asymptotic homogenization to develop a multigrid method for the analysis of periodic materials and to account for the damage phenomena occurring at different scales. Recent works resort to asymptotic homogenization in a wide range of engineering problems, *e.g.* to study metamaterial behavior [Yang et al., 2019, 2020; Abali and Barchiesi, 2020; Abali et al., 2022; Yang et al., 2022], to optimize structures [Suzuki and Kikuchi, 1991; Sigmund, 1995; Hassani and Hinton, 2012], and to evaluate localized stiffness degradation [Visrolia and Meo, 2013]. On the other hand, computational homogenization methods [Moulinec and Suquet, 1998; Feyel and Chaboche, 2000; Kouznetsova et al., 2001, 2002; Miehe and Koch, 2002] do not lead to closed-form overall constitutive equations but retrieve the averaged macroscale response at every macroscopic point of interest by entailing the solution of a microscale boundary value problem attributed to that point. The reader is referred to Kanouté et al. [2009] for a thorough review of homogenization methods. In this chapter, we use asymptotic homogenization for multiscale linear behavior analyses. Therefore, only periodic heterogeneous structures are considered.

Conventional or first-order asymptotic homogenization, which considers only the first term in the asymptotic expansion, works well for cases with a complete separation of scales. This assumption is only valid when the scale of the microstructure or microstructural fluctuations are much smaller than the characteristic dimensions of the macrostructure. For weak separation of scales, however, it generally becomes inaccurate [Ameen et al., 2018]. One solution to overcome this limitation is to keep higher-order terms in the series expansion. Indeed, Boutin [1996] shows that higher-order terms in asymptotic homogenization introduce successive gradients of macroscale strain and tensors charac-

teristic of the microstructure, which result in introducing a non-local effect in the material behavior. Therefore, asymptotic homogenization may offer a better estimate of local fields, even in cases of a weak separation of scales, by a higher-order relocalization process. Nevertheless, the construction of a solution at the vicinity of the boundaries remains beyond the capabilities of this method due to the loss of periodicity assumption in these regions, unless a boundary layer correction is applied. In Fergoug et al. [2022b] a FEM numerical framework has been proposed to perform a higher-order relocalization process associated with a general boundary layer correction method. This work is limited to the assumption that both the heterogeneous microscale mesh, constructed by translating the unit-cell, and the overall macroscale mesh are identical, which can be computationally prohibitive. In the present chapter, we propose an extension of the aforementioned work to deal with different coarser macroscale meshes, requiring less computation time than Direct Numerical Simulations (DNS, *i.e.* when the geometry of the microstructure is explicitly described in simulations). As a result, local fields corrected at the boundaries needed, for example, to predict damage initiation, will be estimated on the coarse macroscale mesh.

Numerical simulations of heterogeneous structures depend on several factors such as the characteristics of the microstructure, the domain of interest, and the applied loads as well as the targeted accuracy and the objective of the simulation. Consequently to avoid a DNS, there is a need to *adaptively* select the appropriate scale for each domain of interest. Toward this end, the concept of *hierarchical modeling* was introduced to couple a multilevel material model in the same simulation. This process of adaptivity is usually steered by criteria used to detect areas where refining the material model is necessary. These criteria can be physically oriented, for example, based on the level of stress, strain or damage [Ghosh et al., 2001] or mathematically oriented by using the macroscale discretization error or the modeling error [Zohdi et al., 1996; Fish et al., 1994a; Ghosh et al., 2007; Temizer and Wriggers, 2011; Vernerey and Kabiri, 2012]. The non-exhaustive representative works that have treated the subject of adaptivity are as follows:

- Zohdi et al. [1996] and Oden and Zohdi [1997] have initiated a hierarchical modeling strategy based on the estimation of a global *modeling error*, which quantifies the error induced by replacing the heterogeneous material with a homogeneous one. Based on the observation that global estimates can be insensitive to *local* features such as stress concentrations or average strains, Oden and Vemaganti [1999, 2000] have proposed an extension of the modeling error to quantities of interest. This error estimation and adaptivity process have been extended to nonlinear problems by Oden et al. [2001]. A disadvantage of this class of methods is that it needs access to the full microscale material fluctuations, and the modeling error estimation is thus conducted through an integral over the corresponding heterogeneous domain, which can be computationally prohibitive.

- Fish and coworkers [Fish and Markolefas, 1993; Fish et al., 1994a; Fish and Belsky, 1995; Fish and Shek, 2000] have proposed a coupling strategy of the macroscale with the microscale of an underlying periodic microstructure at a region of interest identified by *multiscale reduction error estimators/indicators* derived from asymptotic homogenization. The limitation of this method is that it does not take into account the boundary layer effect.

- Gosh and coworkers [Ghosh et al., 2001; Raghavan and Ghosh, 2004; Raghavan et al., 2004; Ghosh et al., 2007] have suggested an adaptive multi-level methodology to create a hierarchy of computational sub-domains with a varying resolution, from homogenized formulations to explicit microstructural modeling. The macroscale computations are done by conventional FEM models while the VCFEM is used for micromechanical analysis. The switching criteria from one level to another can be associated with the gradients of macroscale variables (*e.g.* stress, strain, or strain energy) or the evolution of microscale damage. This method has addressed damage evolution in composites accurately and efficiently.

In this chapter, we present a novel modeling error estimation based on a higher-order relocalization process derived from asymptotic homogenization. The main idea of the proposed estimation is to quantify the terms neglected by conventional first-order homogenization, necessary to capture the gradients of the macroscale field in case of a weak separation of scales. Contrary to Fish et al. [1994b], our estimation quantifies the modeling error that occurs on the boundaries. Indeed, a rapid change of gradients generally occurs near the boundaries, which, ultimately, may be responsible for the failure initiation of the structure [Pipes et al., 1973].
The adaptivity process generally entails minimizing two types of errors, *viz.* the discretization error, inherent to finite element approximation, and the modeling error, as discussed by Fish et al. [1994a] and Zohdi et al. [1996]. To this end, we also study the competition of both discretization and modeling errors for different macroscale meshes and material phase ratios.

Finally, hierarchical modeling raises the challenge of adequately coupling the macroscale and the microscale domains. Several coupling techniques have been proposed in the literature such as the submodeling technique, which consists in performing two independent analyses, one on the macroscale global model with a coarser mesh, and the other on the microscale local model with a refined mesh (submodel), where the displacement obtained with the global model is prescribed to the boundary of the local one. It will be shown later that this technique generally leads, in the context of multiscale analyses, to high modeling errors on the interfaces. Other coupling techniques that differ according to the physics of the problem exist, such as the volume coupling of Arlequin method [Ben Dhia, 1998], and surface coupling techniques such as the mortar coupling [Bernardi et al., 1993; Belgacem, 1999] or the Nitsche coupling [Hansbo and Hansbo, 2002], or more recently a second-order homogenization based coupling [Wangermez et al., 2020]. In this chapter, we propose a multiscale enhancement of the classical submodeling technique where, instead of applying the macroscale displacement on the local domain, a higher-order relocalized displacement field corrected at the boundaries is applied. This is expected to give better results since relocalized fields provide a good estimation of local microscale fields, as will be shown later in this chapter.

Regarding the aforementioned aspects, the present work proposes the following main novelties:

- A higher-order relocalization process with boundary layer correction conducted on macroscale coarse meshes to provide an estimation of local microscale fields. A modeling error, based on this estimation, is proposed.

- A multiscale enhanced submodeling technique based on the relocalized fields corrected at the boundaries to adequately couple the macroscale with the microscale domains.

To the best of our knowledge, such aspects have not been proposed in the literature yet.

The outline of this chapter is as follows. In Sec. 4.2, we first present the studied boundary value problem and briefly recall the relocalization process and the boundary layer correction method. In Sec. 4.3, we detail the proposed procedure to conduct this relocalization process on coarse macroscale meshes. The suggested modeling error estimation is elaborated in Sec. 4.4, and the multiscale submodeling technique is depicted in Sec. 4.5. Each section is accompanied by numerical example to demonstrate the efficiency of the suggested approaches. The analysis is limited to linear elastic material behavior under the small strain assumption.

4.2 Preliminaries

Asymptotic homogenization can be used to determine the effective properties of periodic materials from the knowledge of local mechanical properties over one unit-cell, representative of the microstructure. This method is also able to estimate, by a relocalization process, local fields within a structure without conducting DNS. Nevertheless, the solution provided by the relocalization process is inaccurate in the vicinity of the boundaries due to the loss of periodicity assumption in these regions, unless a boundary layer correction is applied.

In this section, we present the studied boundary value problem and briefly recall the relocalization procedure and the boundary layer correction method to improve the accuracy of estimated fields on the boundaries. We refer the reader to Fergoug et al. [2022a,b] for more details.

4.2.1 Statement of the boundary value problem

A heterogeneous periodic body is considered as a linearly elastic solid in static equilibrium, whose heterogeneity arises from the distribution of separate phases at the microscale. We define the bounded domain Ω, shown in figure 4.1a, occupied by this heterogeneous body and corresponding to the microscale. The boundary $\partial\Omega$ consists of a portion Γ_u, on which the displacements are prescribed to the value $\boldsymbol{u}^d = 0$, a portion Γ_t on which a pressure distribution $P(\boldsymbol{x})$ is applied, and the last portion Γ_s on which the structure is sliding freely. The size of the structure is $L = 12$ mm, $H = 6$ mm, and $W = 1$ mm, with a fiber volume fraction of 25%. The matrix and the inclusions are assumed to be isotropic elastic with coefficients ($E_m = 500$ MPa, $\nu_m = 0.3$) and (E_f, $\nu_f = 0.3$), respectively, where the value of E_f will be varied across the examples. This boundary value problem will be solved under the plane strain conditions.

Due to its heterogeneous nature, the mechanical behavior of the body Ω is assumed to depend on two scales:

- Macroscale with materially homogeneous domain Ω, having L as a characteristic length and global coordinates $\boldsymbol{x} \in \Omega$, and endowed with homogenized proper-

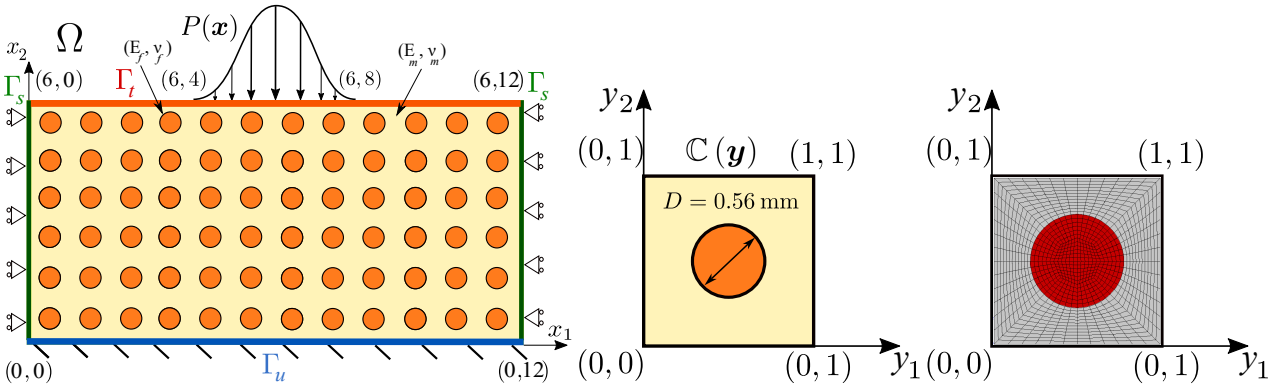

(a) *Structure geometry* (b) *Unit-cell domain* (c) *Unit-cell mesh*

Figure 4.1: *Illustration of the studied fiber-matrix composite. The corresponding microscale mesh is built by repeating the unit-cell Y characterized by a heterogeneous behavior $\mathbb{C}(\boldsymbol{y})$ over the three space directions. The structure is sliding on Γ_s, fixed on Γ_u and a pressure distribution $P(\boldsymbol{x})$ is applied on Γ_t.*

ties $\mathbb{C}^0(\boldsymbol{x})$, obtained from the resolution of the first-order homogenization problem over the unit-cell;

- Microscale, having l as a characteristic length and with local coordinates $\boldsymbol{y} \in Y$, where Y is the unit-cell domain, and endowed with heterogeneous properties $\mathbb{C}(\boldsymbol{y})$.

The coarse and fine scales are related by the parameter ε such that:

$$\varepsilon = \frac{l}{L}, \qquad \boldsymbol{y} = \frac{\boldsymbol{x}}{\varepsilon}. \tag{4.1}$$

The finite element mesh describing the unit-cell is composed of $1,008$ twenty-node brick elements as shown in figure 4.1c. Therefore the microscale mesh describing the entire structure including all heterogeneities is composed of $72,576$ $(1,008 \times 6 \times 12)$ elements, corresponding to $1,527,345$ degrees of freedom.
In section 4.2, we consider that the macroscale mesh is identical to the microscale one, but endowed with homogenized properties $\mathbb{C}^0(\boldsymbol{x})$.

4.2.2 Relocalization procedure

In Fergoug et al. [2022b], an estimation of heterogeneous fields has been proposed by conducting a higher-order relocalization, up to the third-order. The obtained estimates are expected to capture the effect of macroscale successive gradients neglected by a conventional first-order relocalization. The main aspects of the estimation are briefly recalled here and the reader is referred to Fergoug et al. [2022b] for more details.
The proposed estimation is constructed by solving the following problems:

- Homogeneous problem $(\mathscr{P}_{hom})$ with effective behavior $\mathbb{C}^0(\boldsymbol{x})$. Solving this problem enables to compute the macroscale strain and its successive gradients $(\boldsymbol{E}(\boldsymbol{x}), \boldsymbol{\nabla}_x \boldsymbol{E}(\boldsymbol{x}), \boldsymbol{\nabla}_x \boldsymbol{\nabla}_x \boldsymbol{E}(\boldsymbol{x}))$. The gradient of the macroscale strain field, $\nabla_x \boldsymbol{E}$, is numerically evaluated by extrapolating corresponding strain values

between integration points to the nodes and are averaged for each element (at the nodes). Strain values are then appropriately differentiated using the finite element symmetric gradient operator, usually denoted $\boldsymbol{B}$. A similar procedure is used to compute the second gradient of the macroscale strain field $\nabla_x \nabla_x \boldsymbol{E}$.

- First $\left(\mathscr{P}^{1^{st}}_{order}\right)$, second $\left(\mathscr{P}^{2^{nd}}_{order}\right)$, and third-order $\left(\mathscr{P}^{3^{rd}}_{order}\right)$ homogenization problems over the unit-cell. First-, second-, and third-order localization tensors $(\mathbb{D}^0, \mathbb{A}^0, \mathbb{B}^0)$, $(\mathbb{D}^1, \mathbb{A}^1, \mathbb{B}^1)$, and $(\mathbb{D}^2, \mathbb{A}^2, \mathbb{B}^2)$ are obtained from the resolution of these problems, respectively.

The proposed estimates read:

$$\left.\begin{aligned} \boldsymbol{u}^{est}(\boldsymbol{x},\boldsymbol{y}) \;=\; & \boldsymbol{U}(\boldsymbol{x}) \\ & + \boldsymbol{\varepsilon}\, \mathbb{D}^0(\boldsymbol{y}) : \boldsymbol{E}(\boldsymbol{x}) \\ & + \boldsymbol{\varepsilon}^2\, \mathbb{D}^1(\boldsymbol{y}) \vdots \boldsymbol{\nabla}_x \boldsymbol{E}(\boldsymbol{x}) \\ & + \boldsymbol{\varepsilon}^3\, \mathbb{D}^2(\boldsymbol{y}) :: \boldsymbol{\nabla}_x \boldsymbol{\nabla}_x \boldsymbol{E}(\boldsymbol{x}) \end{aligned}\right\} \quad \forall \boldsymbol{x} \in \Omega,\ \forall \boldsymbol{y} \in Y, \tag{4.2}$$

$$\left.\begin{aligned} \boldsymbol{\varepsilon}^{est}(\boldsymbol{x},\boldsymbol{y}) \;=\; & \mathbb{A}^0(\boldsymbol{y}) : \boldsymbol{E}(\boldsymbol{x}) \\ & + \boldsymbol{\varepsilon}\, \mathbb{A}^1(\boldsymbol{y}) \vdots \boldsymbol{\nabla}_x \boldsymbol{E}(\boldsymbol{x}) \\ & + \boldsymbol{\varepsilon}^2\, \mathbb{A}^2(\boldsymbol{y}) :: \boldsymbol{\nabla}_x \boldsymbol{\nabla}_x \boldsymbol{E}(\boldsymbol{x}) \end{aligned}\right\} \quad \forall \boldsymbol{x} \in \Omega,\ \forall \boldsymbol{y} \in Y, \tag{4.3}$$

$$\left.\begin{aligned} \boldsymbol{\sigma}^{est}(\boldsymbol{x},\boldsymbol{y}) \;=\; & \mathbb{B}^0(\boldsymbol{y}) : \boldsymbol{E}(\boldsymbol{x}) \\ & + \boldsymbol{\varepsilon}\, \mathbb{B}^1(\boldsymbol{y}) \vdots \boldsymbol{\nabla}_x \boldsymbol{E}(\boldsymbol{x}) \\ & + \boldsymbol{\varepsilon}^2\, \mathbb{B}^2(\boldsymbol{y}) :: \boldsymbol{\nabla}_x \boldsymbol{\nabla}_x \boldsymbol{E}(\boldsymbol{x}) \end{aligned}\right\} \quad \forall \boldsymbol{x} \in \Omega,\ \forall \boldsymbol{y} \in Y. \tag{4.4}$$

Estimated fields in Eqs. 4.2, 4.3, 4.4 are computed using localization tensors combined with the value of the macroscale strain or its gradients *at this current point*, and not its average over the unit-cell (see figure 4.2). This relocalization process improvement, firstly proposed by Kruch and Forest [1998], requires identical microscale and macroscale meshes in order to locate each unit-cell on the macroscale structure (see figure 4.2). An extension of this relocalization process to different coarser macroscale meshes is presented in section 4.3.

4.2.3 Boundary layer correction

Asymptotic homogenization is unable to provide an accurate estimation of local fields near the boundaries since periodicity is lost in these regions. Indeed, a complex stress (or strain) field occurs within a very local region near the boundaries, frequently referred to as a *boundary layer effect*. Following previous work of Dumontet [1986], we have proposed a general method to correct higher-order estimates on the boundaries, valid for various Boundary Conditions (BCs): Dirichlet, Neumann, or mixed. The main idea of the

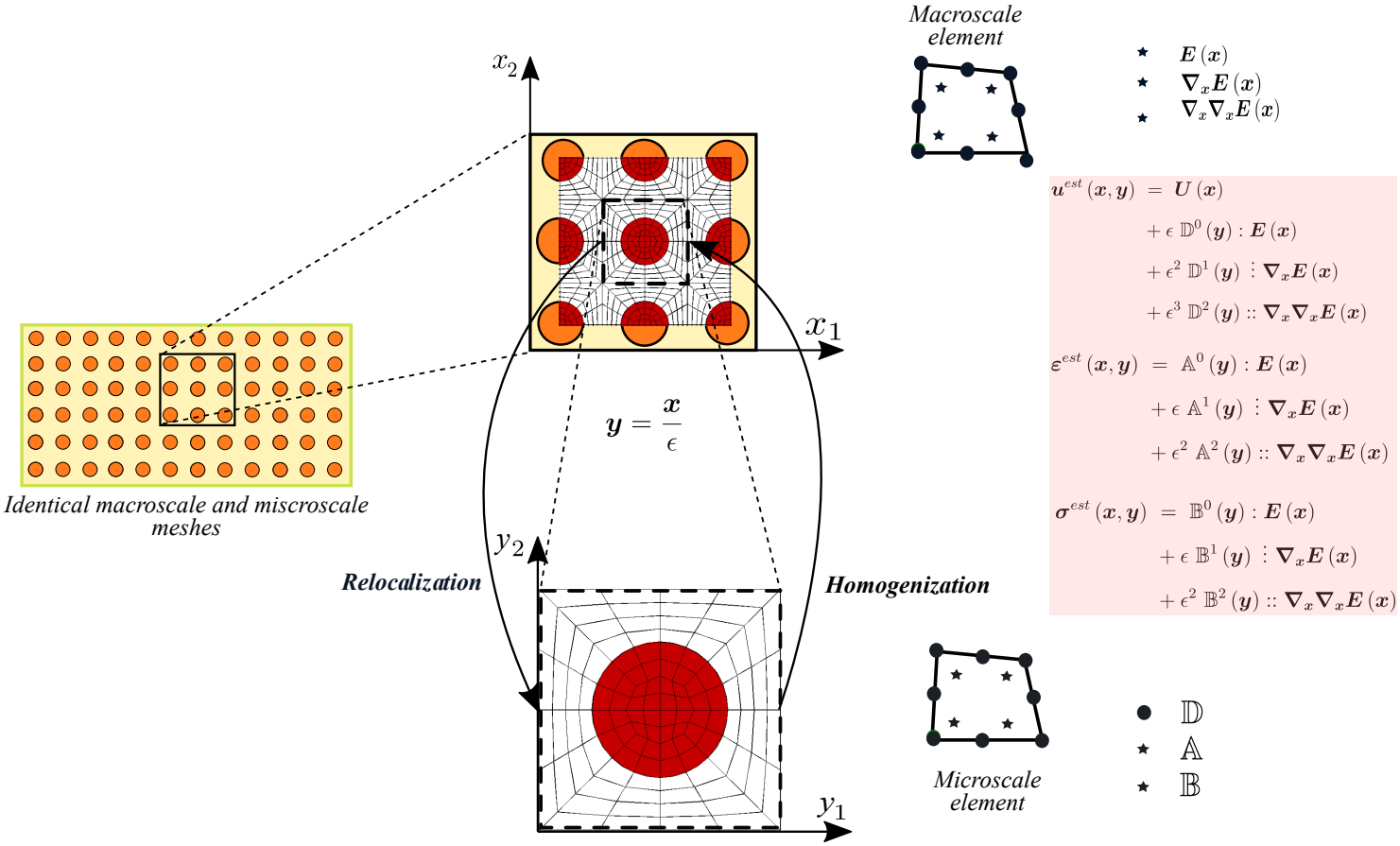

Figure 4.2: *Illustration of the relocalization procedure. The macroscale strain and its gradients* $(\boldsymbol{E}(\boldsymbol{x}), \nabla_x \boldsymbol{E}(\boldsymbol{x}), \nabla_x \nabla_x \boldsymbol{E}(\boldsymbol{x}))$ *are stored at the integration points of the macroscale elements. Strain and stress localization tensors* $(\mathbb{A}, \mathbb{B})$ *are stored at the integration points of the microscale elements of the unit-cell, and the displacement localization tensor* $\mathbb{D}$ *on the nodes. Estimated fields are computed after locating the unit-cell mesh on the macroscale one.*

correction is summarized, for Dirichlet BCs, in figure 4.3. The relocalization process provides a spurious periodic fluctuation $\boldsymbol{v}$ on the boundary. The opposite of this fluctuation is applied to an auxiliary problem subjected to adequate periodic boundary conditions. Solving this problem enables to obtain first, second, or third-order boundary layer displacement, strain, and stress localization tensors $(\mathbb{D}^{0,bl}, \mathbb{A}^{0,bl}, \mathbb{B}^{0,bl})$, $(\mathbb{D}^{1,bl}, \mathbb{A}^{1,bl}, \mathbb{B}^{1,bl})$, and $(\mathbb{D}^{2,bl}, \mathbb{A}^{2,bl}, \mathbb{B}^{2,bl})$, respectively. Afterward, boundary layer correctors $\left(\boldsymbol{u}^{bl}, \boldsymbol{\epsilon}^{bl}, \boldsymbol{\sigma}^{bl}\right)$ are computed by conducting similar relocalization processes, detailed in figure 4.2, on the concerned boundary.

Remark 12 *A particular treatment was considered for boundary layer correction of corner cells, as explained by Fergoug et al. [2022a].*

In what follows, we consider the following fields:

- Microscale fields obtained by solving problem $\left(\mathscr{P}_{ref}\right)$ using DNS, which will be considered as our reference, indexed *ref*, with solution $\left(\boldsymbol{u}^{ref}, \boldsymbol{\varepsilon}^{ref}, \boldsymbol{\sigma}^{ref}\right)$.

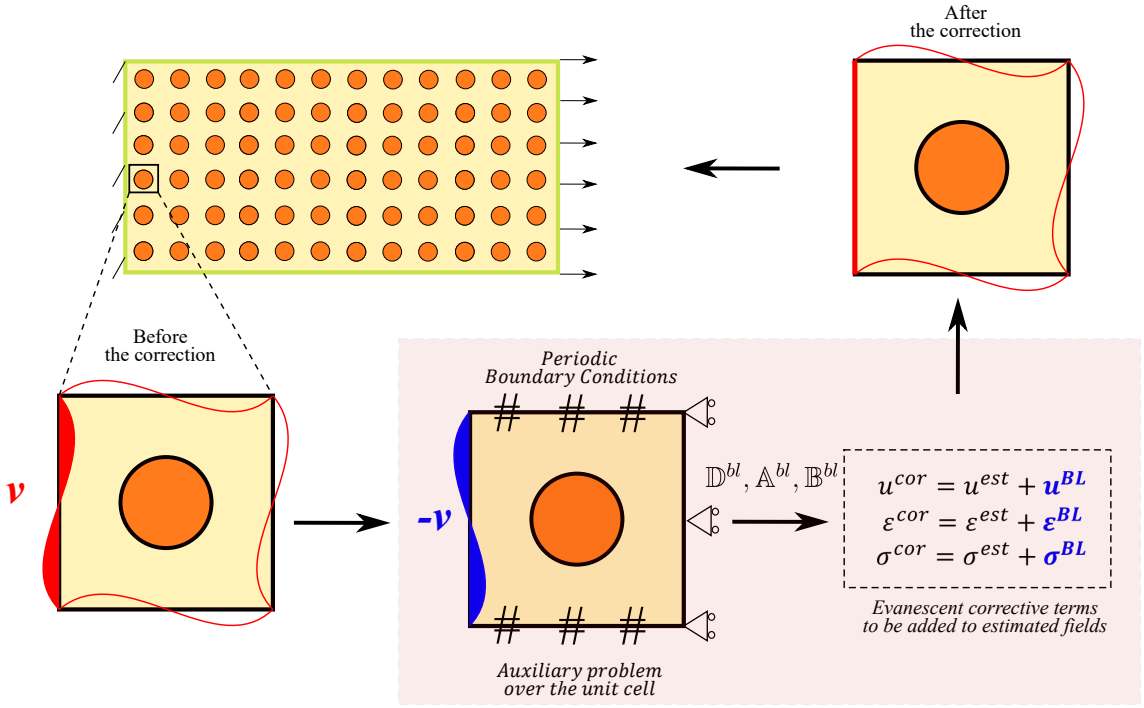

Figure 4.3: *Illustration of the boundary layer correction method for a Dirichlet boundary. Relocalization processes provide a spurious periodic fluctuation $\boldsymbol{v}$ on the boundary. The inverse of this fluctuation is applied to an auxiliary problem over the unit-cell, providing boundary layer displacement, strain, and stress localization tensors. After a relocalization process on the concerned boundary, evanescent corrective terms are computed and added to estimated fields.*

- Homogeneous fields obtained by solving problem $(\mathscr{P}_{hom})$, indexed *hom*, with solution $(\text{displacement } \boldsymbol{U}, \text{strain } \boldsymbol{E}, \text{stress } \boldsymbol{\Sigma})$.
- Proposed first-, second-, and third-order estimates of microscale fields obtained by the first-, second-, and third-order relocalization processes, indexed *est1*, *est2*, and *est3*, respectively.
- Proposed first-, second-, and third-order boundary layer corrections of estimated fields indexed *cor1*, *cor2*, and *cor3*, respectively.

4.3 Extension of the relocalization procedure to arbitrary macroscale meshes

Asymptotic homogenization enables, by a relocalization process, to estimate the microscale fields from the knowledge of the formerly determined macroscale fields.
In this section, we propose an extension of the relocalization process described in section 4.2, to deal with *coarser* macroscale meshes. As a result, global balance and microscale fields are estimated on the macroscale mesh, requiring much less computational cost than DNS.

4.3.1 Proposed relocalization technique

The relocalization process is illustrated in figure 4.4. A cell box, with the same dimensions of the unit-cell mesh, is being moved around the global mesh. Integration Points (IPs) of the macroscale elements inside the moving box are then selected. For each of these macroscale IPs, its nearest microscale IP is then identified after mapping the unit-cell on the current position of the moving box. A first relocalization step is conducted over the global mesh by contracting the strain field (or its gradients) values of the current macroscale IP with relocalization tensors of the identified nearest microscale IP. Afterward, the relocalized field is corrected at the boundaries by using the same previously described approach on the concerned boundary.

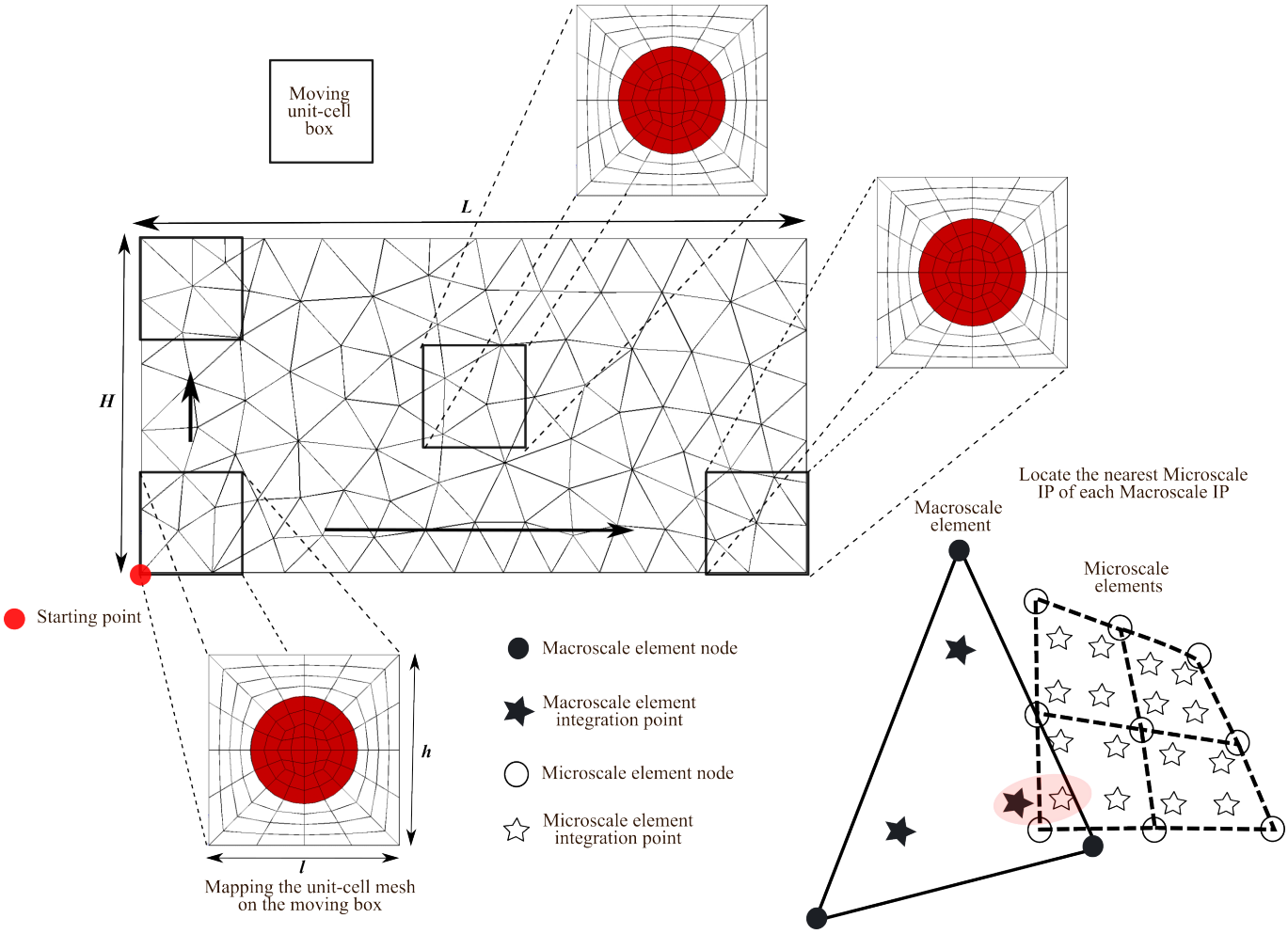

Figure 4.4: *Illustration of the relocalization process on a coarser macroscale mesh.*

The higher-order stress relocalization process is detailed in algorithm 1 (the same procedure is used for strain relocalization). To conduct the displacement relocalization process, the displacement relocalization tensor $\mathbb{D}$, originally stored at the nodes of the unit-cell mesh, is interpolated to integration points. Therefore, the relocalization process can be carried out as previously discussed. The obtained result, which is a displacement correction on the macroscale mesh, is then extrapolated to nodes and added to the macroscale displacement field, as shown for $\boldsymbol{u}^{est}$ in figure 4.2.

Algorithm 1: Stress relocalization with boundary layer correction on the macromesh

Input: Macromesh, unit-cell mesh, $\boldsymbol{E}$, $\boldsymbol{\nabla}_x\boldsymbol{E}$, $\boldsymbol{\nabla}_x\boldsymbol{\nabla}_x\boldsymbol{E}$, $\mathbb{B}$, $\mathbb{B}^{bl}$

Output: $\boldsymbol{\sigma}^{cor1}$, $\boldsymbol{\sigma}^{cor2}$, $\boldsymbol{\sigma}^{cor3}$

Repetition of the unit-cell mesh in the macromesh

$\{L_x, L_y, L_z\} \longleftarrow$ BoundingBox(Macromesh)
$\{l_x, l_y, l_z\} \longleftarrow$ BoundingBox(Micromesh)
$n\_cell\_x = L_x/l_x$, $n\_cell\_y = L_y/l_y$, $n\_cell\_z = L_z/l_z$ ▷ Number of repetitions of the unit-cell mesh on the macromesh

Relocalization with boundary layer correction

for $i \leftarrow 0$ *to* $(n\_cell\_x) - 1$ **do**
  for $j \leftarrow 0$ *to* $(n\_cell\_y) - 1$ **do**
    for $k \leftarrow 0$ *to* $(n\_cell\_z) - 1$ **do**
      unit-cell mesh box moving around the macromesh

      $cell\_x\_min = i * l_x$; $cell\_x\_max = (i+1) * l_x$;
      $cell\_y\_min = j * l_x$; $cell\_y\_max = (j+1) * l_y$;
      $cell\_z\_min = k * l_x$; $cell\_z\_max = (k+1) * l_z$;
      Macroelements IPs contained in the unit-cell mesh moving box

      Macroelem_in_Cell_Box = {Elements s.t. barycentre ∈ unit-cell mesh box}
      for *elem* $\leftarrow 0$ *to Macroelem_in_Cell_Box* **do**
        for *ip* $\leftarrow 0$ *to Nb_of_IP(elem)* **do**
          if *IP_Coords (elem,ip)* ∈ *Moving_Cell_Box* **then**
            (MacroIP_in_Cell_Box).append(IP_Rank,IP_Coords)
          end
        end
      end
      Relocalization

      for *(IP_Rank,IP_Coords)* ∈ *MacroIP_in_Cell_Box* **do**
        IP_Rank_Micro = Locate.Nearest(IP_Coords,Micromesh) ▷ Locate nearest micro IP of the current macro IP
        $\mathbb{B}$ = Reloc_Tensor(IP_Rank_Micro) ▷ Load tensor stored in the identified micro IP
        $\boldsymbol{E}$ = Macro_Strain(IP_rank), $\boldsymbol{\nabla}_x\boldsymbol{E}$ = Macro_GradStrain(IP_rank), $\boldsymbol{\nabla}_x\boldsymbol{\nabla}_x\boldsymbol{E}$ = Macro_GradGradStrain(IP_rank)
        $\boldsymbol{\sigma}^{est1} = \mathbb{B}^0 : \boldsymbol{E}$
        $\boldsymbol{\sigma}^{est2} = \boldsymbol{\sigma}^{est1} + \mathbb{B}^1 \vdots \boldsymbol{\nabla}_x\boldsymbol{E}$
        $\boldsymbol{\sigma}^{est3} = \boldsymbol{\sigma}^{est2} + \mathbb{B}^2 :: \boldsymbol{\nabla}_x\boldsymbol{\nabla}_x\boldsymbol{E}$
      end
      Boundary layer correction

      for *(IP_Rank,IP_Coords)* ∈ *MacroIP_in_Cell_Box* **do**
        if *Moving box with position (i,j,k) is located on boundaries* **then**
          IP_Rank_Micro = Locate.Nearest(IP_Coords,Micromesh)
          $\mathbb{B}^0$ = Reloc_Tensor(IP_Rank_Cell)
          $\boldsymbol{E}$ = Macro_Strain(IP_rank), $\boldsymbol{\nabla}_x\boldsymbol{E}$ = Macro_GradStrain(IP_rank), $\boldsymbol{\nabla}_x\boldsymbol{\nabla}_x\boldsymbol{E}$ = Macro_GradGradStrain(IP_rank)
          $\boldsymbol{\sigma}^{cor1} = \boldsymbol{\sigma}^{est1} + (\mathbb{B}^{0,bl} : \boldsymbol{E})$
          $\boldsymbol{\sigma}^{cor2} = \boldsymbol{\sigma}^{cor1} + (\boldsymbol{\sigma}^{est2} + \mathbb{B}^{1,bl} \vdots \boldsymbol{\nabla}_x\boldsymbol{E})$
          $\boldsymbol{\sigma}^{cor3} = \boldsymbol{\sigma}^{cor2} + (\boldsymbol{\sigma}^{est3} + \mathbb{B}^{2,bl} :: \boldsymbol{\nabla}_x\boldsymbol{\nabla}_x\boldsymbol{E})$
        end
      end
    end
  end
end

4.3.2 Numerical results

To illustrate the effectiveness of the proposed relocalization process, six macroscale unstructured meshes composed of fifteen-node wedge elements are considered, as shown in figure 4.5. The ratio between the numbers of microscale and macroscale degrees of freedom varies from 560 for the coarsest mesh (see figure 4.5a) to 2 for the finest one (see figure 4.5f). A mesh adaptation technique, with a target elements size obtained through the a posteriori discretization error estimator ZZ2 [Zienkiewicz and Zhu, 1992b,d], is used to generate macroscale meshes (see figures 4.5c,4.5d, 4.5e, 4.5f) refined in areas of interest, where stress concentrations occur. For the finest macroscale mesh, the mesh adaptation procedure has been performed while preserving the topology of the fibers (see figure 4.5f). For this example, we consider a ratio $\frac{E_f}{E_m} = 10$ and a relocalization process with boundary layer correction up to the second-order, as it is sufficient to capture strain gradients in the present example.

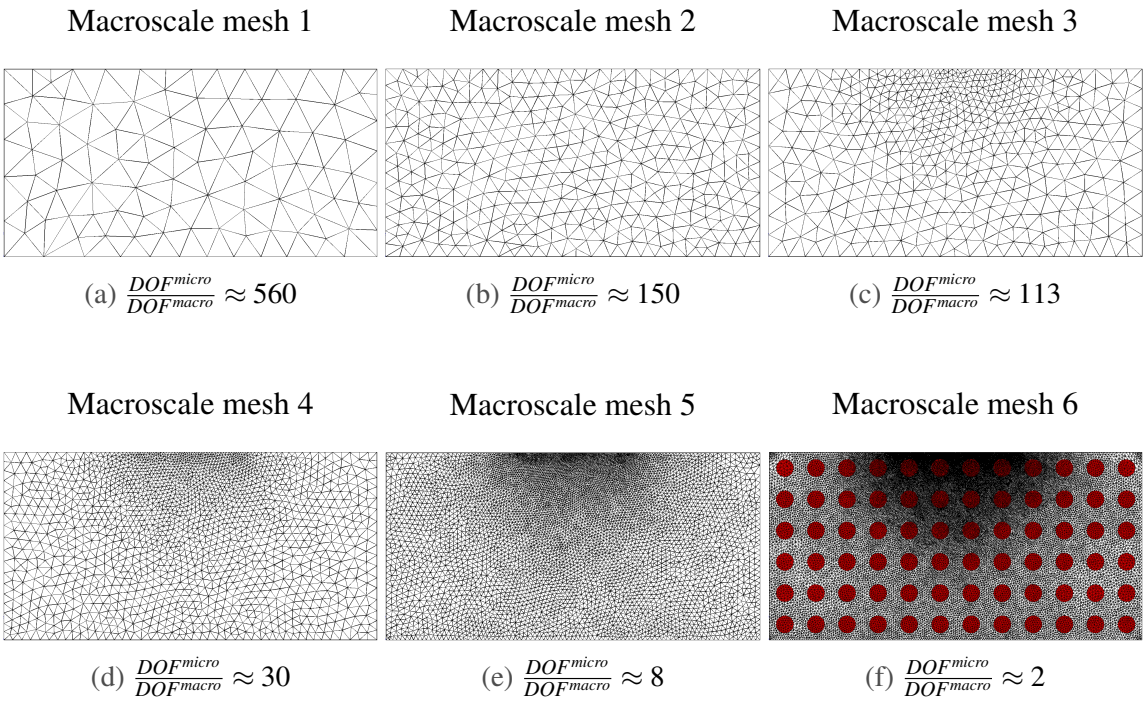

Figure 4.5: *Macroscale meshes on which the global balance and relocalization processes are performed.*

A comparison of σ_{22} and σ_{12} is show in figures 4.6 and 4.7, respectively (other stress and displacement components are presented in appendix C.1). By comparing reference fields, σ_{22}^{ref} and σ_{12}^{ref}, with relocalized fields, one can notice that the quality of the predicted stresses increases by refining the macroscale mesh. Nevertheless, the contribution of different material phase (matrix and fibers) to the stress field becomes visible starting from macroscale mesh 3, which provides an acceptable estimation of reference fields even though it contains 113 times fewer degrees of freedom than the microscale problem. Furthermore, high stress gradients, especially near regions where the load is applied and on the interfaces, are correctly predicted starting from macroscale mesh 3.
This relocalization process provides valuable insights on local responses of the constituents, at any material point, for a given macroscale state computed on a coarse mesh,

which is significantly less computationally expensive than DNS. This is of special interest for identifying local deformation mechanisms and quantities of interest such as damage. Furthermore, estimating local fields on macroscale meshes is a path toward error estimation and efficient multiscale submodeling, as it will be shown in the next sections.

Remark 13 *All localization tensors can be computed off-line and in parallel to reduce the computing time. Also, they can be used for any composite structure involving the same unit-cell with the same material properties of the constituents.*

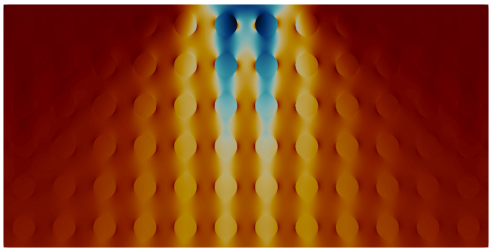

(a) σ_{22}^{ref} *on microscale mesh*

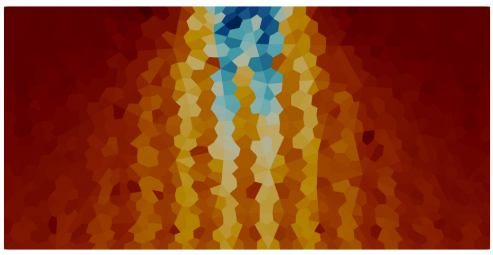

(b) σ_{22}^{cor2} *on macroscale mesh 1*

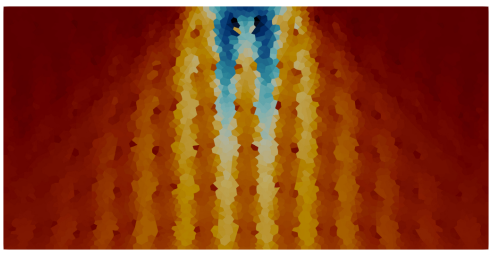

(c) σ_{22}^{cor2} *on macroscale mesh 2*

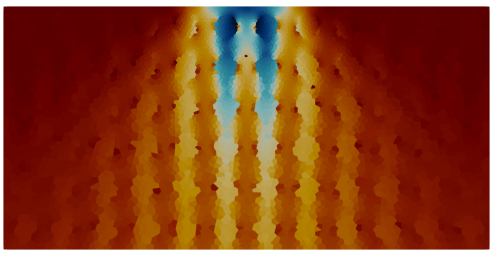

(d) σ_{22}^{cor2} *on macroscale mesh 3*

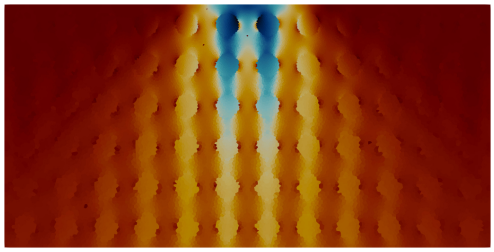

(e) σ_{22}^{cor2} *on macroscale mesh 4*

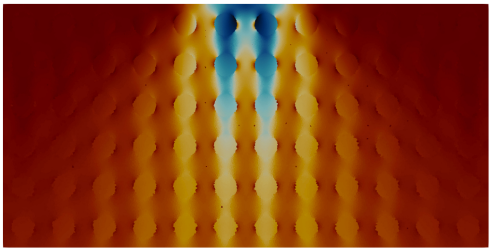

(f) σ_{22}^{cor2} *on macroscale mesh 5*

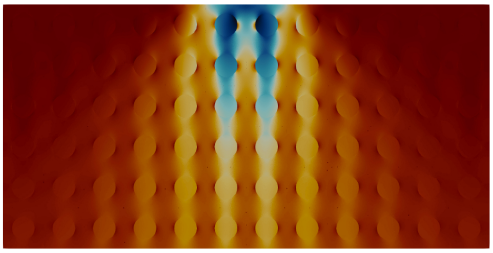

(g) σ_{22}^{cor2} *on macroscale mesh 6*

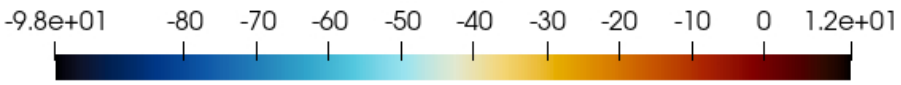

Figure 4.6: *Comparison of* σ_{22} *(MPa) results.*

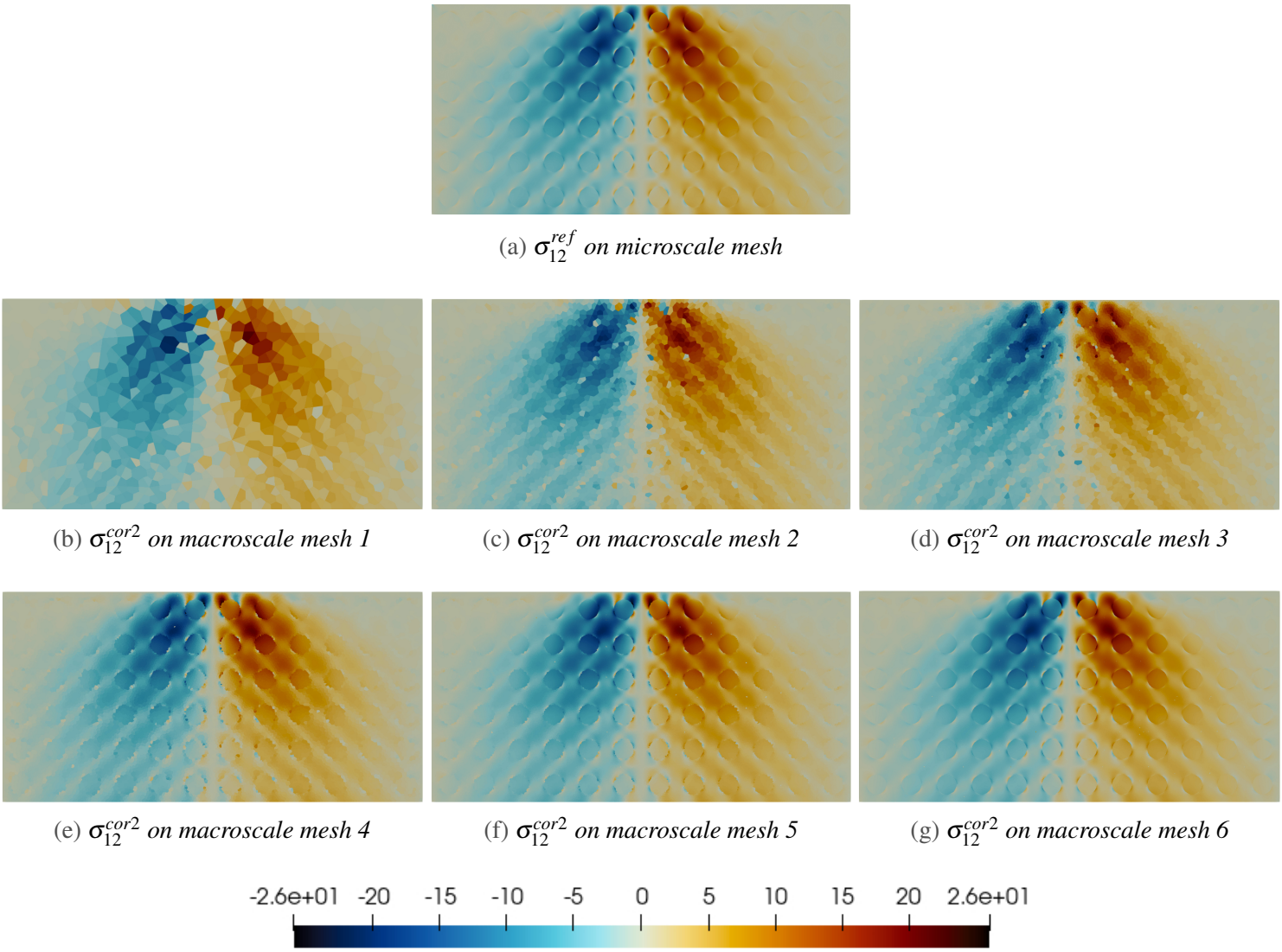

(a) σ_{12}^{ref} *on microscale mesh*

(b) σ_{12}^{cor2} *on macroscale mesh 1*

(c) σ_{12}^{cor2} *on macroscale mesh 2*

(d) σ_{12}^{cor2} *on macroscale mesh 3*

(e) σ_{12}^{cor2} *on macroscale mesh 4*

(f) σ_{12}^{cor2} *on macroscale mesh 5*

(g) σ_{12}^{cor2} *on macroscale mesh 6*

Figure 4.7: *Comparison of* σ_{12} *(MPa) results.*

4.4 Modeling error: A bridge between scales

Solving DNS is generally intractable because of the resulting extremely fine spatial discretization mesh. Nevertheless, there is a need to investigate what could occur at the microscale, since the behavior of heterogeneous structures depends on the characteristics of the heterogeneities. One method to tackle this is to *adaptively* couple a fine heterogeneous material description in some regions of the domain and a coarse, less accurate macroscale model in the other regions. For this purpose, one can use the well known submodeling techniques, which will be investigated in section 4.5.
In this work, a modeling error is used to steer this adaptive modeling process by detecting areas where refining the material model is required.

4.4.1 Formulation of the modeling error estimator

We recall that $\boldsymbol{u}^{ref}$, solution to $\left(\mathscr{P}_{ref}\right)$, is the reference displacement field computed by DNS. This field can be approximated with an asymptotic expansion in powers of the small parameter ε as:

$$\boldsymbol{u}^{ref}(\boldsymbol{x}) = \underbrace{\underbrace{\underbrace{\boldsymbol{u}^0(\boldsymbol{x},\boldsymbol{y})+\varepsilon\boldsymbol{u}^1(\boldsymbol{x},\boldsymbol{y})}_{\boldsymbol{u}^{est1}}+\varepsilon^2\boldsymbol{u}^2(\boldsymbol{x},\boldsymbol{y})}_{\boldsymbol{u}^{est2}}+\varepsilon^3\boldsymbol{u}^3(\boldsymbol{x},\boldsymbol{y})}_{\boldsymbol{u}^{est3}}+\ldots, \tag{4.5}$$

where the quantities $\boldsymbol{u}^n$ are $Y-$periodic functions called *correctors* of the displacement field. The first-, second-, and third-order relocalized displacement fields, $\boldsymbol{u}^{est1}$, $\boldsymbol{u}^{est2}$, and $\boldsymbol{u}^{est3}$, are obtained by truncating the asymptotic expansion to the first-, second-, and third-order, respectively (see equation 4.5).
As stated before, estimated fields are generally incorrect in the vicinity of the boundaries due to the loss of periodicity in these regions. Indeed, matching boundary conditions requires the introduction of boundary layer correctors at each relocalization order. As a result of this correction, $\boldsymbol{u}^{cor1}$, $\boldsymbol{u}^{cor2}$, and $\boldsymbol{u}^{cor3}$ are the first-, second-, and third-order corrected fields on the boundaries, respectively (see algorithm 1).
In this chapter, we define

$$\left\|\boldsymbol{u}^{ref}-\boldsymbol{u}^{est1}\right\|_{L_2(\Omega_e)} = \left(\int_{\Omega_e}\left(\boldsymbol{u}^{ref}-\boldsymbol{u}^{est1}\right)\cdot\left(\boldsymbol{u}^{ref}-\boldsymbol{u}^{est1}\right)d\Omega_e\right)^{\frac{1}{2}}, \tag{4.6}$$

as the measure of the local (element-wise) true modeling error, where Ω_e denotes the domain of an element. Thus, the global true modeling error, $\left\|\boldsymbol{u}^{ref}-\boldsymbol{u}^{est1}\right\|_{L_2(\Omega)}$, reads:

$$\left\|\boldsymbol{u}^{ref}-\boldsymbol{u}^{est1}\right\|^2_{L_2(\Omega)} = \sum_e \|\boldsymbol{u}^{ref}-\boldsymbol{u}^{est1}\|^2_{L_2(\Omega_e)}, \tag{4.7}$$

where Ω denotes the structural domain area.
For this study, the reference problem *is* tractable by Direct Numerical Simulation (DNS) and its mechanical fields are used as reference results to validate our approach. However,

in the more general case where a DNS would be out of reach, common practice would call for a tractable estimate.
Consequently, we choose to estimate the modeling error by replacing $\boldsymbol{u}^{ref}$ with the best estimate of the displacement field yet, *i.e.* $\boldsymbol{u}^{cor3}$. The modeling error is then estimated by:

$$\left\|\boldsymbol{u}^{ref}-\boldsymbol{u}^{est1}\right\|_{L_2(\Omega)} \approx \left\|\boldsymbol{u}^{cor3}-\boldsymbol{u}^{est1}\right\|_{L_2(\Omega)}. \tag{4.8}$$

The proposed modeling error estimator quantifies the terms neglected by a first-order relocalization. These terms are generally negligible in the case of a complete separation of scales. Nevertheless, for weak separation of scales, these terms become significant and necessary to capture gradients of the macroscale field. The proposed estimation also quantifies the modeling error that occurs on the boundaries.

Remark 14 *The modeling error estimation can be formulated using other mechanical fields than the displacement, i.e. the strain, or the stress field* ($\left\|\boldsymbol{\varepsilon}^{cor3}-\boldsymbol{\varepsilon}^{est1}\right\|_{L_2(\Omega)} = \left(\int_\Omega \left(\boldsymbol{\varepsilon}^{cor3}-\boldsymbol{\varepsilon}^{est1}\right):\left(\boldsymbol{\varepsilon}^{cor3}-\boldsymbol{\varepsilon}^{est1}\right)d\Omega\right)^{\frac{1}{2}}$ *and* $\left\|\boldsymbol{\sigma}^{cor3}-\boldsymbol{\sigma}^{est1}\right\|_{L_2(\Omega)}$, *respectively).*

Remark 15 *It is also possible to use an energy norm to quantify the modeling error. Thus, the estimation would read:*

$$\left\|\boldsymbol{u}^{cor3}(\boldsymbol{x})-\boldsymbol{u}^{est1}(\boldsymbol{x})\right\|_{E(\Omega)} = \left(\int_\Omega \left(\boldsymbol{\varepsilon}^{cor3}-\boldsymbol{\varepsilon}^{est1}\right):\left(\boldsymbol{\sigma}^{cor3}-\boldsymbol{\sigma}^{est1}\right)d\Omega\right)^{\frac{1}{2}}. \tag{4.9}$$

4.4.2 Comparison with the discretization error

In general, relocalized solutions, $\boldsymbol{u}^{cor3}$ and $\boldsymbol{u}^{est1}$, are obtained by a finite dimensional approximation, which is, in our case, a finite element approximation $\boldsymbol{u}^{cor3,h}$ and $\boldsymbol{u}^{est1,h}$, obtained on the macroscale mesh. By the Cauchy–Schwarz inequality, one can obtain:

$$\begin{aligned}\left\|\boldsymbol{u}^{cor3}-\boldsymbol{u}^{est1}\right\|_{L_2(\Omega)} \leq & \underbrace{\left\|\boldsymbol{u}^{est1}-\boldsymbol{u}^{est1,h}\right\|_{L_2(\Omega)}+\left\|\boldsymbol{u}^{cor3}-\boldsymbol{u}^{cor3,h}\right\|_{L_2(\Omega)}}_{\text{Discretization error: } \eta_{disc}} \\ & + \underbrace{\left\|\boldsymbol{u}^{cor3,h}-\boldsymbol{u}^{est1,h}\right\|_{L_2(\Omega)}}_{\text{Modeling error: } \eta_{mod}}.\end{aligned} \tag{4.10}$$

Therefore, a bipartite discretization error, indexed η_{disc}, occurs. The first and second parts constituting this error are due to the numerical approximation of $\boldsymbol{u}^{est1}$ and $\boldsymbol{u}^{cor3}$, respectively. To estimate the discretization error, we shall consider that the reference solutions of $\boldsymbol{u}^{est1}$ and $\boldsymbol{u}^{cor3}$ are obtained by conducting the relocalization process and boundary layer correction on the fine microscale mesh (see figure 4.8). Therefore, an interpolation-based nodal field transfer of $\boldsymbol{u}^{est1,h}$ and $\boldsymbol{u}^{cor3,h}$ is necessary from the macroscale mesh to the microscale one is considered (see figure 4.8). This nodal transfer preserves the continuum fields with no information loss since the coarse finite element space is included in the fine one [Dureisseix and Bavestrello, 2006]. The modeling error estimation, indexed η_{mod}, is computed on the macroscale mesh (see figure 4.8).

Remark 16 *On real use cases, relocalization procedure on the microscale mesh is computationally intractable. In this case one can use well known discretization error estimators as the posteriori error estimator ZZ2 [Zienkiewicz and Zhu, 1992b,d].*

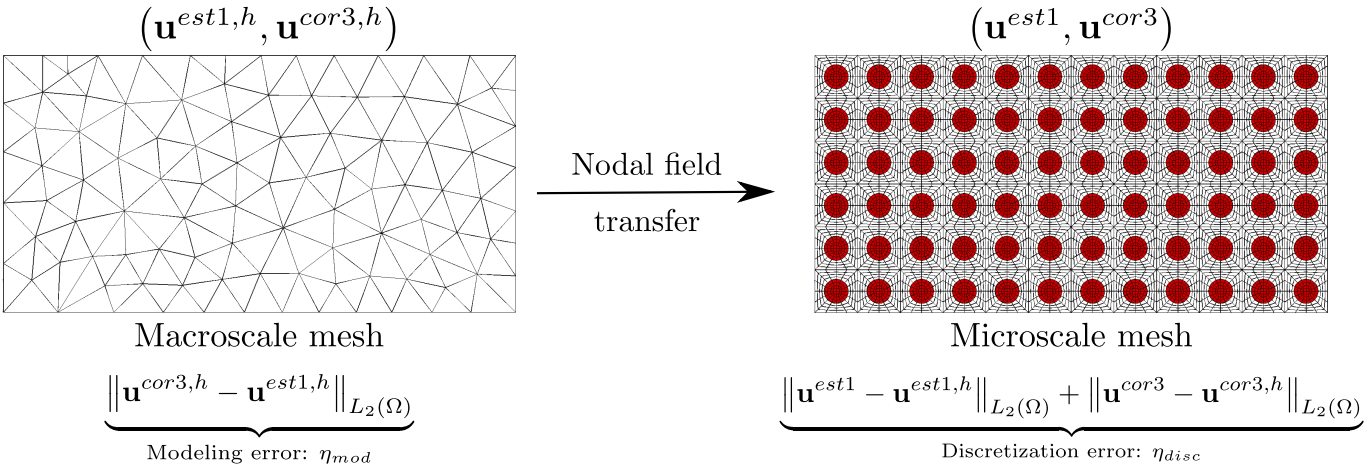

Figure 4.8: *Illustration of the error estimation process. The modeling error is computed on the macroscale mesh. A nodal field transfer of $\mathbf{u}^{est1,h}$ and $\mathbf{u}^{cor3,h}$ to the microscale mesh is conducted to compute the discretization error.*

4.4.3 Numerical results

Relative element-wise contribution to modeling and discretization errors, for a ratio $\frac{E_f}{E_m} = 10$ and $\frac{E_f}{E_m} = 500$, are shown in figures 4.9 and 4.10, respectively. The relocalization process with boundary layer correction is considered up to the second-order, as it is sufficient to capture strain gradient effects since the second gradient of the macroscale field was found to be negligible in this case. A comparison of the reference solution $\boldsymbol{u}^{ref}$, with the obtained relocalized fields, $\boldsymbol{u}^{est1}$ and $\boldsymbol{u}^{cor2}$, is shown in appendix C.2.
Both parts of the discretization error decrease by refining the macroscale mesh and start to cluster mainly on the fiber/matrix interfaces starting at mesh 4, until mesh 6 which preserves the topology of the fibers and, therefore, preserves the interfaces (see figure 4.5f). One can notice that the second part of the discretization error, $\left\|\boldsymbol{u}^{cor2} - \boldsymbol{u}^{cor2,h}\right\|_{L_2(\Omega)}$, is slightly higher than the first part due to numerical errors emanating from the computation of second-order relocalization and boundary layer correctors.

Remark 17 *One can fairly consider that both parts of the discretization error are nearly identical, thus:*

$$\eta_{disc} \approx 2 \left\|\boldsymbol{u}^{est1} - \boldsymbol{u}^{est1,h}\right\|_{L_2(\Omega)} \tag{4.11}$$

The modeling error, contrarily to the discretization error, varies relatively little by refining the macroscale mesh.
Global discretization error, η_{disc}, and modeling error, η_{mod}, for different ratios $\frac{E_f}{E_m}$ are shown in figure 4.11. Global values of the discretization error decrease by refining the macroscale mesh, whereas modeling error remains relatively constant.

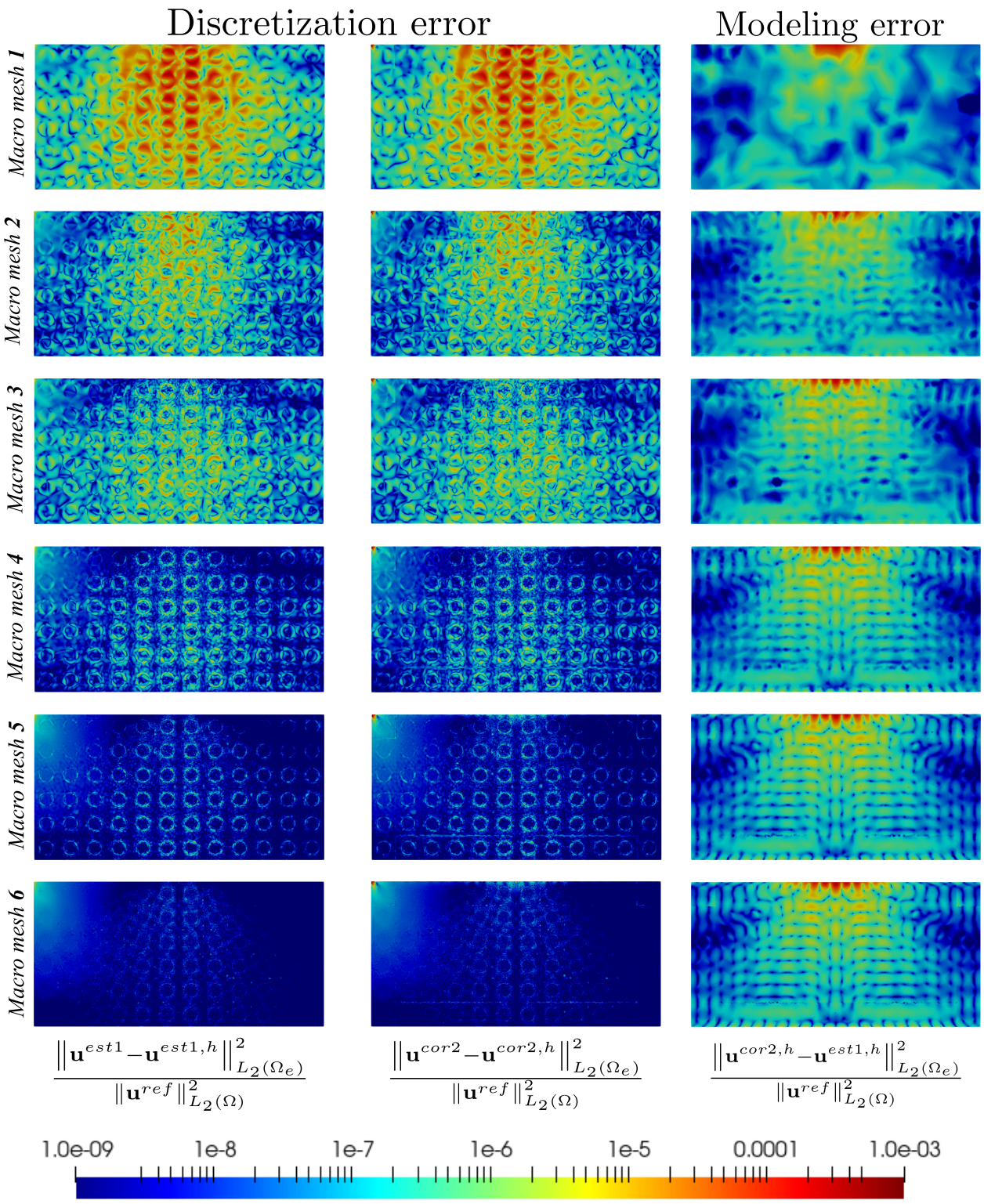

Figure 4.9: *Comparison of relative element-wise contribution to modeling and discretization errors for a ratio* $\frac{E_f}{E_m} = 10$ *on different macroscale meshes illustrated in figure 4.5.*

The modeling (and discretization) error estimation is relatively independent of the mismatch ratio $\frac{E_f}{E_m}$, especially for ratios higher than 50, as shown in figure 4.11. This low con-

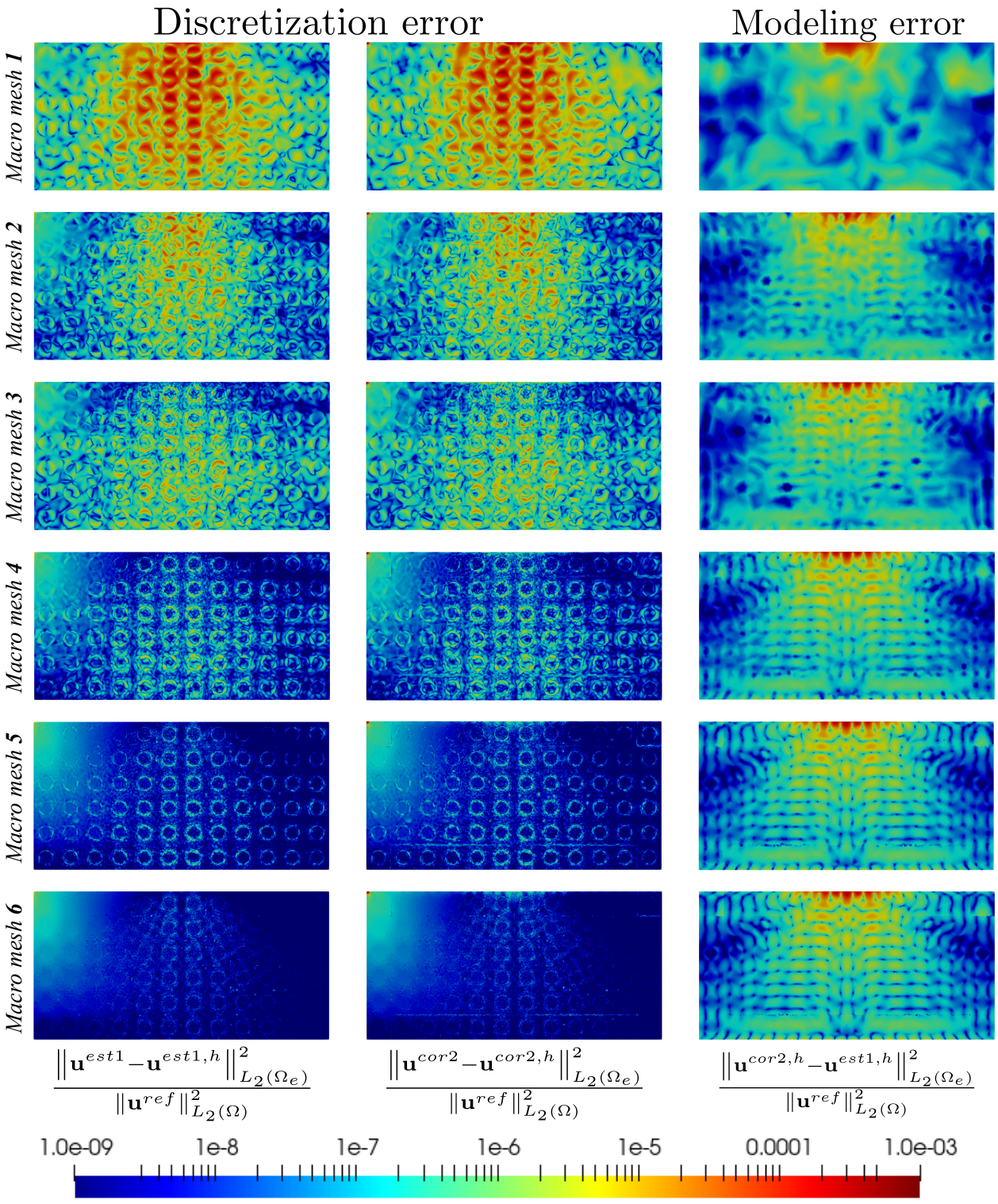

Figure 4.10: *Comparison of relative element-wise contribution to modeling and discretization errors for a ratio* $\frac{E_f}{E_m} = 500$ *on different macroscale meshes illustrated in figure 4.5.*

trast dependency is a key difference with the modeling error estimator proposed by Zohdi et al. [1996], which highly depends on the material phase contrast. This is explained by

the fact that their estimator quantifies the error emanated from the difference between the heterogeneous and the homogeneous materials, which can be high for important contrast ratios. Contrarily, our proposed modeling error estimator is constructed based on the quality of the approximation of heterogeneous fields, explaining the low contrast dependency, a property desirable in a modeling error estimator.

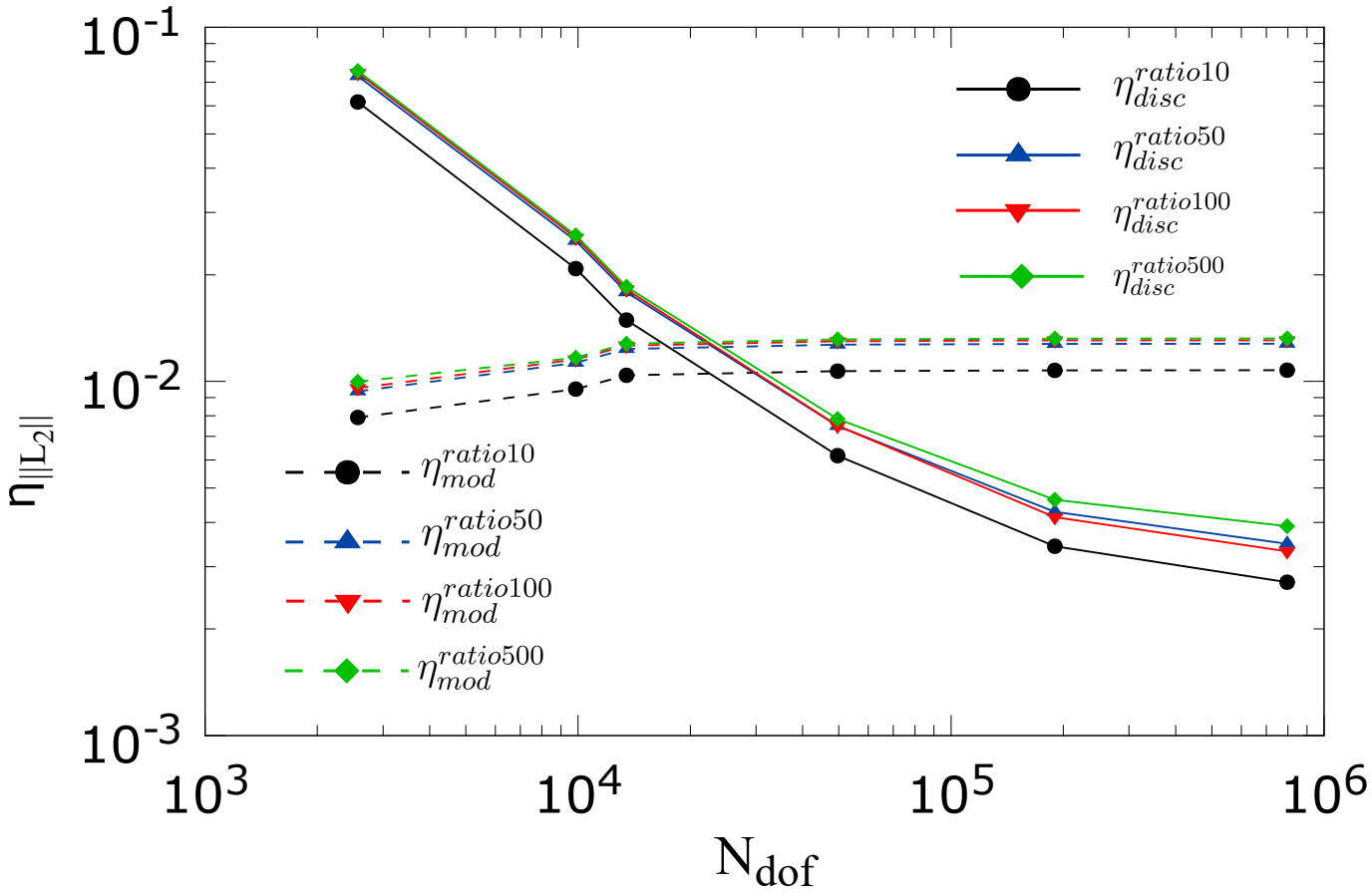

Figure 4.11: *Global discretization error η_{disc} and modeling error η_{mod} for different ratios $\frac{E_f}{E_m}$*

Also, regarding the competition between the discretization and the modeling error illustrated in figure 4.11, one shall consider a mesh refinement procedure to reduce the discretization error, and this until a refinement degree between mesh 3 and mesh 4 where the modeling error becomes dominant. One way to reduce this modeling error is to conduct an adaptive modeling process. This is analogous to mesh refinement, except that the refinement is in terms of the material model, *i.e.* replacing a homogeneous material by a heterogeneous one in regions with high modeling error.

4.5 Multiscale submodeling

The relative modeling error estimation of the stress field, *i.e.*

$$\frac{\left\|\boldsymbol{\sigma}^{cor2}-\boldsymbol{\sigma}^{est1}\right\|_{L_2(\Omega_e)}}{\left\|\boldsymbol{\sigma}^{ref}\right\|_{L_2(\Omega)}}, \tag{4.12}$$

on macroscale mesh 3 and for a ratio $\frac{E_f}{E_m}=500$ is illustrated in figure 4.12. To reduce this

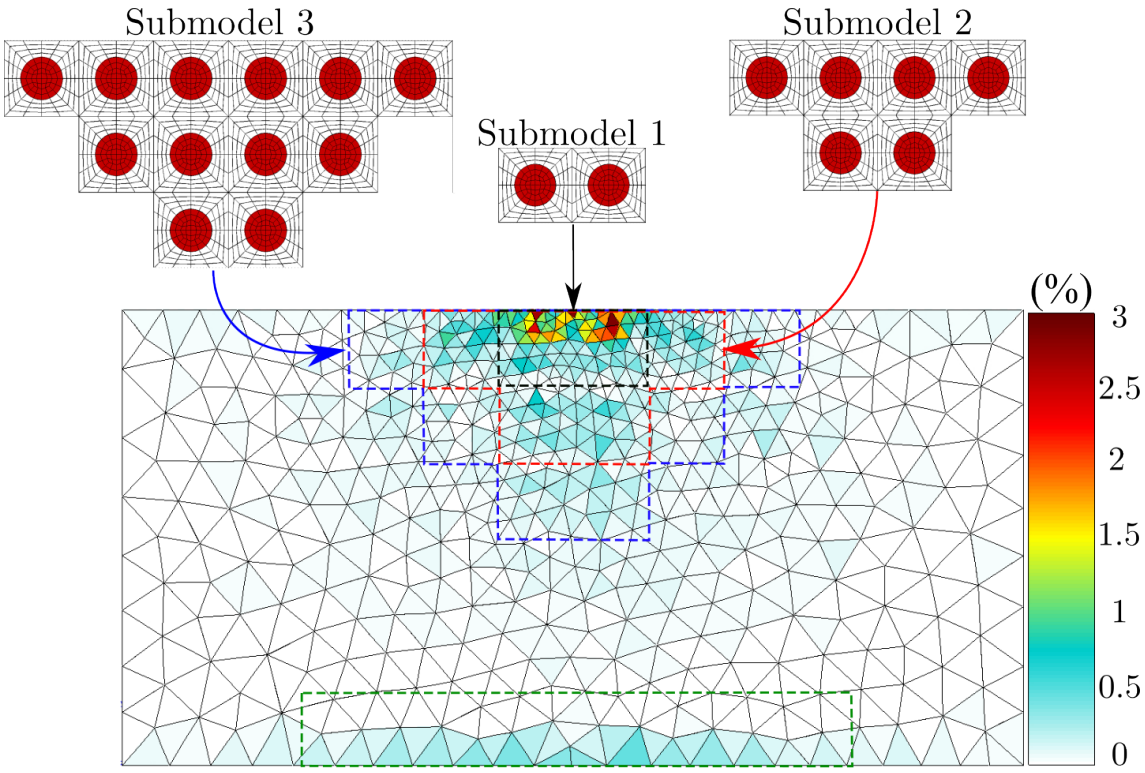

Figure 4.12: *Relative modeling error estimation of the stress field* $\frac{\left\|\boldsymbol{\sigma}^{cor2}-\boldsymbol{\sigma}^{est1}\right\|_{L_2(\Omega_e)}}{\left\|\boldsymbol{\sigma}^{ref}\right\|_{L_2(\Omega)}}$ *on macroscale mesh* 3*, shown in figure 4.5c, and for a ratio* $\frac{E_f}{E_m}=500$*. Different submodels are detected depending on target accuracy. For the sake of conciseness, the modeling error in the fixed boundary region (highlighted in green) is neglected.*

error, one can replace the homogeneous material by the heterogeneous material in regions where the modeling error is relatively high. These regions to be replaced depend on target accuracy, as suggested in figure 4.12. Indeed, replacing the microscale region labeled *submodel* 3 is expected to reduce the modeling error more than inserting *submodel* 2, which itself will reduce the error more than inserting *submodel* 1.

For hierarchical modeling, it is necessary to adequately couple the macroscale homogeneous domain with the selected microscale heterogeneous one. Such coupling is proposed in this section.

4.5.1 Proposed coupling strategy

Submodeling, also called structural zoom or global-local analysis, is largely used in the industry to conduct multiscale analyses since it is supported by most commercial finite element software (*e.g.* Abaqus or Ansys). In this approach, homogenized material properties are first determined, in our case using asymptotic homogenization. The macroscale problem is then solved using these homogeneous properties. The displacements are extracted from the boundary of a macroscale region of interest (Γ_G in figure 4.13). These fields become the boundary conditions (on Γ_L in figure 4.13) for a finite element *submodel* that contains microscale details, as shown in figure 4.13.

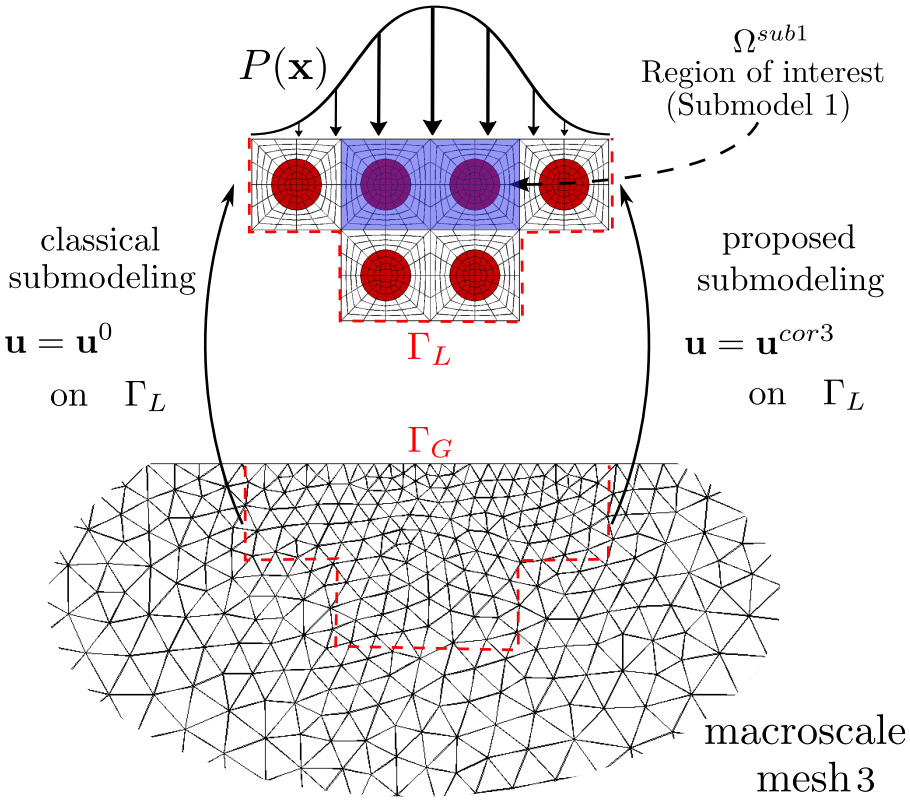

Figure 4.13: *Illustration of the classical and the proposed submodeling techniques.*

Remark 18 *Using displacement field interpolation, the submodel boundary Γ_L nodes do not have to match with the macroscale boundary Γ_G nodes.*

Classical submodeling, *i.e.* applying $\boldsymbol{u}^0$, is expected to fail in appropriately coupling the macroscale with the microscale, and this no matter the size of the submodel, as it will be shown later, for the following reasons:

- The homogenized displacement $\boldsymbol{u}^0$, misses, by definition, the microscale details. The coupling, therefore, neglects the heterogeneous nature of the submodel, which result in high interface coupling errors. Consequently, it is necessary to enlarge the submodel to avoid coupling errors in a region of interest as shown in figure 4.14, which can be computationally expensive.

- Homogeneous fields are only valid for infinite periodic arrays under a uniform state of macro-stress (or macro-strain). This is not the case for weak separation of scale scenarios.
- Homogenized solutions do not take into account the boundary layer effect due to the loss of periodicity conditions on the boundaries.

In what follows, the proposed submodeling is performed by applying $\boldsymbol{u}^{cor2}$ instead of $\boldsymbol{u}^{cor3}$, since the second gradient of the macroscale field was found to be negligible in this case.
The proposed submodeling considers the aforementioned aspects since the displacement field $\boldsymbol{u}^{cor2}$ is heterogeneous by construction, takes into account macroscale strain gradients, and is corrected at the boundaries.
It is worth noting that the submodeling approach is a *descending* process in the sense that there is no feedback from the submodel computation toward the macroscale one. Such feedback is necessary to conduct reliable hierarchical modeling. However, this aspect is left for future works.

4.5.2 Numerical results

To compare the reference solution $\boldsymbol{u}^{ref}$ with the displacement field obtained using classical submodeling $\boldsymbol{u}^{\mathscr{L}}$ or the proposed submodeling $\boldsymbol{u}^{\mathscr{L}^*}$, the following local (element-wise) error in energy norm is defined:

$$\begin{aligned}\|\boldsymbol{e}\|_{E(\Omega_e)} &= \|\boldsymbol{u}^{ref}(\boldsymbol{x}) - \boldsymbol{u}^{k}(\boldsymbol{x})\|_{E(\Omega_e)} \\ &= \left(\int_{\Omega_e} \left(\boldsymbol{\varepsilon}^{ref} - \boldsymbol{\varepsilon}^{k}\right) : \left(\boldsymbol{\sigma}^{ref} - \boldsymbol{\sigma}^{k}\right) d\Omega_e\right)^{\frac{1}{2}},\end{aligned} \tag{4.13}$$

where Ω_e denotes the domain of an element and $k = (\mathscr{L}$ or $\mathscr{L}^*)$. Thus, the global error $\|\boldsymbol{e}\|_{E(\Omega)}$ reads:

$$\|\boldsymbol{e}\|^2_{E(\Omega)} = \sum_e \|\boldsymbol{e}\|^2_{E(\Omega_e)}, \tag{4.14}$$

where Ω denotes the domain of the chosen submodel. We define the local (element-wise) relative error as:

$$\boldsymbol{e}_{rel} = \frac{\|\boldsymbol{e}\|^2_{E(\Omega_e)}}{\|\boldsymbol{u}^{ref}\|^2_{E(\Omega)}}. \tag{4.15}$$

We also consider a quantity of interest corresponding to the relative mean error, e^{mean}_{rel}, in the region of interest Ω^{sub1} illustrated in figure 4.13:

$$e^{mean}_{rel} = \frac{\frac{1}{n_E}\sum_e \|\boldsymbol{e}\|_{E(\Omega^{sub1}_e)}}{\|\boldsymbol{u}^{ref}\|_{E(\Omega)}}, \tag{4.16}$$

where n_E is the number of elements in Ω^{sub1}.
Figure 4.14 shows a comparison of the relative error, defined in equation 4.15, obtained by using the classical submodeling $(k = \mathscr{L})$ and the proposed one $(k = \mathscr{L}^*)$, for the three submodels illustrated in figure 4.12, and for ratio $\frac{E_f}{E_m} = 500$. The macromesh 3, shown in

figure 4.5c, is used for the macroscale computation and the relocalization process. The

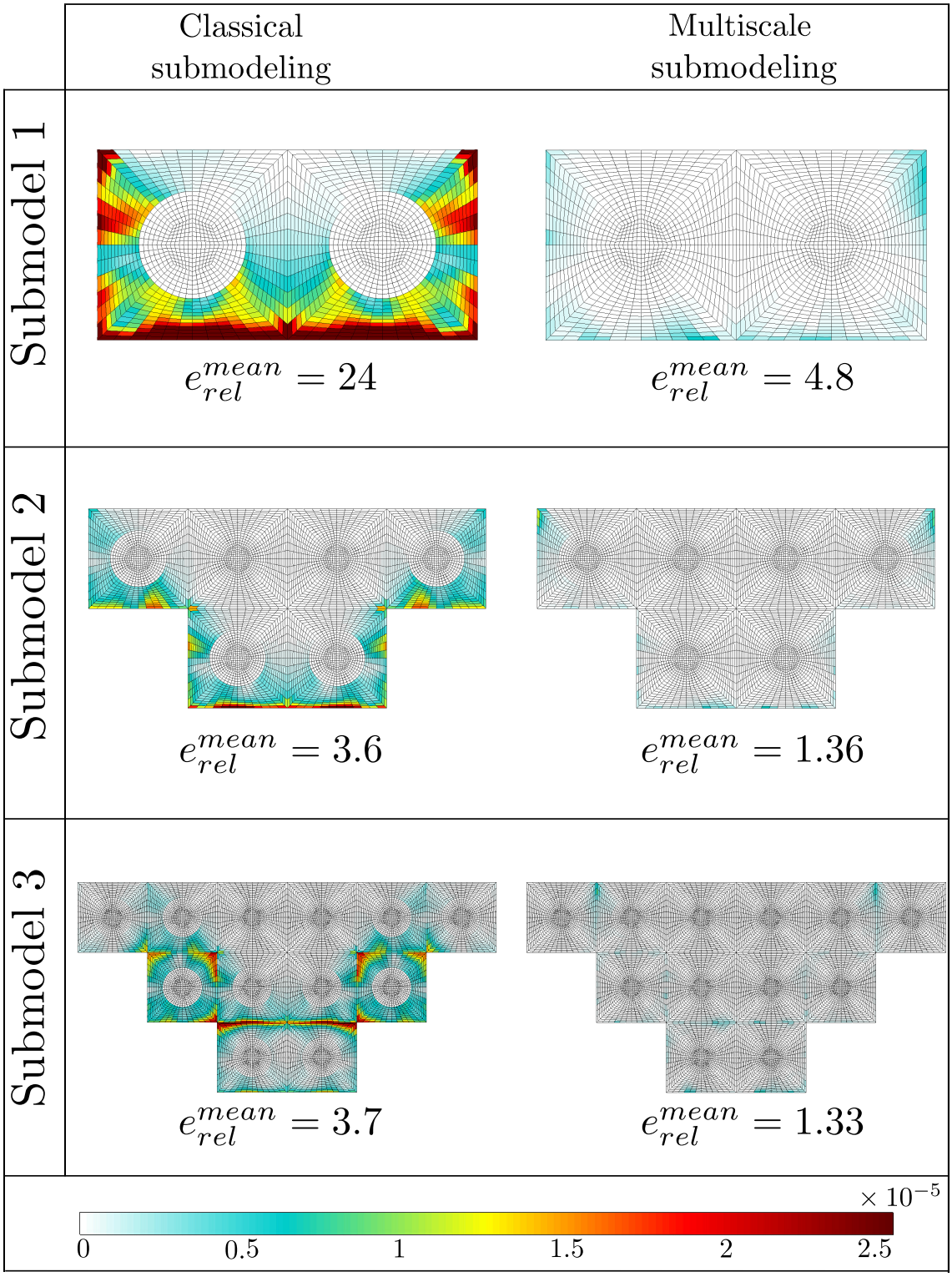

Figure 4.14: *Comparison, for a ratio* $\frac{E_f}{E_m} = 500$*, of the relative error defined in 4.15 and the relative mean error* ($\times 10^{-6}$) *defined in 4.16, both obtained by using the classical submodeling and the proposed multiscale submodeling. The macromesh 3 (illustrated in figure 4.5c) is used for the macroscale computation and the relocalization process.*

relative error is drastically reduced by the proposed submodeling compared to the classical one, for the three submodels and the considered ratio. Indeed, classical submodeling leads to large errors, especially in the vicinity of the coupling interfaces. This coupling error increases by increasing the material phase contrast. The proposed submodeling enables to reduce the relative mean error e_{rel}^{mean} by a factor of ≈ 5 for submodel 1 and a factor of ≈ 3 for submodels 2 and 3.
Comparison of the global relative error, formulated in equation 4.14, obtained by using the classical and the proposed submodeling, is shown in table 4.1. One can notice that the global error increases by increasing the material phase contrast. The proposed coupling reduces the global error by a factor of ≈ 5 for submodel 1, a factor of ≈ 3 for submodel 2 and a factor of ≈ 4 for submodel 3.

Table 4.1: *Comparison of the global relative error* $\frac{\|\boldsymbol{e}\|_{E(\Omega)}}{\|\boldsymbol{u}^{ref}\|_{E(\Omega)}}$ *obtained by using the classical vs the proposed submodeling.*

Ratio/Submodel	1			2			3		
	Classical		Proposed	Classical		Proposed	Classical		Proposed
10	8.50%	*vs*	1.74%	7.03%	*vs*	2.11%	10.79%	*vs*	2.90%
50	9.91%	*vs*	2.06%	8.18%	*vs*	2.51%	12.53%	*vs*	3.41%
100	10.11%	*vs*	2.04%	8.33%	*vs*	2.54%	12.77%	*vs*	3.46%
500	10.26%	*vs*	2.06%	7.51%	*vs*	1.51%	12.96%	*vs*	3.50%

To study the influence of the macroscale mesh on the proposed submodeling, a comparative study is presented in figure 4.15, investigating the relative error and the mean error obtained for a coupling with different macroscale meshes, illustrated in figure 4.5, and for different submodels, shown in figure 4.12. The material phase contrast considered in this study is $\frac{E_f}{E_m} = 500$.

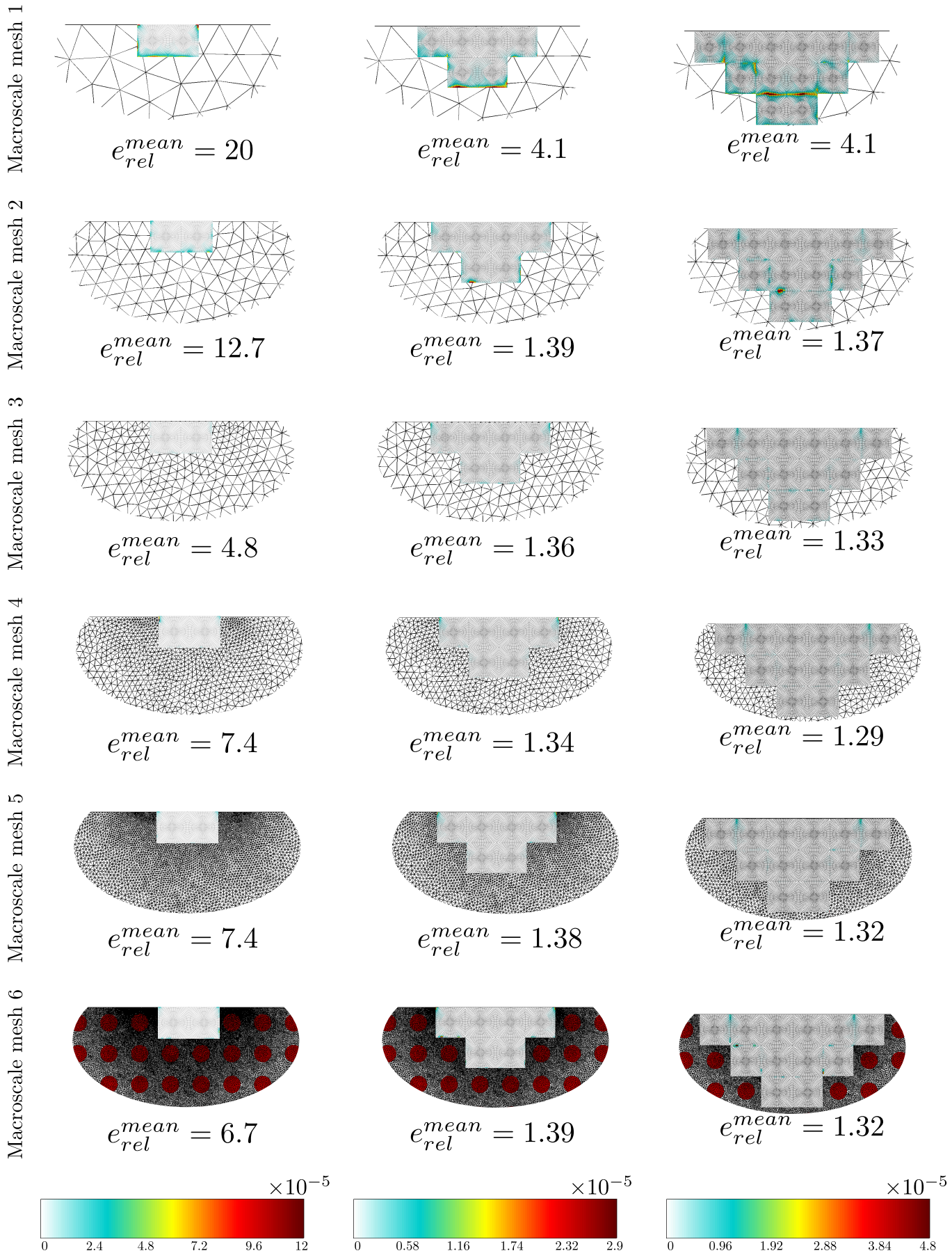

Figure 4.15: *Comparison of the relative error defined in 4.15 and the relative mean error ($\times 10^{-6}$) defined in 4.16 obtained for the proposed multiscale coupling with different macroscale meshes, for different submodels and for a ratio* $\frac{E_f}{E_m} = 500$.

The main features of these results are the following:

- Classical submodeling is almost insensitive to the macroscale mesh. Indeed, the coupling error remains high even after refining the macroscale mesh, irrespective of the submodeling domain size. This is explained by the fact that the homogenized displacement field, applied on the interface of the submodel, is nearly the same for the six macroscale computations as it does not consider the microscale details, but depends only on the effective behavior, unchanged for the six macroscale computations. On the other hand, the proposed coupling is sensitive to the macroscale mesh since the relocalization process depends on this one.
- The multiscale proposed submodeling, with macroscale mesh 1 and 2, is significantly less accurate than with other meshes, since the relocalization process is still largely incorrect, as shown in figures 4.6, 4.7, and 4.11.
- For all the considered cases, the relative local coupling error induced by the proposed submodeling is significantly smaller than the error obtained by the classical submodeling.
- The mean error e_{rel}^{mean} is reduced, besides results obtained for mesh 1, by at least a factor of 2 (for mesh 2 - submodel 1) and at the best by a factor of 5 (for mesh 3 - submodel 1).

A comparison of the global relative error and the relative mean error obtained for a coupling with different macroscale meshes, and for different submodels are shown in figure 4.16 and figure 4.17.
The main features of these results are the following:

- The global and the mean error induced by the classical submodeling are insensitive to macroscale mesh refinement. Contrarily, the errors induced by the proposed submodeling are sensitive to the macroscale mesh refinement since the relocalization process is conducted on this one.
- For all the considered cases, the global error induced by the proposed submodeling is inferior to the one obtained by the classical submodeling. The error is reduced at least by a factor of 1.2 and the best by a factor of 5.
- The mean error in the region of interest Ω^{sub1} decreases by increasing the size of the submodel.
- For all the considered cases, the mean error induced by the proposed submodeling is less than to the one obtained by the classical submodeling. The error is reduced at least by a factor of 1.12 and the best by a factor of 5.

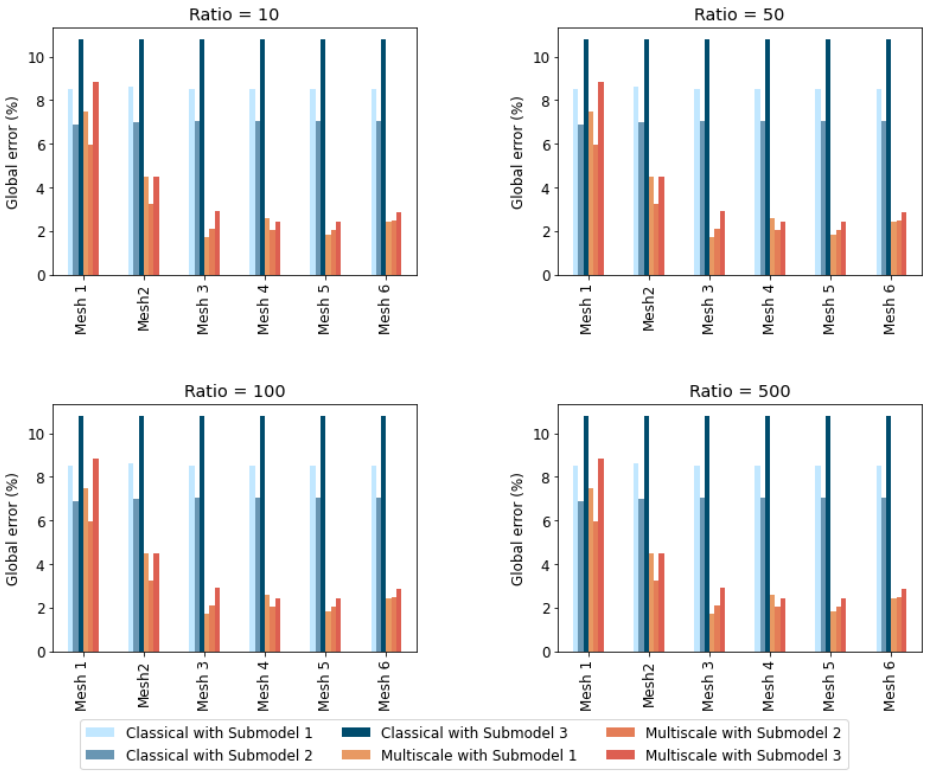

Figure 4.16: *Comparison of the global relative error obtained for a coupling with different macroscale meshes, and for different submodels.*

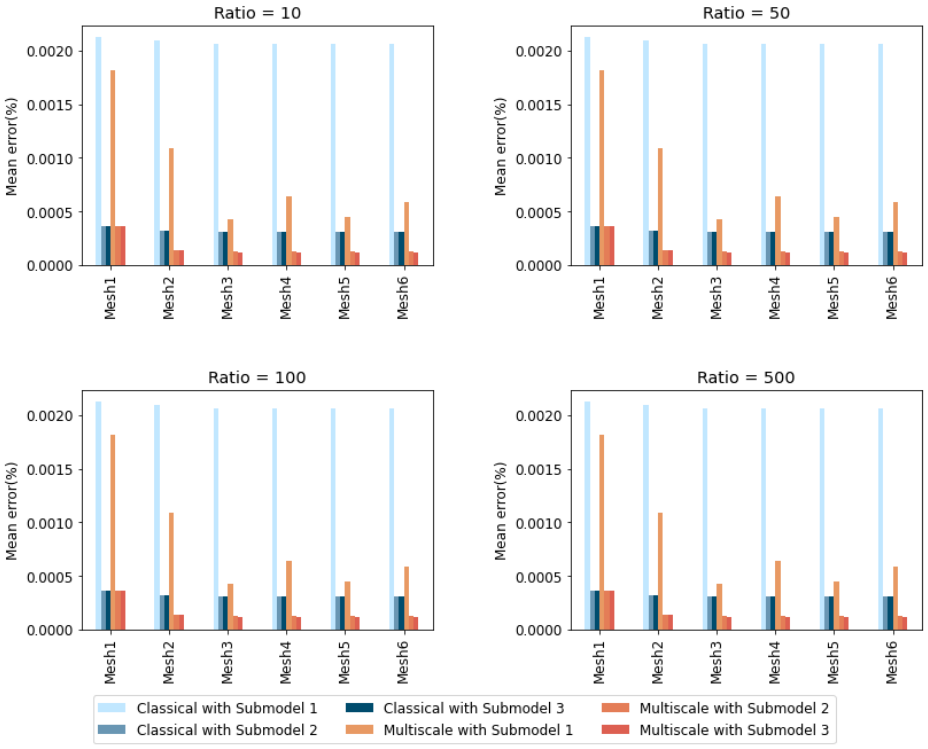

Figure 4.17: *Comparison of the relative mean error obtained for a coupling with different macroscale meshes, and for different submodels.*

4.6 Conclusions

In this work, we have proposed a new numerical method to conduct, on a macroscale coarse mesh, a higher-order relocalization process to estimate local heterogeneous fields within a structure, without conducting any Direct Numerical Simulations (DNS). This relocalization process, contrary to first-order homogenization, takes into account additional terms of the asymptotic expansion, and thus captures the effect of macroscopic successive gradients, generally high in cases of low scale separation. The proposed relocalization process also includes a boundary layer correction to correct estimated fields on the boundaries. As a result, the proposed numerical method provides valuable insights on microscale fields, for a given macroscale state computed solely on the coarse macroscale mesh, much less computationally expensive than DNS.

We have also proposed a modeling error estimation based on the resulting fields computed by the aforementioned relocalization process. Indeed, the suggested error estimation quantifies the terms neglected by the first-order asymptotic expansion. These terms are significant in cases where scales are not well separated and necessary to capture gradients of the macroscale fields. The proposed error estimation is also able to quantify the modeling error on the boundaries due to the loss of periodicity assumptions in boundary regions. This modeling error estimation is used to steer a hierarchical modeling process by detecting areas where refining the material model is necessary.

To couple the microscale domain with the macroscale one, we have suggested a multiscale enhanced submodeling based on the constructed local fields. As a result, the proposed submodeling, contrary to the classical one, considers the heterogeneous nature of the submodel and remains valid in regions with low scale separation, *e.g.* regions with high macroscale strain or stress gradients, and in the vicinity of the boundaries.

The major conclusions that can be drawn from this work are as follows:

- The quality of the estimated stress fields increases by refining the macroscale mesh. Nevertheless, it has been shown that the proposed relocalization process conducted on a macroscale mesh containing ≈ 100 times fewer degrees of freedom than the DNS already provides an acceptable estimation of the local stress field, as illustrated in figures 4.6, and 4.7.

- It is possible to reduce the discretization error by refining the macroscale mesh; the modeling error, however, remains unchanged, as shown in figure 4.11. To reduce this error, hierarchical modeling (or another alternative) should be considered.

- Classical submodeling is less sensitive to macroscale mesh refinement, contrary to the proposed submodeling, as illustrated in figure 4.16 and 4.17.

- The proposed submodeling technique reduces the global coupling error by a factor of 5, compared to classical submodeling, as shown in figure 4.16. It also reduces the mean error in a region of interest by a factor of 5, as shown in figure 4.17.

Reliable hierarchical modeling requires a feedback from the submodel computation toward the macroscale one, which has not been investigated in this work. The suggested methods could also be a path toward the hierarchical modeling of realistic 3D composite structures. This implies the use of irregular structure domains, locally nonperiodic zones, and controlling simultaneously both the discretization and the modeling error.

Chapter 5

Conclusions and Outlook

5.1 Summary of the main results

The main goal of this Ph.D. was to develop a modeling error estimator in order to steer hierarchical modeling of heterogeneous periodic structures. By doing so, I aim to adaptively couple a heterogeneous model in regions with a low separation of scales and a homogeneous, less accurate model in other regions of relatively homogeneous deformation. As a result, hierarchical modeling may significantly reduce computational cost compared to a full heterogeneous computation. Another objective of this Ph.D. was to propose an adequate coupling technique to connect the heterogeneous model with the homogeneous one. Asymptotic homogenization remains the most rigorous and suitable method to deal with periodic structures. It permits not only to determine the macroscopic overall characteristics but to estimate, by a relocalization process, mesostructural effects on the macroscopic response as well.

It has been shown that first-order estimates, obtained from the relocalization process, are a good approximation of the heterogeneous fields in the inner domain of the structure, provided that macroscale gradient fields remain low, *i.e.*, scales are completely separated. Nevertheless, accuracy is lost near the boundaries due to the non-periodicity in the boundary layers. Indeed, I have shown that high stress fields are developed near the boundaries and are neglected by a classical relocalization, which, for example, may result in underestimating a failure criterion if the design is conducted without any boundary layer correction. I have proposed a correction, effective for different boundary conditions (Dirichlet, Neumann, and mixed), to estimate consistent microscale fields in the vicinity of the boundaries. Fundamental idea of this method is to compute correction terms by solving several auxiliary problems on the unit-cell. The type of problem to be solved is determined by the local boundary conditions. These correction terms are added to the standard fields resulting from the relocalization procedure, significantly improving the solution at the boundaries. I have also demonstrated, on a bending case, the scale separation limit of the first-order homogenization method. Indeed, I have shown that first-order estimates become inaccurate, even in the inner domain, when the structure is subjected to important macroscale gradients.

To deal with real engineering cases generally subjected to strong macroscale strain gradients, I have considered higher-order asymptotic homogenization/relocalization, up

to the third-order. As a result, estimated fields are shown to be in perfect agreement with the reference fields inside the structure, even for cases of low scale separation. I have also proposed an extension to the proposed boundary layer correction to rectify higher-order estimates, up to the third order, in the vicinity of the boundaries.

To estimate the modeling error, I first extended the higher-order relocalization process to deal with arbitrary coarse macroscale meshes. As a result, crucial insights on local responses of the constituents are computed on the coarse mesh, which results in a significantly less computationally expensive analysis than a full heterogeneous calculation. The proposed modeling error estimation quantifies the terms neglected by the first-order asymptotic expansion. These terms become significant in cases of a low separation of scales. The proposed error estimation is also able to quantify the modeling error on the boundaries. The competition between the discretization error and the modeling error has been investigated. Furthermore, I have suggested a multiscale enhancement of the classical submodeling in order to adequately couple the homogeneous and heterogeneous domains. It has been shown that the proposed submodeling drastically reduces the coupling errors compared the classical submodeling.

5.2 Main contributions

Most of the development carried-out during this Ph.D. are implemented in the finite element code Z-set [2022]. The main contributions and new developments that I made throughout my Ph.D. are as follows:

- **Higher-order asymptotic homogenization:** Localization tensors are obtained by solving a hierarchical set of elasticity problems with prescribed body forces and eigenstrains, obtained from the solution at the lower-order. I implemented a boundary condition to apply these body forces and eigenstrains in order to compute higher-order asymptotic homogenization, up to the third-order. My implementation has been verified, up to the third-order, based on analytical solutions of localization tensors provided by Boutin [1996], as shown in appendix B.1.

- **Relocalization process and boundary layer correction:** I proposed and implemented a post-processing scheme to conduct higher-order relocalization process, up to the third-order to estimate heterogeneous fields. To correct these estimates on the boundaries, I proposed and implemented a new boundary layer correction method which is constituted from several boundary conditions to be applied on the unit-cell. These boundary conditions depend on the actual location of the boundary to be solved as explained in figure 2.6. I also proposed and implemented a new method to conduct the relocalization process on arbitrary macroscale meshes, as described in figure 4.4. In this method, boundaries are automatically, *i.e.* in the same computation, identified and relocalization fields are then corrected. The method is also able to automatically apply the specific treatment for corner cell illustrated, for example, in figure 2.5e.

- **Modeling error estimation:** I proposed a modeling error estimation based on higher-order relocalization. This estimation is implemented in a post-processing step. Different norms of the error can be considered (L2 norm and energy norm). The modeling error is then used to detect areas where to refine the material model.
- **Multiscale submodeling:** After constructing, on the macroscale mesh, higher-order estimates corrected on the boundaries, I used the submodel boundary condition to apply the resulting estimated field instead of the macroscale one, as per classical submodeling.

5.3 Prospects

Even if the primary research questions outlined in this thesis' introductory chapter have been successfully addressed, certain questions still remain unresolved and new issues arose throughout the Ph.D.

- **Extension to realistic 3D composite structures:** The proposed approaches are adapted for periodic structures. Nevertheless, realistic structures, as the fan blade, display irregular structure domains and locally nonperiodic zones. An extension to such cases would undoubtedly facilitate numerical simulations of engineering structures. Fish and coworkers [Fish and Wagiman, 1993; Fish and Fan, 2008] have tried to account for locally nonperiodicity in the asymptotic homogenization, but this challenging subject requires additional efforts.
- **Simultaneous model and mesh refinement:** Although I have studied the competition between the modeling and discretization error, it would be interesting to propose an multipurpose error estimator able to simultaneously steer both discretization and modeling refinement as done by Temizer and Wriggers [2011]; Vernerey and Kabiri [2012].
- **Reliable hierarchical modeling:** The proposed submodeling is a *descending* process in the sense that there is no feedback from the submodel computation toward the macroscale one. Such feedback is necessary to conduct reliable hierarchical modeling.
- **Higher-gradient macroscale continuum:** In some cases, the conventional Cauchy medium may give a poor prediction of the real deformation state. Consequently, the relocalization process will be inaccurate, even by including higher-order terms, since the resulting macroscale strain and its gradients, considering a Cauchy continuum, are inaccurate and not representative of the deformation state. In these cases, it would be necessary to consider higher-gradient macroscale continua as done in Forest and Sab [1998]; Yvonnet et al. [2020].

5.4 Valorization

Contribution to the Z-set suite

The implemented methods are provided, through an internal Git Repository, for the community of researchers and users of the Z-set suite. Also, a user-guide is written for documentation purposes and to explain how to practically use the implemented methods.

Supervision of a trainee

I supervised, for one year, Mateus AMERICO DE ALMEIDA as part of his specialized master's degree. During the first part (6 months) of the internship at Mines Paris, I accompanied Mateus in his bibliographical research on the asymptotic homogenization method and particularly on solutions to extend this method to non-periodic zones. During the second part of the internship (6 months), I received Mateus at Safran and we worked together on:

- Automatization of the global framework to conduct higher-order relocalization with boundary layer correction in Z-set, see appendix D.1.
- Enhancement of boundary layer correction for corner cells, see appendix D.2.
- Early work on the extension of the asymptotic homogenization method to non-periodic zones, see appendix D.3.

Articles

Two articles have been published and one submitted article:

- **Mouad Fergoug**, Augustin Parret-Fréaud, Nicolas Feld, Basile Marchand and Samuel Forest. A general boundary layer corrector for the asymptotic homogenization of elastic linear composite structures. Composite Structures, 2022, 285:115091. doi: 10.1016/j.compstruct.2021.115091
- **Mouad Fergoug**, Augustin Parret-Fréaud, Nicolas Feld, Basile Marchand and Samuel Forest. Multiscale analysis of composite structures based on higher-order asymptotic homogenization with boundary layer correction. European Journal of Mechanics - A/Solids, 2022, 96:104754. doi: 10.1016/j.euromechsol.2022.104754
- **Mouad Fergoug**, Augustin Parret-Fréaud, Nicolas Feld, Basile Marchand and Samuel Forest. Toward hierarchical modeling of heterogeneous structures driven by a modeling error estimator. Submitted to: Computer Methods in Applied Mechanics and Engineering

One published article in a national conference proceedings:

- **Mouad Fergoug**, Nicolas Feld, Samuel Forest, Basile Marchand, Augustin Parret-Fréaud. Méthode générale pour la correction des couches limites en homogénéisation asymptotique. 15ème colloque national en calcul des structures, Université Polytechnique Hauts-de-France [UPHF], May 2022, 83400 Hyères-les-Palmiers, France. ffhal-03717638

The research results of this thesis were communicated in several international conferences:

- **WCCM 2020**: World Congress in Computational Mechanics (WCCM-ECCOMAS 2020), France (Virtual congress).
- **ADMOS 2021**: 10th International Conference on Adapive Modeling and Simulation, Sweden (Virtual congress).
- **COMPOSITES 2021**: 8th Conference on Mechanical Response of Composite, Sweden (Virtual congress).
- **ECCOMAS 2022**: 8th European Congress on Computational Methods in Applied Sciences and Engineering, Norway.
- **ESMC 2022**: 11th European Solid Mechanics Conference, Ireland.

Appendices

Appendix of Chapter 2

A.1 Finite element resolution of the first-order

This appendix describes the numerical procedure using the Finite Element Method (FEM) in order to solve $\left(\mathscr{P}^{1^{st}}_{order}\right)$ and thus compute the localization tensors $(\mathbb{D},\mathbb{A},\mathbb{B})$ and the homogenized elasticity tensor $\mathbb{C}^0$. We also describe the proposed numerical relocalization scheme used to estimate the full microscopic fields.

Computation of relocalization and homogenized elasticity matrices

The displacement corrector $\boldsymbol{u}^1$, solution of the first-order periodic problem, constitute the components of the corrector displacement matrix $[\mathbb{D}]$. The finite element approximation to Eq. (2.14) is:

$$\begin{aligned}\int_{Y^e} [\boldsymbol{B}]^{\top}_{N_{dof}\times 6}\,[\mathbb{C}]_{6\times 6}\,[\boldsymbol{B}]_{6\times N_{dof}}\,[\mathbb{D}]_{N_{dof}\times 6}\,dY^e &= \int_{Y^e} [\boldsymbol{B}]^{\top}_{N_{dof}\times 6}\,[\mathbb{C}]_{6\times 6}\,dY^e \\ &= \left[\boldsymbol{F}^D\right]_{N_{dof}\times 6},\end{aligned} \tag{A.1}$$

where the script e denotes element quantities from the discretized unit-cell domain Y. $[\mathbb{C}]$ is the heterogeneous elastic stiffness matrix, $[\boldsymbol{B}]$ is the strain shape function matrix, and $[\mathbb{D}]$ is the displacement localization matrix whose components are solutions of Eq. (A.1). The load $\left[\boldsymbol{F}^D\right]$ is a matrix composed of six columns in the 3D cases. Each column is a force vector corresponding to an initial strain loading. To illustrate this, we recall that the nodal forces $\left\{\boldsymbol{f}^{\varepsilon^0}\right\}$ induced by an initial strain ε^0 are defined as:

$$\left\{\boldsymbol{f}^{\varepsilon^0}\right\} = \int_Y [\boldsymbol{B}]^{\top}\,[\mathbb{C}]\,\varepsilon^0 dY. \tag{A.2}$$

Thus, in our case, the loading is six unit initial strain tensors E^{kl} applied to the unit-cell with $kl = \{11,22,33,23,31,12\}$. Indeed, Eq. (A.1) is a set of six matrix equations with six solutions, each providing a column of $[\mathbb{D}]$:

$$D_{ikl} = u^1_i \text{ for } i \in \{1,2,3\},\ kl = \{11,22,33,23,31,12\}, \tag{A.3}$$

where D_{ijk} are components of the displacement localization tensor $\mathbb{D}$. Periodic boundary conditions are imposed on the unit-cell in order to solve problems in Eq. (A.1). The resulting strain and stress fields obtained for each loading case also provide a column of the strain and stress localization matrices $[\mathbb{A}]$ and $[\mathbb{B}]$, respectively. The homogenized elasticity matrix $\mathbb{C}^0$ can be obtained from the volume average of $[\mathbb{B}]$:

$$\left[\mathbb{C}^0\right] = \frac{1}{|Y|}\int_Y [\mathbb{B}]\,dY. \tag{A.4}$$

Practically, the components of $\mathbb{C}^0$ can be computed by solving elementary load cases corresponding to the different components of the macroscale strain E^{kl} and performing a unit-cell average of the resulting microscopic stress components.

Flowchart for the numerical resolution of $\left(\mathscr{P}^{1^{st}}_{order}\right)$

In practice, after discretizing the unit-cell domain, it is sufficient to run the finite element program for six different unit initial strain tensors E^{kl} applied on the unit-cell. With $kl = \{11,22,33,23,31,12\}$ each load case provides a column vector of $[\mathbb{D}]$, $[\mathbb{A}]$, and $[\mathbb{B}]$. Components of the displacement corrector matrix $[\mathbb{D}]$ are stored at the nodes and those of the localization matrices $[\mathbb{A}]$ and $[\mathbb{B}]$ are stored at integration points. The main steps for the numerical resolution of the first-order problem are summarized in Fig. A.1.

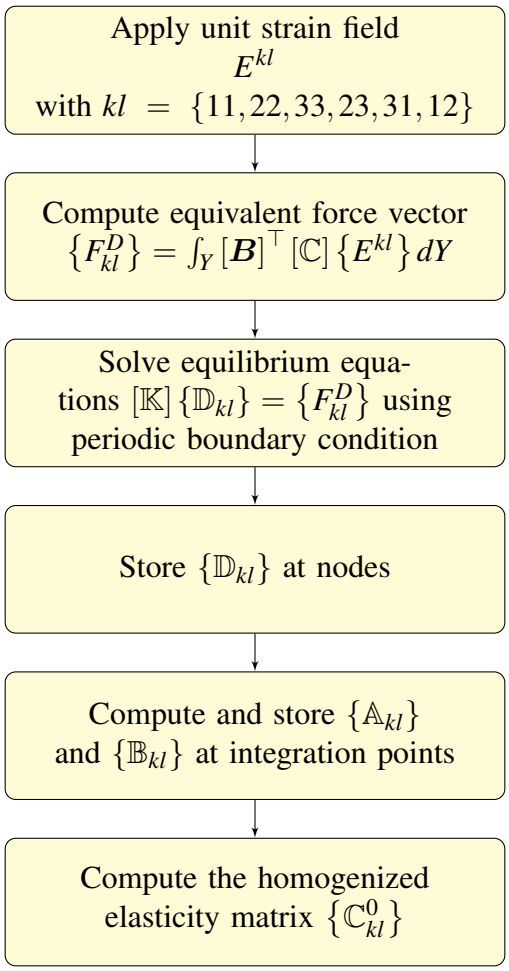

Figure A.1: *Flowchart summarizing the numerical resolution of* $\left(\mathscr{P}^{1^{st}}_{order}\right)$.

A.2 Uni-directional laminated composite in tension

We consider a uni-directional laminated composite made of two layers as presented in Fig. B.1. The size of the structure is $L = 8$ mm, $H = 5$ mm and $W = 1$ mm. The two layers are assumed to be isotropic linear elastic with coefficients ($E_m = 1000$ MPa, $\nu_m = 0.3$) and ($E_f = 10E_m, \nu_f = 0.3$).

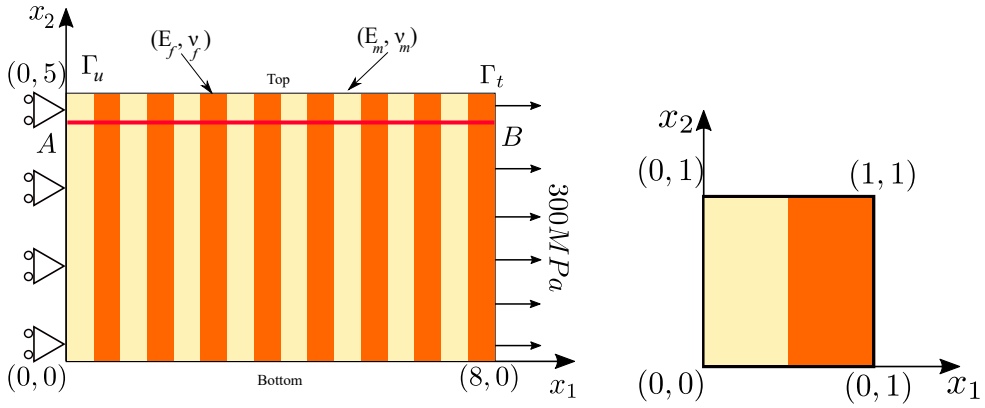

(a) *Structure geometry* (b) *unit-cell domain*

Figure A.2: *Illustration of the uni-directional laminated composite in tension. The structure is sliding on* Γ_u *and surface tension is applied on* Γ_t.

Case 1: Flat Top and Bottom surfaces

In this case, periodicity conditions are applied to Top and Bottom surfaces. Both homogeneous and heterogeneous solution fields depend only on the x_1 variable. Estimated fields using relocalization process are supposed to match exactly with the heterogeneous ones, even on the boundaries as there is no fluctuation of material properties in the x_2 direction (see ε_{11}^{ref}, ε_{11}^{hom} and ε_{11}^{est} in Fig. A.3). Therefore, no boundary layer correction is needed.

Case 2: Free Top and Bottom surfaces

In this case, heterogeneous fields are expected to fluctuate at Top and Bottom surfaces due to the heterogeneity of the material along these free edges. Therefore, a boundary layer correction in these surfaces is necessary in order to correctly estimate heterogeneous fields (see σ_{11}^{ref}, σ_{11}^{est} and σ_{11}^{cor} in Fig. A.3).
Results of stress fields are plotted in Fig. A.4 along the AB line shown in Fig. B.1. The corrected stress field σ_{11}^{cor} captures the fluctuation of the reference field σ_{11}^{ref} contrary to the estimated field σ_{11}^{est} which is constant. The difference between relocalized and corrected fields at $x_1 = [0,1]$ and $x_1 = [7,8]$ in Fig. A.4 is due to the imperfection of the proposed correction for corner cells.

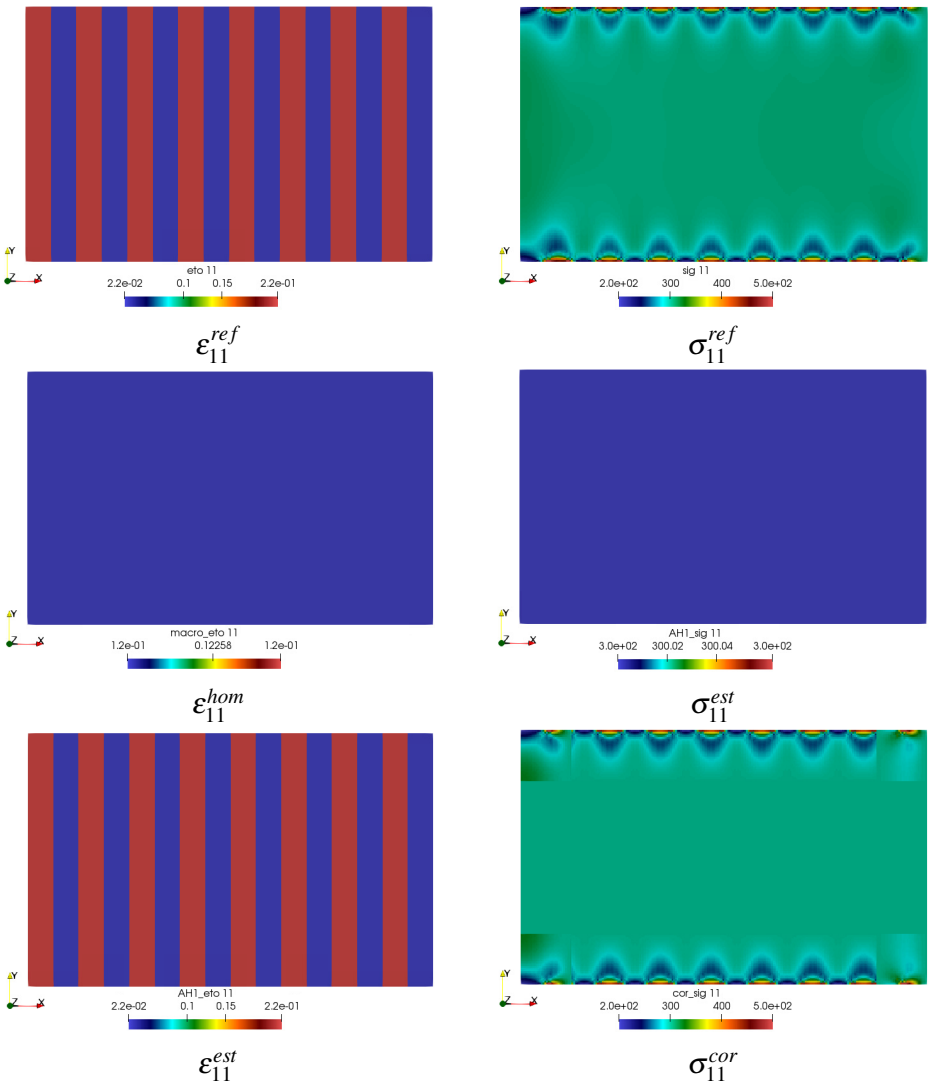

Figure A.3: *Results of the strain fields for case 1 (Periodicity conditions on Top and Bottom surfaces) and stress fields for case 2 (Free Top and Bottom surfaces).*

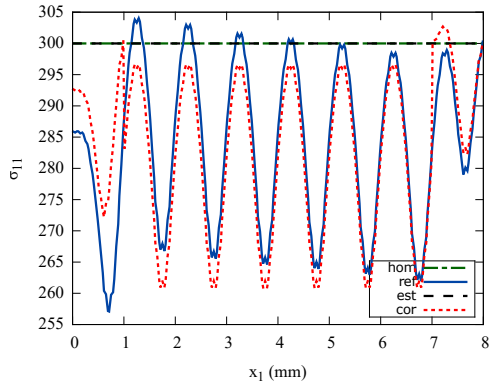

(a) σ_{11} *(MPa)*

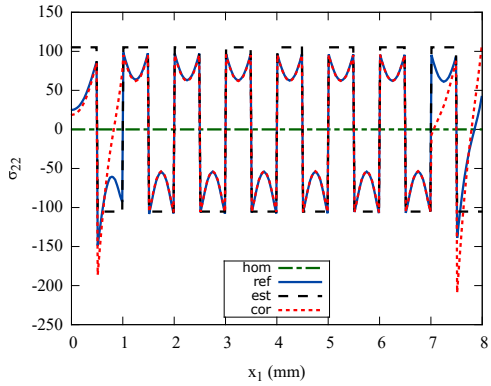

(b) σ_{22} *(MPa)*

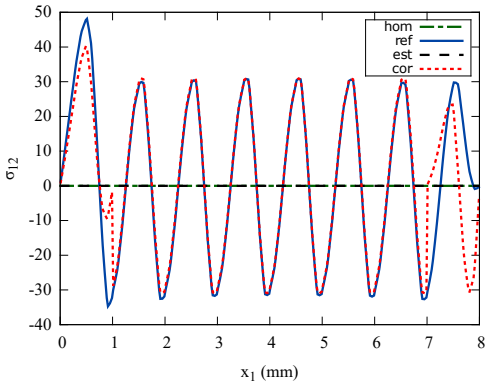

(c) σ_{12} *(MPa)*

Figure A.4: *Results of the homogenized (hom), reference (ref), estimated (est) and corrected (cor) stress fields corresponding to case 2 and plotted along the line AB.*

Appendix of Chapter 3

B.1 Numerical validation of localization tensors

The objective of this appendix is to validate our numerical implementation of higher-order localization tensors, up to the third-order. To do so, we compare the obtained numerical, relocalization and effective, tensors with their analytical solutions provided by Boutin [1996]. For the sake of conciseness, expressions of analytical solutions are omitted.

A stratified composite is considered composed of two isotropic elastic layers a and b with respective thickness $(1-\tau)h$ and τh as shown in Fig. B.1a. The elastic moduli of the phase a and b are (E_a, ν_a) and (E_b, ν_b), respectively. Layers a and b are periodically distributed along the direction y_1, and remain unchanged by any translation along directions y_2 and y_3. Therefore, local fields depend only on variable y_1.

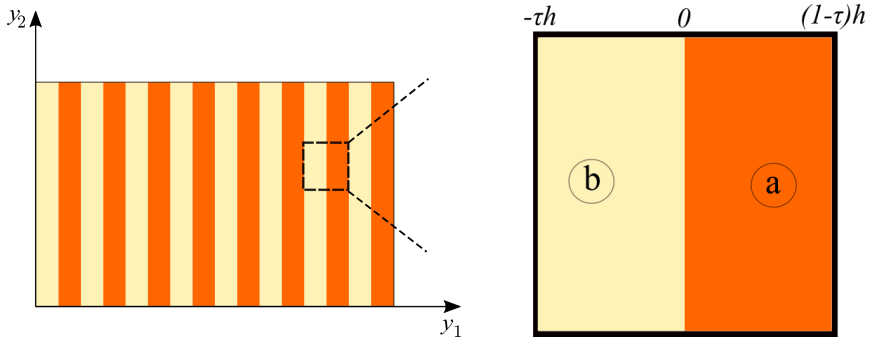

(a) *Stratified composite geometry* (b) *Unit-cell domain*

Figure B.1: *Illustration of the studied problem.*

For numerical simulations, the following material properties are considered: $E_b = 1\text{GPa}$, $E_a = 5\text{GPa}$ and $\mu_a = \mu_b = 0.3$ with $\tau = 0.5$.

First-order problem $\left(\mathscr{P}^{1^{st}}_{order}\right)$ validation

The solutions to these problems are first-order displacement, strain, and stress localization tensors: $\mathbb{D}^0$, $\mathbb{A}^0$, and $\mathbb{B}^0$, respectively.

Components D^0_{111} and A^0_{1111} are shown in Fig. B.2a and B.2b, respectively. Displacement fields, *i.e.* components of $\mathbb{D}^0$, are piecewise linear as shown in Fig. B.2c while strain fields, *i.e.* components of $\mathbb{A}^0$, are constant per layer as shown in Fig. B.2d. Comparison between obtained numerical and analytical solutions of first-order displacement, strain, and stress localization tensors: $\mathbb{D}^0$, $\mathbb{A}^0$, and $\mathbb{B}^0$ are shown in figures B.2c, B.2d and B.2e, which are in perfect agreement.

remark B.1 *By a volume average process on $\mathbb{B}^0$, one can deduce the homogenized elasticity tensor $\mathbb{C}^0$. An orthotropic macroscopic elastic behavior is obtained.*

Second-order problem $\left(\mathscr{P}^{2^{nd}}_{order}\right)$ validation

The solutions to these problems are second-order displacement, strain, and stress localization tensors: $\mathbb{D}^1$, $\mathbb{A}^1$, and $\mathbb{B}^1$, respectively.
Components D^1_{2222} and A^1_{12222} are shown in figures B.2a and B.2b, respectively. Displacement fields are now quadratic functions as shown in Fig. B.3c while strain fields are piecwise linear as shown in Fig. B.3d. Comparison between obtained numerical and analytical solutions of second-order displacement, strain, and stress localization tensors: $\mathbb{D}^1$, $\mathbb{A}^1$, and $\mathbb{B}^1$ are shown in figures B.3c, B.3d and B.3e, which are in perfect agreement.

remark B.2 *Components of $\mathbb{B}^1$ have a zero volume average on the unit-cell. Therefore, the second-order effective tensor $\mathbb{C}^1 = 0$, which is a fifth-rank tensor.*

Third-order problem $\left(\mathscr{P}^{3^{rd}}_{order}\right)$ validation

The solutions to these problems are third-order displacement, strain, and stress localization tensors: $\mathbb{D}^2$, $\mathbb{A}^2$, and $\mathbb{B}^2$, respectively.
Components $(D^2_{12222}, B^2_{222222})$ and $(D^2_{21121}, A^2_{121121})$ are shown in Fig. B.4. Displacement fields are now cubic functions as shown in figures B.4b and B.4f while stress/strain fields are quadratic functions as shown in figures B.4d and B.4h.

remark B.3 *After averaging values of $\mathbb{B}^2$, one can deduce the third-order effective tensor $\mathbb{C}^2$, which is a sixth-rank tensor. Analytical expression of $\mathbb{D}^2$, $\mathbb{A}^2$, and $\mathbb{B}^2$ were not provided in Boutin [1996], but values of $\mathbb{C}^2$ are detailed. We have verified that we obtain, **exactly**, the same values of $\mathbb{C}^2$ provided in Boutin [1996] by our numerical procedure.*

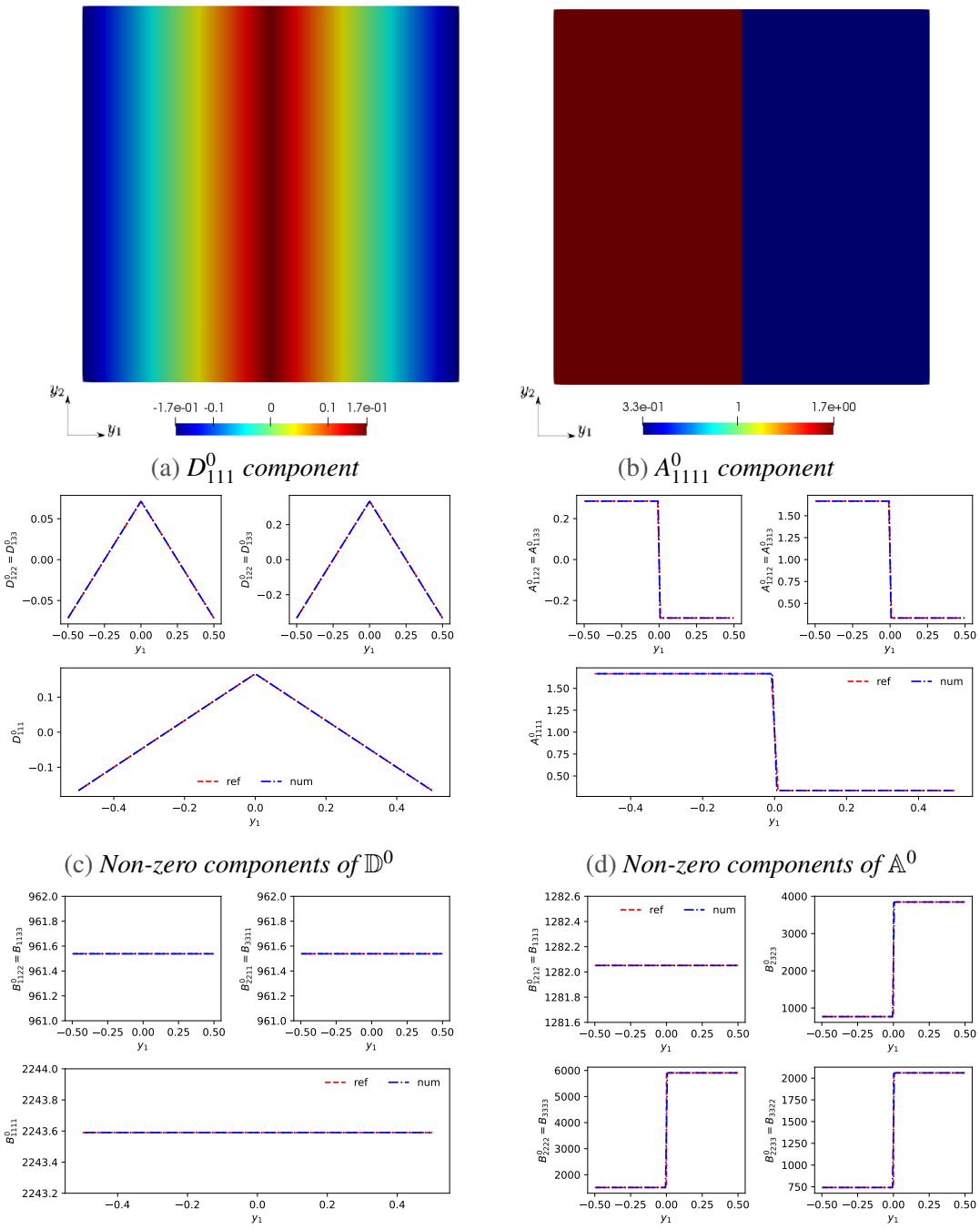

(a) D^0_{111} *component*

(b) A^0_{1111} *component*

(c) *Non-zero components of* $\mathbb{D}^0$

(d) *Non-zero components of* $\mathbb{A}^0$

(e) *Non-zero components of* $\mathbb{B}^0$

Figure B.2: *Results of the first-order homogenization problem* $\left(\mathscr{P}^{1^{st}}_{order}\right)$. *Figures B.2c, B.2d and B.2e show perfect agreement between numerical (in blue) and analytical (in red) results.*

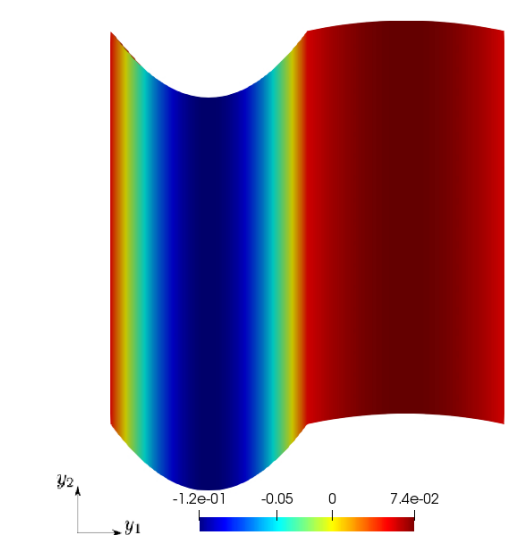

(a) D^1_{2222} *component*
(magnification of 10)

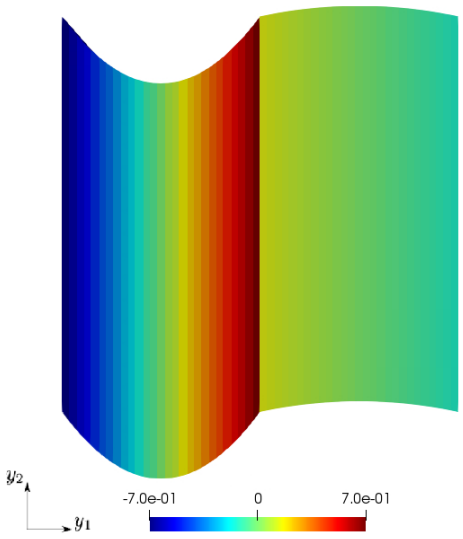

(b) A^1_{12222} *component*
(magnification of 10)

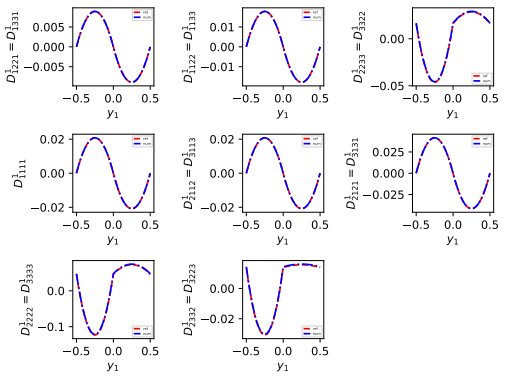

(c) *Non-zero components of* $\mathbb{D}^1$

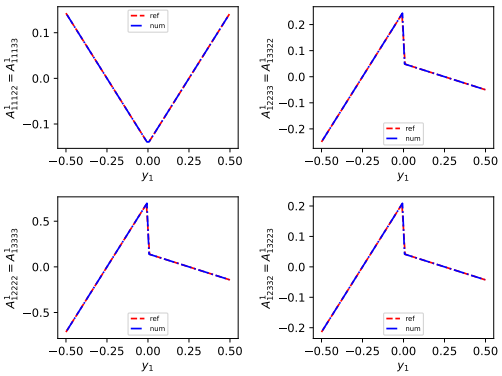

(d) *Non-zero components of* $\mathbb{A}^1$

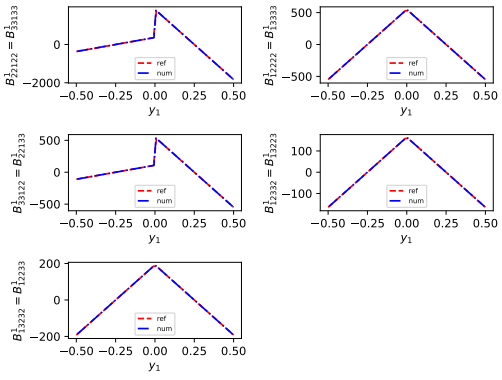

(e) *Non-zero components of* $\mathbb{B}^1$

Figure B.3: *Results of the second-order homogenization problem* $\left(\mathscr{P}^{2^{nd}}_{order}\right)$. *Figures B.3c, B.3d and B.3e show perfect agreement between numerical (in blue) and analytical (in red) results.*

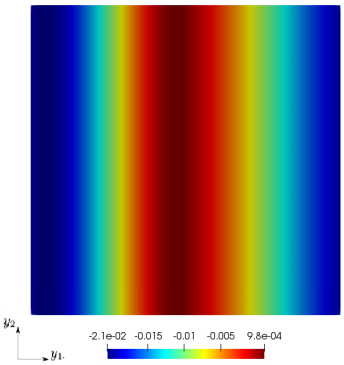

(a) D^2_{12222} *component*

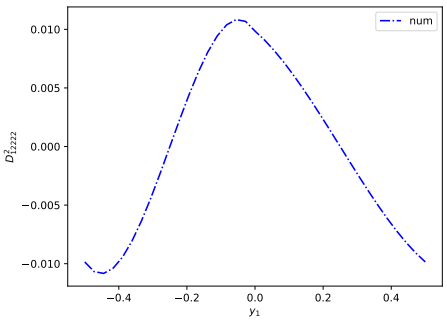

(b) D^2_{12222} *values along* y_1

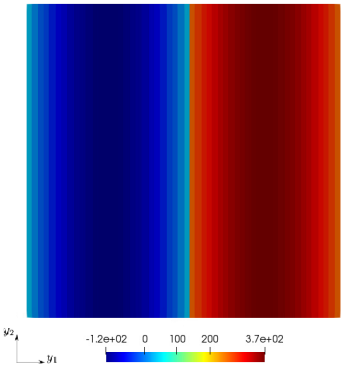

(c) B^2_{222222} *component*

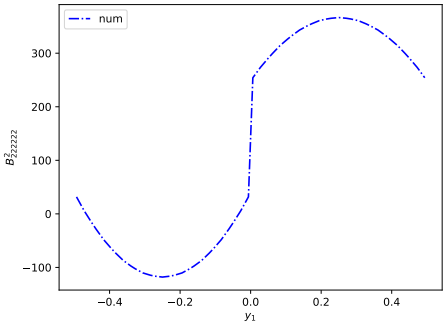

(d) B^2_{222222} *values along* y_1

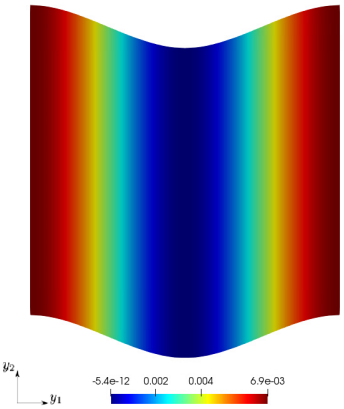

(e) D^2_{21121} *component*
(magnification of 20)

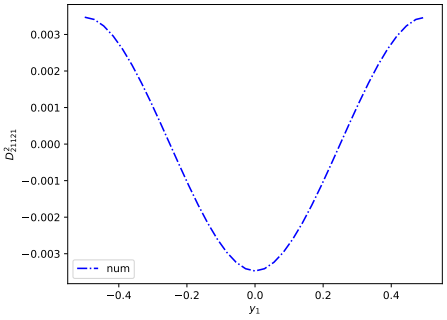

(f) D^2_{21121} *values along* y_1

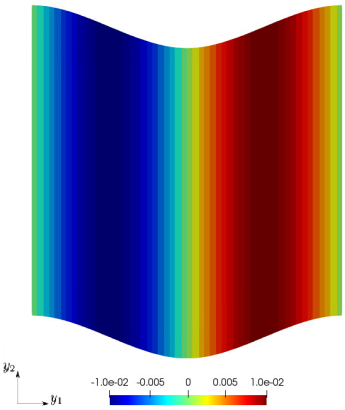

(g) A^2_{121121} *component*
(magnification of 10)

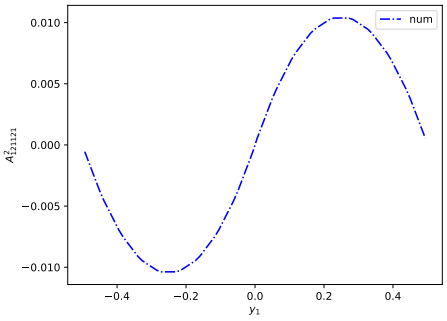

(h) A^2_{121121} *values along* y_1

Figure B.4: *Third-order relocalization components* (D^2_{12222}, B^2_{222222}) *and* (D^2_{21121}, A^2_{121121}).

B.2 Comparative study with He and Pindera [2020a]

The objective of this appendix is to compare our results of higher-order relocalization and boundary layer correction with those obtained in He and Pindera [2020a].
First, second and third-order components of stress localization tensors are shown in Fig. B.5. These results are to be compared with those presented in He and Pindera [2020a] (see their figure 3), where a finite-volume method was used to compute localization tensors. It is noticed that exactly the same results are obtained.

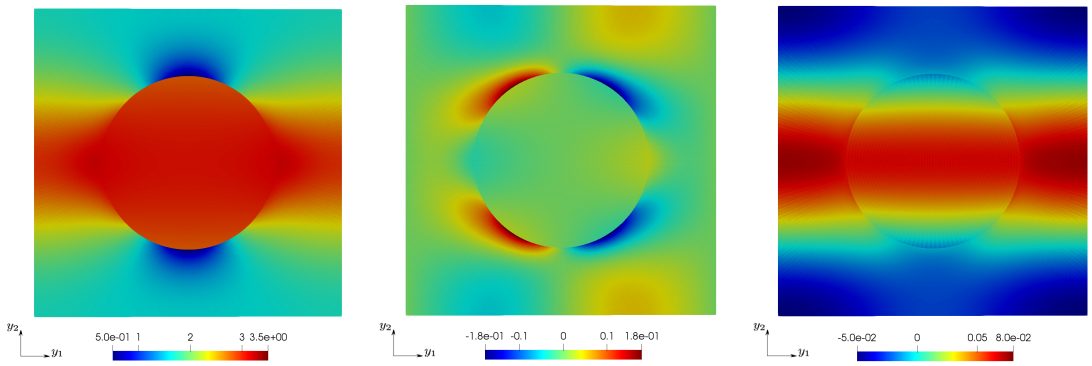

(a) B^0_{1111} *(MPa)* (b) B^1_{11111} *(MPa)* (c) B^2_{111111} *(MPa)*

Figure B.5: *First, second and third-order components of stress localization tensors produced by a unit loadings.*

remark B.4 *The component* B^1_{11111} *has a zero average distribution over the unit-cell, implying that the first component of the second-order effective tensor* $C^1_{11111} = 0$. *In general,* $\mathbb{C}^1 = 0$ *in case of centro-symmetric unit-cell.*

Comparison of different stress fields σ_{11} are shown in Fig. B.6. By increasing the order of the relocalization, estimated stress fields approach progressively the reference. Figures B.6e and B.6f show that a third-order relocalization provides a good estimation in the inner domain of the structure, nevertheless accuracy is lost near the boundaries. Similar results are shown in He and Pindera [2020a] (see their figure 5).
Comparison of stress fields, after the boundary layer correction, are shown in Fig. B.7. It is noticed that the corrected stress, σ^{cor3}_{11}, provides a better estimation near the boundaries (see figure B.7b), contrary to σ^{est3}_{11} in figure B.6f.
In He and Pindera [2020a], a boundary layer correction is conducted by applying the third-order relocalized displacement field in the inner domain of the *fully* detailed, *i.e.* using DNS, boundary.
By comparing our results, it is noticed that a better approximation of σ^{cor3}_{11} is provided by the boundary correction by He and Pindera [2020a], albeit at a higher computing cost. Indeed, instead of conducting DNS, which may be computationally cumbersome when the boundary domain is large, our method introduce corrective terms computed on a *single unit-cell*.

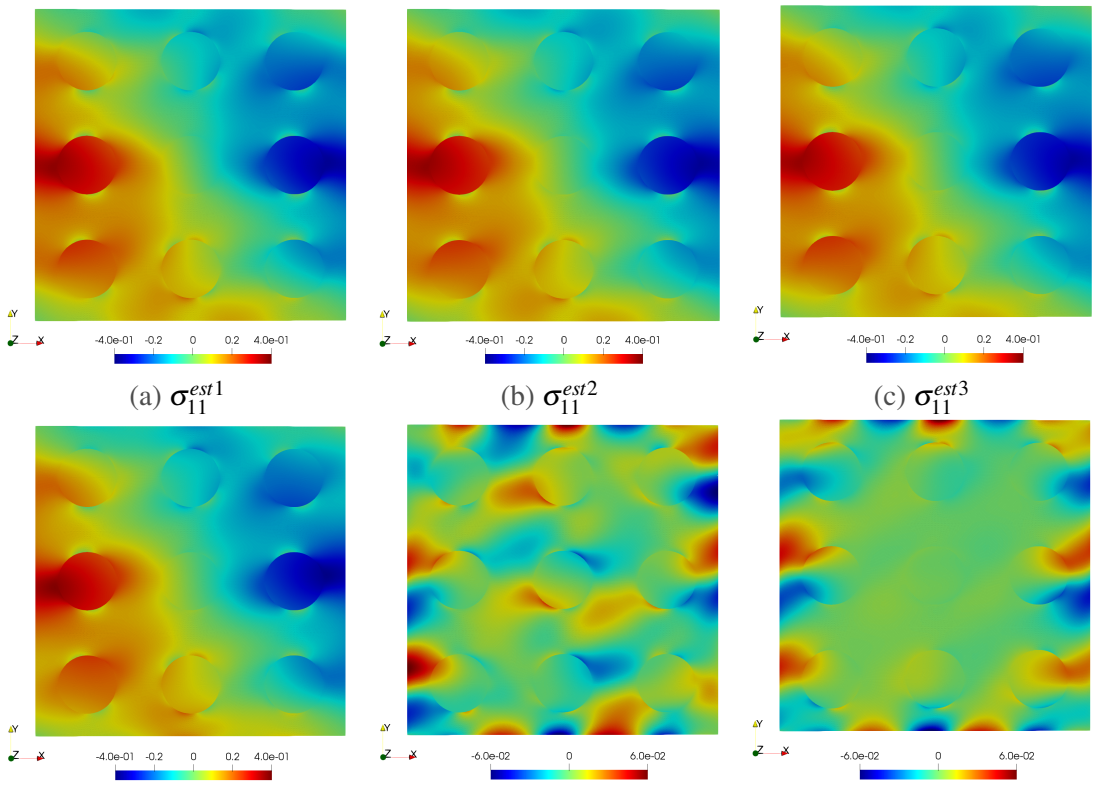

(a) σ_{11}^{est1} (b) σ_{11}^{est2} (c) σ_{11}^{est3}

(d) σ_{11}^{ref} (e) $\sigma_{11}^{est1} - \sigma_{11}^{ref}$ (f) $\sigma_{11}^{est3} - \sigma_{11}^{ref}$

Figure B.6: *Comparison of different stress fields* σ_{11} *(MPa). By increasing the order of the relocalization, estimated stress fields approach progressively the reference, yet remain inaccurate near the boundaries.*

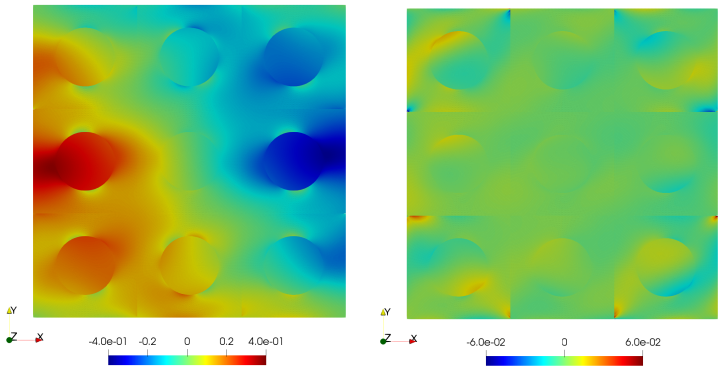

(a) σ_{11}^{cor3} (b) $\sigma_{11}^{cor3} - \sigma_{11}^{ref}$

Figure B.7: *Comparison of corrected stress fields* σ_{11} *(MPa).* σ_{11}^{cor3} *provides a better approximation than* σ_{11}^{est3} *as shown in Fig. B.6f.*

B.3 Limitation of the proposed approach

We consider a plane strain elasticity problem of a laminated composite made of two layers as presented in Fig. B.8. The size of the structure is $L = 8$ mm, $H = 5$ mm and $W = 1$ mm. The two layers are assumed to be isotropic linear elastic with coefficients ($E_f/E_m = 200$, $\nu_m = \nu_f = 0.3$). The structure is fixed on the left whereas a prescribed displacement $u_2 = -2$ mm is applied on the right, as shown in Fig. B.8.

The comparison between the reference displacement field u_2^{ref} and the homogenized one

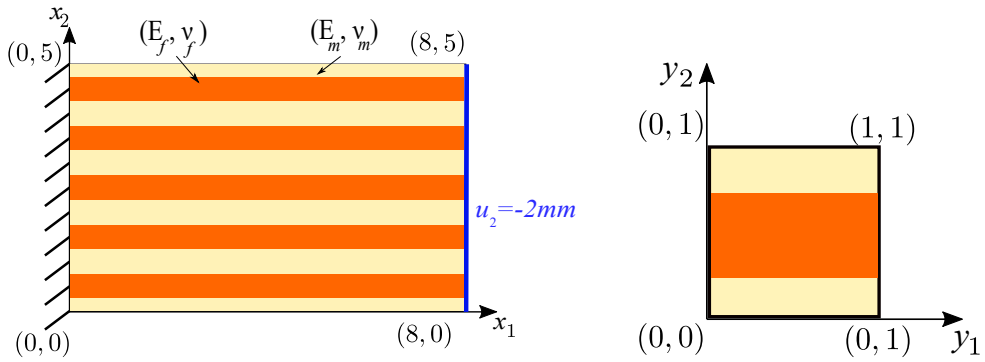

(a) *Structure geometry* (b) *Unit-cell domain*

Figure B.8: *Illustration of a laminated composite in bending. The structure is fixed on the left, a displacement $u_2 = -2$ mm is applied on the right.*

u_2^{hom}, using conventional Cauchy continuum, are presented in Fig. B.9. It can be seen that

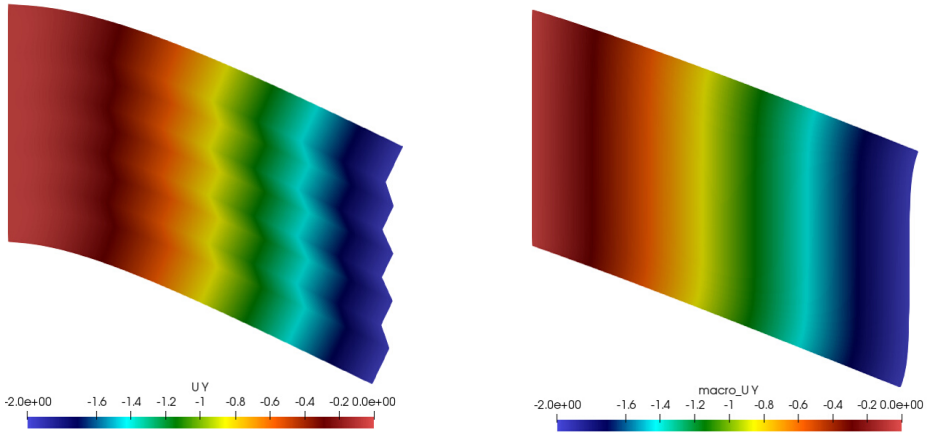

(a) u_2^{ref} (b) u_2^{hom}

Figure B.9: *Comparison between the reference and homogenized displacement field u_2.*

the Cauchy medium gives a poor prediction of the real deformation state. This is due to the fact that it is not able to take into account the clamping conditions. Consequently, the relocalization process will be inaccurate, even including higher-order terms, since the

resulting macroscale strain and its gradients, considering a Cauchy continuum, are inaccurate and not representative of the deformation state, especially near the fixed boundary, which can be seen in Fig. B.10. Cosserat medium was considered at the macroscale

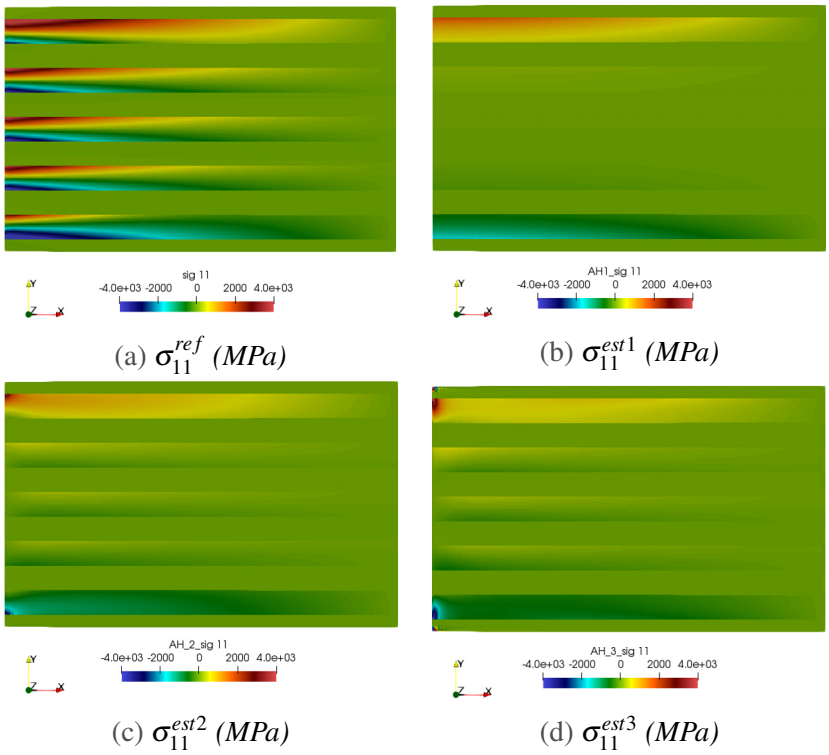

(a) σ_{11}^{ref} *(MPa)* (b) σ_{11}^{est1} *(MPa)*

(c) σ_{11}^{est2} *(MPa)* (d) σ_{11}^{est3} *(MPa)*

Figure B.10: *Results of the reference (σ_{11}^{ref}) field compared with the first-order (σ_{11}^{est1}), second-order (σ_{11}^{est2}), and third-order (σ_{11}^{est3}) estimates for the laminated composite in bending.*

in Forest and Sab [1998] providing better solutions. A higher-order relocalization, using a Cosserat medium at the macroscale, is supposed then to provide better solutions than those presented in Fig. B.10. A macroscopic strain gradient approach would also provide a better solution.

remark B.5 *When considering a structure constructed by one of the two unit-cells presented in subsection 3.5.1 or 3.5.2 and subjected to the same boundary conditions in Fig. A.2a, the macroscale strain and its gradients, using a Cauchy continuum, will be representative of the deformation state. Consequently, higher-order estimates will accurately approximate reference fields. The need of a higher-gradient continuum is, therefore, specific to both the considered microstructure and loading conditions.*

Appendix of Chapter 4

C.1 Comparison of relocalized field on macroscale meshes

Comparison of U_1, U_2 and σ_{11} components, solution of the problem detailed in subsection 4.3.2, are presented in figures C.1, C.2 and C.3, respectively. Same conclusions as in subsection 4.3.2 are drawn. Indeed, the quality of estimated fields increases by refin-

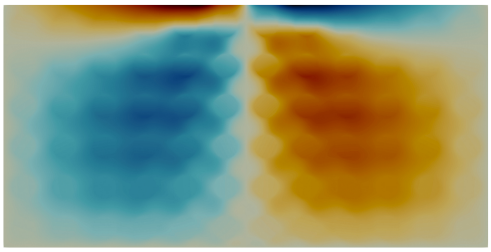

(a) U_1^{ref} *on microscale mesh*

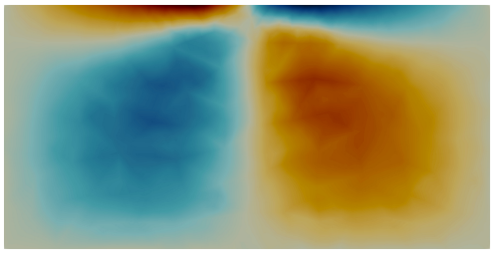

(b) U_1^{cor2} *on macroscale mesh 1*

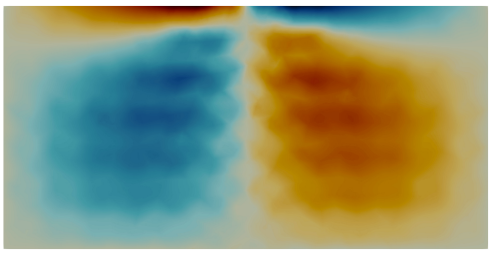

(c) U_1^{cor2} *on macroscale mesh 2*

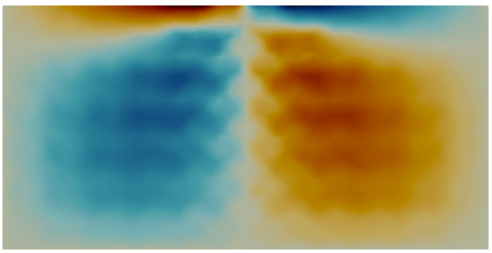

(d) U_1^{cor2} *on macroscale mesh 3*

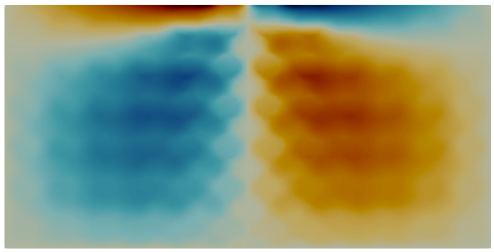

(e) U_1^{cor2} *on macroscale mesh 4*

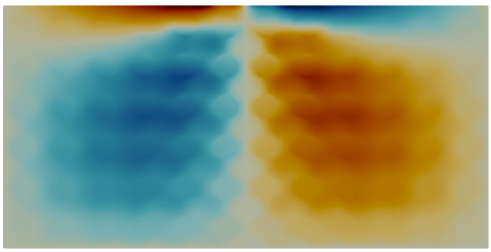

(f) U_1^{cor2} *on macroscale mesh 5*

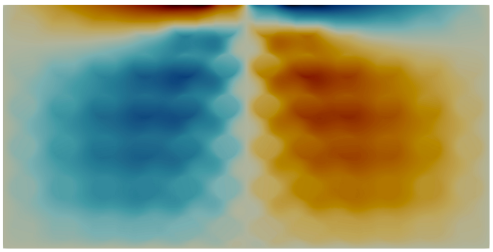

(g) U_1^{cor2} *on macroscale mesh 6*

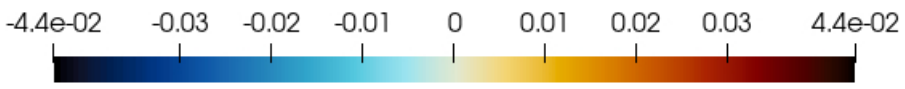

Figure C.1: *Comparison of* U_1 *results.*

ing the macroscale mesh. However, contribution of different material phase (matrix and fibers) to estimated fields begins to be clearly distinguished starting from mesh 3, which provide an acceptable estimation. It is also capable of capturing high gradients developed near region where the load is applied and on the interfaces.

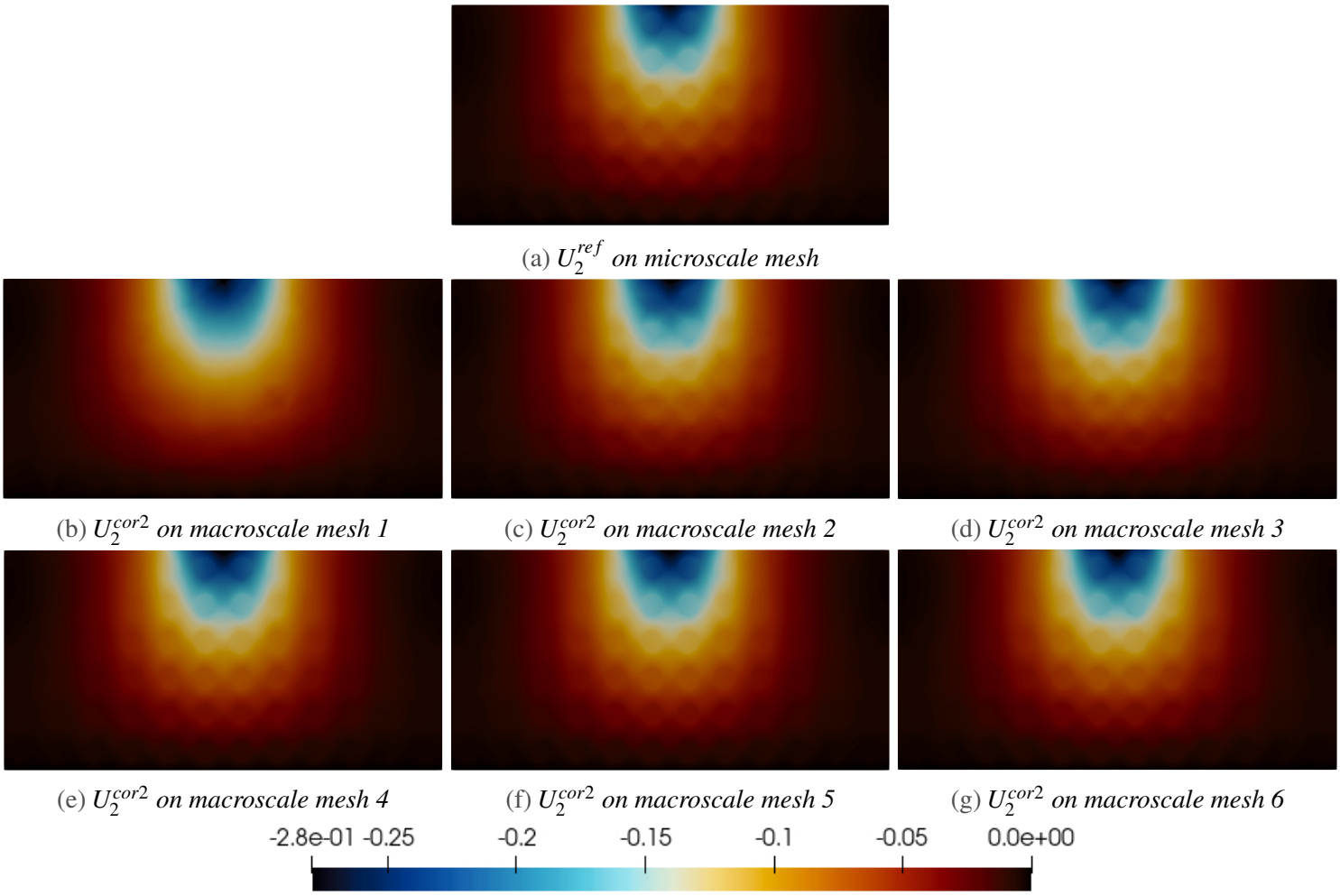

(a) U_2^{ref} *on microscale mesh*

(b) U_2^{cor2} *on macroscale mesh 1*

(c) U_2^{cor2} *on macroscale mesh 2*

(d) U_2^{cor2} *on macroscale mesh 3*

(e) U_2^{cor2} *on macroscale mesh 4*

(f) U_2^{cor2} *on macroscale mesh 5*

(g) U_2^{cor2} *on macroscale mesh 6*

Figure C.2: *Comparison of* U_2 *results.*

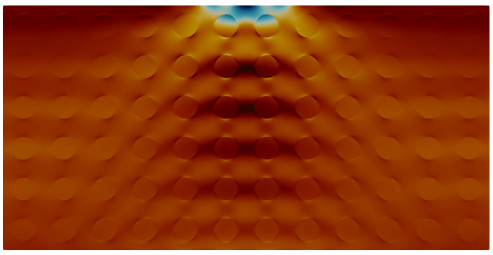

(a) σ_{11}^{ref} *on microscale mesh*

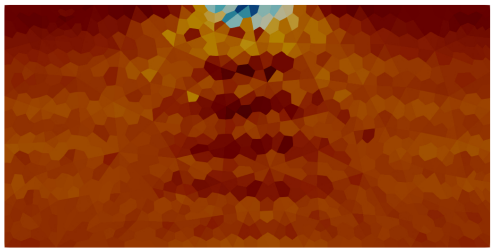

(b) σ_{11}^{cor2} *on macroscale mesh 1*

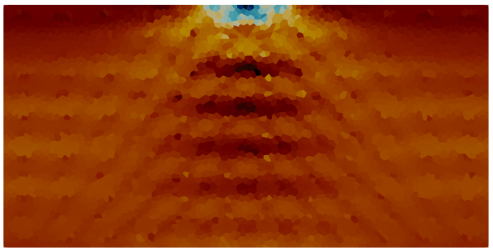

(c) σ_{11}^{cor2} *on macroscale mesh 2*

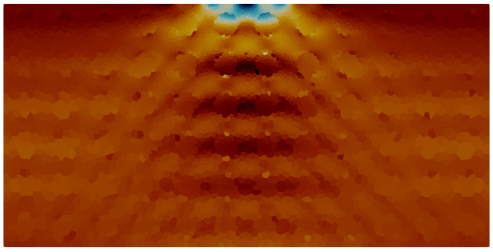

(d) σ_{11}^{cor2} *on macroscale mesh 3*

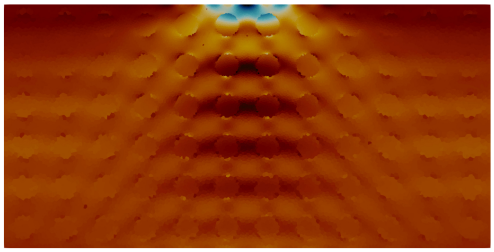

(e) σ_{11}^{cor2} *on macroscale mesh 4*

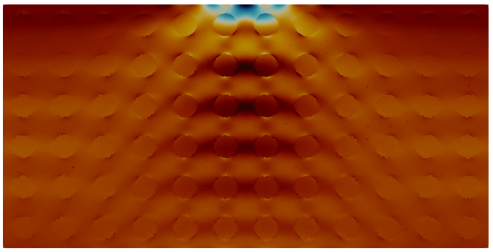

(f) σ_{11}^{cor2} *on macroscale mesh 5*

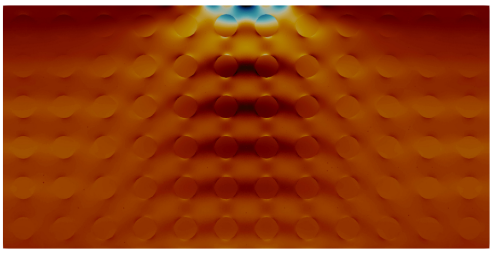

(g) σ_{11}^{cor2} *on macroscale mesh 6*

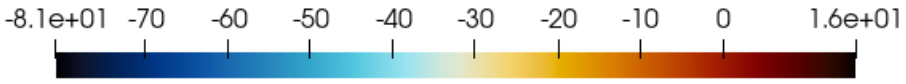

Figure C.3: *Comparison of* σ_{11} *results.*

C.2 Comparison of the reference fields with the relocalized ones

Figure C.4 shows a comparison of the reference solution $\boldsymbol{u}^{ref}$, with the obtained relocalized fields, $\boldsymbol{u}^{est1}$ and $\boldsymbol{u}^{cor2}$ for different ratios $\frac{E_f}{E_m}$. This comparison was conducted by considering an identical macroscale mesh with the microscale one. The second-order relocalized field corrected on the boundaries $\boldsymbol{u}^{cor2}$, highly reduces the modeling error compared to the first-order relocalized field $\boldsymbol{u}^{est1}$. As a result, $\boldsymbol{u}^{cor2}$ provides a better estimation to $\boldsymbol{u}^{ref}$ than $\boldsymbol{u}^{est1}$.
A third-order relocalization is supposed to provide a better solution than $\boldsymbol{u}^{cor2}$ as illustrated in Fergoug et al. [2022b], albeit at a higher computation cost. We have chosen to restrict our study to $\boldsymbol{u}^{cor2}$ since it is sufficient to illustrate our purpose.

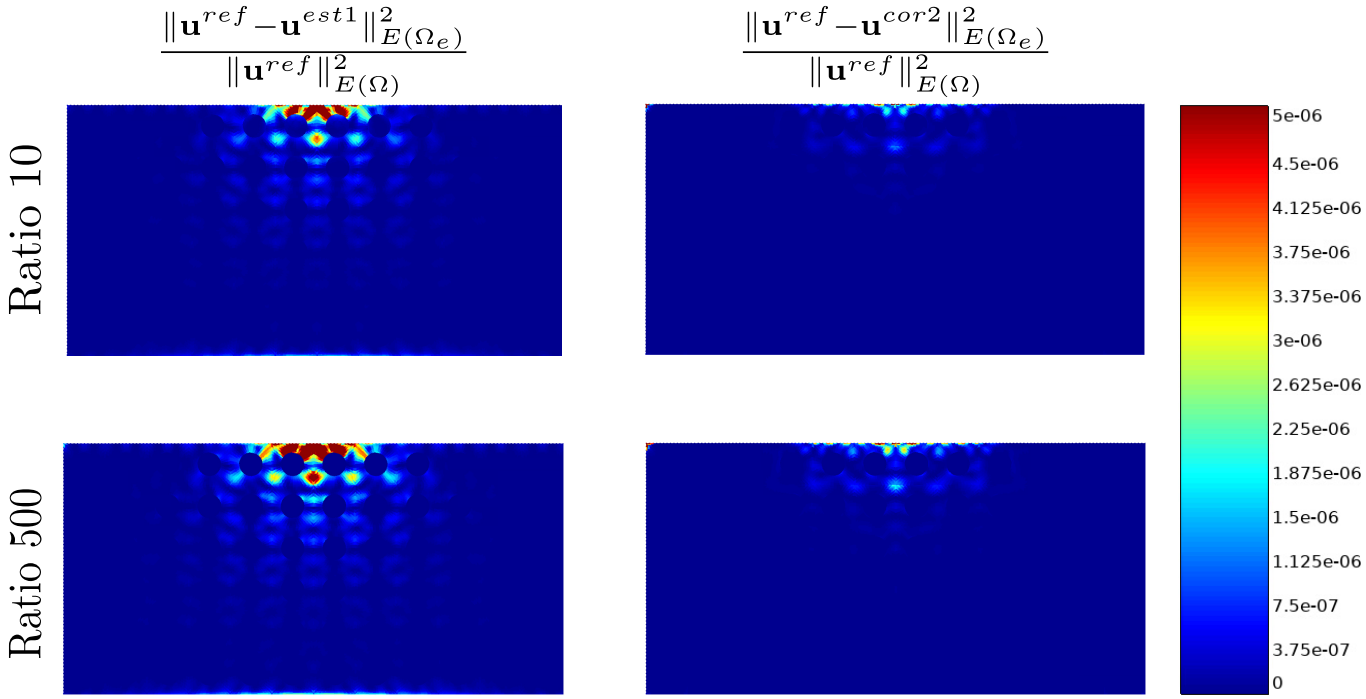

Figure C.4: *Comparison of the relative local error (in the energy norm defined in equation 4.13) between $\boldsymbol{u}^{ref}$ and the obtained relocalized fields, $\boldsymbol{u}^{est1}$ and $\boldsymbol{u}^{cor2}$, for different ratios $\frac{E_f}{E_m}$.*

Work in collaboration with Mateus AMERICO DE ALMEIDA

In this appendix, the main results of the work conducted in collaboration with Mateus AMERICO DE ALMEIDA Americo De Almeida [2022] as a part of his internship are summarized.

D.1 Automatization workflow

To conduct higher-order relocalization with the boundary layer correction, the user must go through several manual steps, which can be difficult, time consuming and can lead to errors. Mateus has proposed a Python tool to conduct, automatically, higher-order relocalization with the boundary layer correction just by entering the geometry of the unit-cell and the dimensions of the used structure, as detailed in the workflow in figure D.1.

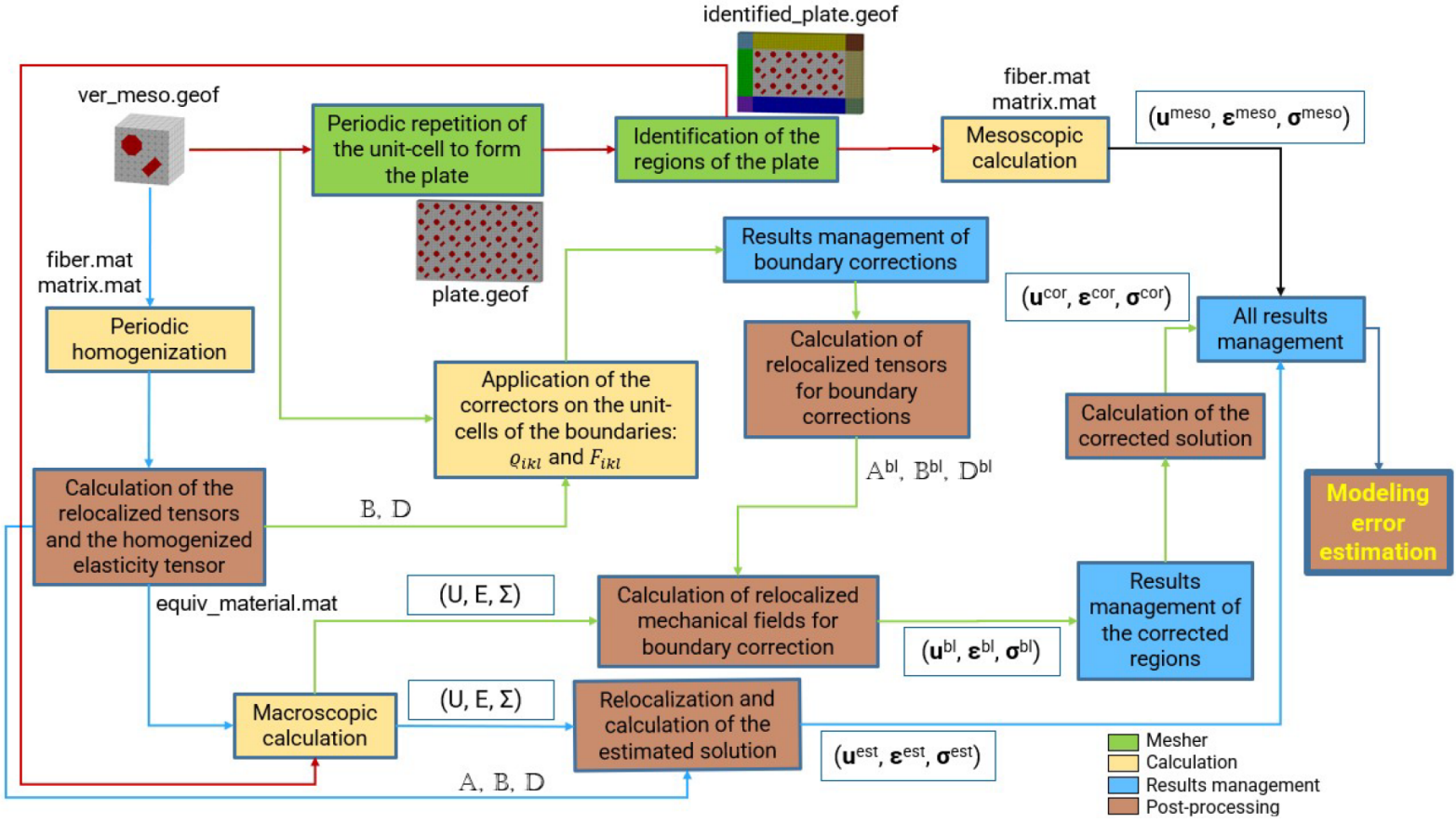

Figure D.1: *Proposed automatization workflow Americo De Almeida [2022].*

D.2 Boundary layer correction for corner cells

The objective of this appendix is to improve the boundary layer correction in corner cells. Indeed, instead of applying the boundary layer correction to one unit-cell, the correction is applied to four unit-cells as shown in figure D.2. Localization tensors are then extracted from the region of interest only (highlighted in blue), corresponding to the studied corner cell.

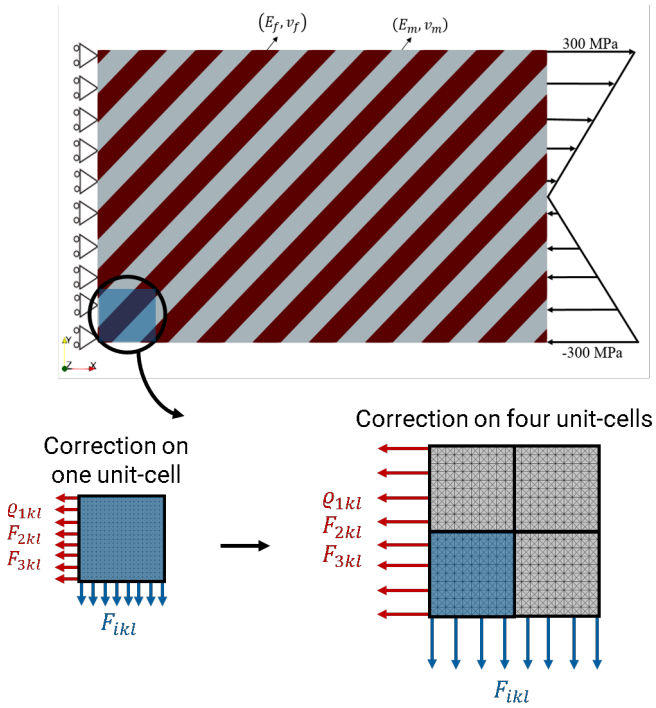

Figure D.2: *Example of the proposed boundary layer correction for corner cells Americo De Almeida [2022].*

A comparison of displacement localization components, D^{bl}_{111} and D^{bl}_{1111}, are shown in figures D.3 and D.4, highlighting the difference between results obtained by the classical and the improved corrections.

A comparison of the local relative modeling error results obtained before and after the improvement of the corner cell correction is shown in figure D.5. One can notice that the modeling error is greatly reduced on corner cells. Particularly, the global modeling error is reduced from 10.9% to 7.3% for the first-order and from 4.7% to 2.6% for the second-order.

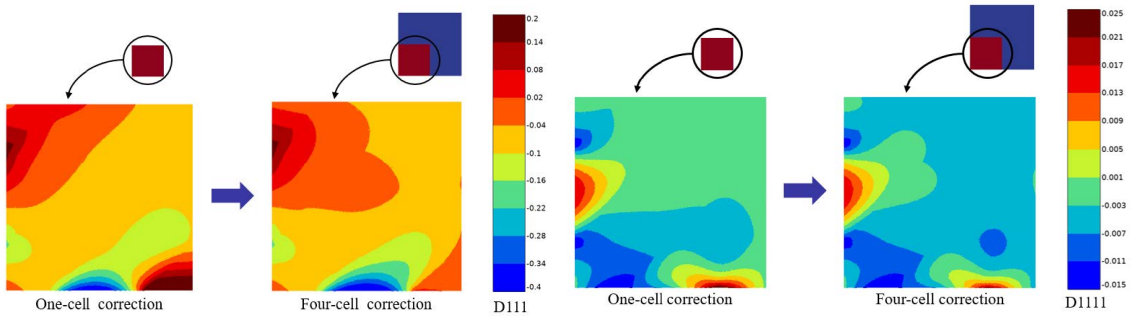

(a) D^{bl}_{111} (b) D^{bl}_{1111}

Figure D.3: *Comparison of displacement localization components.*

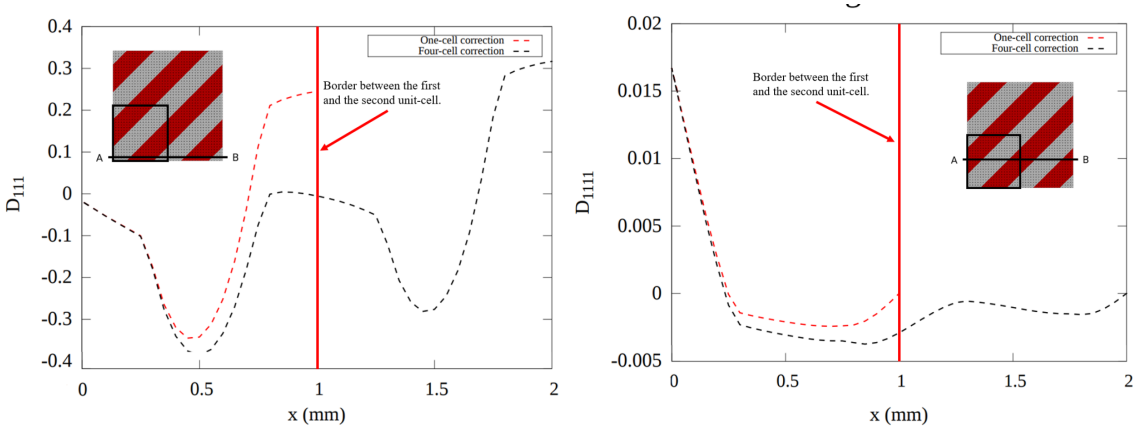

(a) D^{bl}_{111} (b) D^{bl}_{1111}

Figure D.4: *Comparison of values of displacement localization components over the line AB Americo De Almeida [2022] Americo De Almeida [2022].*

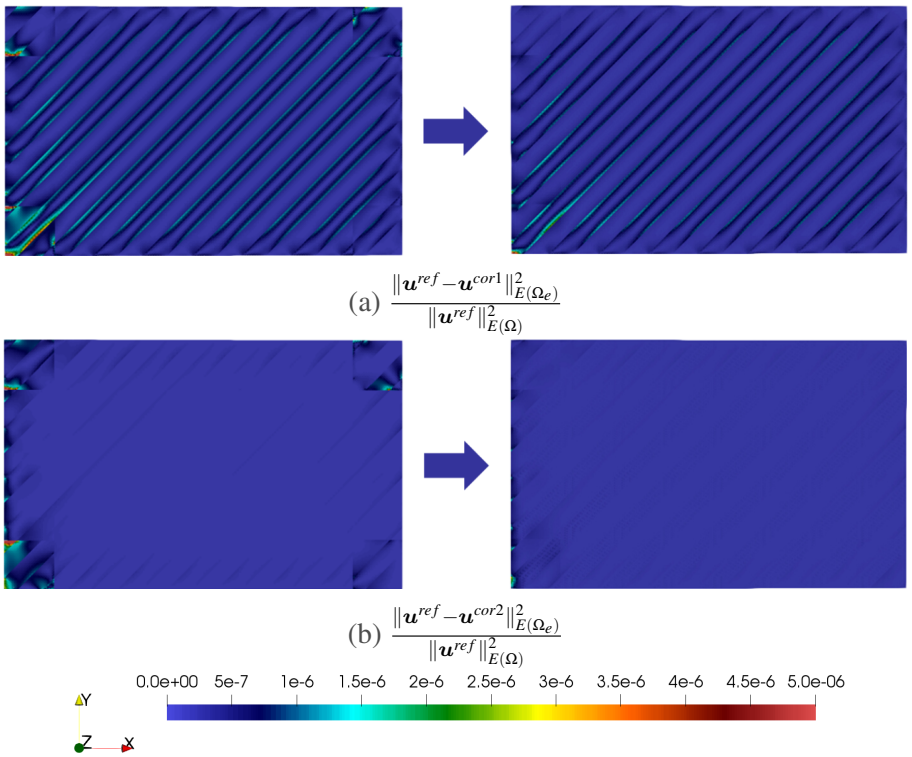

Figure D.5: *Comparison of the local relative modeling error results obtained before and after the improvement of the corner cell correction Americo De Almeida [2022].*

D.3 Extension to nonperiodic structures

We have considered the nonperiodic structure illustrated in figure D.6, where a hole is inserted in the middle of the structure.

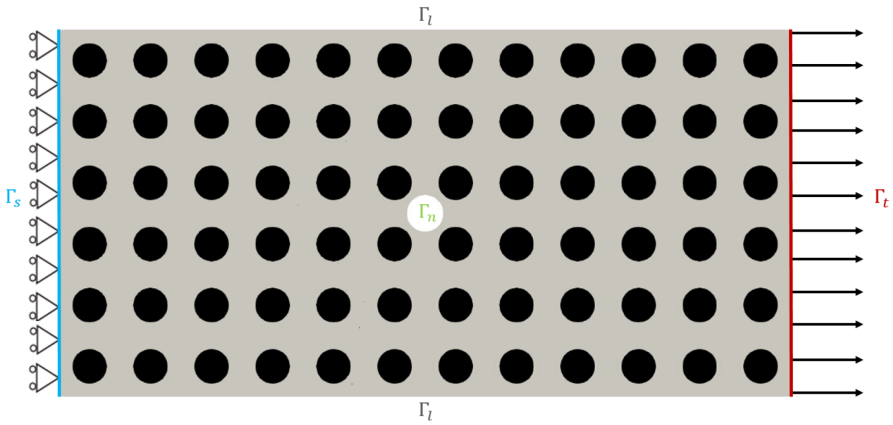

Figure D.6: *Illustration of the studied nonperiodic structure Americo De Almeida [2022].*

The reference field σ_{11} is illustrated in figure D.7a, and the second-order corrected field in figure D.7b. It is clear that the relocalized solution is a good approximation to the reference one except near the hole where the periodicity assumption is lost.

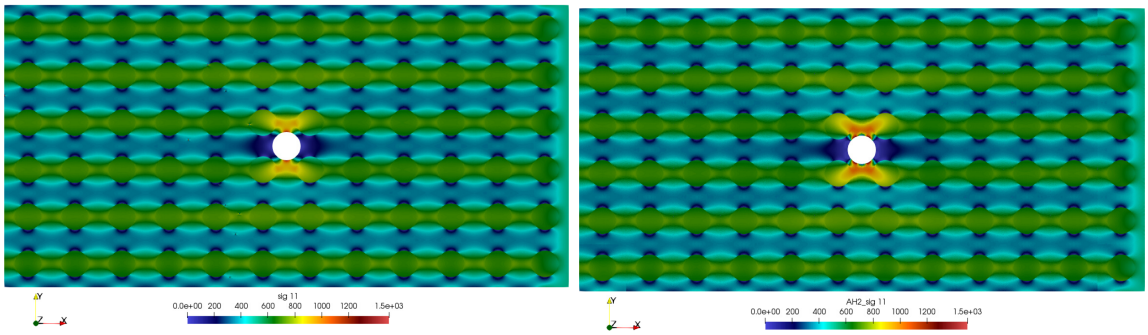

(a) σ_{11}^{ref} (b) σ_{11}^{cor2}

Figure D.7: *Comparison of the reference and relocalized field σ_{11} Americo De Almeida [2022].*

The reference field verifies the following Neumann condition:

$$\boldsymbol{\sigma}^{ref}(\boldsymbol{x}).\boldsymbol{n} = 0, \forall \boldsymbol{x} \in \Gamma_n \tag{D.1}$$

Nevertheless, this condition is not verified for $\boldsymbol{\sigma}^{cor2}$:

$$\boldsymbol{\sigma}^{cor2}(\boldsymbol{x}).\boldsymbol{n} \neq 0, \forall \boldsymbol{x} \in \Gamma_n \tag{D.2}$$

To correct the estimated field, we have considered:

- A first intermediate computation to deduce reaction forces on the boundary Γ_n.
- A second computation where the opposite of these forces are applied as a boundary condition in order to verify the Neumann condition D.1.

The obtained field is illustrated in figure D.8.

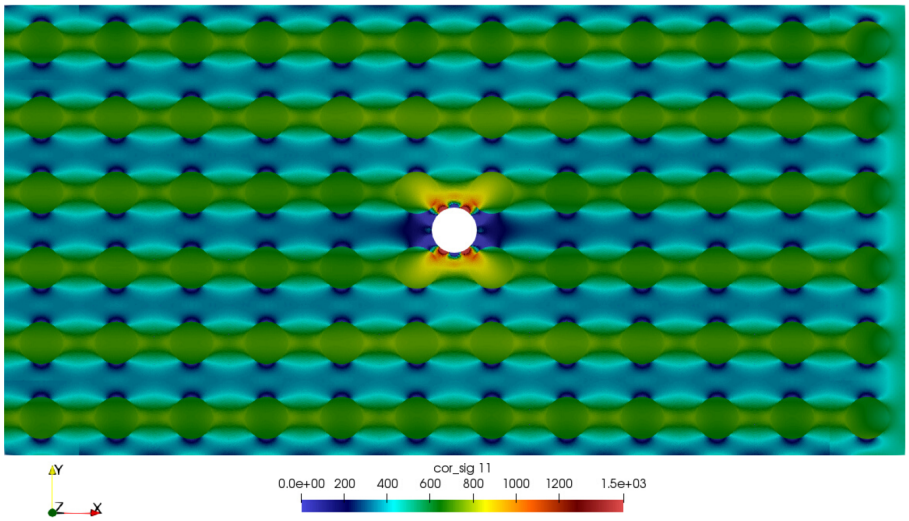

Figure D.8: *Solution of σ_{11} after the proposed correction Americo De Almeida [2022].*

Clearly, the proposed correction is not satisfactory to deal with the nonperiodicity of the solution fields. Further analyses are required to account for locally nonperiodicity in the asymptotic homogenization.

Bibliography

Abali, B. E. and Barchiesi, E. (2020). Additive manufacturing introduced substructure and computational determination of metamaterials parameters by means of the asymptotic homogenization. *Continuum Mechanics and Thermodynamics*.

Abali, B. E., Vazic, B., and Newell, P. (2022). Influence of microstructure on size effect for metamaterials applied in composite structures. *Mechanics Research Communications*, 122:103877.

Abdelmoula, R. and Leger, A. (2005). Local and global effects of small holes periodically distributed on a surface embedded in an axisymmetrical elastic medium. *European Journal of Mechanics-A/Solids*, 24(1):89–109.

Ainsworth, M., Demkowicz, L., and Kim, C.-W. (2007). Analysis of the equilibrated residual method for a posteriori error estimation on meshes with hanging nodes. *Computer methods in applied mechanics and engineering*, 196(37-40):3493–3507.

Allaire, G. and Amar, M. (1999). Boundary layer tails in periodic homogenization. *ESAIM: Control, Optimisation and Calculus of Variations*, 4:209–243.

Ameen, M., Peerlings, R., and Geers, M. (2018). A quantitative assessment of the scale separation limits of classical and higher-order asymptotic homogenization. *European Journal of Mechanics - A/Solids*, 71:89–100.

Americo De Almeida, M. (2022). Evaluation and extension of a modeling error estimation method for multi-scale calculations based on the periodic homogenization theory. Master's thesis, Mines Paris.

Auffray, N., Dirrenberger, J., and Rosi, G. (2015). A complete description of bi-dimensional anisotropic strain-gradient elasticity. *International Journal of Solids and Structures*, 69:195–206.

Babuška, I. and Rheinboldt, W. C. (1978). A-posteriori error estimates for the finite element method. *International Journal for Numerical Methods in Engineering*, 12(10):1597–1615.

Bank, R. E. and Weiser, A. (1985). Some a posteriori error estimators for elliptic partial differential equations. *Mathematics of computation*, 44(170):283–301.

Belgacem, F. B. (1999). The mortar finite element method with lagrange multipliers. *Numerische Mathematik*, 84(2):173–197.

Ben Dhia, H. (1998). Multiscale mechanical problems: the Arlequin method. *Comptes Rendus de l'Académie des Sciences Series IIB Mechanics Physics Astronomy*, 12(326):899–904.

Bensoussan, A., Lions, J.-L., and Papanicolaou, G. (2011). *Asymptotic analysis for periodic structures*, volume 374. American Mathematical Soc.

Benveniste, Y. (1987). A new approach to the application of mori-tanaka's theory in composite materials. *Mechanics of materials*, 6(2):147–157.

Bernardi, C., Maday, Y., and Patera, A. T. (1993). Domain decomposition by the mortar element method. In *Asymptotic and numerical methods for partial differential equations with critical parameters*, pages 269–286. Springer.

Boisse, P., Hamila, N., and Madeo, A. (2018). The difficulties in modeling the mechanical behavior of textile composite reinforcements with standard continuum mechanics of cauchy. some possible remedies. *International Journal of Solids and Structures*, 154:55–65.

Boutin, C. (1996). Microstructural effects in elastic composites. *International Journal of Solids and Structures*, 33(7):1023–1051.

Boutin, C., Auriault, J.-L., and Geindreau, C. (2010). *Homogenization of coupled phenomena in heterogenous media*, volume 149. John Wiley & Sons.

Castaneda, P. P. and Suquet, P. (1997). Nonlinear composites. *Advances in applied mechanics*, 34:171–302.

CFM International (2022). The Power of Flight. www.cfmaeroengines.com.

Cheng, G.-D., Cai, Y.-W., and Xu, L. (2013). Novel implementation of homogenization method to predict effective properties of periodic materials. *Acta Mechanica Sinica*, 29(4):550–556.

Christensen, R. M. (1990). A critical evaluation for a class of micro-mechanics models. *Journal of the Mechanics and Physics of Solids*, 38(3):379–404.

Chung, P. W. and Tamma, K. K. (1999). Woven fabric composites-developments in engineering bounds, homogenization and applications. page 34.

Chung, P. W., Tamma, K. K., and Namburu, R. R. (2001). Asymptotic expansion homogenization for heterogeneous media: computational issues and applications. *Composites Part A: Applied Science and Manufacturing*, 32(9):1291–1301.

Cosserat, E. and Cosserat, F. (1909). *Theorie des corps déformables*. A. Hermann et fils.

Dumontet, H. (1986). Study of a boundary layer problem in elastic composite materials. *ESAIM: Mathematical Modelling and Numerical Analysis*, 20(2):265–286.

Dureisseix, D. and Bavestrello, H. (2006). Information transfer between incompatible finite element meshes: application to coupled thermo-viscoelasticity. *Computer Methods in Applied Mechanics and Engineering*, 195(44-47):6523–6541.

Dutra, T. A., Ferreira, R. T. L., Resende, H. B., Guimarães, A., and Guedes, J. M. (2020). A complete implementation methodology for Asymptotic Homogenization using a finite element commercial software: preprocessing and postprocessing. *Composite Structures*, 245:112305.

Eshelby, J. D. (1957). The determination of the elastic field of an ellipsoidal inclusion, and related problems. *Proceedings of the royal society of London. Series A. Mathematical and physical sciences*, 241(1226):376–396.

Fergoug, M., Parret-Fréaud, A., Feld, N., Marchand, B., and Forest, S. (2022a). A general boundary layer corrector for the asymptotic homogenization of elastic linear composite structures. *Composite Structures*, 285:115091.

Fergoug, M., Parret-Fréaud, A., Feld, N., Marchand, B., and Forest, S. (2022b). Multiscale analysis of composite structures based on higher-order asymptotic homogenization with boundary layer correction. *European Journal of Mechanics - A/Solids*, 96:104754.

Feyel, F. and Chaboche, J.-L. (2000). FE2 multiscale approach for modelling the elasto-viscoplastic behaviour of long fibre SiC/Ti composite materials. *Computer methods in applied mechanics and engineering*, 183(3-4):309–330.

Fish, J. and Belsky, V. (1995). Multi-grid method for periodic heterogeneous media part 2: Multiscale modeling and quality control in multidimensional case. *Computer Methods in Applied Mechanics and Engineering*, 126(1-2):17–38.

Fish, J. and Fan, R. (2008). Mathematical homogenization of nonperiodic heterogeneous media subjected to large deformation transient loading. *International Journal for numerical methods in engineering*, 76(7):1044–1064.

Fish, J. and Markolefas, S. (1993). Adaptive s-method for linear elastostatics. *Computer Methods in Applied Mechanics and Engineering*, 104(3):363–396.

Fish, J., Markolefas, S., Guttal, R., and Nayak, P. (1994a). On adaptive multilevel superposition of finite element meshes for linear elastostatics. *Applied Numerical Mathematics*, 14(1-3):135–164.

Fish, J., Nayak, P., and Holmes, M. H. (1994b). Microscale reduction error indicators and estimators for a periodic heterogeneous medium. *Computational Mechanics*, 14(4):323–338.

Fish, J. and Shek, K. (2000). Multiscale analysis of composite materials and structures. *Composites Science and Technology*, 60(12-13):2547–2556.

Fish, J. and Wagiman, A. (1993). Multiscale finite element method for a locally nonperiodic heterogeneous medium. *Computational Mechanics*, 12(3):164–180.

Fish, J. and Yu, Q. (2001). Multiscale damage modelling for composite materials: theory and computational framework. *International Journal for Numerical Methods in Engineering*, 52(12):161–191.

Forest, S. (1998). Mechanics of generalized continua: construction by homogenization. *Journal de Physique IV*, 8(PR4):Pr4–39.

Forest, S., Pradel, F., and Sab, K. (2001). Asymptotic analysis of heterogeneous Cosserat media. *International Journal of Solids and Structures*, 38(26-27):4585–4608.

Forest, S. and Sab, K. (1998). Cosserat overall modeling of heterogeneous materials. *Mechanics research communications*, 25(4):449–454.

Forest, S. and Trinh, D. (2011). Generalized continua and non-homogeneous boundary conditions in homogenisation methods. *ZAMM - Journal of Applied Mathematics and Mechanics / Zeitschrift für Angewandte Mathematik und Mechanik*, 91(2):90–109.

Gendre, L., Allix, O., Gosselet, P., and Comte, F. (2009). Non-intrusive and exact global/local techniques for structural problems with local plasticity. *Computational Mechanics*, 44(2):233–245.

Germain, P. (1973). The method of virtual power in continuum mechanics. part 2: Microstructure. *SIAM Journal on Applied Mathematics*, 25(3):556–575.

Ghosh, S., Bai, J., and Raghavan, P. (2007). Concurrent multi-level model for damage evolution in microstructurally debonding composites. *Mechanics of Materials*, 39(3):241–266.

Ghosh, S., Lee, K., and Moorthy, S. (1995). Multiple scale analysis of heterogeneous elastic structures using homogenization theory and voronoi cell finite element method. *International Journal of Solids and Structures*, 32(1):27–62.

Ghosh, S., Lee, K., and Raghavan, P. (2001). A multi-level computational model for multi-scale damage analysis in composite and porous materials. *International Journal of Solids and Structures*, 38(14):2335–2385.

Gologanu, M., Leblond, J.-B., Perrin, G., and Devaux, J. (1997). Recent extensions of Gurson's model for porous ductile metals. In *Continuum micromechanics*, pages 61–130. Springer.

Gras, R., Leclerc, H., Hild, F., Roux, S., and Schneider, J. (2015). Identification of a set of macroscopic elastic parameters in a 3d woven composite: Uncertainty analysis and regularization. *International Journal of Solids and Structures*, 55:2–16.

Gras, R., Leclerc, H., Roux, S., Otin, S., Schneider, J., and Périé, J.-N. (2013). Identification of the out-of-plane shear modulus of a 3D woven composite. *Experimental Mechanics*, 53(5):719–730.

Guedes, J. and Kikuchi, N. (1990). Preprocessing and postprocessing for materials based on the homogenization method with adaptive finite element methods. *Computer Methods in Applied Mechanics and Engineering*, 83(2):143–198.

Hansbo, A. and Hansbo, P. (2002). An unfitted finite element method, based on nitsche's method, for elliptic interface problems. *Computer methods in applied mechanics and engineering*, 191(47-48):5537–5552.

Hashin, Z. (1983). Analysis of Composite Materials—A Survey. *Journal of Applied Mechanics*, 50(3):481–505.

Hashin, Z. and Shtrikman, S. (1963). A variational approach to the theory of the elastic behaviour of multiphase materials. *Journal of the Mechanics and Physics of Solids*, 11(2):127–140.

Hassani, B. and Hinton, E. (1998). A review of homogenization and topology opimization II-analytical and numerical solution of homogenization equations. *Computers and Structures*, page 20.

Hassani, B. and Hinton, E. (1999). *Homogenization and Structural Topology Optimization*. Springer London, London.

Hassani, B. and Hinton, E. (2012). *Homogenization and structural topology optimization: theory, practice and software*. Springer Science & Business Media.

He, Z. and Pindera, M.-J. (2020a). Finite volume-based asymptotic homogenization of periodic materials under in-plane loading. *Journal of Applied Mechanics*, 87(12):121010.

He, Z. and Pindera, M.-J. (2020b). Locally exact asymptotic homogenization of periodic materials under anti-plane shear loading. *European Journal of Mechanics - A/Solids*, 81:103972.

Hill, R. (1952). The elastic behaviour of a crystalline aggregate. *Proceedings of the Physical Society. Section A*, 65(5):349.

Hill, R. (1965). A self-consistent mechanics of composite materials. *Journal of the Mechanics and Physics of Solids*, 13(4):213–222.

Hollister, S. J. and Kikuchi, N. (1992). A comparison of homogenization and standard mechanics analyses for periodic porous composites. *Computational mechanics*, 10(2):73–95.

Hsu, P. W. and Herakovich, C. T. (1977). Edge effects in angle-ply composite laminates. *Journal of Composite Materials*, 11(4):422–428.

Huet, C. (1990). Application of variational concepts to size effects in elastic heterogeneous bodies. *Journal of the Mechanics and Physics of Solids*, 38(6):813–841.

Kanit, T., Forest, S., Galliet, I., Mounoury, V., and Jeulin, D. (2003). Determination of the size of the representative volume element for random composites: statistical and numerical approach. *International Journal of Solids and Structures*, 40(13-14):3647–3679.

Kanouté, P., Boso, D. P., Chaboche, J. L., and Schrefler, B. A. (2009). Multiscale Methods for Composites: A Review. *Archives of Computational Methods in Engineering*, 16(1):31–75.

Kelley, F. (1982). Mesh requirements for the analysis of a stress concentration by the specified boundary displacement method. In *Proceedings of the second international computers in engineering conference, ASME*, pages 39–42.

Koley, S., Mohite, P., and Upadhyay, C. (2019). Boundary layer effect at the edge of fibrous composites using homogenization theory. *Composites Part B: Engineering*, 173:106815.

Kouznetsova, V., Brekelmans, W., and Baaijens, F. (2001). An approach to micro-macro modeling of heterogeneous materials. *Computational mechanics*, 27(1):37–48.

Kouznetsova, V., Geers, M., and Brekelmans, W. (2004). Multi-scale second-order computational homogenization of multi-phase materials: a nested finite element solution strategy. *Computer Methods in Applied Mechanics and Engineering*, 193(48-51):5525–5550.

Kouznetsova, V., Geers, M. G., and Brekelmans, W. M. (2002). Multi-scale constitutive modelling of heterogeneous materials with a gradient-enhanced computational homogenization scheme. *International Journal for Numerical Methods in Engineering*, 54(8):1235–1260.

Kruch, S. (2007). Homogenized and relocalized mechanical fields. *The Journal of Strain Analysis for Engineering Design*, 42(4):215–226.

Kruch, S. and Forest, S. (1998). Computation of coarse grain structures using a homogeneous equivalent medium. *Journal de Physique IV*, 08(PR8):Pr8–197–Pr8–205.

Ladevèze, P. and Leguillon, D. (1983). Error estimate procedure in the finite element method and applications. *SIAM Journal on Numerical Analysis*, 20(3):485–509.

Ladevèze, P., Moës, N., and Douchin, B. (1999). Constitutive relation error estimators for (visco) plastic finite element analysis with softening. *Computer Methods in Applied Mechanics and Engineering*, 176(1-4):247–264.

Lefik, M. and Schrefler, B. (1996). FE modelling of a boundary layer corrector for composites using the homogenization theory. *Engineering computations*.

Michel, J. C., Moulinec, H., and Suquet, P. (2000). A computational method based on augmented lagrangians and Fast Fourier transforms for composites with high contrast. *CMES(Computer Modelling in Engineering & Sciences)*, 1(2):79–88.

Miehe, C. and Koch, A. (2002). Computational micro-to-macro transitions of discretized microstructures undergoing small strains. *Archive of Applied Mechanics*, 72(4):300–317.

Mindlin, R. D. (1964). Micro-structure in linear elasticity. *Archive for Rational Mechanics and Analysis*, 16(1):51–78.

Mindlin, R. D. and Eshel, N. (1968). On first strain-gradient theories in linear elasticity. *International Journal of Solids and Structures*, 4(1):109–124.

Monchiet, V., Auffray, N., and Yvonnet, J. (2020). Strain-gradient homogenization: A bridge between the asymptotic expansion and quadratic boundary condition methods. *Mechanics of Materials*, 143:103309.

Mori, T. and Tanaka, K. (1973). Average stress in matrix and average elastic energy of materials with misfitting inclusions. *Acta metallurgica*, 21(5):571–574.

Moulinec, H. and Suquet, P. (1994). A fast numerical method for computing the linear and nonlinear mechanical properties of composites. *Comptes rendus de l'Académie des sciences. Série II. Mécanique, physique, chimie, astronomie.*

Moulinec, H. and Suquet, P. (1998). A numerical method for computing the overall response of nonlinear composites with complex microstructure. *Computer methods in applied mechanics and engineering*, 157(1-2):69–94.

Oden, J. and Vemaganti, K. S. (2000). Estimation of Local Modeling Error and Goal-Oriented Adaptive Modeling of Heterogeneous Materials. *Journal of Computational Physics*, 164(1):22–47.

Oden, J. and Zohdi, T. I. (1997). Analysis and adaptive modeling of highly heterogeneous elastic structures. *Computer Methods in Applied Mechanics and Engineering*, 148(3-4):367–391.

Oden, J. T. and Prudhomme, S. (2002). Estimation of modeling error in computational mechanics. *Journal of Computational Physics*, 182(2):496–515.

Oden, J. T., Prudhomme, S., Hammerand, D. C., and Kuczma, M. S. (2001). Modeling error and adaptivity in nonlinear continuum mechanics. *Computer Methods in Applied Mechanics and Engineering*, 190(49-50):6663–6684.

Oden, J. T. and Vemaganti, K. (1999). Adaptive modeling of composite structures: Modeling error estimation. In *Texas Institute for Computational and Applied Mathematics*. Citeseer.

Oliveira, J., Pinho-da Cruz, J., and Teixeira-Dias, F. (2009). Asymptotic homogenisation in linear elasticity. Part II: Finite element procedures and multiscale applications. *Computational Materials Science*, 45(4):1081–1096.

Pagano, N. J. (1978). Free edge stress fields in composite laminates. *International Journal of Solids and Structures*, 14(5):401–406.

Peerlings, R. H. J. and Fleck, N. A. (2004). Computational Evaluation of Strain Gradient Elasticity Constants. *International Journal for Multiscale Computational Engineering*, 2(4):599–620.

Pipes, R. B., Kaminski, B., and Pagano, N. (1973). Influence of the free edge upon the strength of angle-ply laminates. In *Analysis of the test methods for high modulus fibers and composites*. ASTM International.

Raghavan, P. and Ghosh, S. (2004). Concurrent multi-scale analysis of elastic composites by a multi-level computational model. *Computer methods in applied mechanics and engineering*, 193(6-8):497–538.

Raghavan, P., Li, S., and Ghosh, S. (2004). Two scale response and damage modeling of composite materials. *Finite Elements in Analysis and Design*, 40(12):1619–1640.

Reuß, A. (1929). Berechnung der Fließgrenze von mischkristallen auf grund der Plastizitätsbedingung für Einkristalle. *ZAMM-Journal of Applied Mathematics and Mechanics/Zeitschrift für Angewandte Mathematik und Mechanik*, 9(1):49–58.

Sanchez-Palencia, E. (1983). Homogenization method for the study of composite media. In *Asymptotic Analysis II—*, pages 192–214. Springer.

Sanchez-Palencia, E. (1986). Homogenization in mechanics. a survey of solved and open problems. *Rend. Sem. Mat. Univ. Politec. Torino*, 44(1):1–45.

Sanchez-Palencia, E. and Zaoui, A. (1987). Homogenization techniques for composite media. *Homogenization techniques for composite media*, 272.

Schwartz, D. J. (1981). Practical analysis of stress raisers in solid structures. *SAE Transactions*, pages 4102–4106.

Sigmund, O. (1995). Tailoring materials with prescribed elastic properties. *Mechanics of Materials*, 20(4):351–368.

Smyshlyaev, V. P. and Cherednichenko, K. D. (2000). On rigorous derivation of strain gradient effects in the overall behaviour of periodic heterogeneous media. *Journal of the Mechanics and Physics of Solids*, 48(6-7):1325–1357.

Suquet, P. (2014). *Continuum micromechanics*, volume 377. Springer.

Suzuki, K. and Kikuchi, N. (1991). A homogenization method for shape and topology optimization. *Computer Methods in Applied Mechanics and Engineering*, 93(3):291–318.

Tang, S. and Levy, A. (1975). A boundary layer theory-part ii: extension of laminated finite strip. *Journal of Composite Materials*, 9(1):42–52.

Temizer, I. and Wriggers, P. (2011). An adaptive multiscale resolution strategy for the finite deformation analysis of microheterogeneous structures. *Computer Methods in Applied Mechanics and Engineering*, 200(37-40):2639–2661.

Terada, K. and Kikuchi, N. (1995). Nonlinear homogenization method for practical applications. *American Society of Mechanical Engineers, Applied Mechanics Division, AMD*, 212:1–16.

Terada, K. and Kikuchi, N. (2001). A class of general algorithms for multi-scale analyses of heterogeneous media. *Computer methods in applied mechanics and engineering*, 190(40-41):5427–5464.

Tran, T.-H., Monchiet, V., and Bonnet, G. (2012). A micromechanics-based approach for the derivation of constitutive elastic coefficients of strain-gradient media. *International Journal of Solids and Structures*, 49(5):783–792.

Vernerey, F. J. and Kabiri, M. (2012). An adaptive concurrent multiscale method for microstructured elastic solids. *Computer Methods in Applied Mechanics and Engineering*, 241-244:52–64.

Visrolia, A. and Meo, M. (2013). Multiscale damage modelling of 3D weave composite by asymptotic homogenisation. *Composite Structures*, 95:105–113.

Voigt, W. (1889). Ueber die Beziehung zwischen den beiden Elasticitätsconstanten isotroper Körper. *Annalen der Physik*, 274(12):573–587.

Wangermez, M., Allix, O., Guidault, P.-A., Ciobanu, O., and Rey, C. (2020). Interface coupling method for the global–local analysis of heterogeneous models: A second-order homogenization-based strategy. *Computer Methods in Applied Mechanics and Engineering*, 365:113032.

Willis, J. R. (1981). Variational and related methods for the overall properties of composites. *Advances in applied mechanics*, 21:1–78.

Yang, H., Abali, B. E., Müller, W. H., Barboura, S., and Li, J. (2022). Verification of asymptotic homogenization method developed for periodic architected materials in strain gradient continuum. *International Journal of Solids and Structures*, 238:111386.

Yang, H., Abali, B. E., Timofeev, D., and Müller, W. H. (2019). Determination of metamaterial parameters by means of a homogenization approach based on asymptotic analysis. *Continuum Mechanics and Thermodynamics*.

Yang, H., Timofeev, D., Giorgio, I., and Müller, W. H. (2020). Effective strain gradient continuum model of metamaterials and size effects analysis. *Continuum Mechanics and Thermodynamics*.

Yuan, X., Tomita, Y., and Andou, T. (2008). A micromechanical approach of nonlocal modeling for media with periodic microstructures. *Mechanics Research Communications*, 35(1-2):126–133.

Yvonnet, J., Auffray, N., and Monchiet, V. (2020). Computational second-order homogenization of materials with effective anisotropic strain-gradient behavior. *International Journal of Solids and Structures*, 191-192:434–448.

Z-set (2022). Non-linear material & structure analysis suite. www.zset-software.com.

Zienkiewicz, O. C. and Zhu, J. Z. (1987). A simple error estimator and adaptive procedure for practical engineerng analysis. *International journal for numerical methods in engineering*, 24(2):337–357.

Zienkiewicz, O. C. and Zhu, J. Z. (1992a). The superconvergent patch recovery and a posteriori error estimates. part 1: The recovery technique. *International Journal for Numerical Methods in Engineering*, 33(7):1331–1364.

Zienkiewicz, O. C. and Zhu, J. Z. (1992b). The superconvergent patch recovery and a posteriori error estimates. part 1: The recovery technique. *International Journal for Numerical Methods in Engineering*, 33(7):1331–1364.

Zienkiewicz, O. C. and Zhu, J. Z. (1992c). The superconvergent patch recovery and a posteriori error estimates. part 2: Error estimates and adaptivity. *International Journal for Numerical Methods in Engineering*, 33(7):1365–1382.

Zienkiewicz, O. C. and Zhu, J. Z. (1992d). The superconvergent patch recovery and a posteriori error estimates. part 2: Error estimates and adaptivity. *International Journal for Numerical Methods in Engineering*, 33(7):1365–1382.

Zohdi, T. I., Oden, J., and Rodin, G. J. (1996). Hierarchical modeling of heterogeneous bodies. *Computer Methods in Applied Mechanics and Engineering*, 138(1-4):273–298.

RÉSUMÉ

Les modèles homogénéisés sont souvent utilisés dans l'analyse multi-échelle des matériaux composites en raison de leur efficacité de calcul, cependant ils ne fournissent souvent pas une précision suffisante dans les régions présentant des forts gradients dans les champs de solution. Une approche pour surmonter cette difficulté est de coupler de manière adaptative le modèle homogène avec un modèle hétérogène dans des zones d'intérêt identifiées. J'ai développé un nouvel estimateur d'erreur de modélisation afin de détecter ces régions où le raffinement du modèle de matériau est nécessaire. Cet estimateur est formulé en se basant sur la méthode d'homogénéisation asymptotique d'ordre supérieur associée à une correction originale des effets de bords que j'ai proposée. En effet, il est démontré que l'homogénéisation d'ordre supérieur fournit une estimation précise des champs hétérogènes même dans les cas où la séparation d'échelle entre les longueurs caractéristiques des hétérogénéités et le problème structurel est faible. Cette estimation de l'erreur de modélisation quantifie la différence entre une estimation d'ordre supérieur introduisant l'effet des gradients macroscopiques et une estimation classique de premier ordre. Une stratégie de couplage adéquate est également développée pour coupler efficacement les domaines homogènes et hétérogènes, constituant une étape vers la modélisation hiérarchique des structures élastiques hétérogènes.

MOTS CLÉS

Erreur de modèle, Analyse multi-échelle, Analyse Globale/Locale, Erreur de discrétisation, Homogénéisation, Eléments-Finis

ABSTRACT

Homogenized models are often used in multiscale analysis of composite materials because of their computational efficiency. However they frequently fail to provide sufficient accuracy in regions with considerable gradients in solution fields. One approach to overcome this issue is to adaptively couple the homogeneous model with a full field, heterogeneous model in selected zones of interest which need to be determined somehow. For this purpose, I have proposed a new modeling error estimate based on a higher-order asymptotic homogenization method associated with an original general boundary layer correction, shown to provide accurate estimation of heterogeneous fields even for cases with a weak scale separation between the characteristic lengths of the heterogeneities and the structural problem. This modeling error estimation quantifies the terms neglected by classical first-order homogenization, which become significant for weak separation of scales. An original multiscale coupling strategy is also developed to more effectively couple the homogeneous and heterogeneous domains as a step toward hierarchical modeling of elastic heterogeneous structures.

KEYWORDS

Modeling error, Multi-scale analysis, global-local analysis, Discretization error, Homogenization, Finite Element Analysis